Development of High Resolution Counting Techniques for Body Radioactivity Measurements

BY

Nouri Ali Droughi

A thesis presented as the degree of
Doctor of Philosophy

Glasgow University

September 1997

Scottish Universities Research and
Reactor Centre

ProQuest LLC.
789 East Eisenhower Parkway
P.O. Box 1346
Ann Arbor, MI 48106 – 1346

DECLARATION

The research work described in this thesis was performed in the Health Physics and Nuclear Medicine Department of the Scottish Universities Research & Reactor Centre, East Kilbride, during the period from October 1992 to December 1996, under the supervision of Dr. B. W. East.

This thesis contains the results of some original research by the author and no part of the material offered has been previously submitted by the candidate for a degree in this or any other university in the relevant studies. Where use has been made of the results and conclusions of other authors care has to be taken to ensure that the source of information is always clearly indicated, unless it is of such general nature that indication is impracticable.

Place: SURRC, East Kilbride

Date: 20 September, 1997 **Nouri Ali Droughi**

ACKNOWLEDGEMENTS

I wish to express my deepest gratitude and appreciation to Dr. B.W. East for his expert supervision of the research work and his continuous encouragement through out the research work. At the same time I am very grateful for the much needed help and assistance of Mr. I. Robertson during the building and the final set-up of the monitor shield and the reviewing of first draft of this account. My special thanks also go to Professor R.D. Scott for theoretical discussions, criticism and guidance during the various research assessments which formed part of my training. Also many thanks are due to Dr.T. Preston for his scientific advice and moral support. I would like to also thank Dr. D.C.W.Sanderson, Dr. A.B. Mackenzie for their helpful scientific guidance and encouragement. Thanks are also expressed to Dr. D. Sumner for his interest in the research work and assistance in providing some samples and subjects for measurements.

I am also indebted to Mr. W. Traquair for his technical assistance during strenuous lead moving operation and his moral support. More widely would like to thank all the academic staff, secretaries, technicians and students for their friendship and support in particular, Raj, Idris, David, Willie, Margaret and Irene.

Finally, I would like to thank my wife Latfia for her patience during the many hours that I have spent away from home and her encouragement throughout this research work. I also would like to express my deepest gratitude to my parents, brothers and sisters and my wife's family for their great moral support. Special thanks are due to the Libyan energy secretariat for their provision of scholarship and to the Libyan interest section for their concern and guidance without which this work would not have been possible.

Dedication

I would like to dedicate this work to the most precious people in my life:
my wife Latfia and the newly arrived twins Nezar and Nooralhooda
And to my mother Raga and to the memory of my late father
Ali Droughi

ABSTRACT

Development of High Resolution counting techniques for body radioactivity measurement

In vivo whole- and partial-body counting has been dominated by scintillation detectors because of their high counting efficiency for gamma-rays. However, large semi-conductor detectors are now becoming available and it is logical to apply them to body counting in order to take advantage of their very high resolution since they can give usable efficiencies. With the increasing interest in low-energy gamma and X-ray emitters such as plutonium and americium in the body, semi-conductor detectors namely the Low Axial - to diameter length- known as LOAX (a product name of EG&G Ortec), specifically designed for this energy region, can also be used for these measurements. Efforts to measure internally deposited transuranic elements *in vivo* have largely been concentrated on the accurate detection of the radionuclides in various parts of the body. This requires that the detectors are reliable and adequately sensitive.

As an integral part of this study a great deal of effort has been spent on the modification of the shadow-shield whole-body counter at SURRC. The shadow-shield was reorganized to accommodate up to four n-type LOAX detectors and one 80% p-type HPGe-detector along with the two NaI(Tl) detectors already present. This detector arrangement has transformed the monitor into a " hybrid " detection system capable of measuring low, intermediate and high energy gamma-emission from radionuclides. This research work has investigated the detection characteristics of the hyper-pure germanium detectors in the shadow-shield monitor as an improved method for quantitative measurement of internally deposited radionuclides. It provides a comprehensive background data analysis of the shadow-shield arrangement and

discusses the various methods of background prediction for the HPGe-detectors used.

The detection capability of the " hybrid " counter has been thoroughly examined by measuring standard sources and a number of different types of anthropomorphic phantoms. Specially made tissue equivalent phantoms labelled with various activities of isotopes of ^{241}Am, ^{210}Pb and ^{238}U have been measured and used for the calibration. Combining the results of the calibration factors in terms of sensitivity, minimum detectable activity (MDA) and the scattering contribution of human subject measurements a number of optimum methods for data analysis have been presented for HPGe-detectors in the shadow-shield arrangement and discussed.

To establish the usefulness of the equipment for body measurement, the MDA is what is of interest. The main criterion tried for carrying out data analysis of the small (low counts) peaks expected was to see whether the collected counts constituted a peak above established background or not. The utilisation of the available computer programs was not very helpful in this respect and the straight-forward method of visually comparing the spectrum with background from controlled subjects was examined. Using this method, the MDA taking 2σ as the definition, corresponded to 3 Bq for ^{241}Am 59.5 keV for a one hour count and to 10 Bq for ^{210}Pb. Other methods were also used to define the exact region of interest for the low energy peaks, for example, the counts within each peak were manually calculated and their respective activity and MDA were tabulated.

The results of special measurements of four human subjects that were known to contain various levels and types of the radioactivity of interest due to their various life styles, are presented. Also a number of whole dead sheep and various bones collected from decayed animals in the South West of Scotland area have been measured and found to contain a significant level of americium radionuclide mainly due to contamination by Sellafield discharges and lead radionuclide due to the presence of natural uranium decay products. The final reported activity levels were

determined using calibration factors that were calculated using their appropriate phantom " internally " deposited activities. An activity of as low as 4 Bq was determined in one subject and as high as 100-150 Bq of ^{241}Am in sheep and bone samples from the South West Scotland.

These final results have proved the applicability and the considerable sensitivity of the detection system in the actual detection of real cases of internally deposited low-level and low-energy radioactivity. A number of interesting and valuable *in vivo* gamma-ray spectra obtained from the measurements of human subjects as well as soil samples showing various activities of ^{241}Am, ^{210}Pb and other radionuclides are presented in the appendix A.

Table of contents

Chapter 1

Measurements of body radioactivity by external radiation detection

Chapter 2

A description of the whole-body counting equipment and its development

Chapter 3

Background studies

Chapter4

Calibration of the Whole-body Monitor using Surrogate Human Phantoms

Chapter 5

Chapter 6

Conclusion ,summary and recommendations

List of Figures

Chapter 1

Chapter 2

Chapter 3

Chapter 4

Chapter 5

List of Tables

Chapter 1

Chapter 2

Chapter 3

Chapter 4

Chapter 5

Chapter 6

Chapter 1

Measurements of body radioactivity by external radiation detection

1.1 Introduction

Mankind is continuously subject to exposure from internal radioactivities naturally present in the body. These internal exposures arise from the presence of ^{40}K, ^{14}C and traces of the long-lived uranium and thorium series radionuclides and their daughters. The detection or dosimetry of internally deposited radionuclides is generally termed *in vivo* or Internal Dosimetry. The first ever internal measurement carried out on human subjects was on the radium dial painters going back to the year 1929 (Raabe, 1994) where an ionization chamber was used to estimate the amount of radium intake.

The use of man-made radionuclides and ionizing radiations in various scientific, medical and technological fields, including nuclear energy, will also potentially add to these "natural" exposures and under extreme circumstances could pose potential health hazards. One important objective in radiation protection programmes is to prevent or limit the intake of radioactivity by radiation workers and the general public both under normal operating conditions and accidents.

During the last three decades a greater awareness of radiological protection issues has developed; more conservative radiation protection philosophies have evolved; there have been revisions of the regulations relating to occupational and public exposures; and greater interest in the possible effects of low-level radiation doses has been taken. In particular, the public has become concerned about the apparent health effects near nuclear installations where materials like plutonium are handled. This radionuclide is very difficult to detect *in vivo* because of the low-energy of its electromagnetic emissions but an associated radionuclide, ^{241}Am, is somewhat more energetic giving a greater possibility of detection *in vivo*. Consequently, there has been a marked increase in the emphasis which has been placed on the counting of low-energy low-level radionuclides in the body.

The accurate assessment of internal exposure to radioactive materials requires reliable and adequately sensitive methods for the activity measurement in specific organs and in the whole-body.

Also, in recent years, a number of scientific documents have reported an apparent increased risk of various types of cancer following exposure to low dose radiation. Some of these reports have noted an increased incidence of childhood leukemia around some British nuclear establishments (Roman et al., 1987). Part of the increase of childhood leukemia was attributed to early paternal exposure in nuclear workers (Gardner et al., 1990), but apparent effects were also noticed in residents in the close proximity of operating nuclear installations such as Sellafield and Dounreay (Gardner and Winter, 1984) and (Mole, 1987). All of these reports have caused a certain alarm and triggered further investigative studies by various medical and scientific committees. After the investigation in 1983 by Yorkshire Television and their programme about the increased induction of childhood leukaemia in Seascale in Cumbria, close to the Sellafield nuclear facility, the British government set up an advisory group chaired by Sir Douglas Black to study further and investigate the causes of the so-called leukaemia "cluster". After a preliminary investigation a report confirmed the findings and made a number of important recommendations (Black, 1984). Based on these recommendations a Committee on Medical Aspects of Radiation in the Environment (COMARE) was further established which added to the list of reports concerning the various aspects of the same phenomena (COMARE, 1986,1988,1995). Almost all of these reports have recommended that critical population groups (i.e. a small homogenous group of individuals who, due to their habits or ways of life represent the most highly exposed individuals in the population), be screened for low-level activity to establish further the link with disease or eliminate it as a possibility.

In the nuclear industry, internal radiation measurement procedures consisting of biological monitoring and in some cases, body counting, are routinely carried out to monitor radiation workers handling radioactivity or working in a radioactive environment. These are intended to ascertain the effectiveness of the various safety procedures and to ensure that the internal dose is well within the recommended safe limits. Similar measurements have been carried out on the general population, for

example, after the Russian accident at Chernobyl in 1986, in order to estimate internal intake from the consumption of contaminated food caused by world-wide radiation fallout. A large number of the Scottish general public were screened and their intake pattern of ^{137}Cs and ^{134}Cs was followed over a long period of time (2 years) using two large NaI(Tl) detectors housed in the shadow-shield whole-body counter (East and Robertson, 1988) and (Watson, 1988). This demonstrated the applicability and usefulness of this type of monitoring which, if it could be extended to radionuclides such as ^{241}Am, would be extremely relevant. There is great interest in plutonium and americium and their possible contribution to human radiation exposure resulting from nuclear fallout in general and from particular situations such as the liquid waste discharges of British Nuclear Fuels Ltd. (BNFL) from their nuclear fuel reprocessing plant at Sellafield. This plant has discharged low-level radioactive waste within the permitted levels (authorized limits) into the Irish sea since 1952. The quantity of caesium, plutonium and americium radionuclides discharged annually has varied considerably from the 1970s up to the 1990s as indicated by Figure 1.1 a & b (MacKenzie & Scott, 1993) and (MAFF, 1990). A major review of the historical discharges to sea and atmosphere from the Sellafield site was presented in 1995 by Gray et al. (Gray et al., 1995).

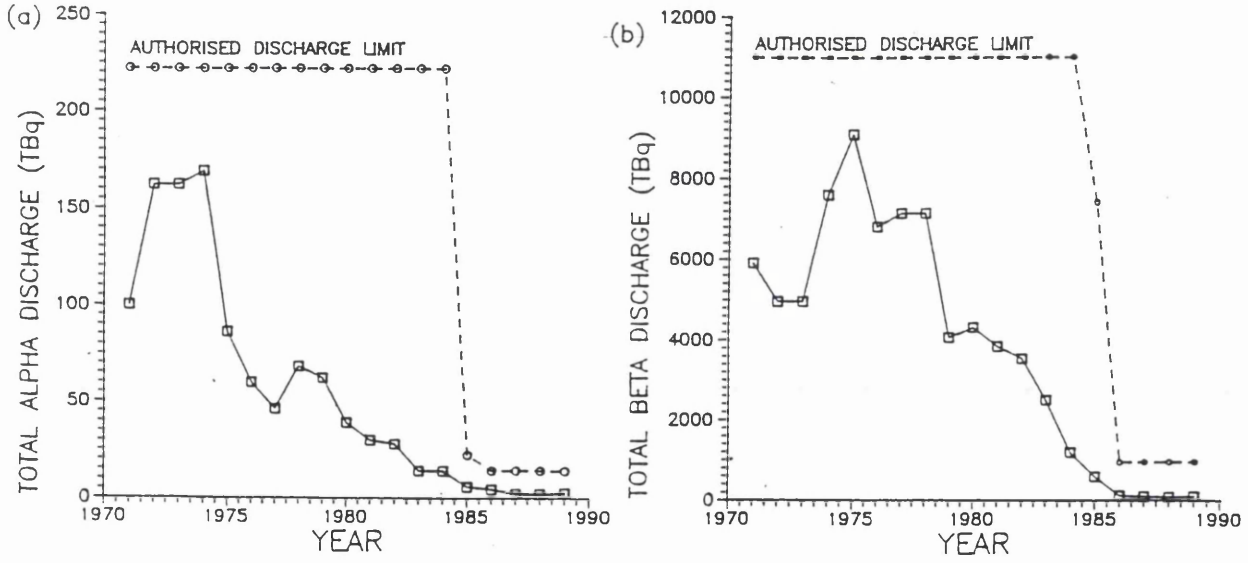

Figure 1.1 Total annual quantities of: (a) alpha emitting radionuclides and; (b) beta emitting radionuclides released from Sellafield (MAFF, 1971-1989).

Latterly, a general trend of decreased discharge of both alpha and beta emitters by two orders of magnitude or more has been observed (BNFL, 1971-1990). Therefore, it is important to evaluate the radiological significance of these discharges into the environment, and identify "critical pathways" leading to the maximum human radiation exposure (Pentreath, 1980). The external and internal exposure resulting from the Sellafield discharges has been assessed by the Ministry of Agriculture Fisheries and Food (MAFF) and their main estimates of these exposures are plotted in Figure 1.2 a & b (MAFF, 1971-1989). It can be seen that while the discharges over the same period have decreased two orders of magnitude, the internal exposure has fallen by only one order of magnitude.

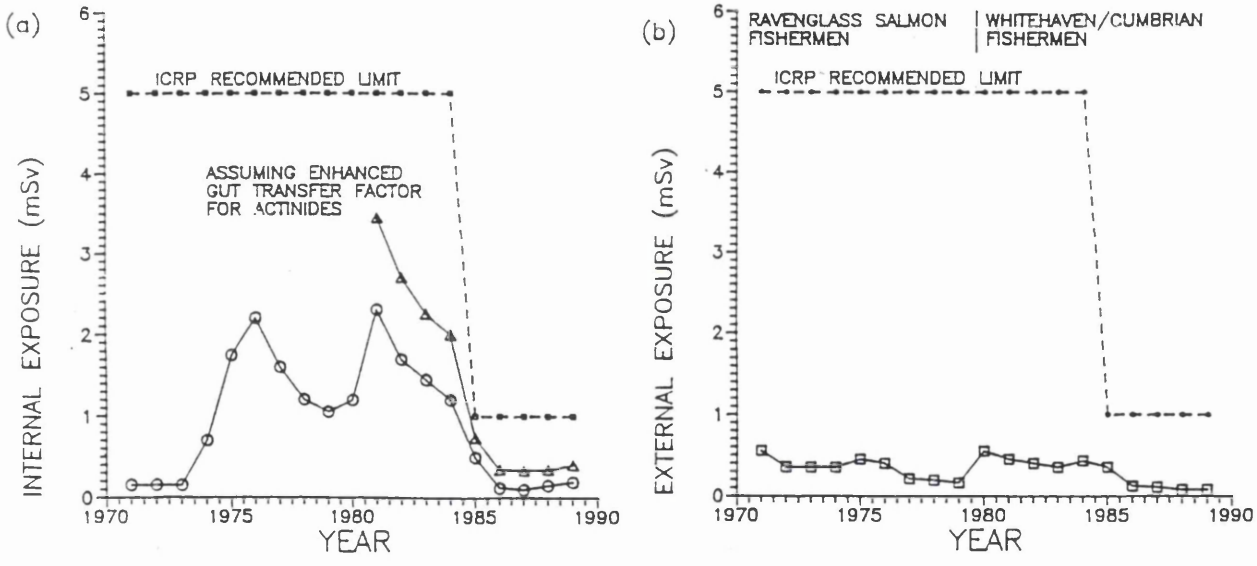

Figure 1.2 MAFF estimate for: (a) critical group internal exposure (0) and internal exposure assuming an enhanced gut uptake factor for actinides (Δ), and; (b) critical group external exposure to radiation as a result of the Sellafield discharge (MAFF, 1971-1989).

As can be seen that from figure 1.2, the internal exposure for the critical group has decreased from a maximum of 2.3 mSv in 1981 (3.45 mSv if enhanced gut uptake of actinides is assumed) to 0.19 mSv in 1989 (0.4 mSv if enhanced gut uptake of actinides is assumed). It is also noted that the external exposure has dropped from a maximum of 0.55 in 1980 to 0.079 mSv in 1989. This fact implies that during the period of reduced effluent releases, radionuclides present in the environment from

previous discharges continued to make a significant contribution to the critical group exposure. One additional fact that might explain the unmatched reduction of discharge to exposure is due to the difference in half-lives of both ^{241}Pu (14.4y) and ^{241}Am (433y) which means there is continuous growth of Am from the decay of Pu . Because of its toxicity and widespread use plutonium has been studied exhaustively. It is known that reactor produced plutonium consists of a mixture of isotopes such as (238, 239, 240, 241, 242). The relative amount of each isotope depends upon the irradiation history of the material being measured and time since separation but ^{239}Pu and ^{240}Pu cannot be separately analysed by alpha spectrometry so they are normally quoted as a composite fraction- ^{239,240}Pu. However it is established that the ratio of (^{238}Pu / ^{239,240}Pu) is about 0.03-0.05 for the global fallout plutonium and about 0.5 for the Chernobyl derived plutonium (Kozhevrov, 1991). When dealing with plutonium contamination assessments, the isotopic composition is determined from mass- or alpha-spectrometry. This procedure enables the determination of the specific activities and X-ray yields of all plutonium isotopes involved in the accident and thus the Pu:Am activity ratio analysed (Burns et al., 1994) and (Palmer and Rhoads, 1989). For these reasons the ^{241}Am is therefore used as a tracer for plutonium especially for cases of class (y) (which refers to its biological half-clearance times from certain pulmonary compartments in the lungs of 500 days) intake or fresh intakes of soluble aerosols. However, due to the differential metabolism of plutonium and americium, it may be prudent to rely on the measurement of plutonium lung burden by means of the low-energy X-rays. On the other hand ^{241}Am with its alpha, photon, and X-ray emission has more than 50 individual practical applications which make it by far the most used actinide element. Among other things, it has been widely used in smoke detectors through the use of its alpha emission ionization properties. Although most of the americium produced in nuclear reactors is regarded as a contaminant, its separation method and uses of this radionuclide in numerous applications increase the potential for exposure of both occupational i.e. radiation workers and environmental exposure i.e. the general public as whole. For these reasons, its measurement characteristics will be emphasized and thoroughly studied in this research work.

1.2 Review of whole-body counting

Whole-body counting is a colloquial term used for the measurement of X- and gamma radiations emitted from radionuclides deposited inside the body by using external detectors close to the body surface. As the name implies, the whole-body is measured simultaneously. Where external detectors are used to measure radiation from a specific organ, this is referred to partial body counting, such as lung counting, liver counting, skull counting etc. The method is a " direct " measurement and can provide data which can be used to verify uptake models, resulting from environmental contamination etc. A limitation is that only activity present at the time can be found and to fix the activity present at some previous time, metabolic models or retention curves that describe the behaviour of the radionuclides in the body must be used.

A typical whole-body counting facility consists of a detection system and radiation shielding components. Shields commonly used fall into two categories. The first type are complete iron or steel rooms often made of pre-World War II naval armour plating which has a low radioactive content, for housing the detectors and the measured subjects in a very low background environment. They are expensive and difficult to build. The second type is a considerably cheaper approach consisting of a " shadow-shield " form of shielding which uses a minimum amount of lead so that the subject is not completely shielded, but the parts of the subject being measured pass into or are placed in the shielded compartment during counting. This is the type of arrangement used in this work.

As mentioned, the first ever *in vivo* measurement of radioactivity in the human body was carried out by Schlundt in 1929 using an ionization chamber (Johnson, 1989). All through the years of World War II and for the period up to 1957, there was steady progress in the development of various techniques of *in vivo* measurements using different types of detectors. However, the real breakthrough came when Marinelli, 1957 used a single large NaI(Tl) scintillation detector suspended over the body of a subject to be counted (Knoll, 1994). The subsequent production of larger and larger NaI-crystal sizes has made them the mainstay of direct internal monitoring techniques. The first results to be published using a shadow-shield facility, constructed of lead, iron and wood, were reported by Palmer and Roesch in 1965,

(Hickman, 1994). In most whole-body counting systems, NaI(Tl) detectors were used to measure the gamma-rays emitted by internally deposited radionuclides in the body. Their counting efficiency was sufficient to detect naturally occurring ^{40}K in the human body. It was also possible to measure other radionuclides *in vivo* such as ^{137}Cs from radioactive fallout (Boddy, 1966) and those used in medical procedures such as ^{59}Fe, ^{57}Co, ^{56}Co and ^{131}I.

During the last two decades, the uses of whole-body counting systems have been diversified. Because of increasing concern about the effect of low-level radiation, high resolution semiconductor detectors, namely Ge(Li) and HPGe-detectors have been a prime focus for developing the latest state-of-art whole-body monitor technology. Their potential precision and accuracy for whole-body counting, permitting the measurement of very low-level natural and man-made gamma-ray radioactivity has been the attraction.

These detectors have been used in a number of laboratories throughout the world (Palmer and Rieksts, 1984). The first such system consisting of eight planar HPGe detectors, mounted in arrays of four on two downward looking cryostats, was described in 1976 (Falk et al., 1979) and (Falk and Tyree, 1984) . The Oak Ridge National Laboratory (ORNL) HPGe-system was next to be reported and consisted of six planar detectors arranged in a closely packed rectangular array designed to cover one lung field (Berger and Lane, 1981). Following this, a single HPGe-detector was used to evaluate the performance of an array for *in vivo* detection of uranium (Pomory and Malm, 1984 a & b). The potential of a planar HPGe-detector vis-à-vis a "phoswich" detector for the assessment of Pu in lungs was investigated by Newton (Newton et al., 1984). He used a single HPGe detector, 50mm diameter x 10mm thick to simulate a four detector array. The Atomic Weapons Research Establishment (AWRE) in the UK, have used two arrays of planar HPGe detectors in addition to phoswiches for monitoring of actinide lung contamination (Lane et al., 1985). One array of six planar detectors is placed over each side of the chest of the measured subject. Palmer (Palmer et al., 1984) employed six individual HPGe-detectors in an array for the measurements of radioactivity in lungs. Palmer and Lane have compared the limit of detection for actinides in the chest for a Ge array and two phoswich systems and concluded that the former were superior in many respects particularly for

recognizing the radionuclides in cases of low-level internal contamination. They also found that Ge-arrays can complement the findings from phoswich detectors (Sharma et al., 1989) and (Pomroy and Malm, 1984 a & b). However, they also found that Ge arrays appear to be less suitable than phoswiches for measurements in the 14-20 keV region of ^{239}Pu.

In recent years the results of Cohen et al. (1992), Hickman and Cohen, (1988); Boecker, (1991); Pushparaja, (1992); Bunl et al., (1993), and Smith et al., (1994) have shown considerable improvements in sensitivity, which is defined as the least amount of a radionuclide in the body that can be quantified by a whole-body count. The current detection system with greatest sensitivity for the detection of ^{239}Pu and ^{241}Am is located at the Pacific Northwest Laboratory (PNL) and consists of an array of high purity germanium detectors used for *in vivo* monitoring of workers (Palmer and Rieksts, 1984). Their reported minimum detectable activity (MDA) for the low energy X-rays (17 -20.4 keV) of Pu is in the range of 3000-6000 Bq while it is in the range of 7-13 Bq for the 59.5 keV photon of ^{241}Am (Toohey et al., 1991).

The high energy resolution of these detectors and the steady improvement in detection efficiencies which have been achieved is mainly due to the manufacturing advances in germanium technology which can produce bigger and bigger crystals. In addition, there has been a decrease in relative costs, which has helped their more widespread use for *in vivo* measurements. There is a large volume of published literature covering the development of whole-body counting and *in vivo* counting techniques: (IAEA, 1970, 1984, Swinth et al., 1978, NCRP, 1985 and Palmer et al., 1988).

1.3 Purpose (Aims of the research work)

The main purpose of this research was firstly to apply the design criteria outlined in the previous M.Sc. research work by the author (Droughi, 1992) and build up an optimum semiconductor shadow-shield whole-body counter comprising two types of HPGe-detectors capable of detecting low, medium and high-energy gamma-ray emitters. The ultimate and extremely difficult aim was to construct a detection system with a low enough limit of detection for actinides to be able to measure them in

members of the public. This work took the form of constructing a shadow-shield "Hybrid" detection system comprising a number of two to four n-type low-energy photon-detectors and one p-type 80% high purity germanium detector added on to an existing NaI configuration. It has to be noted that the number of LOAX detectors used through out the experimental procedures varied according to the availability of these detectors since they are required for some other purposes.

Secondly, the aim was to calibrate the detection system using various point sources and different organ models and tissue equivalent phantoms. Adapted computational stripping procedures and synthesized gamma-ray spectra techniques were to be applied in order to elucidate the low count-rate spectra involved which often do not lend themselves to reduction by available gamma analysis programmes . A number of synthesized gamma-ray spectra were produced for this purpose as activity reference data for the various counting geometries.

Thirdly, to utilize this system to investigate *in vivo* the variability of background levels for the main energy peaks of interest and to determine the particular minimum detectable activity (MDA) for the shadow-shield system. The high resolution obtained with germanium detectors enables easier identification of radionuclides compared with NaI detectors and can offset problems of variable scattering when measuring the human body. An important aspect of calibration was to assess the effects of scattered radiation on the background in different phantoms and different individuals.

Fourthly, to make practical *in vivo* measurements of individuals from affected areas, such as South West Scotland thought to be effected by Sellafield discharges to test the detection capability and sensitivity of the system. In addition, it was also possible to use the system for counting *in morto* samples such as whole sheep and their skeletons found in the open in affected areas. Where possible, trial measurements of non-exposed subjects from the general population and other special subjects known to be injected or exposed to certain types of radiation were to be tested along with some animals and soil samples known to be contaminated by nuclear installation effluent discharges.

By reviewing previous work on the methods of assessment of internally deposited radionuclides (Palmer et al., 1988) and studying the latest ICRP Lung model (ICRP 66, 1994) and the biokinetics models for specific nuclides, it is evident that the detection of low- energy photon emitting, low-level internally deposited radioactivity in the lung, liver and skeleton from exposures which have occurred many years earlier, is a formidable task.

1.4 The main radiation emission properties of actinides

The term low-energy photon emitter (LEP) in this context, mainly refers to the alpha-emitting heavy elements or actinides, namely uranium and the transuranic elements, in particular ^{241}Pu and ^{241}Am. A list of the radiations from actinides of interest in this work is given in Table 1.1.

In vivo counting techniques are based on the direct detection and quantitation of gamma and or X-ray photons emanating from within the body by the use of appropriate detection systems located externally.

^{241}Am $t_{½}$=432.7y		^{239}Pu $t_{½}$ =2.41x10^{4} y		^{241}Pu $t_{½}$ =14.4y	
Energy keV	% Abundance	Energy keV	% Abundance	Energy keV	%Abundance
Alpha		Alpha		Alpha	
5477	85%	5156	73.3	4854	2.92x10^{-4}
5435	12.6%	5143	15.1	4896	2.01x10^{-5}
5378	1.7%	5106	11.5	4972	3.08x10^{-5}
Gamma Rays	% Intensity	Gamma-Rays	% Intensity	Gamma-Rays	% Intensity
26.345	2.4	38.66	0.0105	59.543	8.29x10^{-4}
59.537	35.9	51.624	0.0271	103.680	1.02x10^{-4}
X-rays	% Intensity	X-rays	% Intensity	X-rays	% Intensity
13.9	13.3	13.6	1.48	13.6	2.29x10^{-3}
17.5	19.4	17.06	2.09	17.04	3.07x10^{-3}
20.98	4.9	94.66	2.42x10^{-3}	20.3	7.12x10^{-4}

Table1.1 Main energies of radiation, emitted by ^{241}Am, ^{239}Pu and ^{241}Pu along with their percentage abundance. (Sharma et al., 1989) & (ICRP 38).

Radionuclides that emit photons with energies in the range 10-100 keV, such as those shown above can only be measured with great difficulty because of attenuation of their radiations in body tissues. Table1.1 presents the main emitted particles, gamma-ray and X-rays for ^{241}Am, ^{239}Pu, and ^{241}Pu. It has to be noted that ^{241}Pu is overwhelmingly a low energy beta emitter with negligible alphas. For ^{241}Am only 17.8 keV low-energy x-rays are emitted in 19.4% of its disintegrations which are severely attenuated in the body. Lead-210, which is found in small quantities in the bones of uranium mine and mill workers (Palmer et al., 1984) emits 46.5 keV γ-rays in 4% of its disintegrations.

In contrast, radionuclides such as ^{60}Co and ^{137}Cs that emit high energy γ-rays are easily measured, even when present only in very small amounts in the body (Toohey et al., 1991). Table 1.2 lists a range of photon emissions from actinides along with the total linear attenuation coefficient of the main human tissues (Sharma et al., 1989).

Radionuclide	Photon energy keV	Total Linear Attenuation Coefficient (mm^{-1}) of human tissues.			
		Muscle	Adipose	Lung	Rib
^{239}Pu	13.6	0.205	0.107	0.0506	0.82
^{241}Pu	17.06	0.107	0.0591	0.0263	0.414
^{241}Am	20.98	0.0714	0.0422	0.0176	0.261
^{241}Am	59.54	0.0197	0.0171	0.0048	0.0299
^{238}U	63 & 93	0.0173	0.0159	0.0045	0.022
^{235}U	186	0.0143	0.0131	0.0037	0.0182

Table 1.2 Linear attenuation coefficient of various human tissues for the significant energies of actinides.

It can be seen from this table, the measurement of these low-energy photons is a very difficult task due to the severe attenuation within the body tissues and their low relative abundance and low specific activity. The principal aim of any radiation monitoring programme for a radiation worker is to be able to determine the

Committed Equivalent Dose Effective (CEDE) or Collective Effective Dose (CED) when a significant intake has occurred. The current legislation in the UK requires the assessment of CEDE to whole body or CED to an organ based upon 3/10ths of the annual limit of 50 mSv to the whole body or 500 mSv to an organ and so any monitoring procedure must at least have sufficient sensitivity to achieve this.

The general population that might be exposed directly or indirectly to nuclear effluent discharges into sea and air, or fallout due to a nuclear explosion is subject to much lower dose limits, namely a recommended maximum of 1 mSv per year, so that even greater sensitivity is necessary to meet the recommendations of COMARE committee reports (Black Report, 1984) such as that chaired by Sir D. Black. The mechanisms and further description of the various models of biological effects of low level ionising radiation have been provided in a number of references namely the UNSCEAR (United Nation Scientific Committee on the Effect of Atomic Radiation) reports of the united nations (UNSCEAR 1990 & 1994).

1.5 Detailed experimental research procedures

Since it is known that the main organs that accumulate the actinide radionuclides are the lung, liver and skeleton it is necessary to design and outline appropriate methods for their measurement. The principal factors that influence the detection sensitivities and errors of low-energy photon measurement in these organs are: detector geometries; number of detectors used; detector positioning; configuration and the distribution of activity.

The aim of the research studies is to obtain detailed experimental data for subject and background measurements using HPGe-detectors. Comprehensive measurements of calibration factors and MDA levels for static and scanning geometries of various point sources, a commercially available phantom called the Lawrence Livermore phantom and tissue equivalent phantoms will be used to assess the HPGe-detector's capability. As a trial of detection capability, the system was used to measure two subjects, one being injected with ^{237}Pu as part of a Harwell experiment (Newton, 1994) and the second known to be exposed to high levels of radon in her capacity as

an amateur mineral prospector and collector in Devon and Cornwall. The latter subject measurements led to the measurement of a number of a special soil samples for further scrutiny and comparison purposes.

In order to evaluate the monitor for the high energy gamma photon measurement, a volunteer who ingested a known amount of Heather honey which contained 92 Bq of ^{137}Cs was monitored over a one year period. Also, further tests measuring sheep and sheep internal organs from an area affected by nuclear reprocessing plant effluent discharges (Dumfries) provided useful data. To investigate further the effect of man-made radioactivity in the area on the general population, a farmer, taken to represent the farming community, was measured and the collected results are analyzed and discussed. The subject from the area is known to be involved with farming activities in the surrounding area.

In addition, a special phantom (Ego) containing several radionuclides emitting both low and higher energy photons was measured as part of a European inter-comparison study carried out by the German authority **B**undesamt**f**ur **S**trahlenschutz (BfS). Since NaI detectors, an 80% Ge detector and low-energy photon (LOAX) HPGe-detectors were all mounted in the body monitor shielding, cross-comparisons were readily carried out.

CHAPTER 2

A description of the whole-body counting equipment and its development

2.1 SURRC shadow-shield design

A separate prototype shadow-shield design was initially built in the health physics laboratory at SURRC using available 10 cm thick chevron lead bricks. This lead was washed thoroughly and the construction followed the design criteria from work carried out earlier by the author (M.Sc. thesis, Droughi, 1992). The aim was to provide an experimental shadow-shield arrangement as shown in Figure 2.1, utilizing one large volume p-type 80% HPGe-detector having an L-shaped cryostat, inserted at the top side-wall of the shield while the two n-type low-energy HPGe-detectors were inserted horizontally from the top surface of the shield using two separate apertures. (These low-energy detectors were characterized by a low axial-to-diameter length and given the name " LOAX " by the manufacturer (EG&G Ortec Instruments 1993/1994)).

From preliminary background studies it became apparent that the lead bricks were contaminated giving a much higher background than expected. This rendered the system unusable for low background *in vivo* measurements. Despite the cleaning, it was found that ^{60}Co and ^{137}Cs were present in the lead bricks used, as shown in the pulse height spectrum in Figure 2.2. In an attempt to decontaminate the lead bricks, further cleaning was carried but the reduction factor obtained by this procedure was only 10 with the contamination still persisting. The background was therefore considered to be unacceptable for the intended purpose of the counter for low-level low-energy *in vivo* measurements and the decision was taken to relocate the detectors to an existing whole-body monitor shield originally described in full detail by Boddy (Boddy et al., 1975).

As shown in Figure 2.3, the right side of the roof surface of the shadow-shield was reorganized in order to accommodate the 80% HPGe-detector and two LO-AX detectors. The 80% HPGe-detector was inserted from the side about 20 cm from the upper NaI(Tl) detector and at (18 + 57) = 75 cm from the edge of the side-shield at the copper holder.

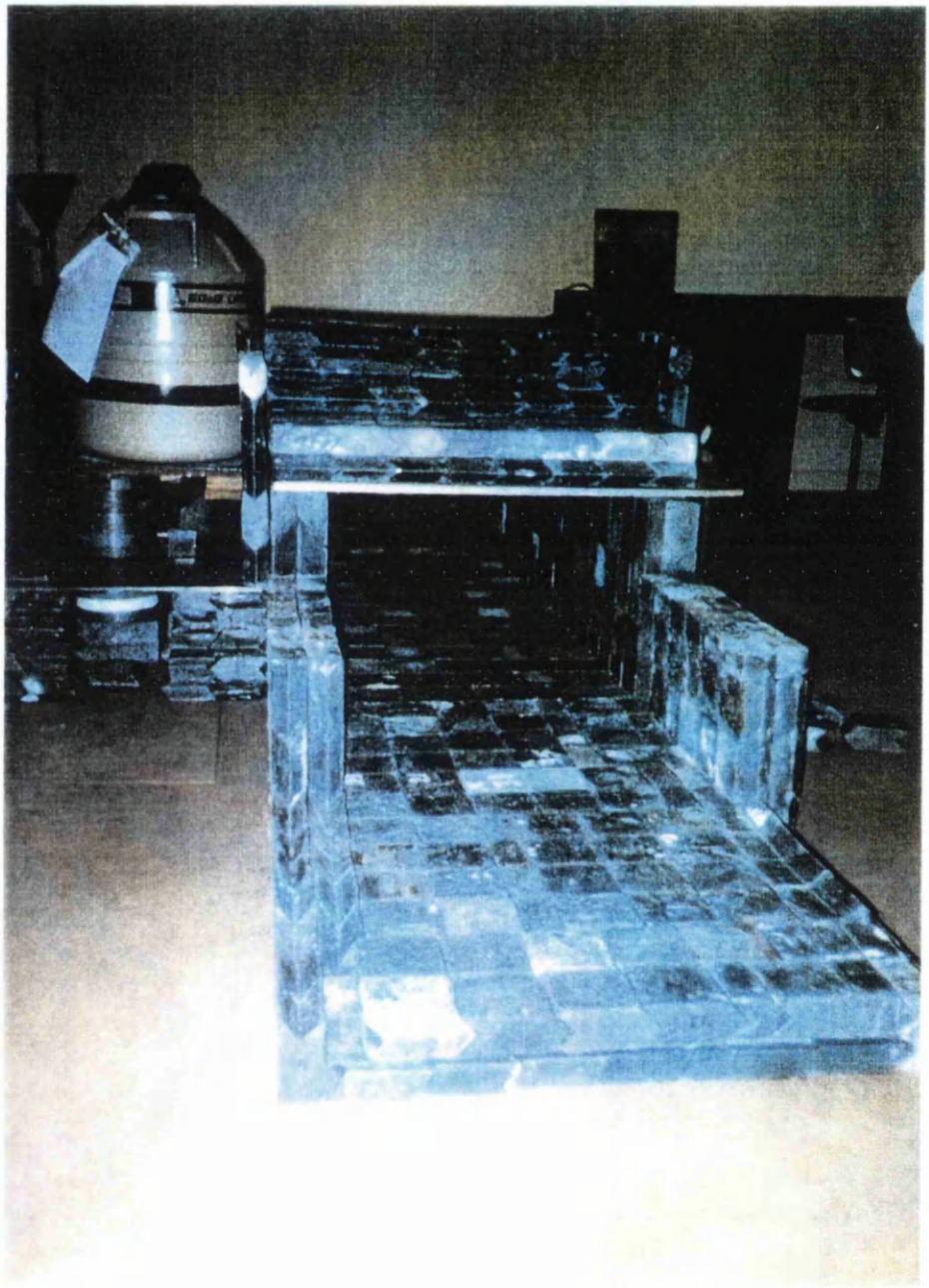

Figure 2.1 Shows the preliminary prototype shadow-shield arrangement.

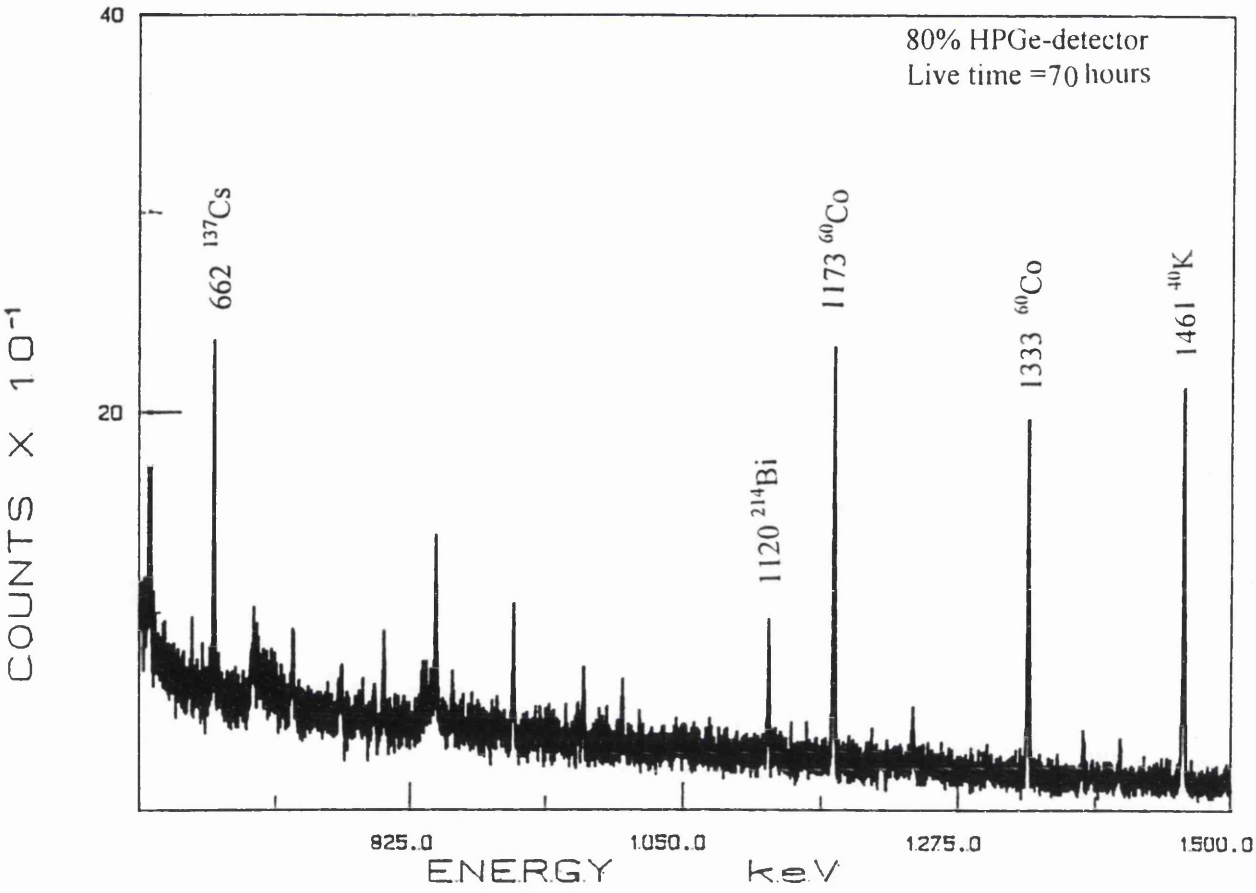

Figure 2.2 Gamma-ray spectrum of the background count of the shadow-shield showing the ^{60}Co and ^{137}Cs contamination.

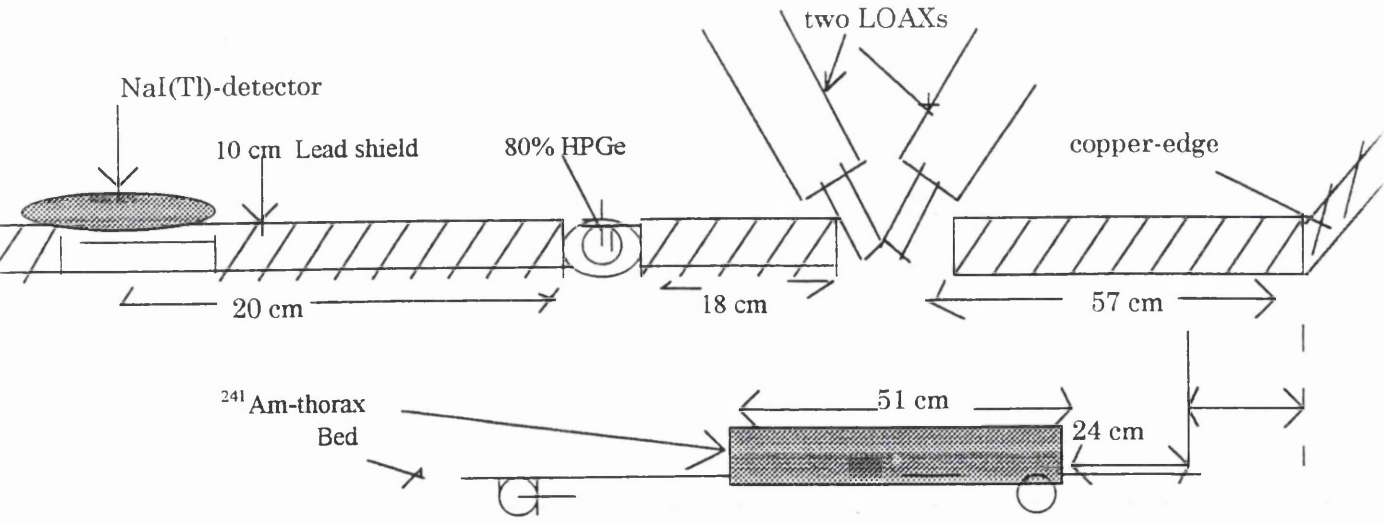

Figure 2.3 The detector arrangement at the modified Shadow-shield whole-body monitor configuration.

To the right side of the 80% HPGe-detector and at a distance of 20 cm, four separate apertures (10 cm x 10 cm) were made to accommodate the semi-vertical insertion of LOAX detectors from above. The four crystals were positioned inside 14 cm thick lead and protruded only about 3 cm beyond the inside roof surface. The separation between the four apertures was only 2.5 cm, and the maximum distance between the detector surfaces and bed surface was about 29 cm. A photograph depicting the detector set-up is shown in Figure 2.4. The LOAX HPGe-detectors were located at a distance of 57 cm from the right side edge of the shielding and the turret was lined from all sides by the 10 cm thick lead forming the top of the monitor. In addition lead shot, contained in polyethylene bags, was used to fill small, irregular gaps around the detector probes.

Detailed background assessments were made and again due to the high resolution of these detectors traces of ^{60}Co and ^{137}Cs contamination were again detected. This had not previously been observed so clearly with the NaI(Tl) detectors over many years of use. Therefore, a decontamination procedure was followed for all the chevron lead bricks used around areas where the shield was modified. In order to ensure the effectiveness of the decontamination operation, the whole lead turret surrounding both NaI(Tl) detectors was dismantled and a comprehensive cleaning procedure for the lead and steel plates followed.

The final background gamma-ray spectra obtained for both detection systems are shown in Figure 2.5 where it can be seen that some improvement was obtained. This is discussed in more detail in chapter 3 particularly section 3.1.3, 3.2 and 3.3.

Figure 2.4 Photograph of the shadow-shield configuration.

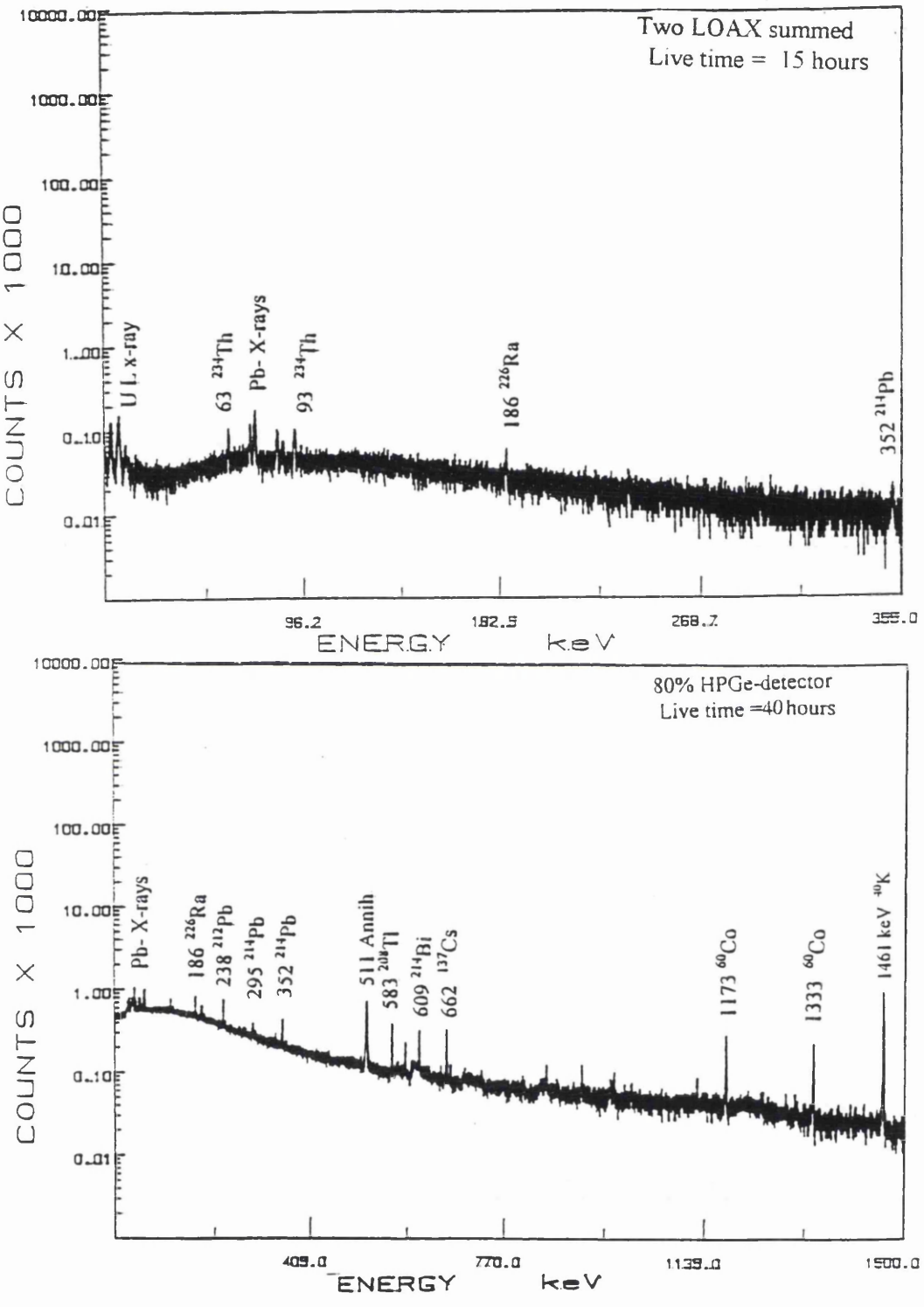

Figure 2.5 Gamma-ray spectra of the final shielding arrangement after decontamination; (a) the 80% HPGe-detector count; (b) the two LOAX detectors.

2.2 The hybrid system

The final structure of the shadow-shield configuration provided a unique combination of detectors with various characteristics which made it a potentially very versatile "hybrid" system. The essence of the "hybrid" system was that two-NaI(Tl) detectors (29.5 cm x 29.5 cm) provided high sensitivity while one large volume p-type 80% HPGe-detector and two or four n-type LOAX detectors provided high gamma-ray resolution. The following section describes the Ge-detectors in detail and outlines all their performance results. Descriptions and detection characteristics of the NaI(Tl) system can be found in a number of references (Boddy, 1966), (East & Robertson, 1989) and (Droughi, 1992).

2.2.1 The LOAX HPGe-detectors

The principal advantages of the n-type LOAX detectors used to build the system are related to the lower capacitance of their coaxial configuration along with their large active frontal area (Seymour et al., 1989). They are supplied with 0.3 μm Be-windows. These technical characteristics along with the inherent higher interaction probability (efficiency) of germanium than for Si(Li), for photons provides a good specification for *in vivo* measurement of actinide radionuclides. In comparison with Si(Li) detectors, which also have high efficiency for the detection of X-and gamma-rays in the range from 1 to 20 keV the germanium types have a larger energy range extending up to 200 keV which is useful in this context.

Although the energy resolution of the Si(Li) and HPGe-detectors may be comparable, their sensitivity to the background will differ. It has been demonstrated by the Mössbauer experiment, that germanium detectors are advantageous in the detection of photon of energy greater than 14 keV, and results in more counts in the full-energy photon peak relative to background continuum (Knoll, 1994). Figure 2.6 gives the ratio of the linear absorption coefficients (cm^{-1}) for both silicon and germanium for the photoelectric to incoherent as a function of energy (Seymour et al., 1989).

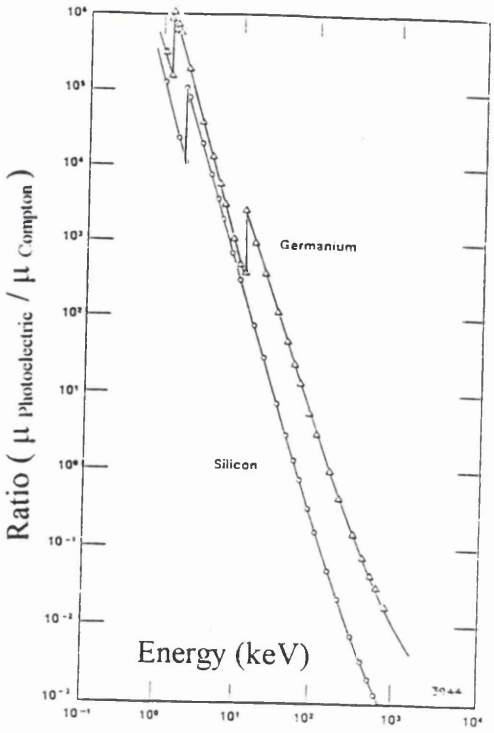

Figure 2.6 Photoelectric to Compton scattering ratio for germanium and silicon crystals.

For the 17.75 keV photon (^{239}Pu), it was calculated that, the HPGe-detector would have approximately a 14:1 photopeak area-to-total area advantage over the Si(Li) detector of similar resolution. This result is expected because the probability of Compton scattering is proportional to the atomic number (Z). However, for the photoelectric process the absorption cross section coefficient varies with energy approximately as $E^{-3.5}$ and also varies as Z^5 (Knoll, 1994). Therefore, for energy above the K-absorption edge of germanium at 11 keV, a significant advantage in sensitivity is gained over the silicon detector. For LOAX detectors, typical sensitivities for ^{235}U for a 30 minute count at 10 cm distance are about 3 Bq for a single detector and about 0.1 Bq for a seven-detector array (Cohen et al., 1992).

The four HPGe LOAX detectors (EG&G ORTEC) in the monitor were closed-end coaxial n-type detectors, each detector being nominally 51 mm in diameter and 20 mm long giving an active volume of approximately 40 cm^3. They were fitted with beryllium windows. Table 2.1 gives the complete technical data for all the detectors and a profile of them is shown in Figure 2.7. Their diameter-to-length ratio is 2.5 or greater and this gives a lower capacitance than larger HPGe detectors. The detector assemblies are coupled to a low capacitance, field-effect transistor (FET) preamplifier which is cooled to 77 K. Such a set up produces very low electronic noise relative to

which is cooled to 77 K. Such a set up produces very low electronic noise relative to its large area entrance window (EG&G Catalogue, 1994). The detector assemblies are mounted in PopTop™ transplantable capsules so they can be interchanged from one dewar to another. The small size compact dewar can be used to provide approximately 48 hours of operating time. Also because of their compactness, the detector elements could be closely packed to obtain useful efficiency for body counting.

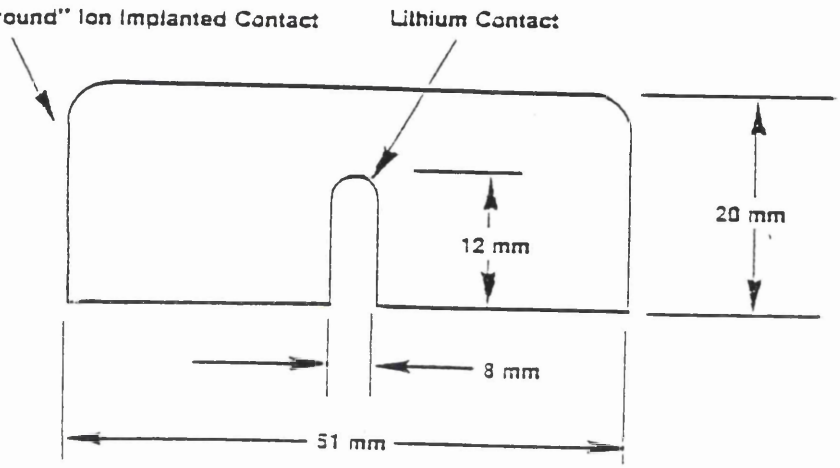

Figure 2.7 A profile of LOAX detectors.

LO-AX Model 51370/20-P	Dimensions		
Crystal diameter	51.1 mm		
Crystal length	18.9 mm		
End-cap-to Crystal	3 mm		
Volume	38.8 cm^3		
Operating Voltage	2500 V		
Resolution	Warranted	EG&G	SURRC
5.9 keV of ^{55}Fe	370 eV	328 eV	400 eV
122 keV of ^{57}Co	625 eV	557 eV	650 eV
80% HPGe-detector Gem-80220-P	**Dimensions**		
Crystal diameter	75.7 mm		
Crystal length	75.2 mm		
End-cap-to Crystal	4 mm		
Volume	338.8 cm^3		
Operating Voltage	3500 V		
Resolution	Warranted	EG&G	SURRC
122 keV of ^{57}Co	1.4 keV	0.787 keV	1.38 keV
1332 keV of ^{60}Co	2.2 keV	1.9 keV	1.9 keV
Peak-to Compton ratio	74:1	76:4	65:1

Table 2.1 Characteristic data for the LOAX and 80% HPGe-detectors.

2.2.2 Large-Volume HPGe-detector

One of the most significant developments in recent years for practical whole-body counting is the availability of large-volume HPGe-detectors which can now provide much improved sensitivity as well as the very high energy resolution for which they are renowned. (High purity means less than 10^{10} atom cm^{-3} of impurity). Use of these large volume HPGe-detectors either singly or in arrays, is providing fast subject counting and radioactivity localization information (Palmer, 1991). A significant number of counting laboratories throughout the world are now using them for low-level measurements. HPGe detectors have replaced earlier technology which used the lithium drifting process. They have the advantage that they do not require continuous cooling and can be allowed to warm to room temperature from time to time without damage (Knoll, 1994). This makes them very convenient to use, especially when experimental designs are being tried. There has also been significant development in the production technology of high purity germanium crystals with regard to their volume. A crystal with an efficiency of 30% for detection of the 1332 keV ^{60}Co gamma-ray relative to a 7.6 x 7.6 cm NaI detector has a volume of 120 ml and has been available for some years. Crystals with relative efficiencies of up to 150% are now being produced.

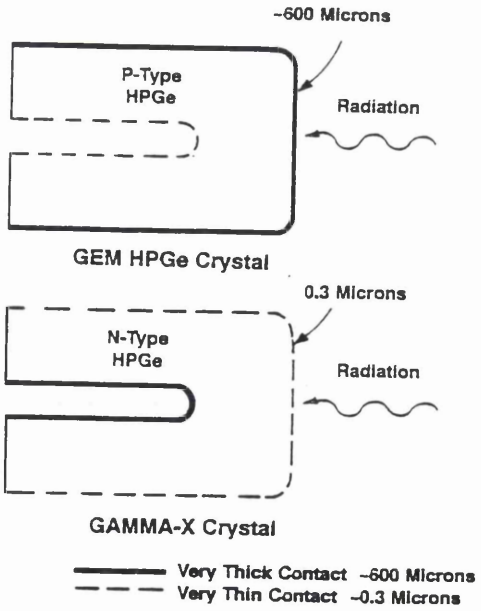

Figure 2.8 Cross section of various types of HPGe-detector crystal contacts and their ion implantation outline.

The measured peak to Compton ratio for the coaxial 80% detector used for this research work was found to be 65:1. This greater resolution allows a smaller region of the background to be used under the photopeak and also a more accurate prediction of the background contributed by the human body because there is less interference from higher energy gamma-rays from other activity in the body. In addition the peak-to-background ratio will be better for the coaxial configuration than for the planar configuration because there is a greater probability that events will deposit their full energy in the detector up to some maximum energy at what is called the "knee" of the efficiency curve after which the efficiency starts to drop (Seymour et al., 1989).

Germanium detectors are very stable in gain and in multiple arrangements, the output of each detector goes to a preamplifier and then to an amplifier which has an adjustable gain, as well as an adjustable DC level (Ortec Model 571 & 572) which allows a complete matching of all detectors over the entire energy range.

2.3 Electronic set-up

The two detection systems, that is, the 80% and two or four LOAX HPGe-detector array were connected to a Multi Channel Buffer (MCB) (EG&G ORTEC Model 919 Spectrum MASTER™) via a multipexer to route the signals appropriately. The 919 MCB is an Advanced Data Collection And Management system (ADCAM). The individual signals can be fed to a mixer / router system which allows either combined or individual signals from up to four detectors to be analysed using this high performance technology MCB which acts as a multichannel analyzer. The multiplexer is used to take a number of inputs from separate detectors through a single analog-to-digital converter (ADC), which means that, while it is digitizing one pulse, the other inputs have to queue, which can cause considerable dead times, especially for high count rate measurements. This was the only drawback of the system, but due to the low count rates being measured in most of the work, it only gave significant effects when measuring standard sources with higher activities. Where possible, it was better to calibrate one detector at one time to reduce the dead time effect.

The Spectrum Master, was interfaced to a personal computer (PC) to provide data handling functions of acquisition/ storage/ display and analysis shared between the specific hardware and PC-based software. With the high speed multiplexer / router up to four separate detectors, each with a maximum of 16 k-channel allocation, and with independent start/ stop/ pre-set and pileup rejection circuitry could be run. This instrument can be configured to provide from 2 k up to 16 k channels for each pulse height spectrum and the four memory segments may be of unequal sizes, making the 919 an ideal solution for a system in which germanium detectors are mixed with other types of detectors such as NaI.

A detailed block diagram of the whole system is given in Figure 2.9, showing the 80% HPGe-detector connected separately to the 919 MCB and the two or four LOAX detectors connected either separately or through a summing amplifier (Ortec model 533) to the 919 MCB. The PC ran an MCA emulation programme called MAESTRO™ MCA for the display and the quantitative analysis of the collected spectra and final printout of the report files.

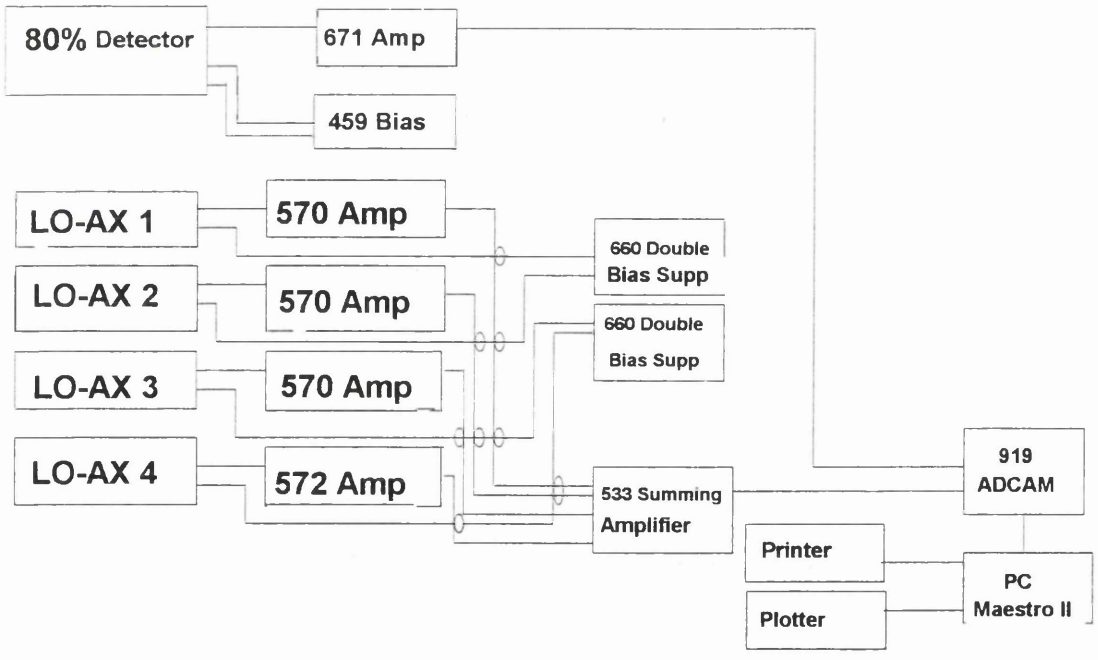

Figure 2.9 Electronic block diagram of the semiconductor whole-body monitor set-up.

The MAESTRO™ emulation software was capable of providing a number of advanced functions: peak centroid and shape calculation; net and gross area of peaks with statistical uncertainty; spectrum strip / normalization / compare / and summation / energy calibration; setting and analysis of region-of-interest; spectral plotting and complete control of the MCA hardware.

2.4 Summing amplifier

This type of summing amplifier accepted up to four input signals and provided an algebraic sum of them at its output. The most difficult aspect of its utilization was the adjustment of the different input signals so that the resolution of a given gamma peak was not degraded appreciably. In order to be certain that all the energy peaks fell in the same channels, widely spread energies, such as either 59.5 and 122 keV were used with 276 and 302 keV for calibration purposes. Energy linearity needed to be maintained throughout measurement procedures and regularly checked and adjusted. The main purpose of the summing amplifier was to utilise fully the detector outputs when dealing with spectra containing low counts. Counts of the main energy peaks of ^{241}Am (59.5 keV), ^{133}Ba (276, 302, 356 and 384 keV), ^{57}Co (122 keV) confirmed that the summed count for four detectors was four times that of a single detector. At the same time the resolution (FWHM) deteriorated only by 15% for the 59.5 keV and 18% for the 122 keV peaks. Figure 2.10 shows examples of gamma-ray spectra of the four LOAX detectors both for single and summed data.

As well as the summing amplifier, spectra were also analysed using computer software that was capable of adding up to 200 different spectra of similar energy calibration. This method of spectra summation and the results obtained are discussed in detail in chapter 5.

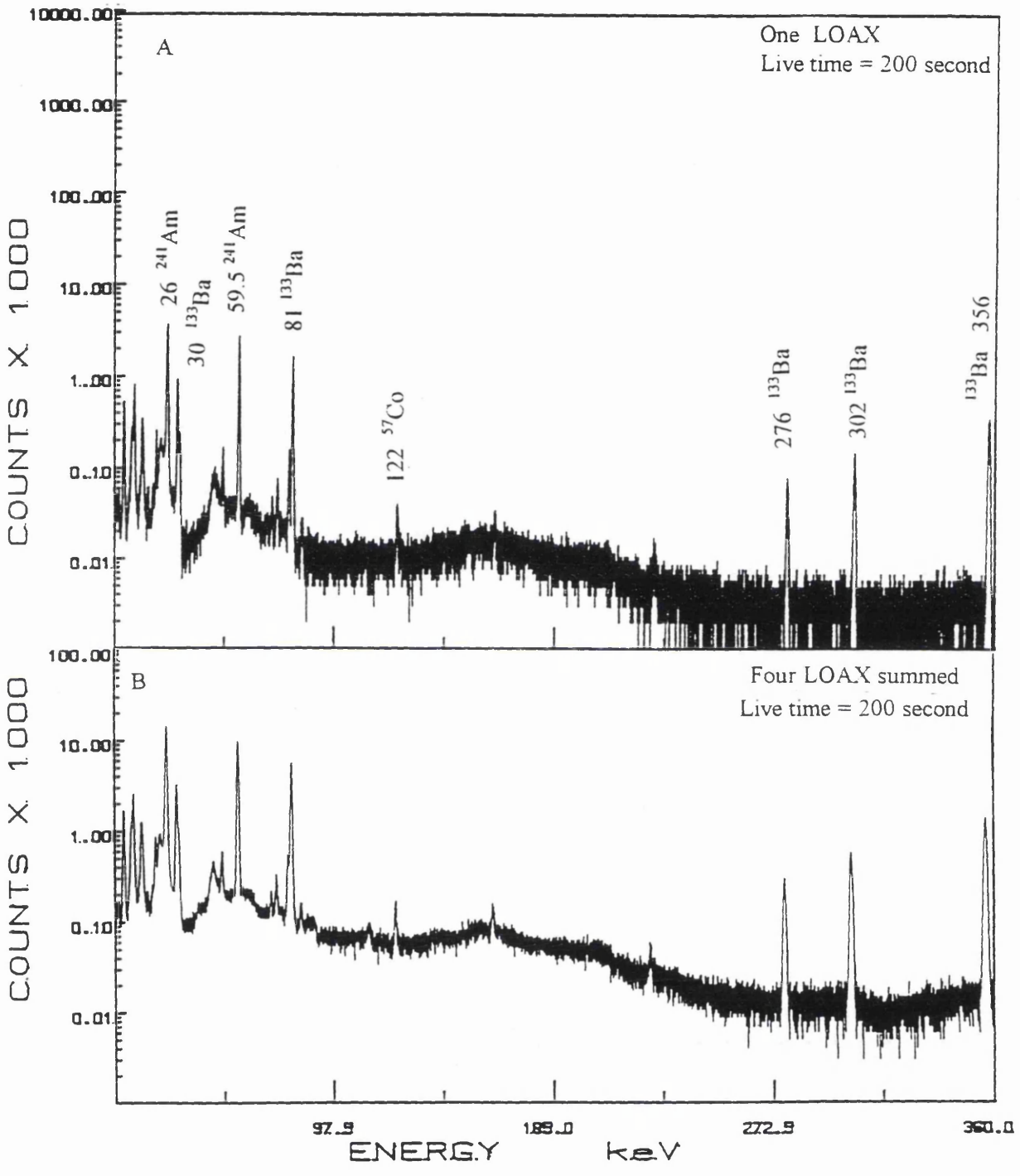

Figure 2.10 Two spectra of LOAX detectors measuring ^{241}Am, ^{133}Ba and ^{57}Co: (a) single detector; (b) summed spectra of four detectors.

2.5 Optimization of the SURRC shadow-shield design

As the name implies, the ideal shadow-shield arrangement is that which covers a minimum space around the detector and the measured subject such that no external gamma-ray can reach the detector. The shield built around the detectors can thus be visualised as casting a shadow on the detectors and counting space. Figure 2.11 gives an impression of the disposition of detectors and counting space in the SURRC hybrid shadow shield. Where the LOAX detectors penetrated the roof of the space, gaps in the shielding were filled with bags of lead shot. The 80% detector can just be seen in the roof channel behind the two LOAX detectors while the two original NaI detectors are above and below behind it. The dewar of the 80% detector which is outside the shield was also completely surrounded by 5 cm lead bricks to ensure that no radiation reached the detector crystals directly by streaming through gaps.

The inside surfaces of the shadow-shield were covered with sheets of cadmium (3 mm) and copper (5 mm) to produce a "graded" shield. The copper can be seen in the photograph. Graded shielding was used to absorb the characteristic X-rays which were produced when gamma-rays interacted with the lead shield. These appeared at 70-85 keV and could interfere with the low-energy photons such as those from ^{241}Am at 17.5, 26.3, 59.5 keV and the 46.5 keV from ^{210}Pb. The way in which the graded shield worked was that the cadmium absorbed the lead X-rays and emitted further X-rays at 28 keV (Sharma et al., 1989). These were in turn absorbed by the copper which emitted X-rays at 8 keV, thus effectively removing them from the working background range. In addition, the LOAX detector crystals were covered by polyethylene sheet and 2mm thick copper tubing, 3.8 cm diameter and 20 cm long. These components were held in place tightly by the plastic cap. The whole length of the 80% detector housing was also covered on the top and sides with graded shielding.

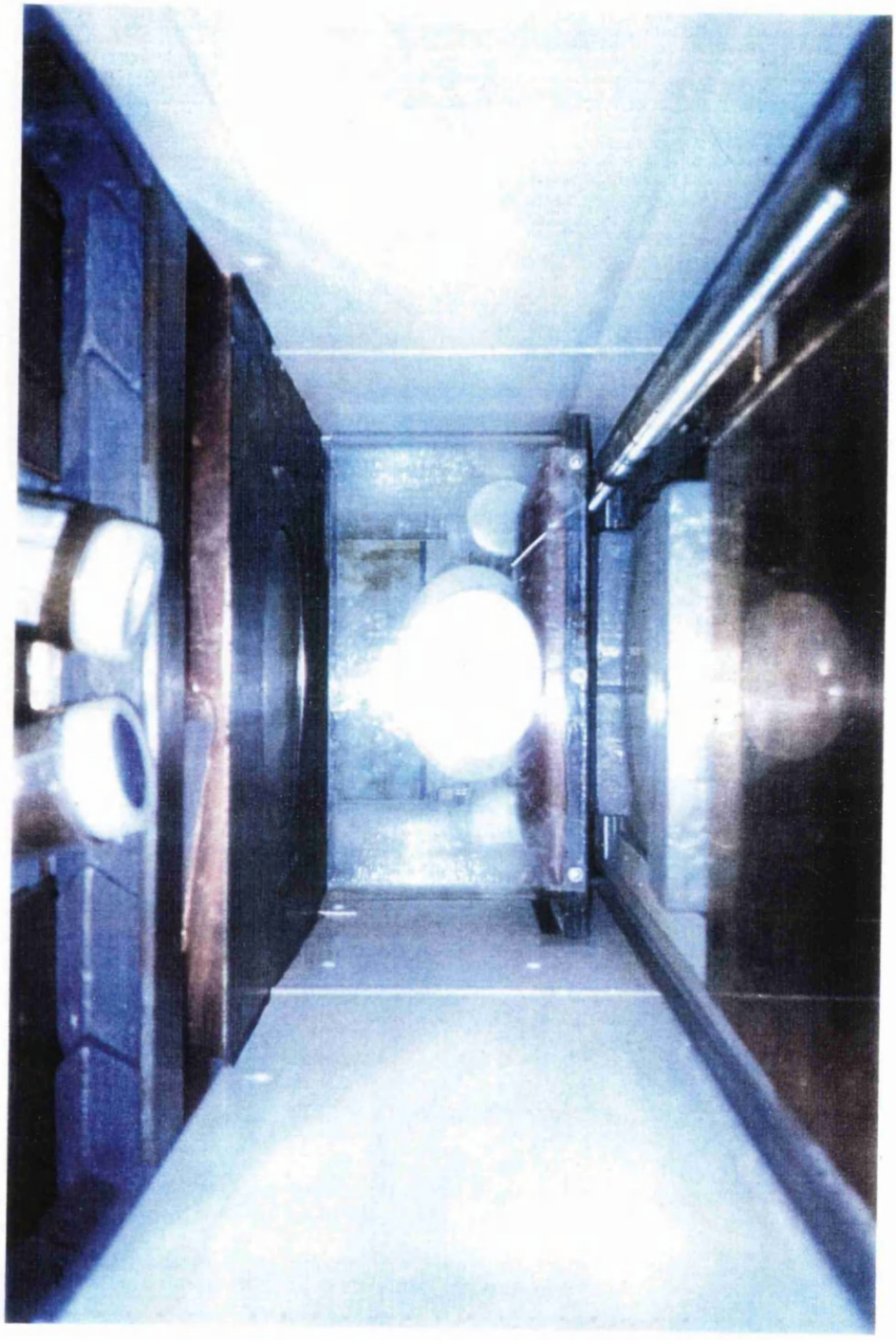

Figure 2.11 The internal arrangement of the three detector systems inside the shielding configuration.

Figure 2.12 depicts the reduction of the characteristic X-rays in the LOAX detector after covering with copper tubes and cadmium sheet. A reduction factor of almost two was observed for the main characteristic X-rays at 74 and 77 keV. This reduction is clearly shown in the lower spectrum of Figure 2.12. But due to the fact that the measuring surface of the detectors cannot be covered by this graded shield, therefore, there will always be characteristic X-ray in spectra obtained.

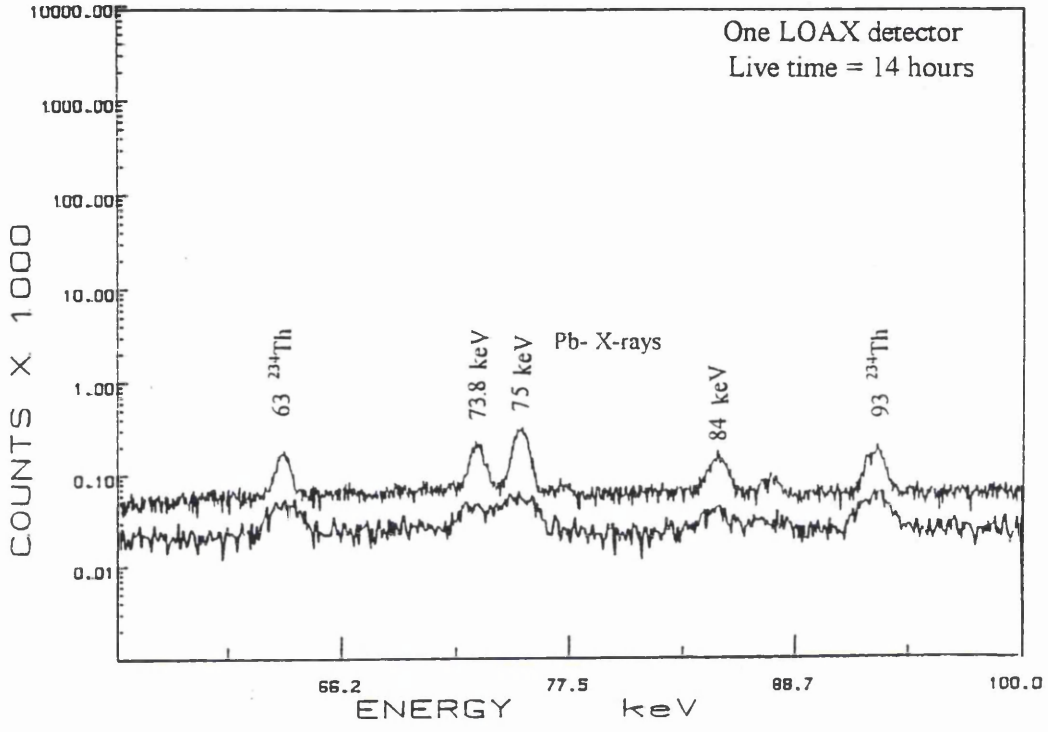

Figure 2.12 Characteristic X-ray reduction of gamma-ray spectrum of one LOAX HPGe-detector: effects of Cu/Cd shield.

2.5.1 Facility design

The laboratory area and the monitor were kept clean by the use of door floor mats, in addition to the routine daily mopping of the whole laboratory floor, in order to reduce the dust transport. Also an additional heating system was installed to keep the room at constant ambient temperature while maintaining an adequate air flow to prevent the build up of the radon progeny in the air. The mild steel bed rail track and its supporting structure, which could possibly have a trace source of ^{60}Co, was removed and replaced by one made of aluminum. A special very low-background foam material was used as an auxiliary bed support to raise the measured subject as

required. This manoeuvre was sometimes used to reduce the distance between detector and subject to increase sensitivity.

2.6 *In vivo* measurement geometries

Two main requirements for an ideal *in vivo* counting geometry are; high sensitivity of detection and an invariant response to internally deposited radioactivity. To achieve these requirements two main *in vivo* counting methods were used. The first was the *static* method, whereby the subject is positioned as close as possible to the detector crystals concentrating for example, on the anterior surface of an organ in the body with the subject in a supine position. The three main organs of interest in the present work were the lung, the liver and the skull. This method is effectively partial body counting and it depends very much on how well the calibration of the detectors simulates the true distribution of radionuclides in the human subject. It is extremely useful for measuring low-energy photons, where the sensitivity of the detection system needs to be maximized. With the present spatial arrangement of the two or four LOAX detectors in their fixed counting position as shown in Figure 2.11, either one or two LOAX detectors will be positioned on top of each lung. Using Monte Carlo simulation techniques Scott et al. (Scott et al., 1977) showed that the optimum configuration for two detectors is to position each detector approximately 20 cm below the top of the shoulder and 10 cm from the midline of the sternum and this was done.

The second counting method is known as the *scanning* count whereby the subject, in a supine or prone position is moved on a motorized bed past the detectors. This method was also used extensively in the present work.

2.7 Data processing of gamma spectra

2.7.1 Gamma-ray spectra description

The main features of the gamma-ray spectra in germanium detectors and in particular, the background, depend on the energy of the incoming photons, the shielding and the construction of the detector. These features may be explained by the examination of

the interaction processes of gamma photons namely; photoelectric effect; Compton scattering; and pair production. The total absorption of the incoming gamma-ray produces a spectrum consisting of a full-energy peak which is proportional to the gamma-ray energy of the source. The photoelectric effect will produce a full-energy peak with a marginal contribution from the other types of interactions. Along with this peak the Compton continuum extending from zero energy up to the Compton edge is observed. The total counts in the peak are a combination of the counts arising from the measured source in addition to background. The main contributor to the background especially at the lower energy end of the spectrum, is the Compton continuum. It mainly arises from gamma-ray interactions within the detector or from other gamma-rays in the background radiation interacting with the shielding and the detector crystal. They cause non-specific counts as a result of partial capture of full-energy gamma-ray or full capture of photons that have been degraded outside the detector crystal as shown in Figure 2.13.

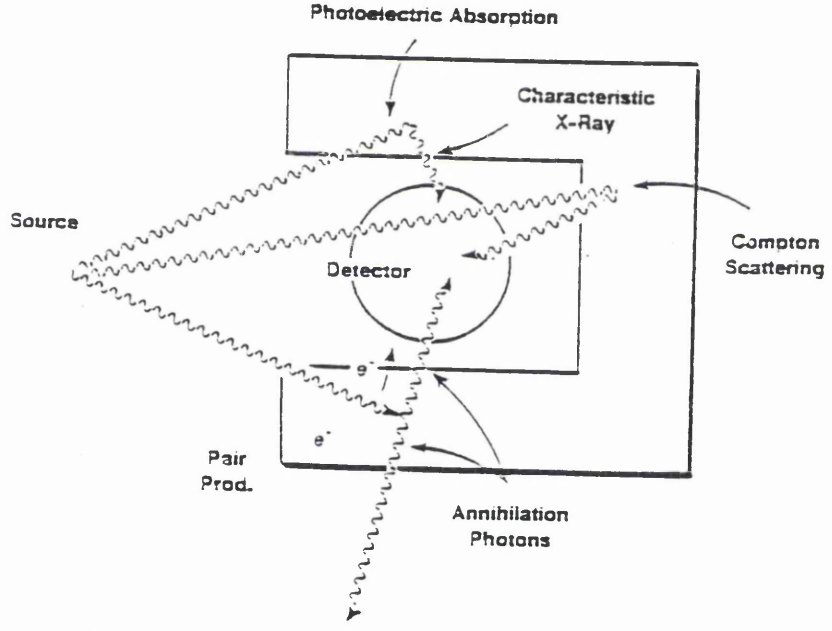

Figure 2.13 The various types of gamma-ray interaction around a detector shield arrangement.

2.7.2 Well defined gamma peaks

The distribution of counts in a given gamma-ray peak is approximately Gaussian about a central point and is a measure of the photon energy and emission

rate (Debertin and Helmer, 1988) of a radionuclide. In order to handle complex gamma-ray spectra, a number of commercial computer programmes were available which used routines consisting of an algorithm which searched the spectrum for peaks, statistically fitted them to Gaussian or modified Gaussian shapes, and then computed the background under the peak by extrapolation. The computer software programme used for the analysis of some of the data in this study was called Minigam as an independent peak search programme and was supplied in addition to the Maestro™ II (A63-BI) emulation software (EG&G Ortec). The functions provided by this software were to: locate the peaks in a spectrum; determine their resolution; identify the radionuclide from each energy peak; differentiate between single and multiple peaks; determine the gross and net area of the peak. Most of these programmes were based on the Mariscotti method of analysis (Mariscotti, 1967), which provided a method of automatically identifying peaks in the spectrum by testing the derivative of the gross counts of the data collected. The data were then smoothed by averaging the entire spectrum channel by channel, and setting the centroid channel from the average value.

2.7.3 Poorly defined low-level peaks

For ill-defined or non-apparent peaks frequently encountered in *in vivo* measurements, these programmes could not handle the data adequately. For this reason a different method of spectral analysis was employed. Low-level peaks were selected by careful inspection and their energy range specified manually. Quantitative analysis was then carried out using the Maestro II programme to print a report file of the gross and net counts in the peak. This manual tracing of the specified energy ranges was carried out for both the suspected contaminated and "clean" subjects or the blank. The obtained gross and net counts of the collected gamma-ray spectra are compared and analysed statistically for the verification of presence or absence of trace activity levels of the suspected contaminant. This method of peak identification of ill-defined peaks was applied through out this research study.

In the literature there are a number of methods used to calculate the total and the net peak area. One method was found to use the first channel on each side of the peak region as representative of the gross (or integral) area of the peak by the use of $G = \sum C_i$, where C_i are the counts in the i^{th} channel as shown in Figure 2.14.

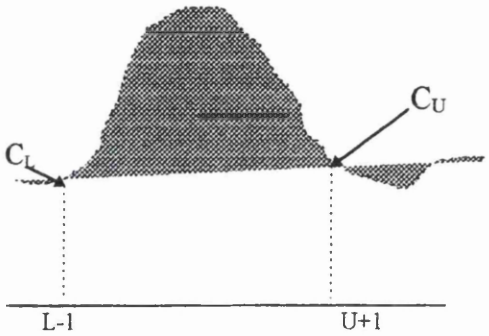

Figure 2.14 Peak area calculation using single channel method.

The background beneath the peak is estimated as:

$$B = n\,(C_{L-1} + C_{L+1}) / 2 \quad \text{.....Equation 2.1}$$

Where; n is the number of channels within the peak region and C_{L-1} and C_{L+1} a single channel at the upper and lower edges of the peak region to estimate the background beneath the peak. The net peak area (Net) is calculated by; Net =G - B, where G is the gross peak area counts and B is the background counts as calculated with equation 2.1.

The background is considered to be the area of the trapezium beneath the peak. It is actually the mean background count per channel beneath the peak multiplied by the number of channels within the peak region. It has to be noted that using a single channel, the number of total counts beneath the peak can be estimated, but it could not differentiate which channel to be used as background and which channel to be included in the true peak counts. For this reason background under the peak can be made more precise (i.e. less uncertain) and best be estimated using more channels to estimate the mean count per channel under the peak. Figure 2.15 shows the general principle of the channels distribution. A number of channels on each side of the peak

are taken and averaged, the area of the trapezium beneath the peak calculated to give the background.

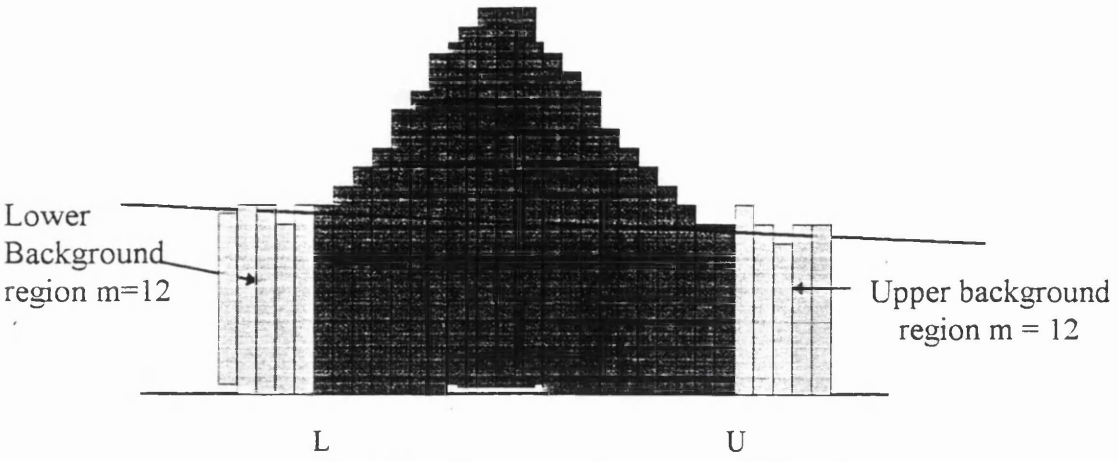

Figure 2.15 Net peak area and background calculation using the trapezium method

This method of background calculation is called the trapezium method for the calculation of the net peak counts of a number of gamma spectra in this research work. This method was carried out by labelling a fixed number of channels above and below the main peak area manually with the aim of obtaining a better allowance for the background variation. Thus, the estimate of the background was obtained by printing the files that contained all the labelled channels for the main peak and the selected extra channels above and below it. In order to calculate the main counts under the peak, the gross counts from the associated channels above and below the main peak were taken to delineate a trapezium beneath the peak, Wasson and Quittner methods (Neton, 1988). The area of this trapezium was subtracted from the given gross peak area using the following equation;

$$A = \sum_{i=L}^{U} C_i - n\left[\sum_{i=L-m}^{L-1} + \sum_{i=U+1}^{U+m}\right]/2m \qquad \text{.....Equation 2.2}$$

The statistical uncertainty of the net peak area calculations using this method was carried out by taking the variance of the net peak area given by the sum of the variances of these two terms giving: var. (Net) =var. (G) + (var.(B). Substituting for

the individual variances and using equation 2.2, the following equation can be deduced:

$$\mathrm{var}(A) = \sum_{i=L}^{U} C_i + n^2\left[\sum_{i=L-m}^{L-1} + \sum_{i=U+1}^{U+m}\right]/4m^2 \quad \text{.....Equation 2.3}$$

It has to be noted that the total uncertainty in the peak background channels is used unlike the single background counts where the variance of the count is numerically equal to the count itself. For this reason the standard deviation expression to be used for a peak area calculation is :

$$\sigma_{Net} = [\ Net + B(1 + n/2m)\ ]^{1/2} \quad \text{.....Equation 2.4}$$

Where: B- is the background count rate,
Net- is the net count rate,
C_i - counts in the i^{th} channel,
C_{L-1} -counts in the channel immediately beyond the lower channel,
C_{L+1}- counts in the channel immediately beyond the upper channel,
σ_{Net} - standard deviation of the net count rate

The uncertainty of this method depends upon the number of channels used to estimate the background regions. This method was more precise in determining the low counts under the peaks, especially if the peaks were small and were situated on top of a Compton continuum region. Its main disadvantages were that it did not provide satisfactory results for overlapped peaks or for two peaks that lie in close proximity of each other, in addition to its being a time consuming method of analysis.

2.7.4 Detector Calibration

In order to identify the radionuclides responsible for the peaks in a gamma-ray spectrum, energy calibration of the spectrum is required using standard radionuclides which emit gamma-rays of known energy. Figure 2.16 a & b shows the energy calibration curve obtained using both the 80% and LOAX HPGe-detectors. In addition, to ensure that the germanium detector's energy response is stable and linear over long counting periods, a number of point standard sources were measured on a regular, routine basis. The point sources used were mainly ^{241}Am, ^{133}Ba and ^{57}Co for the LOAX detectors, while a ^{226}Ra standard source of 18.5×10^4 Bq activity (in equilibrium with its decay products) was used for the 80% HPGe-detector. They were positioned in reproducible geometries at a distance of 25 cm from the detector

end-caps. Table 2.2 lists the main energy data and gamma intensities of the nuclide used for the LOAX energy calibration while Table 2.3 lists the main radium

Nuclide	Half-life	Energy	Rel. intensity
^{241}Am	432 y	59.5	36
^{133}Ba	10.57 y	81	34
		276	7.17
		302	18.32
		356	62
		384	8.93
^{57}Co	272 d	14.4	9.6
		122.1	85.6

Table 2.2 Main low-energy radionuclide characteristics used for energy and efficiency calibration for the LOAX HPGe-detectors.

decay radionuclides, energies and relative intensities for the 80% detector. The detector efficiencies were also determined and the curve for two LOAX HPGe-detectors summed is presented in Figure 2.17. Using the radium standard source two efficiency curves were constructed for the 80% HPGe-detector shown in Figure 2.18 for static and scanning counting modes and the respective gamma-ray spectrum is shown in Figure 2.21. Also a typical radium gamma-ray spectrum is presented for the two LOAX in Figure 2.19 and the spectrum of standard sources for the 80% HPGe-detectors in Figure 2.20. An efficiency curve was made for the 80% HPGe measuring the standard point source in scanning counting mode in air and the sources under a water chest phantom for comparison purposes is shown in Figure 2.22. It could be clearly seen that the detection sensitivity dropped by an order of magnitude when sources were measured under 20 cm of water thickness. In addition gamma-ray spectra for the two LOAX detectors were obtained measuring the ^{55}Fe standard point source, demonstrating the very low-energy 6 keV detection capability with the LOAX system in Figure 2.23 a & b. The spectrum shown in: (a) used the ^{55}Fe alone while in; (b) ^{55}Fe was counted simultaneously with ^{57}Co. It could be seen that both low-energy photons, namely 6 and 14 keV, can be clearly distinguished in the measured spectrum.

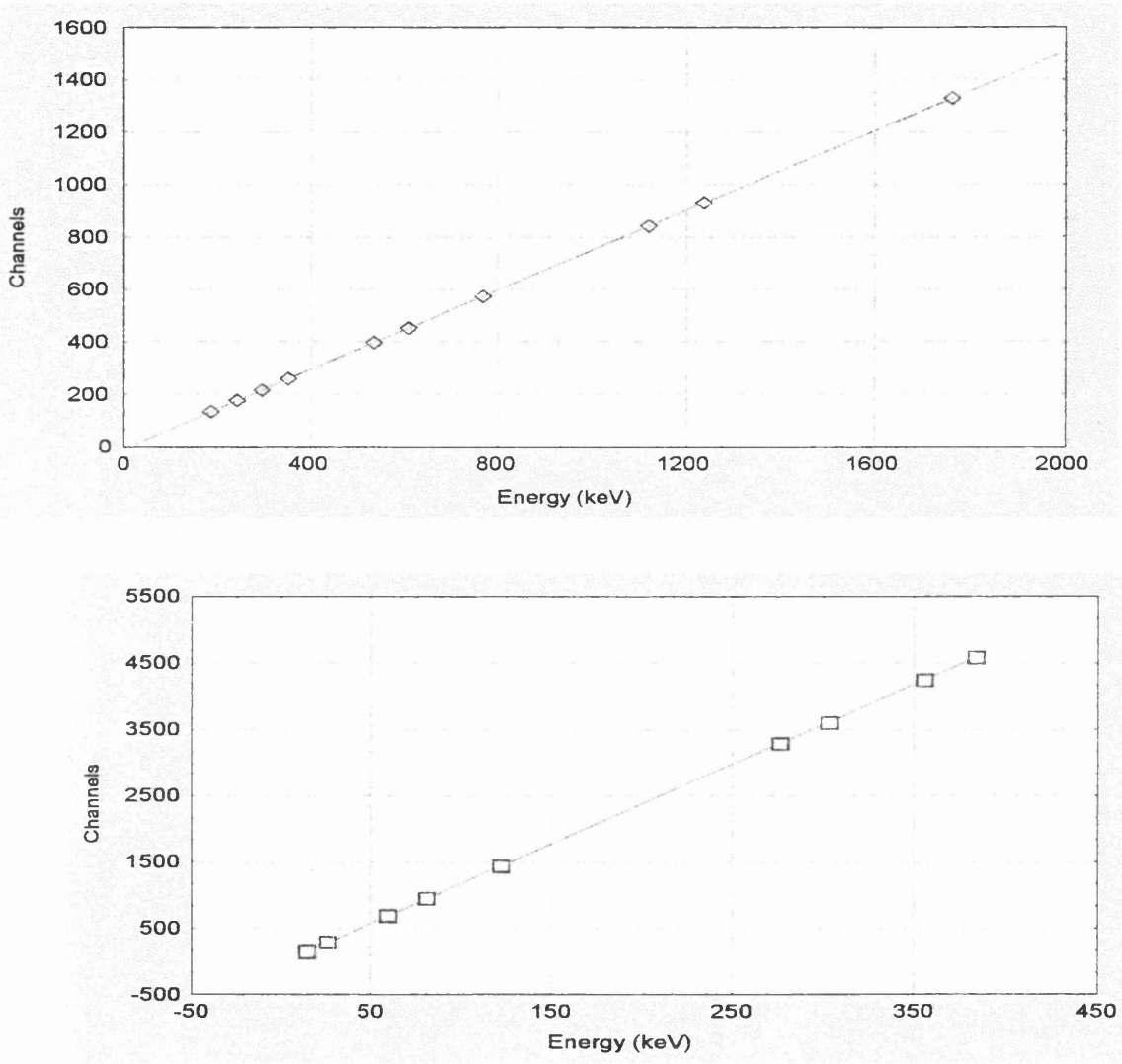

Figure 2.16 Energy calibration curves for both HPGe-detectors: (a) 80% HPGe-detector; (b) two LOAX-detectors.

Nuclide	Energy (keV)	Relative Intensity
^{226}Ra	186.21±0.01	9.00±0.10
^{214}Pb	241.98±0.01	16.06±0.19
^{214}Pb	295.21±0.01	42.01±0.53
^{214}Pb	351.92±0.01	80.42±0.81
^{214}Bi	609.31±0.01	100±0.92
^{214}Bi	768.36±0.01	10.90±0.15
^{214}Bi	934.06±0.01	6.93±0.10
^{214}Bi	1120.29±0.01	32.72±0.39
^{214}Bi	1238.11±0.01	12.94±0.17
^{214}Bi	1377.67±0.01	8.87±0.15
^{214}Bi	1509.23±0.02	4.78±0.09
^{214}Bi	1729.59±0.02	6.29±0.10
^{214}Bi	1764.49±0.01	34.23±0.44
^{214}Bi	1847.42±0.03	2.53±0.09
^{214}Bi	2118.55±0.03	10.77±0.05
^{214}Bi	2204.22±0.04	3.32±0.20

Table 2.3 List of the major ^{226}Ra-decay data for the energy and their relative intensity.

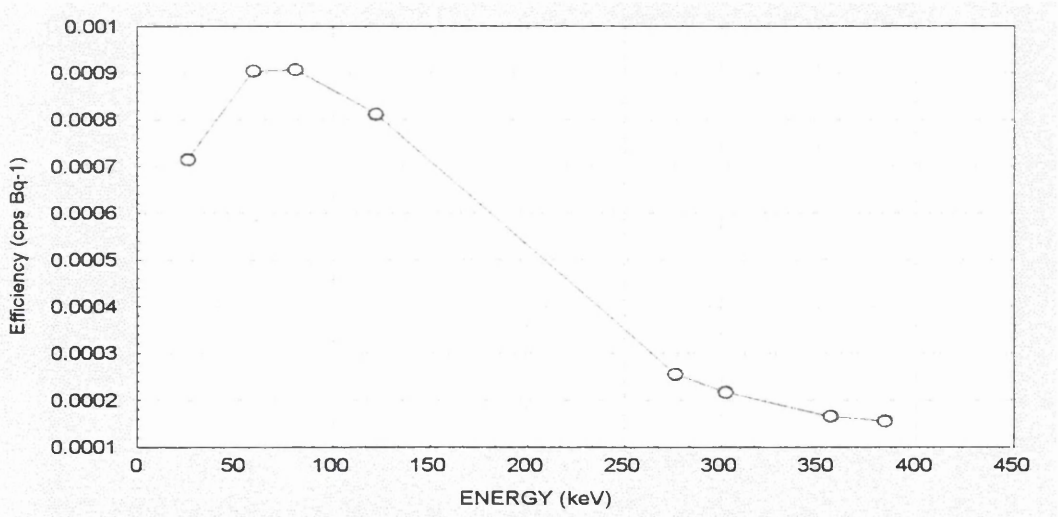

Figure 2.17 Efficiency calibration curve for the two LOAX detector using ^{241}Am, ^{133}Ba, ^{57}Co in static mode only.

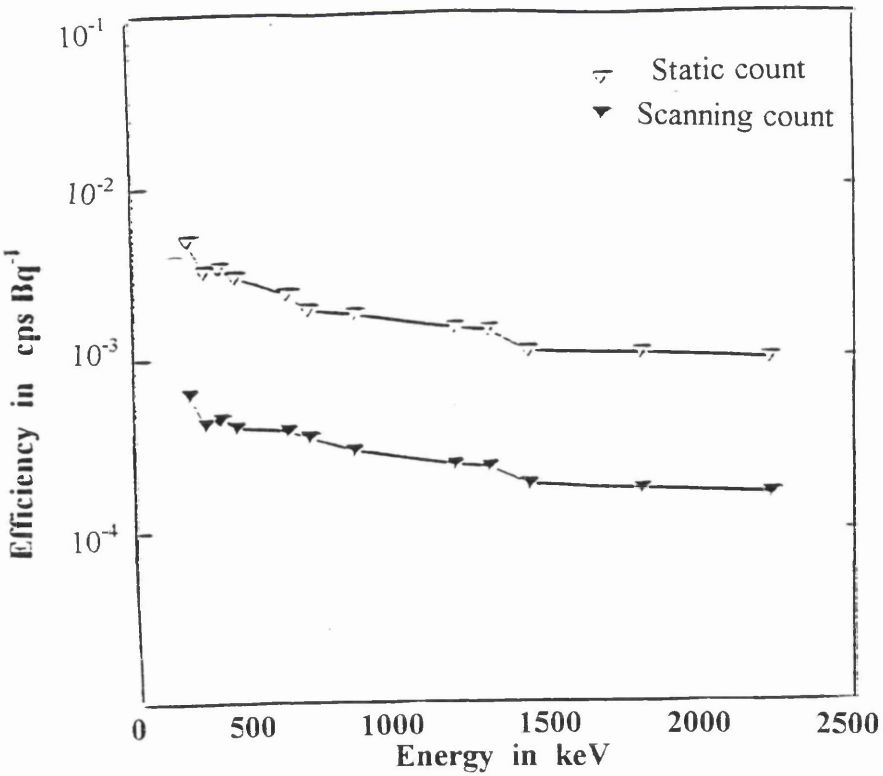

Figure 2.18 Efficiency calibration curve for the 80% HPGe-detector in scanning and static counting modes using ^{226}Ra standard source.

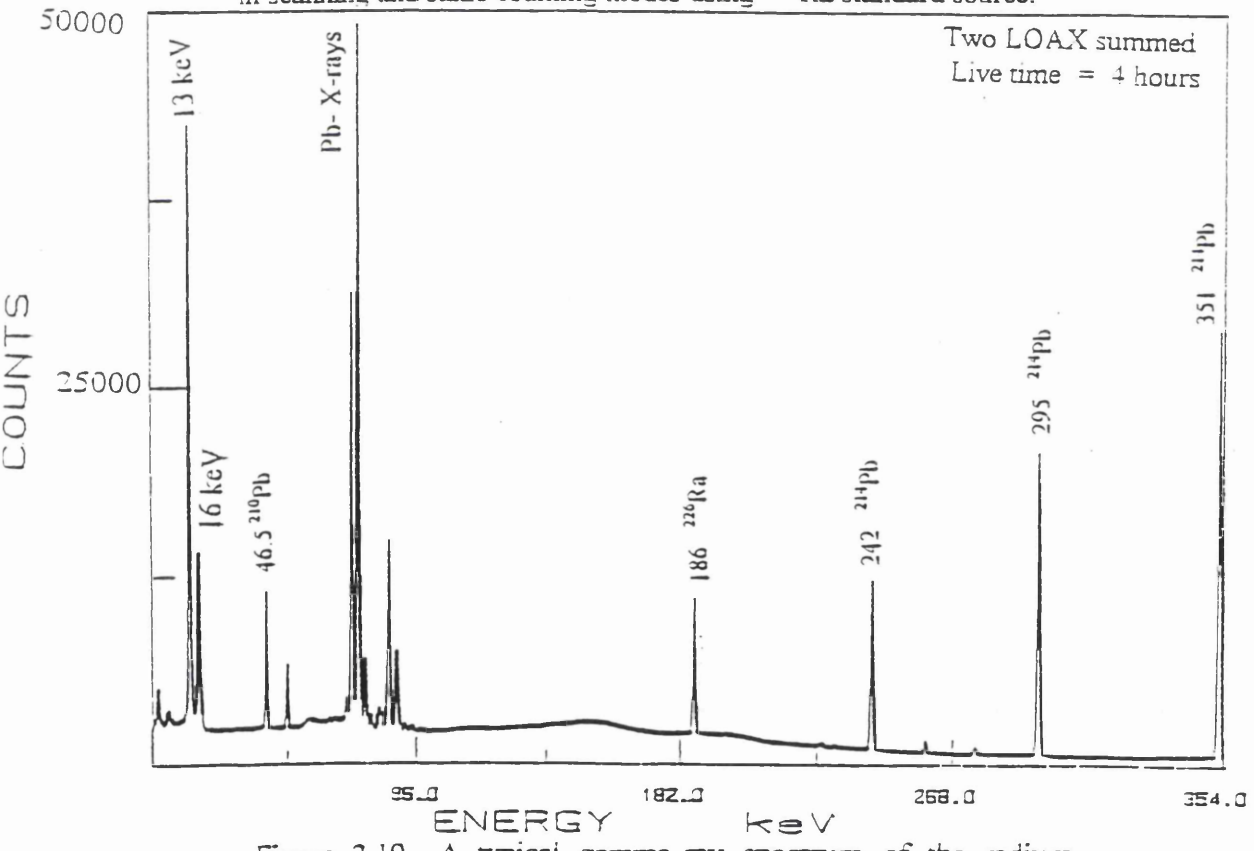

Figure 2.19 A typical gamma-ray spectrum of the radium source measured using two LOAX detectors summed.

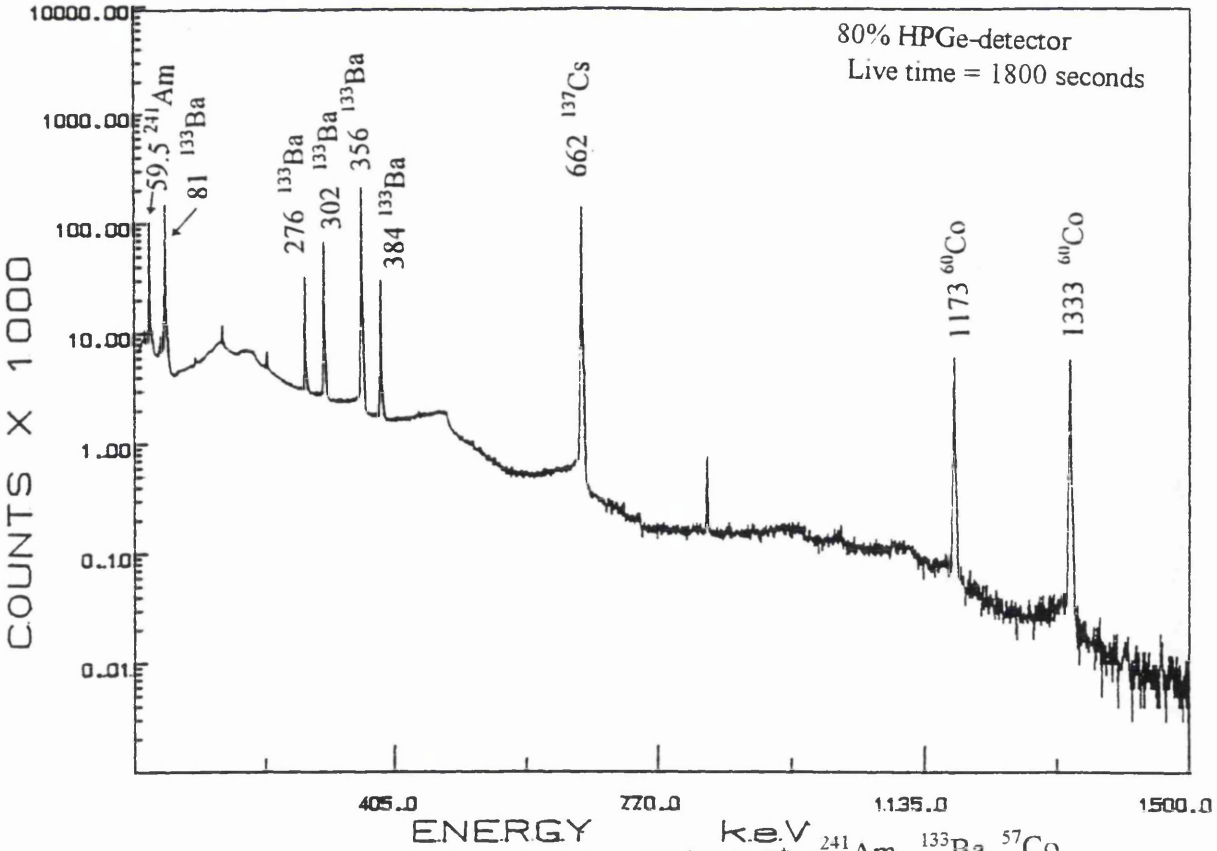

Figure 2.20 A typical gamma-ray spectrum of ^{241}Am, ^{133}Ba ^{57}Co, and ^{60}Co standard source measured using the 80% HPGe-detector.

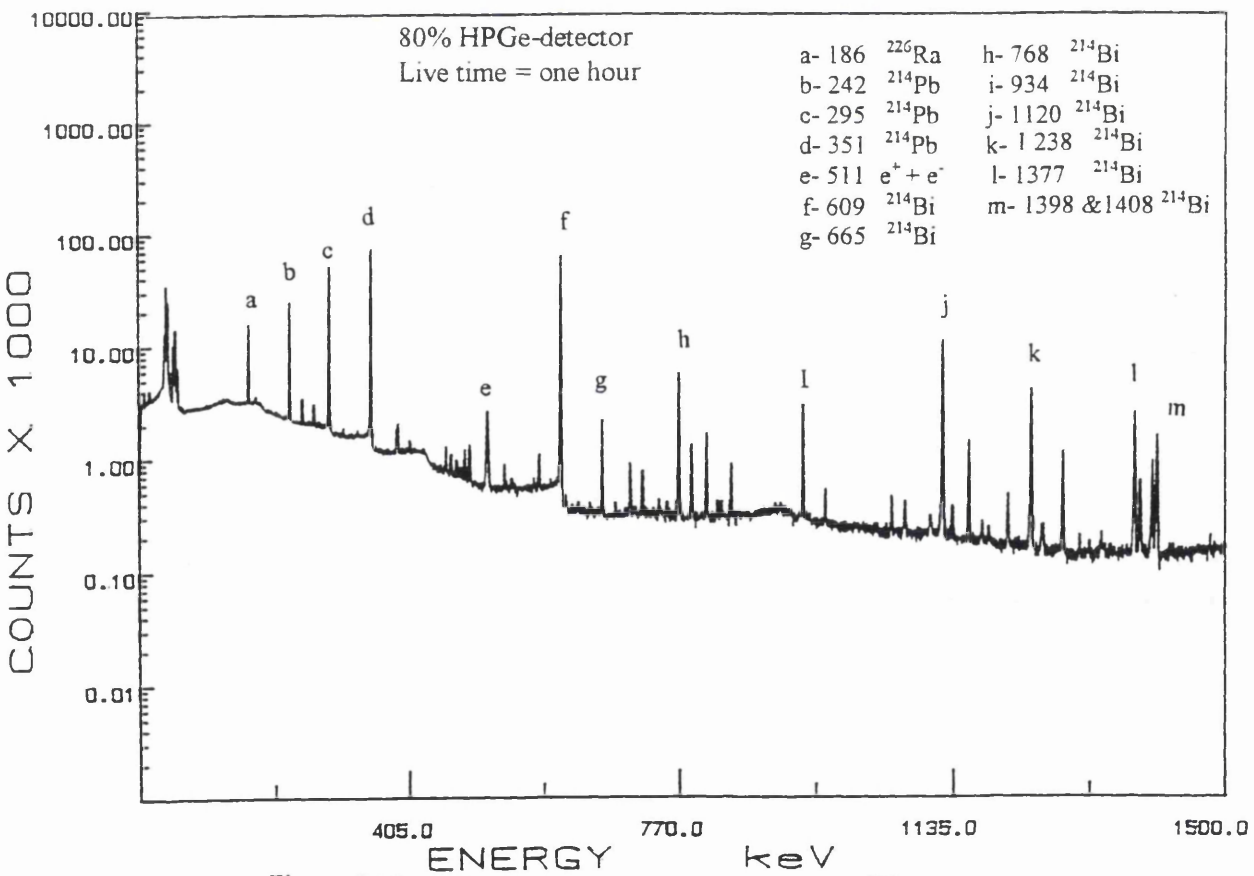

Figure 2.21 A typical gamma-ray spectrum of ^{226}Ra standard source measured using the 80% HPGe-detector.

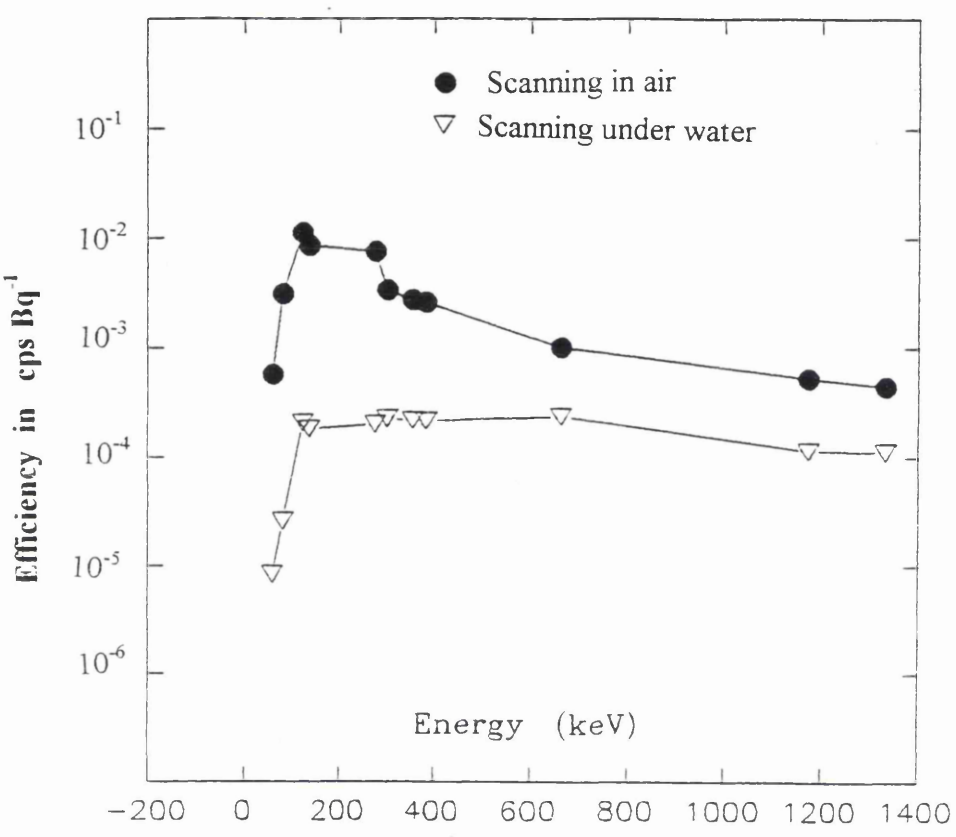

Figure 2.22 Efficiency curves for the 80% HPGe-detector measuring standard sources of ^{241}Am, ^{133}Ba, ^{57}Co, and ^{60}Co using scanning counting mode in with and without absorber.

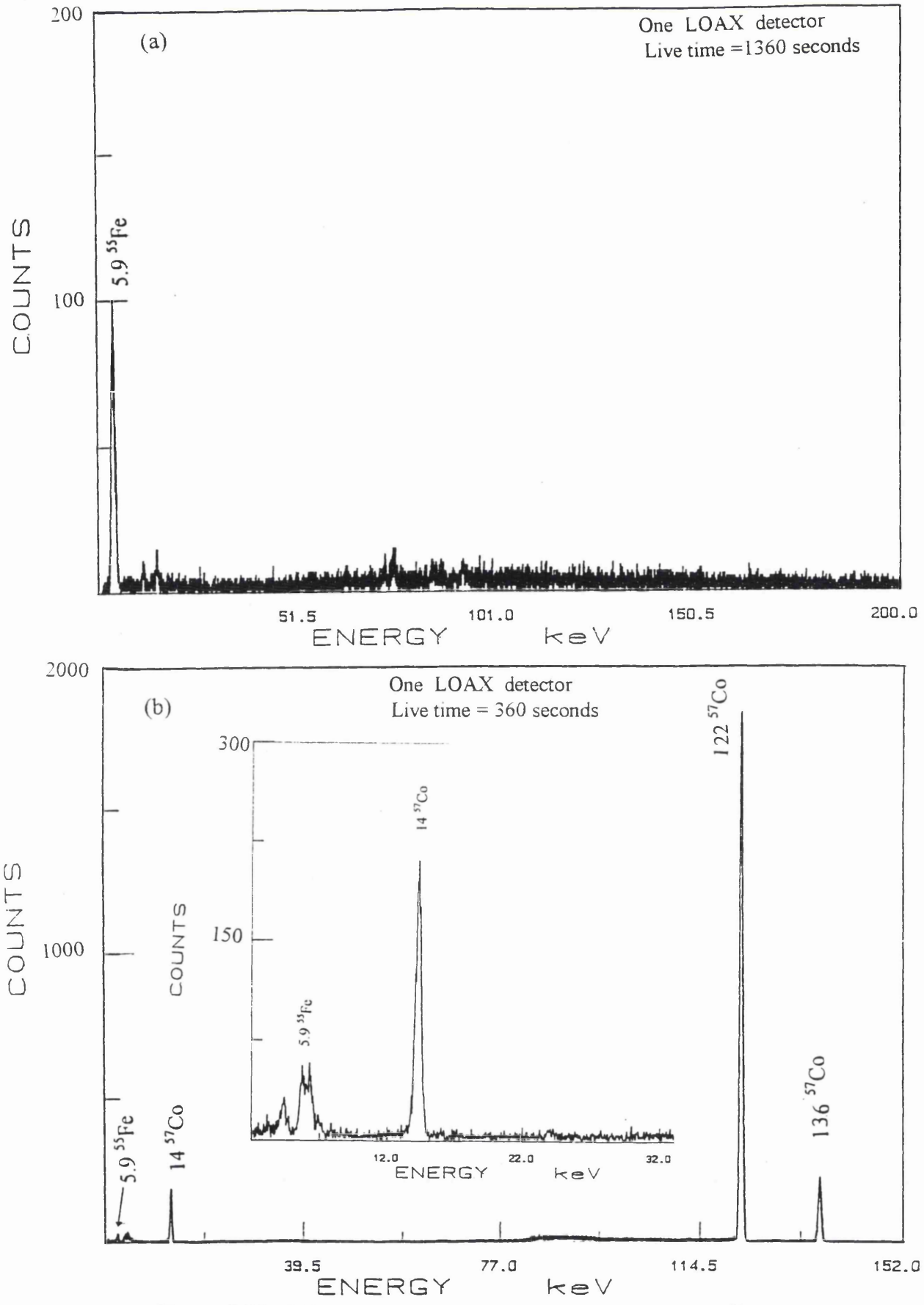

Figure 2.23 LOAX detector γ-ray spectra: (a) measuring ^{55}Fe standard point source alone at 2cm distance; (b) measuring ^{55}Fe and ^{57}Co simultaneously.

2.8 Synthesized spectra

In order to obtain an appreciation of the practical detection limits of the monitoring system, and as an alternative to calculation methods, a series of synthesized spectra were produced. The aim was to add spectra, representing decreasing activities of the radionuclides of interest, to the spectrum of the background or blank until the associated gamma peaks became undetectable. This simulated the situation where trace quantities of radioactivity were being measured at very low levels.

A water phantom and a subject were measured to obtain background or "blank" spectra. Tissue equivalent phantoms with known activities were also measured in the same geometry for the same counting time. Using the Maestro II programme, multiple fractions of the spectra from the known activities were successively added to the background spectra. Table 2.4 shows the results of adding fractions of the spectrum from an "externally" e.g. surface labelled ^{241}Am skull phantom to an *in vivo* skull background. This added fraction is labelled as "stripping factor" which is defined as: the activity value subtracted from a standard phantom and consequently added to the background spectrum. The multiple factors used to modify the original ^{214} Am spectrum are given together with the gross and net values computed for the 59.5 keV synthesized peak.

Stripping factor	Synthesized activity Bq	Gross counts cps $\pm\sigma$ 1	Net counts cps $\pm\sigma$ 1
0.0000	0.000	0.038±0.003	0.002±0.001
0.0001	0.051	0.038±0.003	0.002±0.001
0.0002	1.028	0.039±0.003	0.003±0.001
0.0004	2.056	0.042±0.003	0.006±0.001
0.0006	3.084	0.043±0.004	0.009±0.002
0.0008	4.112	0.046±0.004	0.011±0.002
0.001	5.140	0.047±0.004	0.016±0.002
0.002	10.28	0.058±0.004	0.029±0.003
0.004	20.56	0.077±0.005	0.043±0.003
0.006	30.84	0.099±0.005	0.053±0.004
0.008	41.12	0.119±0.006	0.066±0.004
0.01	51.40	0.139±0.006	0.134±0.006

Table 2.4 Net and gross count rates for the synthesized ^{241}Am activity extracted from an externally labelled ^{241}Am skull phantom and added to a subject background spectrum (^{241}Am phantom activity 5.14 kBq).

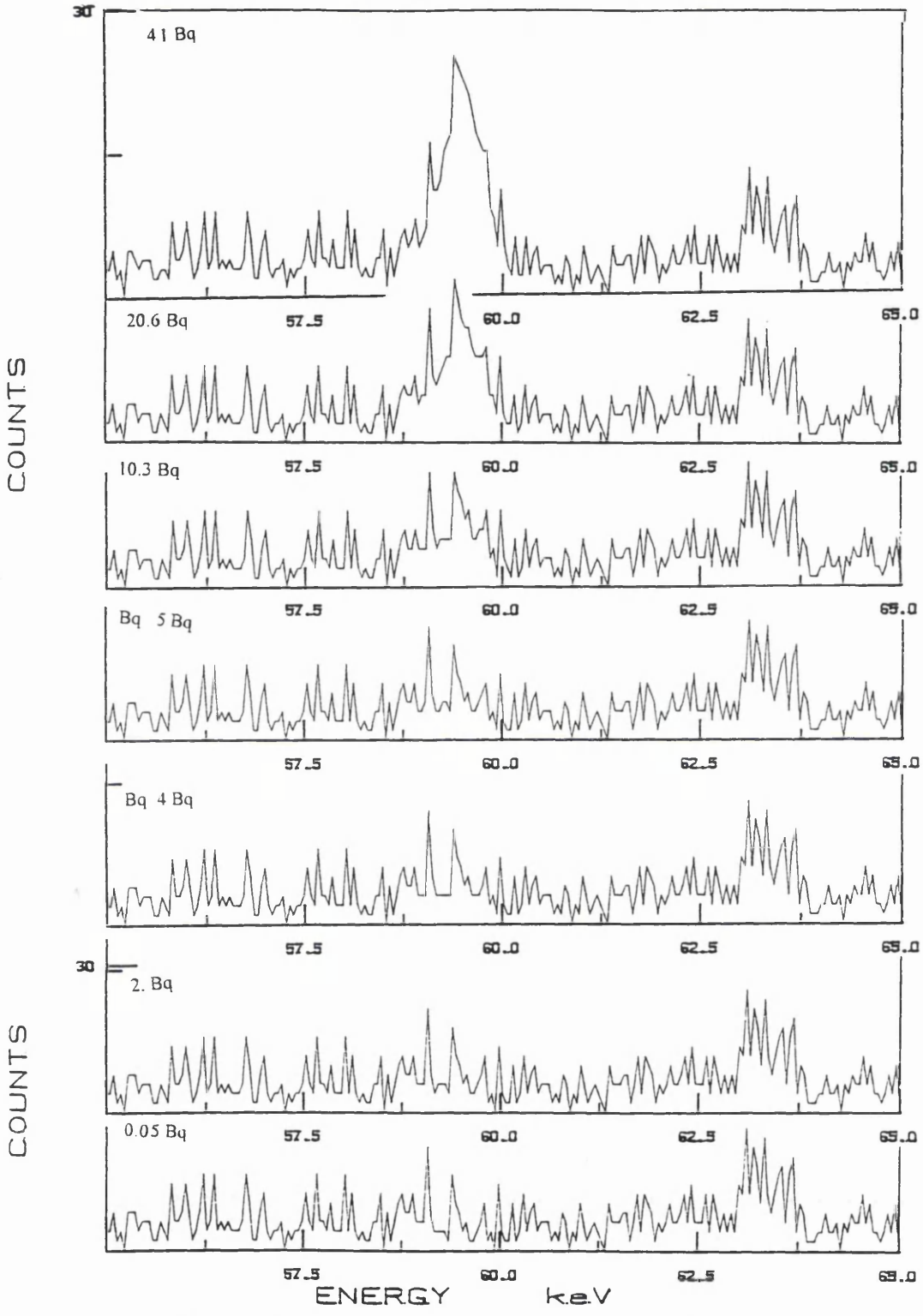

Figure 2.24 Shows all the synthesized spectra from Table 2.4 of the standard ^{241}Am skull phantom added to *in vivo* subject spectrum.

Figure 2.24 shows most of the gamma-ray spectra obtained from this synthesis procedure and illustrates the appearance of the americium peak for each activity. Where, Figure 2.25 shows only three of these spectra on a larger scale to show the difference of the appearance of the low-level activity spectra. These synthesized spectra were used for comparison with other collected spectra to verify the presence or otherwise of trace activities. A number of practical application of this method was employed in the analysis of some samples in sections 5.6 and 6.3.2.

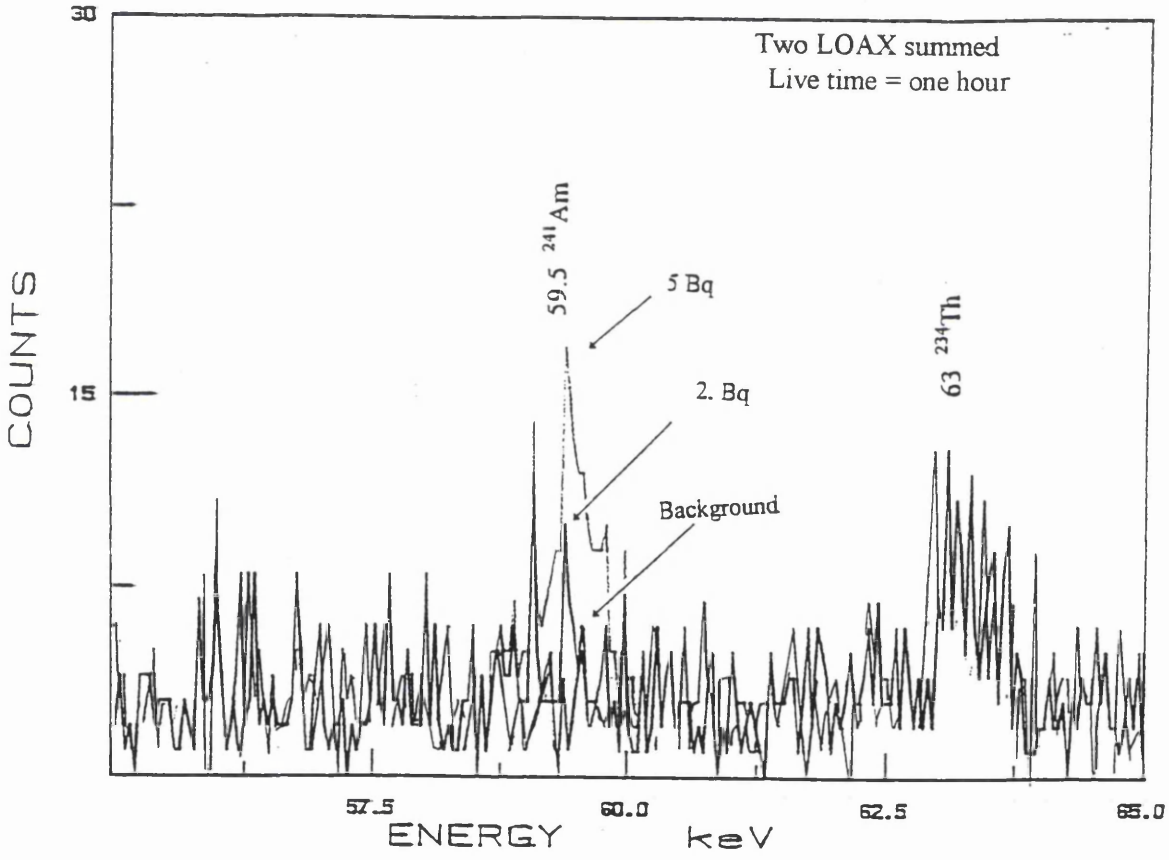

Figure 2.25 Two synthesized low activity ^{241}Am spectra in comparison with background *in vivo* count.

Chapter 3

Background studies

3.1 Background sources

There are four principal sources of background radiation which need to be considered when performing *in vivo* measurements of low-energy photon emitters using a shadow-shield configuration. These are; natural external radioactivity and radiation; natural radioactivity in the construction materials of the detector; man-made radioactivity in these materials; and radioactivity in the body of the subject not immediately of interest. Background spectra obtained using the 80% and two LOAX detectors in their final shield configuration are shown in Figure 2.5 a & b. These spectra can be taken as illustrative examples of the main peaks to be found in a background count. They were used as standards for other measurements and as references when monitoring possible background changes or alteration of detector characteristics with time.

3.1.1 Natural external radioactivity and radiation

Sources of natural activity were the primordial and cosmogenic radionuclides and cosmic radiations. Cosmic-rays produce high energy particles, mainly π-mesons, μ-mesons and electrons which interact with both the shielding and the detectors to increase the background inside the detector area. Neutrons and gamma-ray photons arose from meson decay and interactions with the shielding material surrounding the detector. These in turn cause a number of activation products with peaks which appear in the gamma-ray spectrum recorded over a period of 40 hours in the final shielding arrangement as shown in Figure 3.1. The nuclear reactions involved are presented in Table 3.1. It was noticeable that the highest contribution was due to the e^--e^+ annihilation peak.

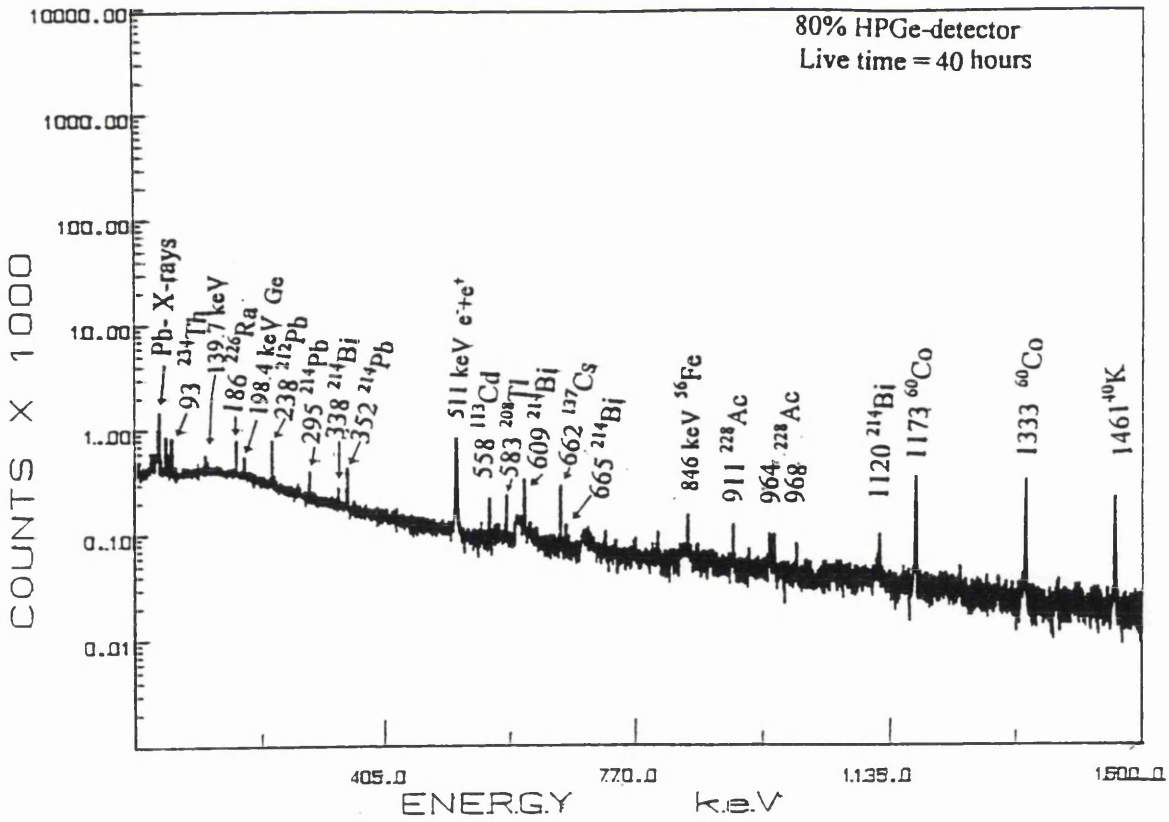

Figure 3.1 Gamma-ray spectrum of the 80% HPGe-detector showing the main activation background peaks.

Accepted energy keV	Measured energy keV	Intensity cps x 10^{-3}	Nuclear reaction
53.53	53.40	1.07	$^{72}Ge(n,\gamma)\ ^{73m}Ge$
66.70	67.0	3.59	$^{72}Ge(n,\gamma)\ ^{73m}Ge$
139.69	139.77	2.16	$^{74}Ge(n,\gamma)\ ^{75m}Ge$
159.71	160.1	0.35	$^{76}Ge(n,\gamma)\ ^{77m}Ge$
198.31	198.4	4.44	$^{70}Ge(n,\gamma)\ ^{71m}Ge$
511.00	510.69	42	$e^- - e^+$ annihilation
558.20	558.15	4.02	$^{113}Cd(n,\gamma)\ ^{114}Cd$
843.76	843.0	1.50	$^{27}Al(n,n')\ ^{27}Al$
1460.81	1460.09	10.8	^{40}K

Table 3.1 Main background peaks and neutron activation processes in the 80% HPGe detector taken from 40 hour count.

3.1.2 Natural radioactivity in the construction materials of the shield and detector

Gamma emitting daughters from the decay of the ^{238}U, ^{235}U and ^{232}Th decay series were present at different trace levels as contaminants in the detector material and in the massive 8 tonnes of lead in the shield structure. Since the HPGe-detectors were made of crystal material with an impurity concentration of less than one part in

10^{12}, and there were no naturally occurring radioactive germanium isotopes, there was no contribution to the background from this source.

Lead is used as the main shield and for 10 cm a 1 MeV γ-ray would be attenuated by a factor of a 3200. Figure 3.2 shows the half-thickness values for gamma attenuation in lead and some other materials. Clearly, greater thicknesses would provide additional attenuation, but this would also increase the probability of undesirable cosmic-ray interaction within the shield so increasing the background. Thus increasing the lead thickness could add to the background undesirably. However, a further source of contamination was ^{210}Pb (46.5 keV, $T_{1/2}$ = 21 y) occurring as a natural gamma-ray emitter of the ^{238}U decay series. Also, the lead shielding could contain other impurities due to the addition of antimony or due to external surface contamination arising from the moulding processes. In addition to this, excitation of the lead could give rise to characteristic lead X-rays with energies in the range 74-85 keV. This could be reduced by the use of the graded shielding as described earlier.

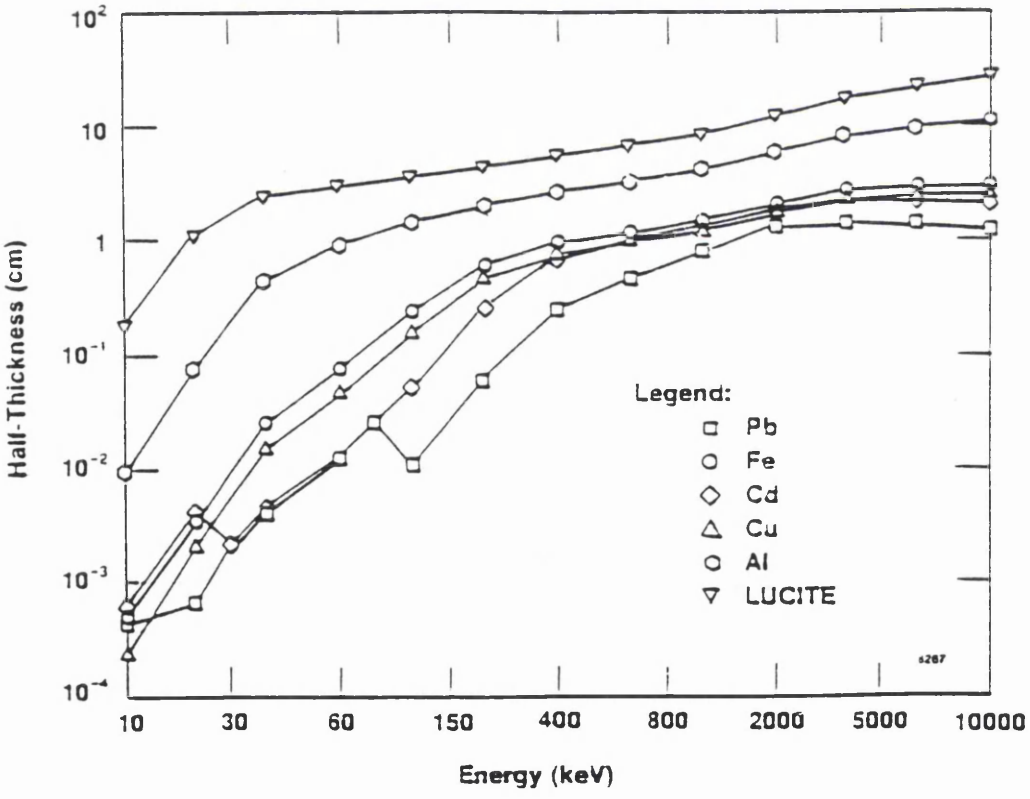

Figure 3.2 Half-Thickness Values vs. energy for commonly used shield materials (EG&G Ortec Catalog, 1994).

3.1.3 Man-made contamination

A number of man-made radionuclides appeared in the background gamma-ray spectrum shown in Figure 3.1. These were identified as ^{60}Co and ^{137}Cs and found to be mostly surface contamination. An attempt was made to reduce these contaminants by completely dismantling the shadow-shield as shown in Figure 3.3. A decontamination process was carried out by washing individual bricks with hot water and 5% "Decon* " solution. Also the lead bricks that were located close to the detector were buffed with an electric tool to remove about 1mm of their outer surface. Figure 3.4 shows the reduction factors obtained by this decontamination procedure for both radionuclides. It can be seen that the reduction factors were approximately 10 times for ^{60}Co and 15 times for ^{137}Cs.

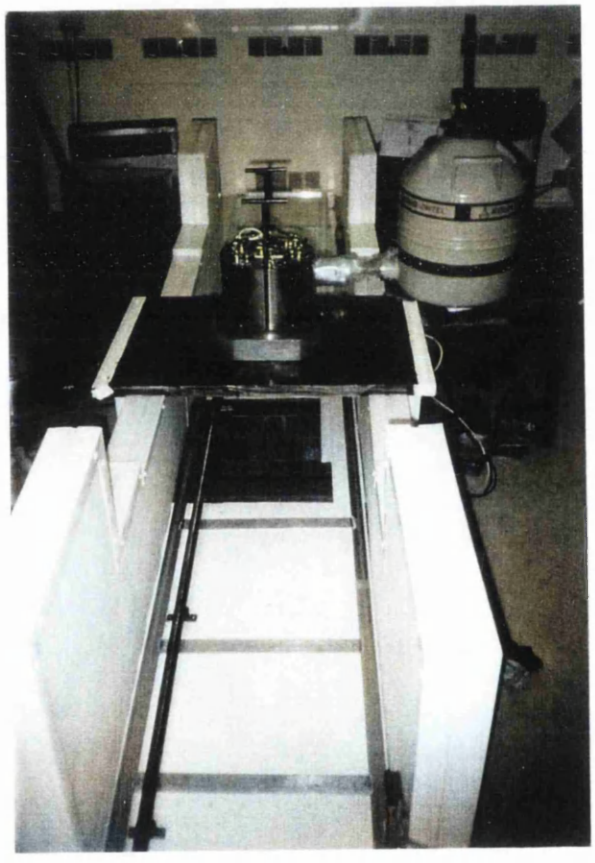

Figure 3.3 Dismantled shadow-shield arrangement for decontamination purposes.

* Commercial name for a totally effective surface-active cleaning agent used for de-contamination procedure. Manufactured by Decon Laboratory Ltd., England.

In addition to the above, it was found that two of the four purchased LOAX detectors had traces of ^{241}Am contamination with count rates of 0.08-0.1 cps in the 59.5 keV region. On return to the manufactures EG&G Ortec, it was confirmed that the ^{241}Am was present as a trace contaminant of the crystal housing. Replacement of this successfully solved the contamination problem and the level fell to the average background range of 1.3×10^{-3} -1.5×10^{-4} cps.

Finally, it was also noted that when the UTR300 research reactor was operating, the 80% HPGe-detector and the two NaI(Tl) detectors detected the 1295 keV gamma-ray peak of ^{41}Ar which appeared as an activation product in the reactor exhaust to the atmosphere. It was thought that traces of this could reach the laboratory atmosphere. No *in vivo* measurements were carried out when this elevated background was present. This problem is specific to counters located at reactor sites.

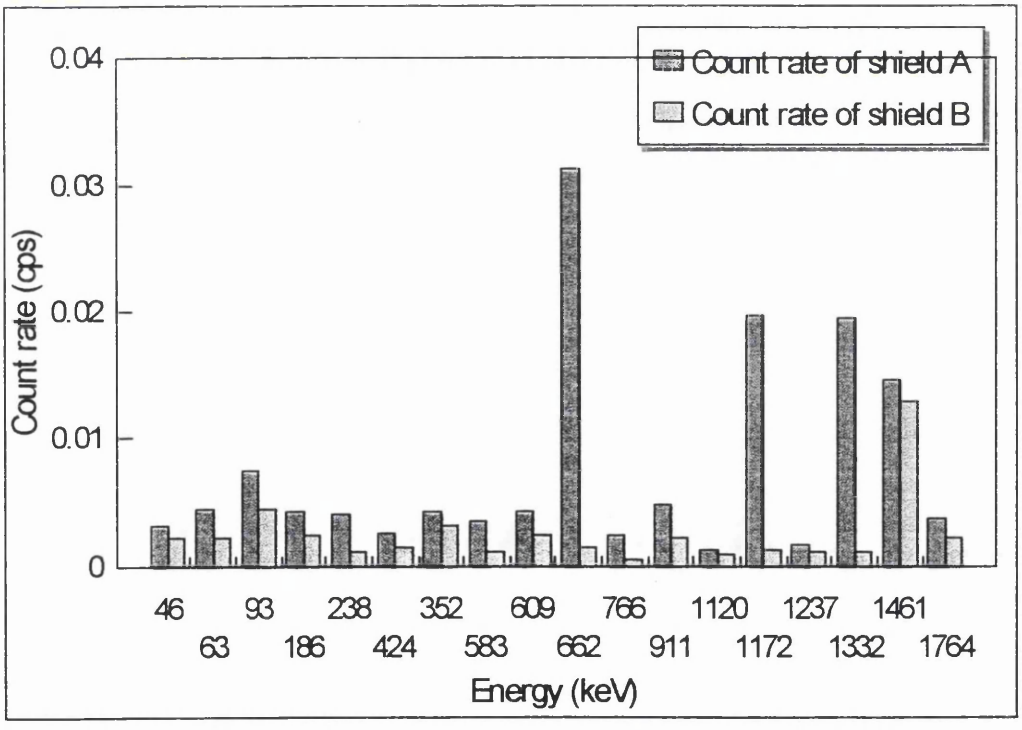

Figure 3.4 Count rates of various gamma-ray energies of the shadow-shield lead (A) before and (B) after decontamination process of the shield at NaI(Tl) whole-body monitor.

3.1.4 Radioactivity in the subjects being measured

Apart from the ^{41}Ar, it would be expected that the various contributing background factors to the detector would remain fairly constant. However, a significant source of variability in body counting is due to the amount of natural and man-made radioactivity present in the body of the measured subject. The human body maintains about 140 g of potassium in homeostatic equilibrium, of which 0.0117 % is composed of ^{40}K shown in Figure 3.5 which corresponds to about (4.4 kBq) of activity (ICRP, 1975). This activity is mostly distributed through out the soft tissue of the body. There are a number of factors that effect the ^{40}K levels in human subjects, the main ones being height and weight as well as the muscle to fat ratio (the lean body mass factor). They all have an important effect on the activity of ^{40}K in different subjects. Thus different subjects will produce different contributions to the background.

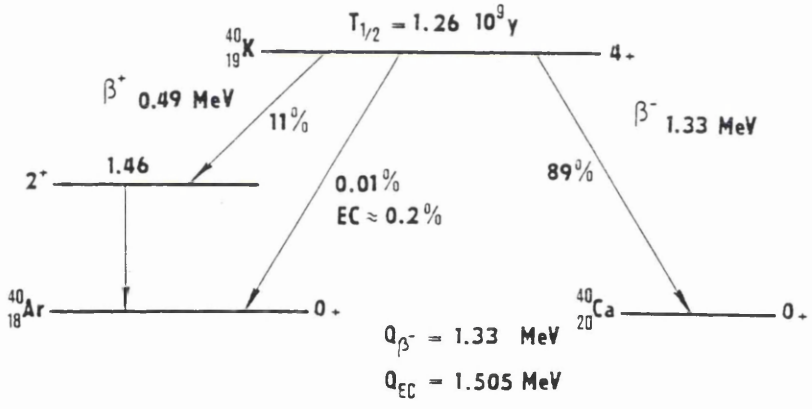

Figure 3.5 ^{40}K decay scheme (ICRP 38, 1983)

An additional source of variation is ^{137}Cs that can be present in different levels in human subjects due to the world-wide spread of fallout from atmospheric atomic bomb tests and the Chernobyl accident in 1986. Several other activities are also present in the body as shown in Table 3.2 (Bertrand et al., 1983). Carbon-14, although it has a comparable activity to potassium, does not contribute to the gamma background because it is a pure beta emitter.

Nuclide	Activity Bq
^{40}K	4440
^{14}C	3700
^{210}Pb	22.2
^{222}Rn	3.7
Natural Uranium	25.9
^{226}Ra	1.85
^{228}Ra	0.925
Total	8195

Table 3.2 Various endogenous radiation levels of activity in a human body (Bertrand et al., 1983).

The possibility of external traces of contamination was also an important consideration for this highly sensitive *in vivo* measurement procedure. For this reason subjects were asked to remove outer clothing and change into a clean overall before entering the monitor for measurement. At some other laboratories preparation for *in vivo* monitoring includes taking a shower in addition to changing into clean overalls. However, long years of experience had shown that this was not necessary at SURRC.

3.2 Observed background effects

The two nuclides, ^{137}Cs and ^{40}K, gave the highest Compton scattering in the body, hence, they constituted the principal component of background radiation when measuring subjects. Table 3.3 presents comparative count rate data for the 80% detector measuring: a water phantom; a subject; a K-phantom; and a mixed K/U phantom. Both phantoms contained five time the physiological (140 x 5= 700 g) level of K. It can be seen that there was no significant increase of counts in the peaks of interest at 46.5, 63 and 93 keV between the water phantom and the subject. However, the effect is more significant for NaI detectors as has been has been reported by (Droughi, 1992) and Grag (Rahola et al., 1984). It also has to be noted that, the

background per unit area of the germanium detectors over the body is three times higher in the 12 to 25 keV energy region and 1.7 times higher in the 50 to 65 keV region than that for the phoswich detectors (Palmer and Rieksts, 1984). At the same time because of the superior energy resolution of the germanium detectors their background levels are more than 10 times better (lower) than the Phoswich detectors. Even though the human body is an ideal scattering medium, the observed effect of ^{40}K gamma-rays at 1460 keV on the lower energy peaks below 200 keV was not significant and found to be approximately 1-5% in comparison of the water phantom and a subject. It must also be noted that Berger and Lane (Berger and Lane, 1981) demonstrated that for *in vivo* measurements of a typical subject with no other contaminants than those expected to occur from natural processes, the background could triple the count rate in the ^{239}Pu X-ray region (13-20 keV) compared to that count rate obtained from just an empty shielded room. It could be seen when measuring a subject or phantom containing radioactive materials the counts of low-energy peaks increases accordingly.

Energy	Water phantom (cps±2σ) x10^{-4}	Subject count (cps ±2σ) x10^{-4}	K-phantom (cps±2σ) x10^{-4}	K/U-phantom (cps±2σ) x10^{-4}
46.5	6.0 ± 4	6.4±4	7.8±4	9.6±5
63	8.0±5	8.4±5	10.5±5	19.3±7
93	10.0±5	11.1±5	13.8±6	21.6±7
186	6.0±4	8.0±4	11.2±5	21.0±6
352	5.0±3	4.6±3	5.8±4	5.6±4
609	3.0±1	2.8±2	3.3±3	3.6±3
662	3.0±2	3.5±2	3.9±3	3.8±3
1461	2.0±1	18±7	59±12	61±13
1764	0.7±1	0.7±1	0.6±1	0.6±1

Table 3.3 Various counted phantoms, subjects and their relative effect on the count rates of different energy peaks, one hour counts.

3.3 Shadow-shield effectiveness study

The effectiveness of the shadow-shield arrangement was investigated by the comparison of the main energy peaks present in the background with the two detector systems, the LOAX array and the 80% HPGe, under the following shielding conditions;

1 Detectors completely out of the shield in the laboratory (open count).

2 Detectors in the shield in the normal counting position with the configurations:

a) both sides (front and back entrances) of the counting space open.

b) one side (back entrance) of the counting space closed.

The partial shield enclosure of the detectors was of interest because these configurations could be used for special counts such as particular static counts of subjects or *in vitro* samples.

A large number of background counts were taken with configuration (a) with and without a water phantom in position. This simulated the static counting position for a subject and provided reproducibility data. Figure 3.6 a, b, and c shows the gamma-ray spectra obtained using the two LOAX detectors summed and the following sections describe in more detail the results for both detection systems separately.

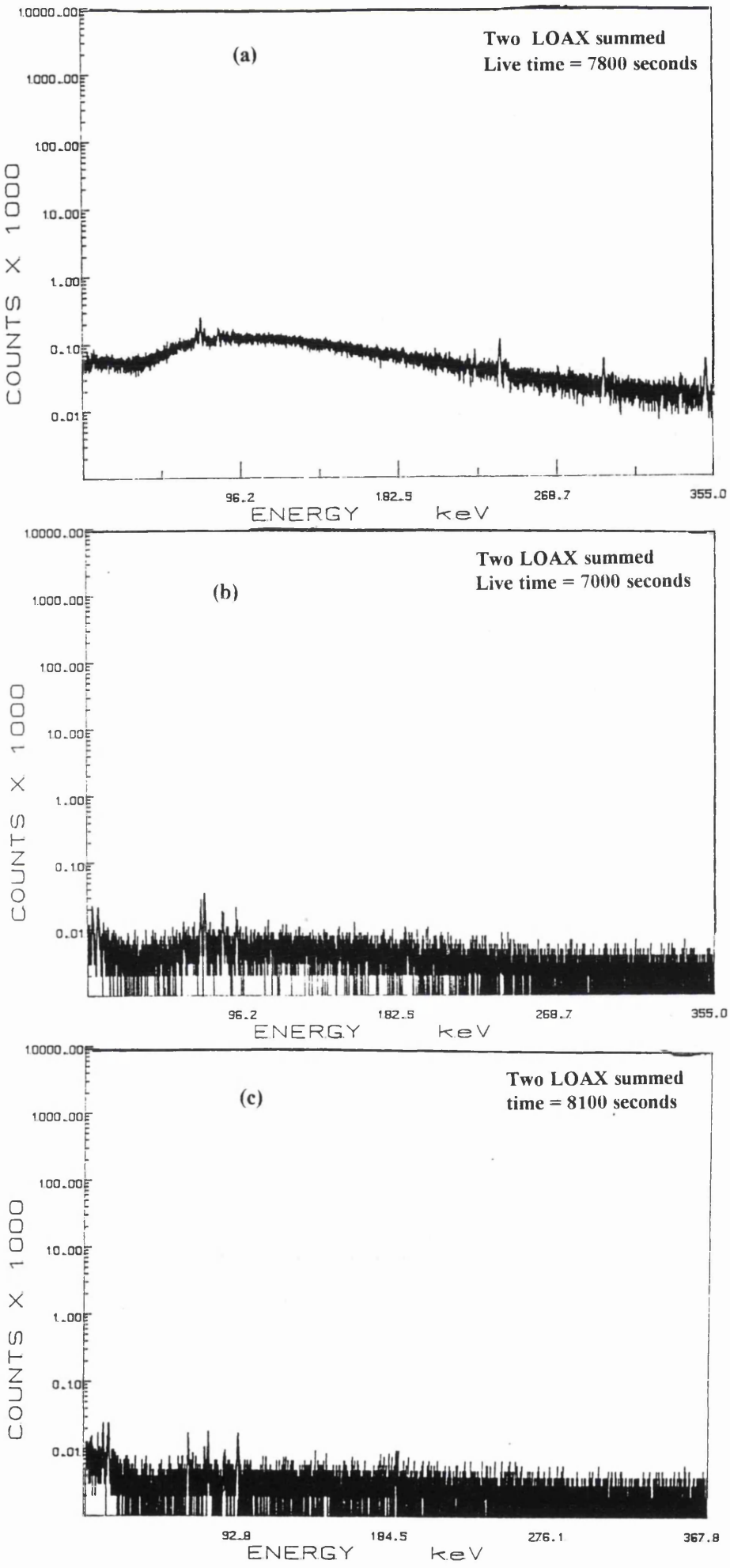

Figure 3.6 Gamma-ray spectra for the three shielding arrangement using the two LOAX detectors summed.: (a) detectors out of shield; (b) two sides open; (c) one side of the turret closed.

3.3.1 The LOAX backgrounds

Although the shielding system was designed to hold up to four LOAX detectors, they were not always available, so many counts were taken using two summed LOAX detectors. All the detection systems were left running all the time, so most of the background counts were obtained overnight and over weekends. Because it was intended to adjust the position of the subject to optimise sensitivity, counts were taken by placing the complete water phantom in the static counting position at different heights from the detector surface in order to determine the variability of the background. Counts were also made with the counting space empty and the gross and net count rates of the main peaks and the characteristic X-rays were found to be higher for an empty counting space and to decrease as the water phantom was raised-up closer to the detector surfaces. This fact was due to the shielding effect of the water phantom which reduced backscatter into the detectors.

The detailed count rates for the main low-energies for the two LOAX detectors are presented in Table 3.4. Four shielding configurations were used namely: the detectors being out of shield; detectors in shielding position with one side of the chamber being closed; the last two counts having the two sides open while the chamber empty and the other with subject in position. The count rates are shown for the three shielding configurations along with the subject count in the normal operating arrangement. The detected gross count rates for 63 keV were 1.16±0.18 cps , 0.033±0.003 cps, 0.044±0.004 cps and 0.063±0.004 cps for the four shielding arrangements respectively.

It was noted that the highest difference was between the open and normal condition while the difference was minimal between the complete enclosure and one side open i.e. the normal operating condition. This proved that the shadow-shield was effective and the slight background increase was not affecting the detection capability of the detector assembly. The increase of count rate for the LOAX detectors for the particular low-energy peaks was minimal and less than 3%, but the overall increase was noticeable in the whole spectrum continuum.

Energy keV	Detector out of shield completely cps±1σ for 1 hour	One side of the chamber closed cps±1σfor 1 hour	Two sides of the chamber open cps±1σ for 1 hour	Subject count both sides open cps±1σ for 1hour
13	0.619±0.013	0.058±0.004	0.063±0.004	0.062±0.004
16	0.675±0.014	0.072±0.004	0.077±0.005	0.078±0.005
26	0.649±0.013	0.018±0.002	0.024±0.003	0.029±0.003
46.5	0.708±0.014	0.016±0.002	0.021±0.002	0.034±0.003
59.5	0.789±0.015	0.012±0.002	0.021±0.002	0.027±0.003
63	1.16±0.018	0.033±0.003	0.044±0.004	0.063±0.004
93	1.67±0.022	0.041±0.003	0.055±0.004	0.071±0.004
186	1.02±0.017	0.023±0.003	0.035±0.003	0.034±0.003

Table 3.4 Gross count rates of measurement of subject and various shielding arrangement using two LOAX detectors summed.

This means that they were slightly affected by the interaction of the high energy 1461 keV of photons ^{40}K. Also data for the background index (cps keV^{-1}) for the three configurations for the three energy ranges: 0-100 keV, 100-200 keV and 200-300 keV are outlined in Table 3.5. This clearly shows that the background index of the complete enclosure shield was compatible with that for the shadow-shield configuration arrangements. It is doubtful whether the increase of the background index when measuring K- phantoms due to the 1461 keV gamma-ray is statistically significant.

Energy range keV	Closed turret cps	Water phantom cps	K-phantom cps
10-100	$7.37x10^{-3}$	$1.84x10^{-2}$	$1.91x10^{-2}$
100-200	$4.81x10^{-3}$	$1.43x10^{-2}$	$1.49x10^{-2}$
200-300	$3.23x10^{-3}$	$6.76x10^{-3}$	$7.13x^{-3}$

Table 3.5 Total count rates of specific energy region of the γ-ray spectra of different shielding phantom arrangements for two LOAX detectors summed.

The LOAX detectors were assembled into an array in order to increase the volume of germanium available and thereby increase the sensitivity. The effect of summing the backgrounds from these detectors was investigated at the gamma energies of interest. It was found that the backgrounds with different numbers of LOAX detectors for the 63 keV peak of ^{234}Th were; $0.007\pm2x10^{-3}$ cps, $0.017\pm2x10^{-3}$ cps and $0.040\pm3x10^{-3}$ cps for one, two and four summed LOAX detectors respectively. Also the backgrounds for the 93 keV peak were $0.008\pm3x10^{-3}$ cps, $0.021\pm2x10^{-3}$ cps and $0.061\pm4x10^{-3}$ cps

for one, two and four detectors respectively. It was noticed that the background going from two to four summed detectors was increased by almost two and four times for the 63 and 93 keV energy ranges respectively. The explanation for this, was that two of the detectors were located towards the outside of the array where the background was expected to be slightly higher. Although the detector volume had been increased, there was thus a slight increase in background which could influence the ultimate limit of detection.

3.3.2. The 80% HPGe-detector data

A typical long background count spectrum for the 80% HPGe detector in the final shield is shown in Figure 2.5b. The average count rates (cps) for the 46.5, 63, 93 keV peaks were ($0.0006\pm4x10^{-4}$), ($0.0008\pm5x10^{-4}$) and ($0.0011\pm6x10^{-4}$), respectively when measuring the water phantom statically. A one hour count of a normal subject under the same counting conditions gave ($0.0007\pm4x10^{-4}$ cps), ($0.0009\pm5x10^{-4}$ cps) and ($0.0012\pm6x10^{-4}$ cps) for the same gamma-ray energies. The ^{40}K in the measured subject appeared to have no significant effect on the count rate for the main low-energy peaks as shown above.

Table 3.6 presents the various count rates (cps) for the energy ranges of interest for the three shielding arrangements: having the chamber completely closed; both sides open with water phantom; again both sides open and K-phantoms in place. The difference can be noticed between completely closed especially at low-energy end of the spectrum where lead X-rays play an important role in the increase of the count rate. This effect was reduced when both sides of the chamber were open and a phantom was in place. Also, comparison of columns 3 and 4 shows the effect of the K-phantoms where the count rates of the low energy ranges were increased due to ^{40}K by approximately 24.8 %.

Scattered radiation due to the open-ended nature of the counting space, did not contribute appreciably to the low-energy region of the spectrum. It has to be noted that the external background and the lead x-rays contribution will be completely restricted and its effect would be much reduced in a complete shielded room type of whole-body monitor.

Energy range keV	Close chamber cps $x10^{-3}$	Water phantom cps $x10^{-3}$	K-phantom cps $x10^{-3}$
40-100	6.86	1.28	1.55
100-200	3.30	1.16	1.40
200-400	4.01	5.90	7.15
400-600	2.20	2.80	3.45
600-700	1.60	2.10	2.41
700-1000	1.03	1.27	1.67
1000-1500	0.58	0.74	1.34
1500-2000	0.26	0.40	0.34

Table 3.6 Total count rates (cps) of specific energy regions of the γ-ray spectra of different shielding and phantom arrangement using the 80% HPGe-detector.

3.4 Methods of subject background determination

The accurate high sensitivity determination of low-level low-energy radionuclides in the human subject requires a reliable method for background prediction. There are a number of methods being used for HPGe-detectors which have been extensively investigated by a number scientists at different laboratories (Falk et al., 1979; Spitz et al., 1983; Hickman and Cohen 1988; Newton et al., 1981 and Palmer and Riesksts, 1984). Some of these methods will be presented and employed for the background prediction of human subjects in this research study and will be discussed further.

The background of human subjects was usually influenced by two main processes. The first was the non-stochastic process caused by ^{40}K and other deposited nuclides in the body of the measured subject. The second was mainly a stochastic process caused by the photon scattering within the detection system and its surrounding materials as shown in Figure 3.6. Because of these two process, the background contribution from each subject had to be estimated using a special mathematical function determined from a database of control subjects (Hickman and Cohen, 1988). The prediction of the background variance was also based on mathematical functions. As will be discussed further in section 3.5, the statistical analysis of the background shows the lower the variance of the predicted background, the better the overall detection capabilities of the system. It was also important that the function used to estimate the background must not introduce any bias and should accurately represent the background population. However, this method is not dealt with in this research and further explanation could be found in Debertin and Helmer (1988). The various

methods and techniques used for human background prediction and applied in different parts of this research work were based on net count rate calculations. Each of these methods of measuring the subject background has its own advantages and limitations depending on the level and type of contamination being evaluated. Due to the high peak-to-Compton ratios for the main HPGe-detection system used, the following background determination methods were used;

1- The most common method was the utilization of anthropomorphic phantoms filled with water and a certain amount of potassium chloride (KCl) usually about 140 g to simulate the ^{40}K present as the natural body content ICRP 54 (ICRP, 1988) of reference man. Phantoms could be simple to construct and were easily measured routinely. A limitation was that a correction factor was sometimes needed to allow for differences between simple phantom models and the human body.

2---The second method which could be used was the " matched subject " method which, as the name implies, meant the selection of a subject known to be free of contamination from the general public who matched the height and weight of the subject being measured. The main disadvantage of this technique was the difficulty of obtaining a control subject for each individual contaminated subject. Although an attractive method, it has been found that subjects with the same body dimension did not necessarily produce the same background count rate (Cohen, 1984). This was also seen in the data collected from two matched subjects measured by our own detection systems under the same counting conditions. The pulse height gamma-ray spectra of two matched subjects were (slightly) different as shown in Figure 5.9 a & b.

3--- The third common method used when contamination was thought to be likely to occur, is to use the subject as his own background. Thus a background measurement was recorded for the subject prior to starting work with radioactive material. This measurement could be used as an accurate estimation of the subject's normal background due to the scattering effects of his ^{40}K and any other radionuclides present at the time of measurement. A requirement was that the individual maintained a constant body weight and shape. Also, the energy calibration of the detection system had to be stable.

3.5 Background determination for low-energy peaks using HPGe-detectors

3.5.1 The statistical significance of background

The low counts observed in the Compton continuum in HPGe detectors allowed the possibility of observing low-energy peaks with low activities. The identification of full energy peaks that rise above the continuum is easy visually or by use of special peak search algorithms. While this fact holds for prominent peaks, low-count peaks in the low-energy region (16-100 keV for the LOAX and 40-200 keV for the 80% HPGe-detector) of the spectrum might be hidden under the Compton continuum. This fact puts more stringent requirements for the overall sensitivity for the identification of those unseen "hidden" peaks for *in vivo* measurements. To detect the lowest possible activity for the low-energy photons required the predetermination of the background peaks and the levels of the smallest possible indication (or peak rise) of positive net activity that could be identified and detected. To study these phenomena further, the following sections will describe the various parameters in more detail.

3.5.2 Critical limit (L_C)

In order to determine whether the net count of the measured peak area is significant or not, it is essential that some statistical criterion has to be used to establish whether or not a peak is significant. Since a peak becomes non-significant only when it becomes "lost" in the background, identifying the presence of a peak cannot be done by reference to the peak area alone but must take into account the uncertainties of the background. To determine whether a net count near zero is truly zero or represents a true positive count, there must be some level which can be called the critical limit, above which the count can be accepted as a valid net count. Operationally this is applied by comparing the net count rate obtained with quoted values for the L_C for the same energy. If the net counts obtained are above the L_C then an activity has been detected and could be quoted as a value with its associated uncertainty. Graphically this could be illustrated in Figure 3.7 for a series of background counts having a mean net count of zero but distributed in a Gaussian fashion above and below zero. The standard deviation, or the distribution of the counts was represented by σ_0. The count is taken to be statistically significant if $A > k_\alpha \times \sigma_0$ and the count is not

significant if $A \leq k_\alpha \times \sigma_0$. The k_α factor is taken to be a predetermined degree of confidence limit of 95%. Further discussion of these concepts has been presented in detail elsewhere (Currie, 1968; Summerling et al., 1981 & 1985; Brodsky, 1986 and Droughi, 1992).

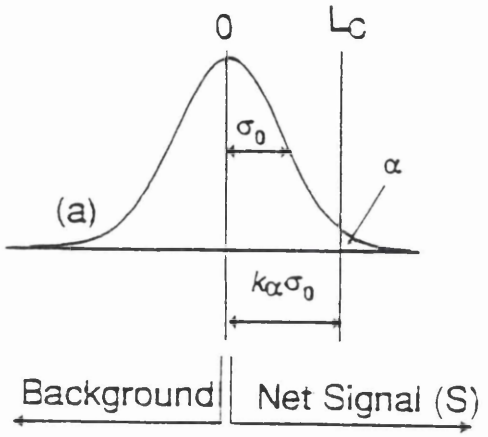

Figure 3.7 Relationship and description of the Critical and Detection Limit concepts.

This critical limit was defined as the lowest number of counts in a specified peak of a particular radionuclide that could be detected with a given level of statistical significance (e.g. 95% confidence limit) above the background level. According to this definition it was obvious that the background of the detection system governed the limit of the detection. The critical limit was coincident with the point at which the peak was "lost" or "disappeared" into the background. Thus, the limit could only be found by reference to the energy range of the peak. The formula used for calculating the critical limit was that derived by Currie (Currie, 1968):

$$L_C = 2.3\ \sigma_b \quad \text{(at 95\%confidence limit)} \quad \text{.....Equation 3.1}$$

where the main parameters defined as:

2.3 is the value of the standardized normal deviate (false positive and false negative) that is expected with a probability of 0.05.

σ_b is the standard deviation of background counts from a K-phantom taken as the blank. Table 3.7 presents the critical limit for the 80% HPGe-detector based on the background counts of the main energy peaks of interest.

Energy nuclide keV	Net count rate cps $x10^{-3}$	Calculated error (σ_b) for net cps 1h	Calculated $L_C = 2.33\sigma_b$ cps
^{210}Pb 46.5	7.44	1.4×10^{-3}	3.3×10^{-3}
^{241}Am 59.5	1.11	5.6×10^{-4}	1.3×10^{-3}
^{234}Th 63	1.12	5.6×10^{-4}	1.3×10^{-3}
^{234}Th 93	1.31	6.0×10^{-4}	1.4×10^{-3}
^{226}Ra 186	0.093	1.6×10^{-4}	3.7×10^{-4}
^{214}Pb 295	0.057	1.3×10^{-4}	3.0×10^{-4}
^{214}Pb 352	0.049	1.2×10^{-4}	2.8×10^{-4}
^{214}Bi 609	0.026	8.5×10^{-5}	2.0×10^{-4}
^{137}Cs 662	0.032	9.4×10^{-5}	2.2×10^{-4}
^{214}Bi 1120	0.014	6.2×10^{-5}	1.4×10^{-4}
^{60}Co 1332	0.026	8.5×10^{-5}	2.0×10^{-4}
^{40}K 1461	0.094	1.6×10^{-4}	3.8×10^{-4}

Table 3.7 Net background count rates (cps) of the main energy peaks for the 80% HPGe-detector and the calculated limit of detection L_C.

3.5.3 Minimum Detectable Activity (MDA)

To determine clearly the least amount of activity that can be measured by any detection system, the minimum detectable activity has to be defined. The MDA is defined as the lowest amount of activity which could be detected with a particular level of statistical significance above background levels. When measuring a subject there is a 95% probability that the measured activity has a statistical probability, β of non-detection (type II error) known as false negative and α, the type I error also known as false positive (Storm and Stansbury, 1992). This implies that a great care has to be taken when measuring a low count activity so that neither type of error would occur.

This activity should be high enough to be just above the critical limit for it to be detected and defined as activity, which in turn, will be above the detection system's background. However, in the literature a number of more elaborate formulae for the calculation of MDA can be found in various references. The formula of particular interest and used through out this research work is given by the following:

$$MDA = 2\sigma_b / f \text{ ---------Equation 3.2}$$

where:

σ_b ---- Standard deviation of blank or background count.

f ---- Calibration factor that convert counts into units of radioactivity (sensitivity factors).

It has to be noted that even though the values for the L_C are quoted it, is the MDA values are widely used and considered to be of greater importance for evaluating the detection systems.

For the purposes of comparing the results of this research work with that of previous workers in the field the above formula will be applied. Brodsky (1986) found MDAs for ^{235}U and ^{238}U to be 7.4 Bq and 110 Bq, respectively, for *in vivo* counting, and the best state-of-the-art values were attained by Palmer et al. (1991 and Toohey et al. (1991) with MDAs of 4 Bq and 70 Bq for the same uranium radionuclides respectively. Using the same above formula, the Canadian human monitoring laboratory quote 220 Bq and 6 Bq for the 17 and 59.5 keV photons of ^{241}Am respectively and 4.4 Bq for ^{235}U using 4x70 mm germanium detectors in 1800 sec static count. [private communication through the Internet system with Kramer, G. (the director of laboratory)].

3.6. Calculation of the background using trapezium methods

The trapezium method uses "predictor" regions taken immediately above and below the peak of interest. Because of the properties of the Compton continuum of the germanium detectors, the predictor regions provide a good estimate of the background under the peak for specific counting conditions.

The LOAX-detectors were set to operate on a gain of 0.081 keV/channel which gave an energy range of 2-386 keV over 4k channels. This set-up allowed for a 12 channel predictor region to be taken above and below each main peak for the energies above 93 keV. At the same time lower number of channels i.e. 6 channels, were taken for the 63, 59.5 and 63 keV because of the close proximity of these peaks in gamma-ray spectrum. The net peak activity of the main peaks was determined by calculating the arithmetic average of both predictor regions above and below it, and the result is subtracted from the main peak counts using equation 2.3. This net counts calculation procedure and its uncertainty propagation was carried out using equation 2.4 on a number of peaks to determine their background counts using different geometries as indicated in Tables 3.8 and 3.9.

Energy		One side of chamber closed		Both sides open		Both open with water phantom	
keV		cps	1σ % error	cps	1σ % error	cps	1σ % error
U X-rays	13	0.034	18	0.031	18	0.027	17
---	16	0.046	22	0.046	21	0.041	20
---	19	0.005	7	0.009	9	0.008	9
^{210}Pb	46	0.002	4	0.001	6	0.002	6
^{241}Am	59	0.003	6	0.001	3	0.002	5
^{234}Th	63	0.018	13	0.017	13	0.016	14
Pb-x-rays	84	0.012	11	0.027	16	0.017	13
^{234}Th	93	0.029	17	0.025	16	0.014	11
^{226}Ra	186	0.008	9	0.007	9	0.026	15

Table 3.8 Net background count rates and one hour error percentage for the main energy peaks using the trapezium method.

However, for the 80% HPGe-detector, due to the low gain, the channel width was 0.326 keV/channel. Because a wide energy range was covered by the spectrum (from 20- 2800 keV), the number of channels (3-6 channels) under a given peak was therefore limited compared to the LOAX detectors of 12 channels). This also meant that peaks were close together so that the number of channels available as predictors was less. Thus, the predictor regions i.e. the number of channels taken, especially at 59.5 keV peak for the ^{241}Am and at 63 keV peak for ^{234}Th, were limited to only 3-6 channels on each side of the peak to calculate the background. Table 3.9 outlines the count rates of the main peaks of the 80% HPGe-detector using the trapezium method taking three summed background counts totaling 61 hours, duration for each shielding arrangement. For this reason the error shown was taken as the percentage average of the mean count rates separately. These tables shows the net count rate did not change appreciably under the three shielding geometries.

Energy		One side of chamber closed		Both sides open		Both open with water phantom	
Nuclide	keV	cps	1σ % error	cps	1σ % error	cps	1σ % error
^{210}Pb	46	0.003	5	0.004	6	0.010	10
^{241}Am	59	0.002	4	0.001	2	0.004	3
^{234}Th	63	0.004	6	0.002	4	0.007	6
^{234}Th	93	0.012	11	0.008	9	0.007	8
^{226}Ra	186	0.008	9	0.007	8	0.007	9
^{214}Pb	352	0.008	5	0.007	6	0.007	10
^{214}Bi	609	0.006	8	0.008	9	0.014	12
^{137}Cs	662	0.006	8	0.007	8	0.009	9
^{40}K	1461	0.007	8	0.011	10	0.115	33

Table 3.9 Net background count rates and calculated percentages error for one hour using the 80% HPGe-detector using the trapezium methods.

Chapter 4

Detector calibration and determination of performance using anthropomorphic phantoms

4.1 Introduction

The accurate evaluation of internally deposited photon-emitting radionuclides by the use of semiconductor detectors requires well defined methods to calibrate the detectors in order to convert the measured counts into the amount of activity deposited within the organ or tissue under study. Ideally, the calibration techniques must take into consideration the distribution of activity in the body as well as the spatial geometrical relationship i.e. solid angle and the distance between the detector and the measured phantom or subject. The method used here was to take anthropomorphic "phantoms" constructed to simulate the size, shape and weight of the body and add known amounts of radioactivity.

The following sections describe in more detail the types of phantoms used for calibration and present all the relevant data collected for the calculations of sensitivities and MDAs. In the final section the relationship between the: MDA values for the main radionuclides; the Intake Retention Factors (IRF); and the Minimum Detectable Intake (MDI) for internal radiation measurements are discussed.

4.2 "BOMAB" Phantom Calibration Standards

A very common type of phantom widely used for the routine calibration of whole-body counters is the BOMAB "**Bo**ttle-**Ma**nikin-**Ab**sorption" phantom shown in Figure 4.1. It consists of 10 polyethylene containers of sizes which, when appropriately assembled, are roughly equal to the size, weight and shape of "standard man". The containers are usually filled with demineralised water containing known activities of radionuclides. Although they provide a good calibration, these phantoms differ in their scattering

characteristics because they do not accurately simulate the true distribution of radionuclides in the human subject. One set of these polyethylene phantoms was usually filled with demineralised water which was sufficiently tissue-equivalent to provide the absorption and scatter of background radiation within the shield of the whole-body detection system for a situation where there was no activity present. Other phantoms were loaded to represent whole-body activity and in particular, included the nuclides ^{134}Cs , ^{137}Cs , ^{40}K and ^{238}U.

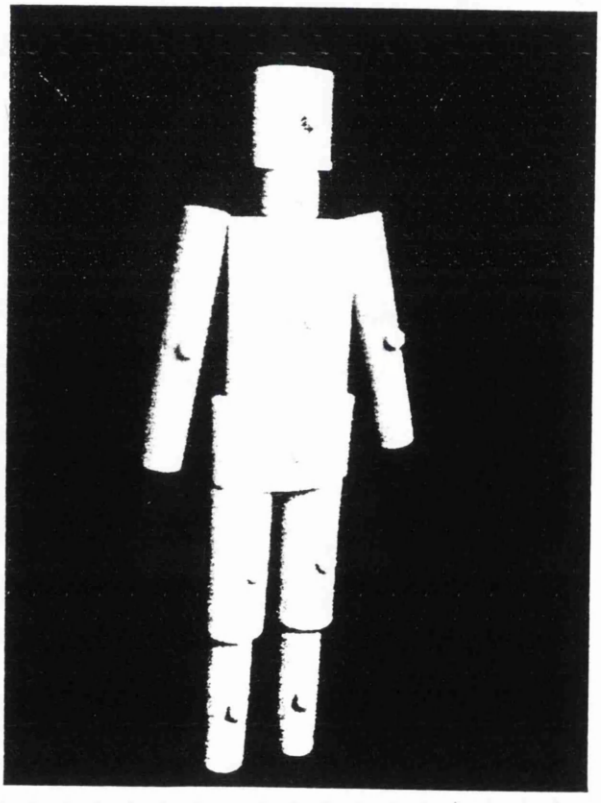

Figure 4.1 A typical BOMAB "**Bo**ttle-**Ma**nikin-**Ab**sorption" phantom.

4.2.1 K-phantom measurements

A complete K "BOMAB" phantom was prepared by taking five times the normal human potassium level. Therefore the total amount of potassium chloride used was (140 x 5 x 1.907) = 1334.9 g. This was divided and distributed according to the percentage weight of body organs as shown in Table 4.1.

The phantom was measured using the 80% HPGe detector in both static and scanning geometries 8 cm and 3 cm from the detector by adjusting the height on the bed. Table 4.2 represents the count rate obtained for the scanning counts of the various sections of the K phantom for which the measured average sensitivity was 0.0219±0.0025 cpm g^{-1} K for the 80% HPGe-detector. This average measured sensitivity value was used for the calculation of total body potassium for subject measurements which will be dealt with in section 5.2.3 of chapter 5. The total activity in Becquerels was calculated by taking the specific activity of ^{40}K = 32 Bq g^{-1} K. The measured MDA of the 80% detector was found to be 1 g of K for a 60 minute count equivalent to 2σ. Normalised sensitivity factors were calculated and found to be in the range of 106-144%. The highest variability was found when measuring the chest section separately due to its size and less K distribution than measuring the whole phantom .

Counts were also taken with the LOAX detectors and it was noticed that the background values for the low-energy peaks increased slightly with the introduction of the K phantom. By examining Table 3.6, it could be seen that the count rates for the K phantom were marginally higher than for the water phantom. This fact confirmed that the gamma-ray spectra obtained using the LOAX detectors in the presence of the K-phantom were affected as could be seen in Figures 4.2 & 4.3. These detectors had a low efficiency for the high energy gamma-rays which was considered to be an advantage in reducing these Compton effects. Also, Figure 4.2 depicts the gamma-ray spectra obtained from a 4 hour count of the water phantom; K-phantom; and potassium/uranium mixed phantom known as (K/U) using two LOAX summed detection systems. The

difference between the three spectra is very minimal and only a slight increase in the lower part of the spectrum was indicated. At the same time Figure 4.3 shows a comparison of gamma-ray spectra between the water and K phantoms for the 80% detector where the increase in Compton effects could be clearly noticed.

Phantom section	Fraction of Total (%)	Normal K Content (g)	Kx5times Conc. (g)	Required KCl forx5Conc.(g)	Actual KCl (g)
Head	5.6	7.8	39.2	74.7	74.8
Neck	1.5	2.1	10.5	20.0	20.0
Chest	27.6	38.6	193.0	368.4	368.4
Pelvis	16.5	23.1	115.5	220.2	220.2
Thigh R	10.6	14.8	74.2	141.5	141.5
Thigh L	10.6	14.8	74.2	141.5	141.5
Leg R	7.0	9.8	49.0	93.4	93.4
Leg L	7.0	9.8	49.0	93.4	93.4
Arm R	6.8	9.5	47.6	90.8	90.8
Arm L	6.8	9.5	47.6	90.8	90.8

Table 4.1 K - phantom preparation details.

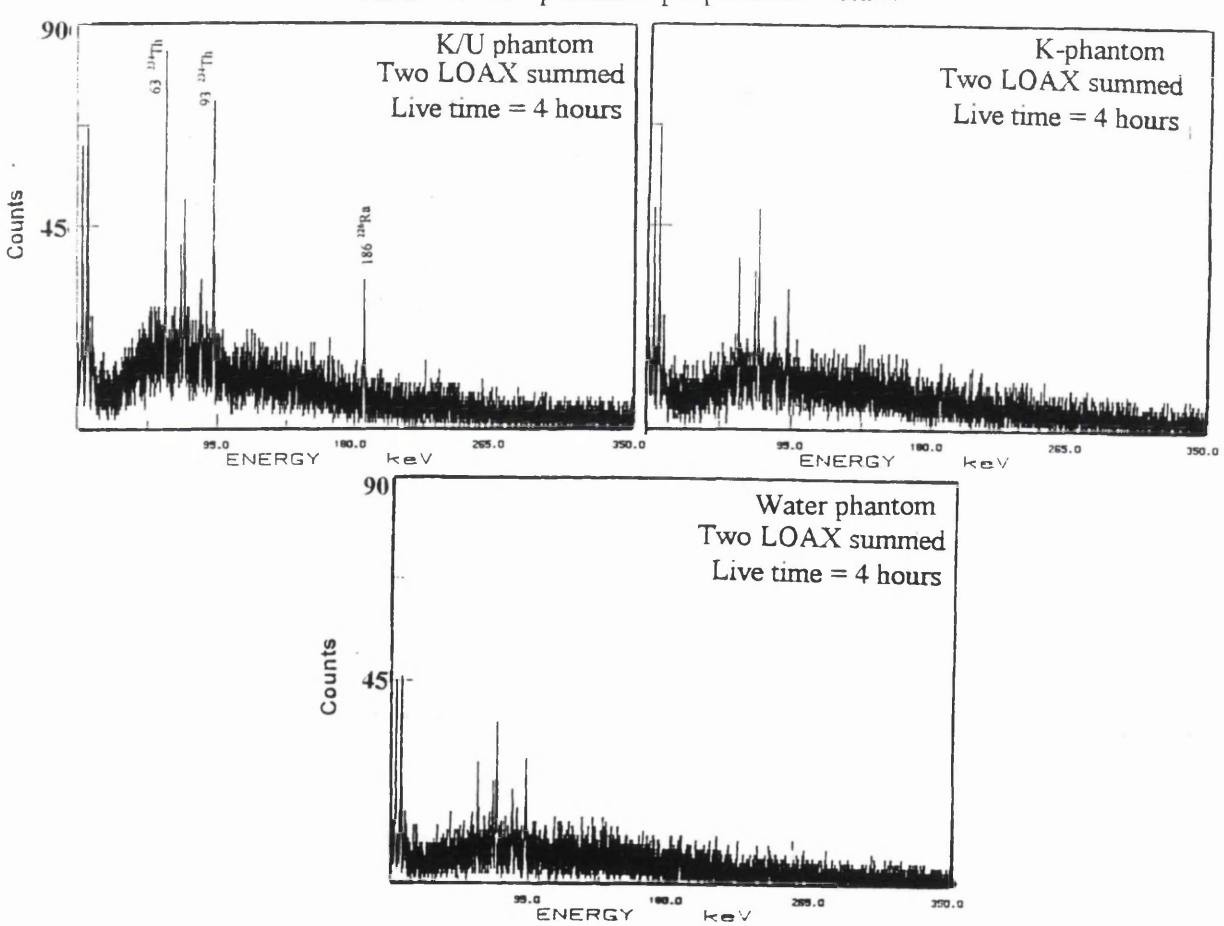

Figure 4.2 Comparison between water; K; and K/U phantoms γ-ray spectra using two LOAX detectors summed.

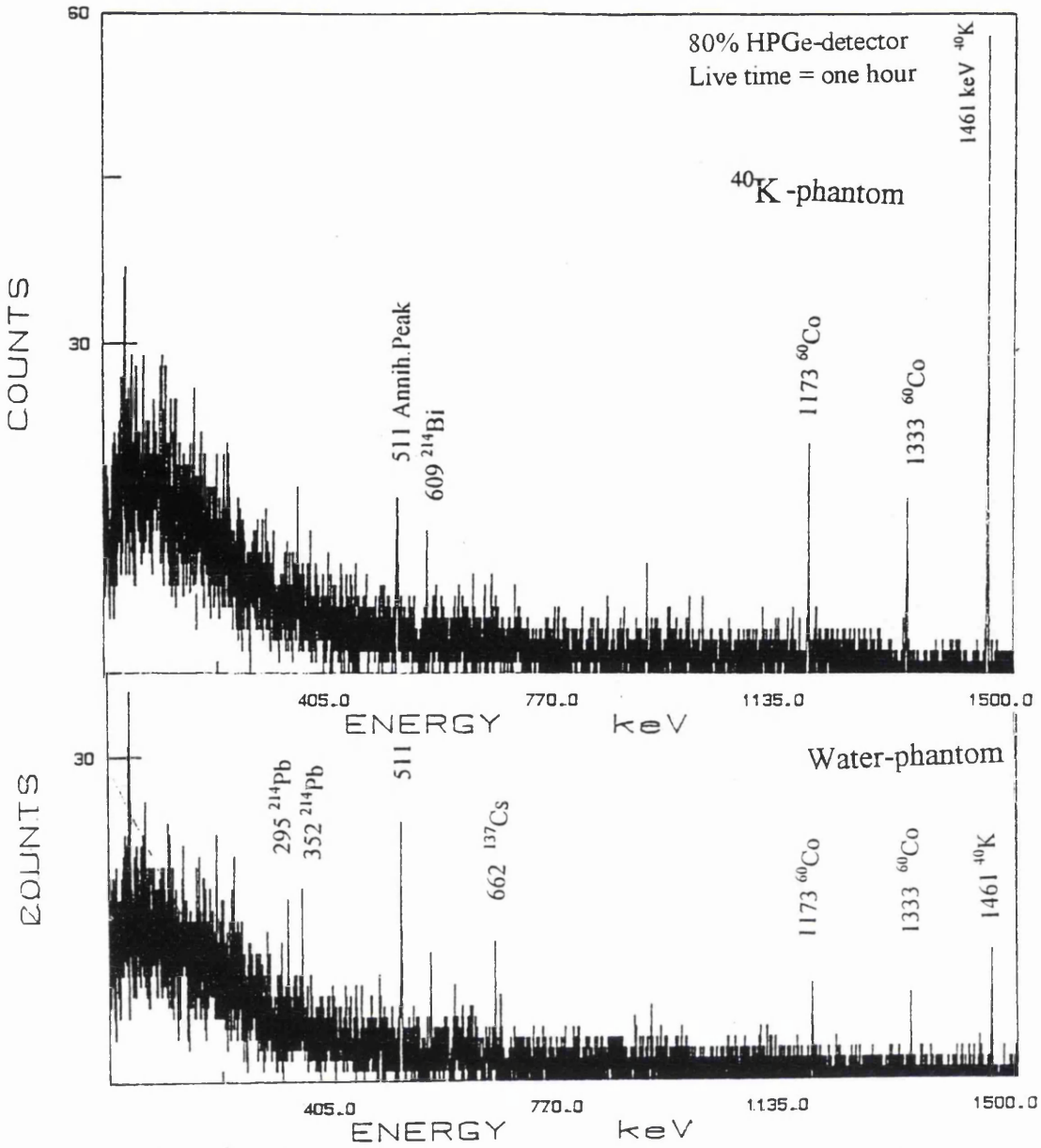

Figure 4.3 Comparison between typical gamma-ray spectra obtained using the 80% HPGe-detectors measuring K- and water phantoms.

Phantom sections	Net (cpm) of ^{40}K 1461 keV	Wt. of K (g)	80%HPGe-detector Sensitivity (cpm g^{-1}) (%)*	
All phantom parts	**13.6**	**700**	**0.019±0.002**	**100%**
All phantom-legs	**12.5**	**602**	**0.021±0.002**	**107**
Chest+pelvis+arms	**8.3**	**404**	**0.021±0.002**	**106**
Chest+pelvis+arms head+ nick	**10.0**	**453**	**0.022±0.003**	**114**
Chest	**2.6**	**93**	**0.028±0.003**	**144**
Average	—	—	**0.022±0.003**	**113**

Table 4.2 Scanning count rates and measured sensitivities of various sections of K phantom using the 80% HPGe-detector. *Normalised factors in percentage.

4.2.2 Mixed uranium and K measurements (K/U)

In order to calibrate the detection systems for uranium, uranyl nitrate ($UO_2(NO_3)_2$ $6H_2O$) was added to the potassium phantom as described in Table 4.3, column 5 gives the exact uranium added to the different phantom sections. It is the equivalent of 1 gramme of natural abundance material was used. The measurements were made using the 63 and 93 keV ^{234}Th peaks making the assumption that it was in equilibrium with the ^{238}U and taking into consideration a 10% error of the added activities. A typical gamma-ray spectrum for two LOAX detection systems is shown in Figure 4.2.

Phantom section	Fraction of total (%)	Normal content K (g)	$UO_2(NO_3)_2.H_2O$ Wt (g)	U Activity taken Wt (g)
Head	5.6	7.8	0.118	0.121
Neck	1.5	2.1	0.032	0.033
Chest	27.6	38.6	0.582	0.595
Pelvis	16.5	23.1	0.348	0.345
Thigh R	10.6	14.8	0.224	0.229
Thigh L	10.6	14.8	0.224	0.219
Leg R	7.0	9.8	0.148	0.133
Leg L	7.0	9.8	0.148	0.113
Arm R	6.8	9.5	0.143	0.138
Arm L	6.8	9.5	0.143	0.145
Total		140 g	2.11	2.07=0.981 g U

Table 4.3 ^{238}U phantom preparation data.

The phantom was measured in scanning mode as a whole phantom and then subsequently with sections removed starting with the legs, thighs and arms until finally measuring the chest alone. Each count was taken for 2000 seconds duration. The collected count rates were used to calculate sensitivities and the MDA using equation 3.2, for both detection systems i.e. the 80% and four LOAX HPGe-detectors. It has to be noted that the number of LOAX detectors used through out the calibration procedures varied according to their availability. The highest sensitivity for scanning with the 80% HPGe-detector was 9±2 cpm g^{-1} and for the four LOAX HPGe-detectors was 13±3 cpm g^{-1} at 93 keV and their respective MDAs were 37 mg and 29 mg U for a count of 33 minutes. This is the same time used for measuring subjects in scanning modes. Figures 4.4 and 4.5 depict

graphically the reduction of observed activities with the removal of various phantom parts for the 80% and two LOAX detectors.

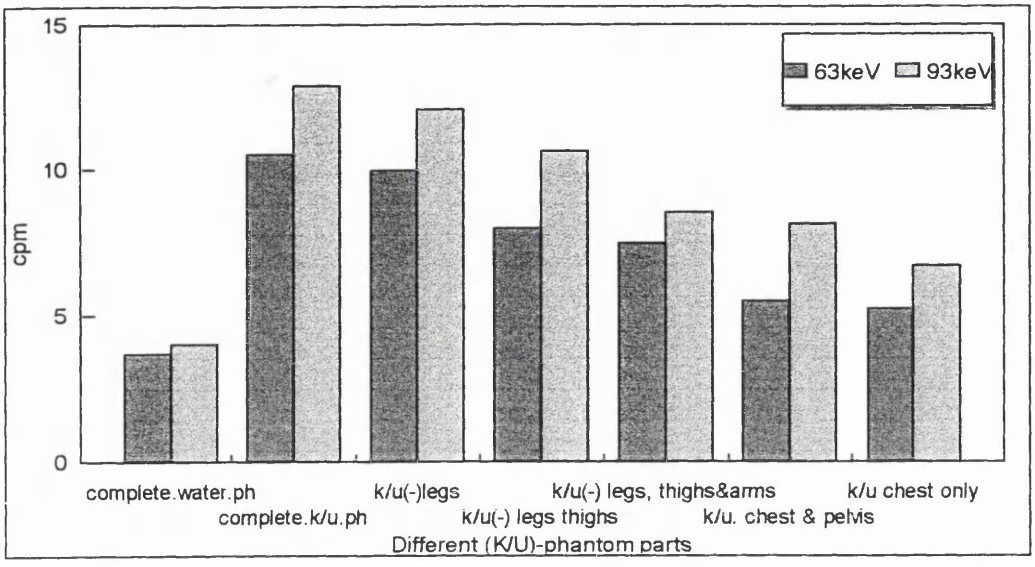

Figure 4.4 The reduction of scanning count rate with the removal of different parts of the K/U phantom using the 80% HPGe-detector.

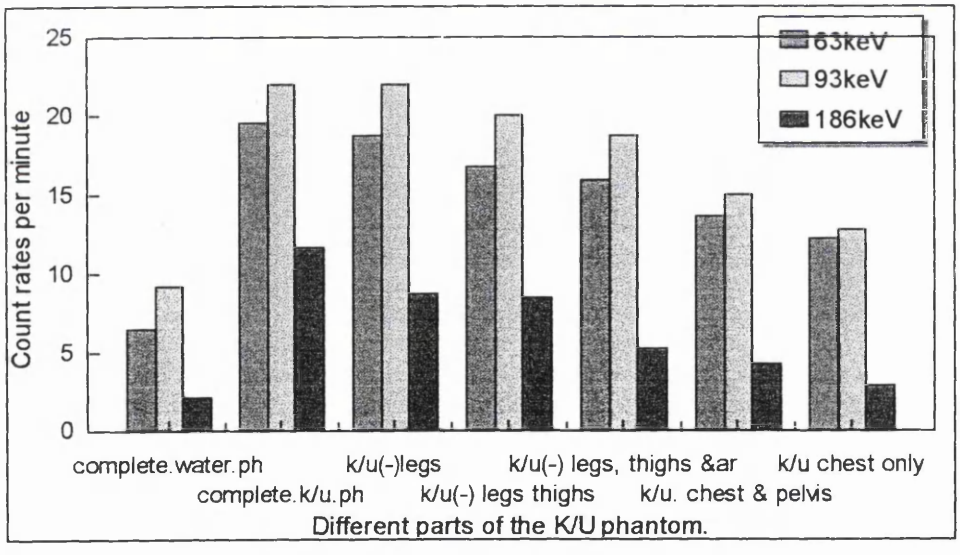

Figure 4.5 K/U phantom scanning counts of the various parts using the four LOAX detectors summed.

One hour counts were taken using one LOAX detector on both K/U and K-whole phantoms scanned separately, and the gamma-ray spectra obtained were compared at the low-energy end of the spectrum region as can be seen in Figure 4.6. It was clearly noticed that the 93 keV peak is best for quantifying the uranium measurement.

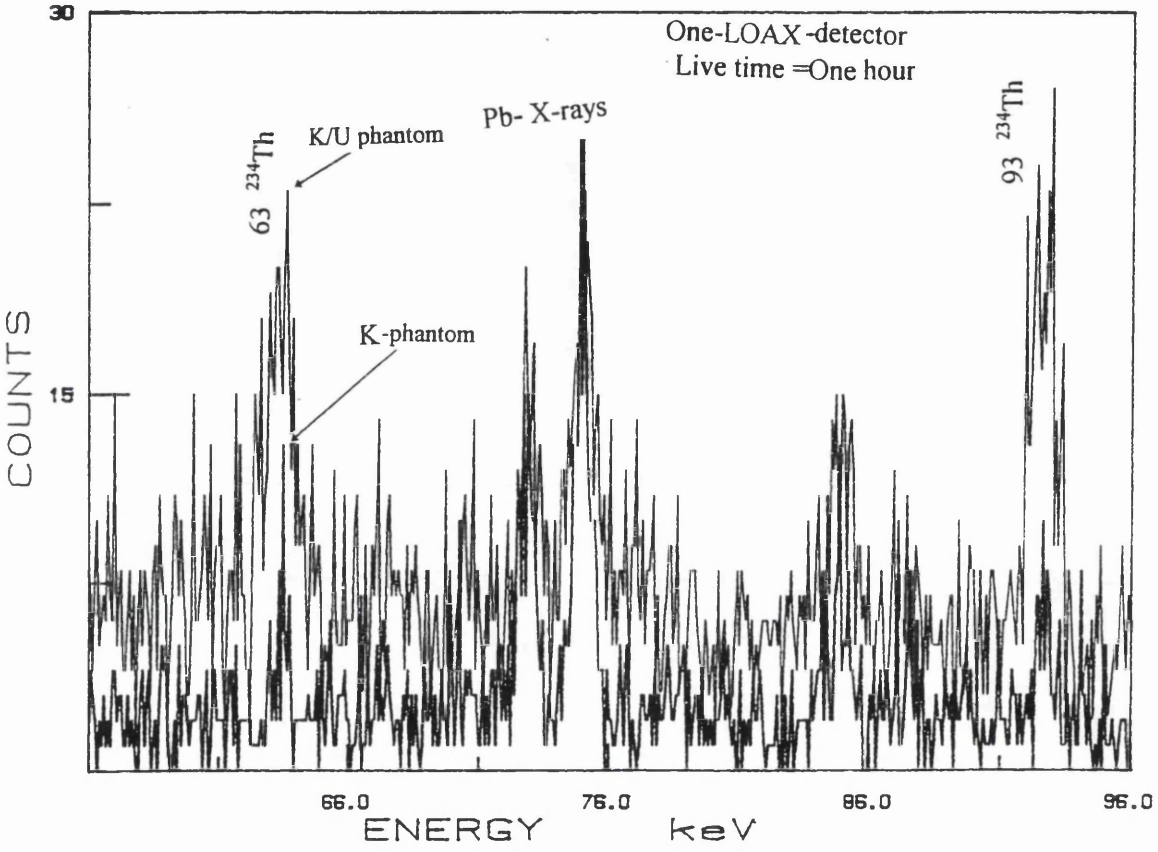

Figure 4.6 Comparison of scanning counts using one LOAX detector measuring K/U and K-phantoms for one hour.

The phantom was also measured using both detection systems in the static mode. The 80% HPGe-detector was over the chest area and the four LOAXs were over the lower abdomen and pelvis. The calculated sensitivity for both detection systems for one hour static counts were found to be 13±3 cpm g^{-1} and 29±5 cpm g^{-1} respectively, and their MDA values were calculated using Equation 3.2 to be 28 mg and 14 mg U. The gamma-ray spectra obtained are shown in Figure 4.7 a & b for both detection systems.

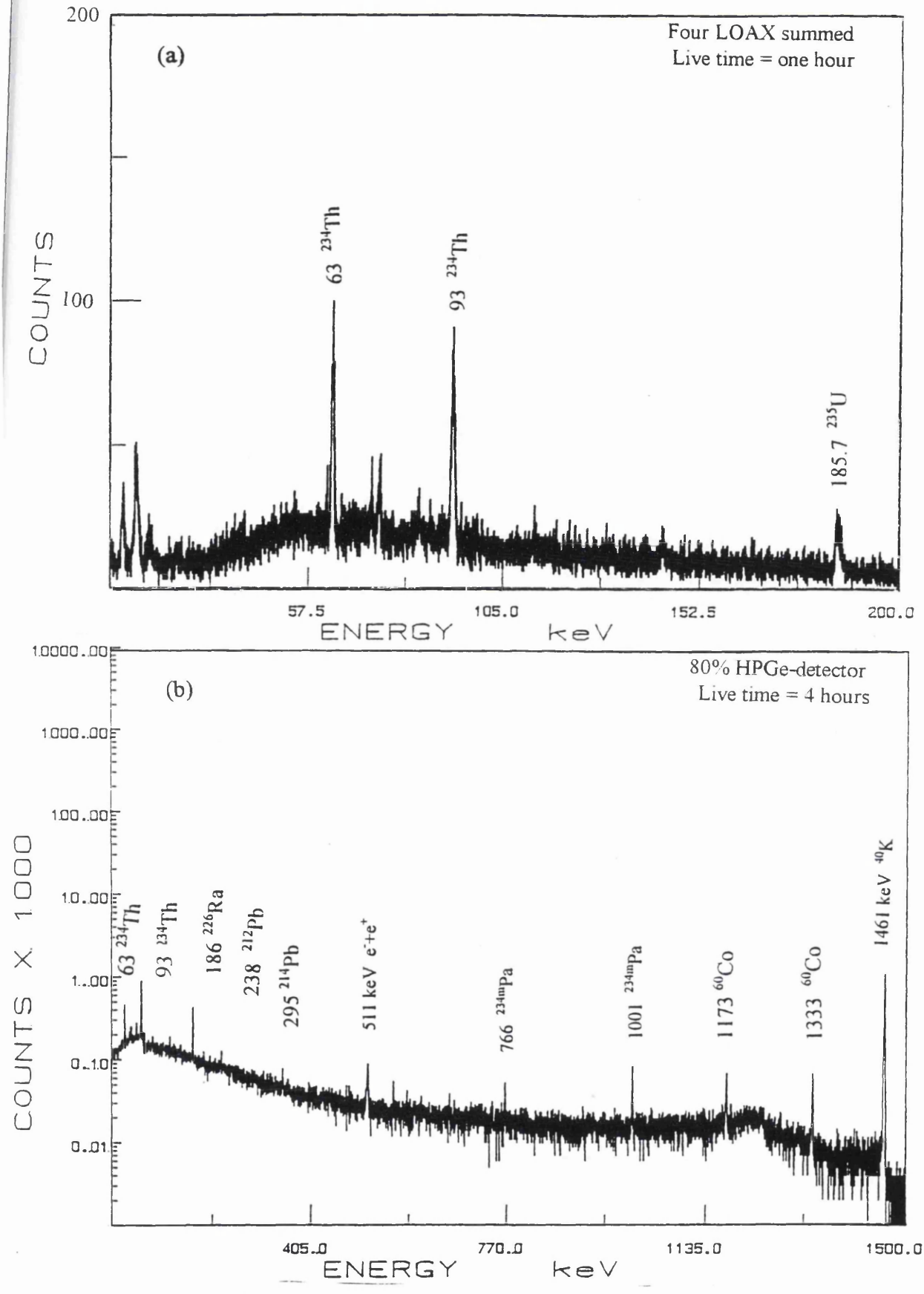

Figure 4.7 Gamma-ray spectra of K/U-phantom: (a) using the four LOAXs and; (b) the 80% HPGe-detector.

In addition to these observations, the chest section was measured separately under the 2 LOAX detectors at different heights and the sensitivity factors as well as the MDAs were found at those heights as outlined in Table 4.4. The chest section was then raised and inverted (to avoid the filler cap) so as to be as close as possible to the detectors. This gave the highest sensitivity factor of 1.26 cps g^{-1} U and a MDA of 4 mg for the 93keV peak (σ_b=2.66x10^{-3} cps) taking two standard deviations of the background count rate. Also the same geometry was used for the 80% detector and the sensitivity found to be 0.56 cps g^{-1} U and a MDA of 7.1 mg for the same 93 keV peak for a one hour count taking two standard deviations of background σ_b=2x10^{-3} cps. These values compared very well with the maximum permissible lung burden for natural uranium of 26 mg. For the same geometry (raised and inverted) the chest section was scanned under both detectors and the sensitivity dropped to 0.17 cps g^{-1} U and the MDA increased to 34 mg for the 80% detector. A sensitivity of 0.34 cps g^{-1} U and a MDA of 26 mg were obtained for the two LOAX detectors summed. Also the same chest section was measured using two LOAXs at three different heights namely: with 8 cm, 5 cm and 1 cm separation. Table 4.5 gives the detailed sensitivities and MDAs for 1 hour static counts in these positions. It was evident that the sensitivity increased as the chest was raised closer to the detectors with a corresponding decrease in MDA. To check the separate response of the LOAXs, the K/U chest section was measured using the same geometry with one, two and four detectors. The data are presented in Table 4.6. The MDA was improved by a factor of greater than 2 as expected when summing two detectors, but it was found to increase by a lesser extent of proportionality, when summing four detectors. This was due to the higher relative increase of background. Finally, using the 80% HPGe-detector the whole K/U phantom was positioned in static mode and measured for one and four hours respectively. Taking the net counts of both the main peaks and the calculated background errors for both counting times of 1 and 4 hours for the K-phantom, the detection sensitivity and MDA were calculated and tabulated in Table

4.7. The sensitivity remained constant, while the MDA was reduced by half for the longer counting time.

Energy keV	Sensitivity at 1cm distance cps g^{-1}	2σ MDA mg	Sensitivity at 4cm distance cps g^{-1}	2σ MDA mg	Sensitivity at 8cm distance cps g^{-1}	2σ MDA mg
13	0.34	17±3	0.21	29±9	0.12	46±18
16	0.56	31±6	0.23	38±11	0.15	115±46
46.5	0.06	35±7	0.04	29±9	0.01	78±31
63	0.92	4±1	0.39	10±3	0.23	17±7
93	1.20	4±1	0.55	8±2	0.34	13±5
186	0.36	11±2	0.16	25±8	0.14	30±12

Table 4.4 Measured sensitivity and calculated MDA for main energy peaks of (chest of K/U phantom) ^{238}U using the two LOAX HPGe-detectors at three different distances.

Energy keV	Net cps cps ± 1σ	Background rate cps ± 1σ	Sensitivity cps g^{-1} U	2σ MDA mg U
63	**$0.061\pm4\times10^{-3}$**	**$0.008\pm2\times10^{-3}$**	**0.22**	**14±4**
93	**$0.144\pm7\times10^{-3}$**	**$0.013\pm2\times10^{-3}$**	**0.51**	**8±2**
186	**$0.089\pm6\times10^{-3}$**	**$0.013\pm2\times10^{-3}$**	**0.32**	**13±4**
766	**$0.015\pm3\times10^{-3}$**	**$0.004\pm1\times10^{-3}$**	**0.05**	**75±23**
1001	**$0.027\pm4\times10^{-3}$**	**$0.004\pm1\times10^{-3}$**	**0.1**	**42±13**

Table 4.5 Count rates and calculated values of sensitivity and MDA for main energy peaks of chest section of (K/U phantom) ^{238}U using the 80% HPGe-detector.

Energy keV	One LOAX detector single BKGR cps±2×10^{-3}	Sensitivity cps g^{-1}	2σMDA mg U	Two LOAX detector summed BKGR cps±2×10^{-3}	Sensitivity cps g^{-1}	2σ MDA mg U	Four LOAX summed BKGR cps±3×10^{-3}	Sensitivity cps g^{-1}	2σ MDA mg U
63	0.014	0.37	11±6	0.019	0.86	4.6±2	0.038	1.46	4.0±2
93	0.017	0.49	8±4	0.019	1.22	3.3±1	0.042	2.03	3.0±1

Table 4.6 Main energy peaks calculated sensitivities and MDA for measuring chest section of K/U-phantom by one, two and four LOAX-detectors summed.

Energy keV	one hour σ_b(cpm)	1 hour-count of whole K/U phantom Net counts cpm±σ(1h)	Sensitivity cpm g^{-1} U	2σMDA mg	4 hour count of whole K/U phantom Net counts cpm±σ(4h)	Sensitivity cpm g^{-1} U	2σMDA mg
63	0.089	2.51±0.20	2.54	70±21	2.50±0.20	2.55	36±5
93	0.148	3.38±0.28	3.45	86±26	3.48±0.27	3.57	32±5
186	0.140	3.49±0.24	3.58	78±23	3.40±0.24	3.47	40±6
766	0.076	0.45±0.09	0.46	332±100	0.489±0.09	0.50	152±23
1001	0.029	1.12±0.14	1.12	52±16	0.808±0.12	0.82	34±5

Table 4.7 Measured counts per minute, calculated sensitivity and MDA for whole K/U phantom measured in static geometry under the 80% HPGe-detector for one and four hours.

Also a comparison was carried out between one and four hour count of both complete phantoms measured separately in static mode using the 80% HPGe-detector. Representative gamma-ray spectra for the main low-energy peaks are presented in Figure 4.8. From the figure shown, it could be clearly seen that low-count peaks appear in the background of the K phantom. These are the 63 and 93 keV peaks of the ^{234}Th and are typical of a subject spectrum.

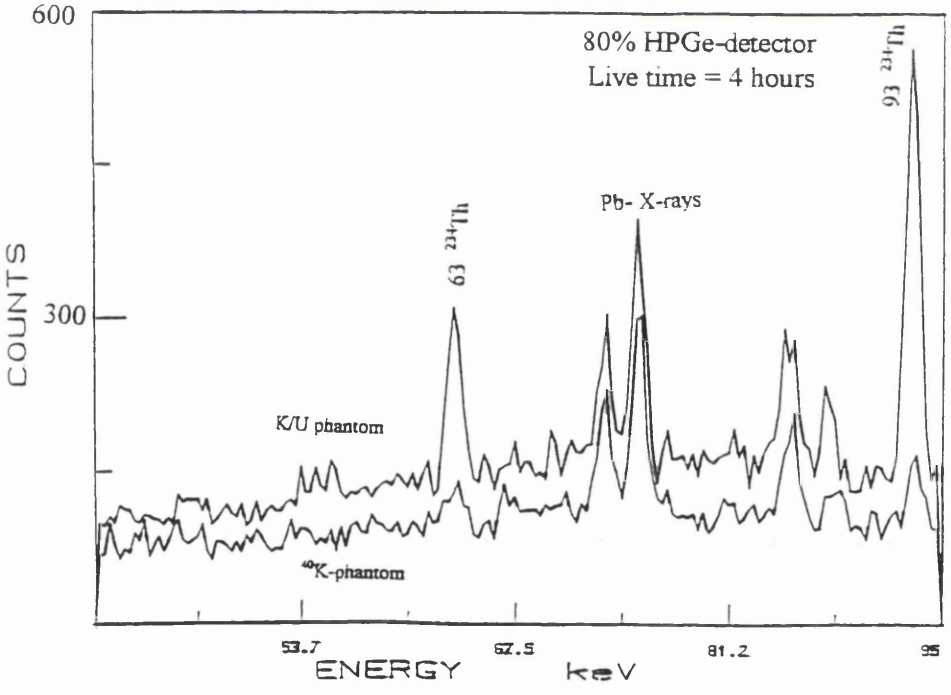

Figure 4.8 A comparison between the complete K and K/U phantoms in static mode under the 80% HPGe-detector.

4.2.3 Uranium bottle phantoms

To investigate further the detection capability of the whole-body monitor detectors, four plastic phantom bottles were prepared having 1000, 100, 10, 1 mg of natural uranyl nitrate [$UO_2(NO_3)_2 6H_2O$]. The four phantoms were prepared from a stock solution of 0.2247 g of uranyl nitrate in 100 ml demineralised water which gave 1 mg of U per 100 ml and then added to the bottles with 2000 ml demineralised water. All four phantoms and the blank which contained only demineralised water were measured under the four LOAXs and the 80% HPGe-detector. Figure 4.9 shows the complete spectrum obtained for the 10 mg U bottle measured at a distance of approximately 4 cm from four LOAX detectors for a one hour count. At the same time, Figure 4.10 shows the stepwise increase of the main peak activities for the 63 and 93 keV for 1, 10, 100, and 1000 mg uranium phantoms measured with the four LOAXs detectors. Table 4.8 gives the calculated sensitivities and the MDA for the two systems respectively. Graphically, it could be seen that 1 mg U peaks at 63 and 93 keV are shown just above the background peak of the blank water bottle measured under the same geometry and counting time of 1 hour.

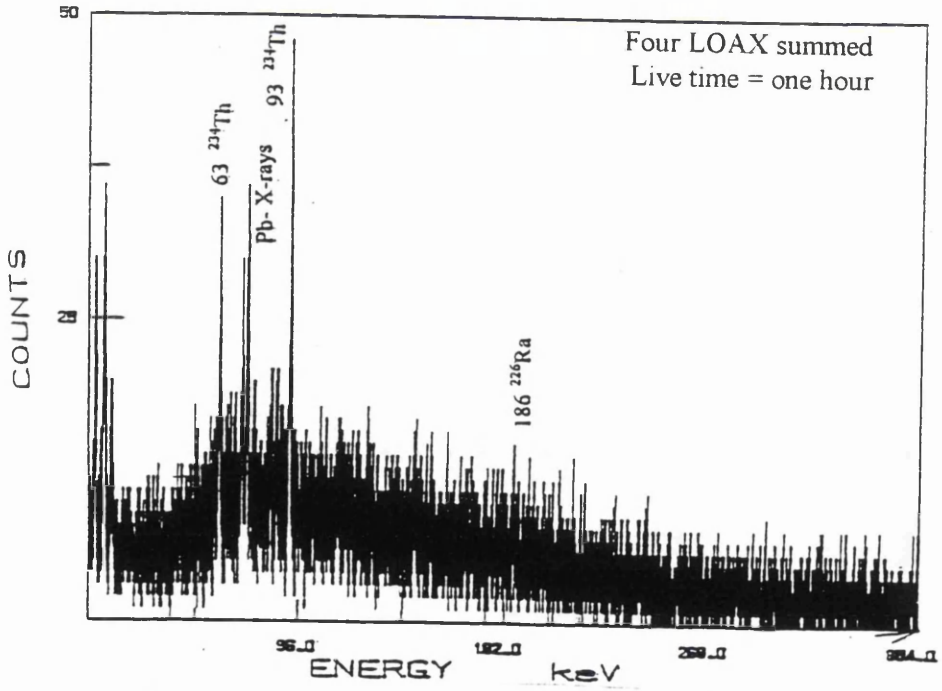

Figure 4.9 The gamma-ray spectrum obtained for 10 mg U at 4 cm from the four LOAX HPGe-detectors summed.

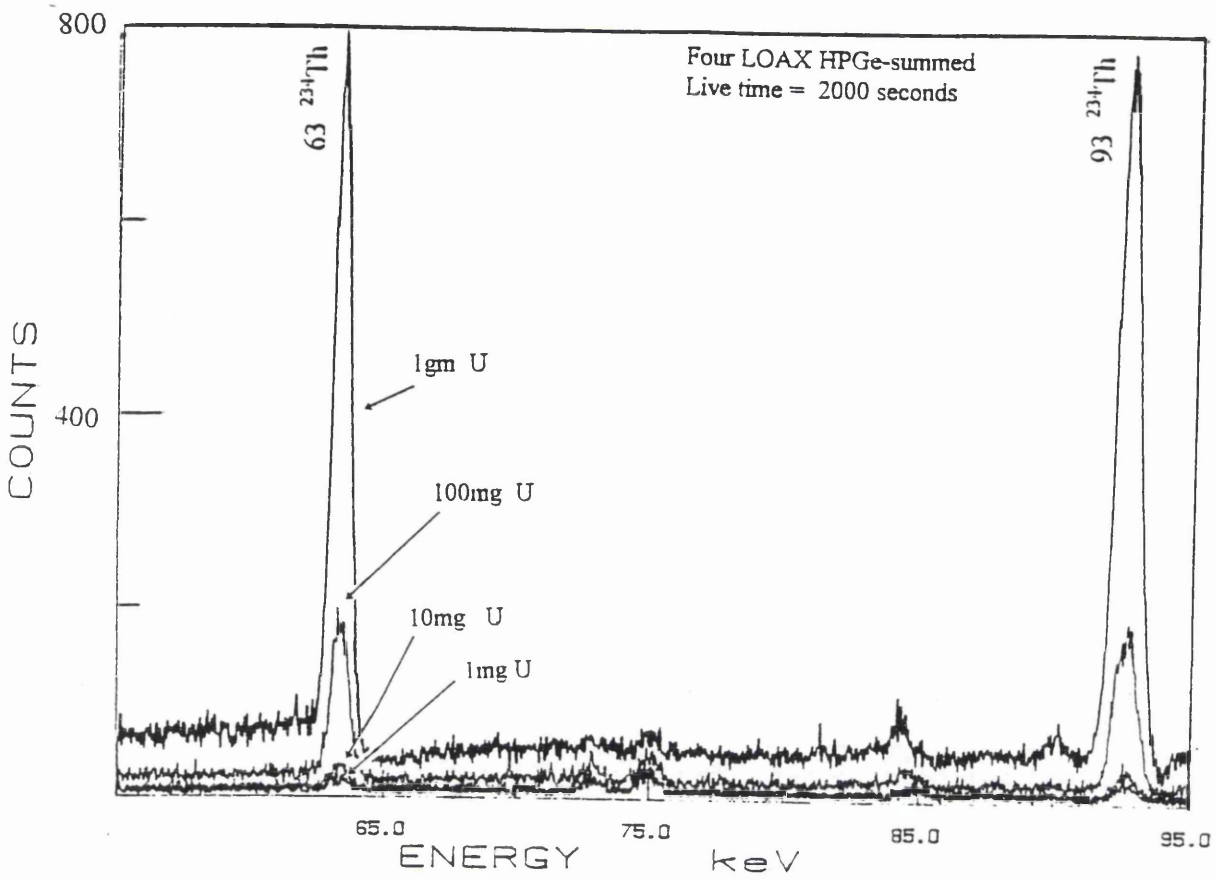

Figure 4.10 The stepwise increase of activity for the spectra obtained measuring the set of uranium phantoms; 1, 10, 100, 1000 mg with the four LOAX detectors summed.

From Table 4.8 it could be seen that the MDA values varied when counting low activity due to background interference. However, it leveled off when measuring higher activity and it became independent of counted uranium activity as you would expect it.

Weight of U in bottle	Data for the four LOAX					
	63 keV		2σ	93 keV		2σ
	cps±1σ	(cps mg^{-1})	MDA (mg)	cps±1σ	(cps mg^{-1})	MDA(mg)
Blank	0.056±0.004	---	----	0.071±0.004	---	---
1mg	0.023±0.006	0.023	0.35±0.1	0.022±0.006	0.022	0.36±0.1
10mg	0.045±0.007	0.005	1.78±0.3	0.094±0.008	0.009	0.86±0.1
100mg	0.663±0.015	0.007	1.20±0.2	0.851±0.016	0.009	0.94±0.1
1gm	5.84±0.04	0.006	1.32±0.2	7.09±0.04	0.007	1.12±0.2

Table 4.8 Calculated detection sensitivities and MDA values for the uranium bottle phantoms using four LOAX detectors.

4.2.4 Depleted uranium metal samples

To study further the isotopic distribution and the ^{238}U parent-daughter relationships and to investigate the MDA of the whole-body monitor detectors, metal samples of depleted uranium weighing 1, 10, 100, 1000, 5000 and 10,000 mg were placed in separate plastic bags and measured using the two LOAX array and the 80% HPGe to examine the MDAs. The samples were measured in static mode separately under each detector system and the measured count rates for the main energies were tabulated in Table 4.9. Generally it could be seen that the count rates increase with the increase of the weight of the uranium sample but not in constant proportionality. This fact probably was due to the self absorption of the these energies by the thickness of the various weights of the uranium it self. This could be clearly seen in Figure 4.11 from the gamma-ray spectra collected using four LOAX detectors summed, measuring the blank, 1 mg and 10 mg uranium metal samples. Figure 4.12 shows the gamma-ray spectra of the blank and 10 mg of metal uranium using the 80% HPGe-detector. The aim was to ascertain at what activity the uranium was no longer detectable. This was designed to cross-check whether or not the MDAs previously found were correct.

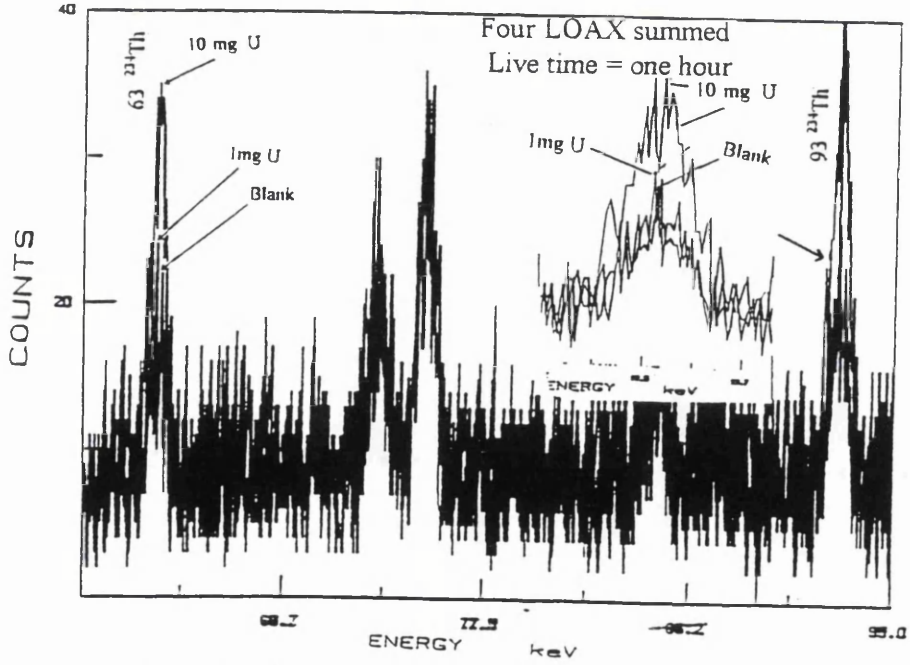

Figure 4.11 Comparison of detection limits between gamma-ray spectra of blank, one mg, and 10 mg of metal uranium using four LOAX detectors summed.

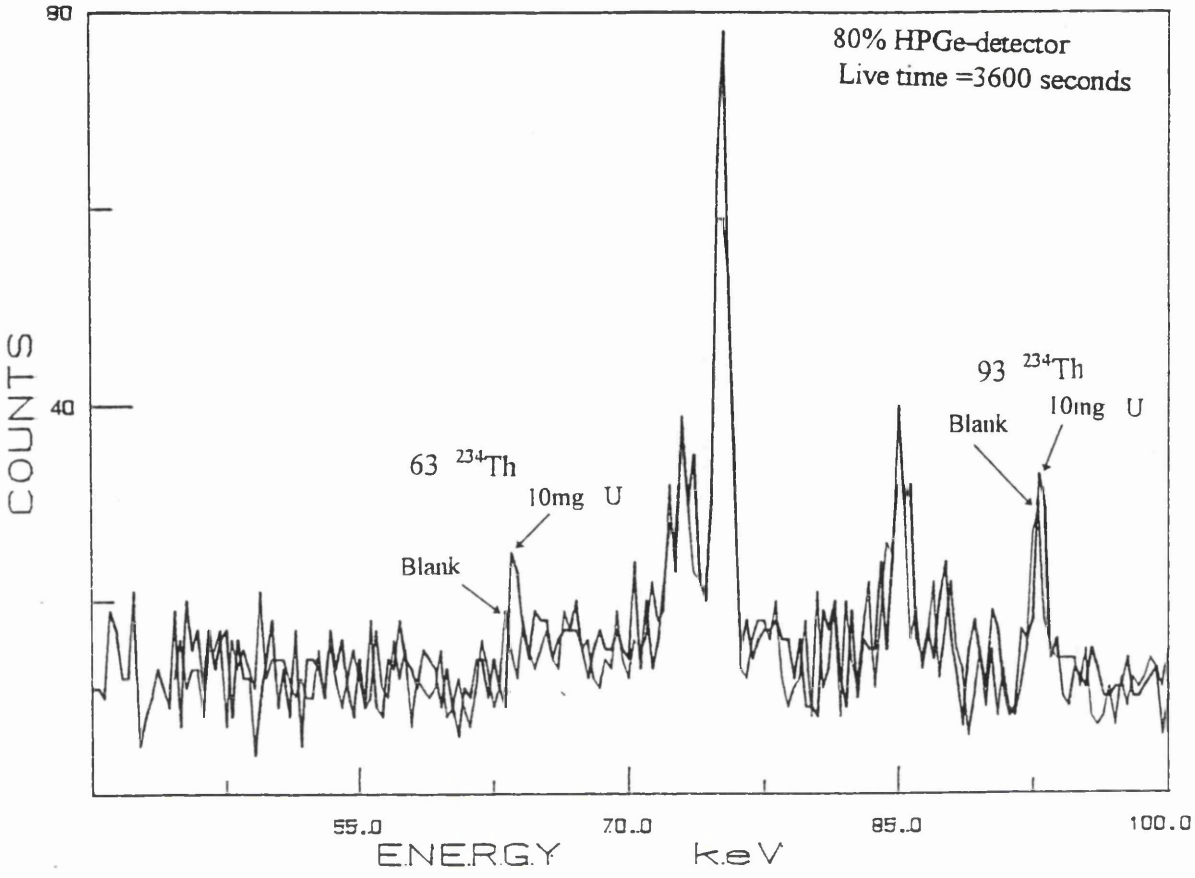

Figure 4.12 Comparison of detection limits between blank and 10 mg metal uranium using the 80% HPGe-detector.

It could be clearly seen that the 80% detector had a detection limit of approximately 10 mg whilst the combined four LOAX detectors give a value well below 10 mg, probably down to about 2 mg. Also, the different samples were measured in scanning mode under the detection systems at 8.5 cm from 80% HPGe-detector and a number of calibration curves were constructed. At the same time a number of static measurements were taken on each sample and a set of calibration curves were made using the net count rates for each of the main energy peaks versus the weight of each measured metal sample. A representative calibration curve for the static count is shown in Figure 4.13,

and Table 4.10 represents a complete table of the two sets of results was prepared by taking the slope to calculate the sensitivity and using the background counting rate to calculate the MDA for both counting modes. These calibration procedures were carried out for static and scanning counts of the metal uranium samples measured. From Table 4.10, it can be seen that the static mode had much higher counting efficiency and it was about ten times better as the count ratio indicates.

Weight of U- metal	Data for the two LOAX		Data for the 80%HPGe-detector energies		
	63 keV	93 keV	63 keV	93 keV	186 keV
Blank	0.88±0.12	1.25±0.02	3.82±0.25	3.88±0.25	3.27±0.23
1mg	2.1±0.3	3±0.3	3.0±0.4	7±0.5	2.5±0.4
10mg	11±1	17±1	26±1	83±1	24±1
100mg	27.83±1	68±1	96±1.3	485±3	126±2
1gm	96±1	231±2	302±2.3	961±4	435±3
10gm	667±3	1691±5	471±3	1690±5	857±4

Table 4.9 Net counts per minute for the depleted uranium metal sample counted in static mode using two LOAX and the 80% HPGe-detectors.

Energy keV	Static Sen. Cpm g^{-1} U	Static 2σ MDA mg U	Scanning cpm g^{-1} U	Scanning 2σ MDA mg U	Ratio scan./static
63	0.0055	11	0.036	72	7
93	0.0019	4	0.015	30	8
186	0.0027	6	0.028	56	10
766	0.0043	8	0.045	90	10
1001	0.0019	4	0.028	56	14

Table 4.10 Data taken using calibration curves of count rates versus ^{238}U metal weight of samples at 8.5 cm distance of 80% HPGe-detector.

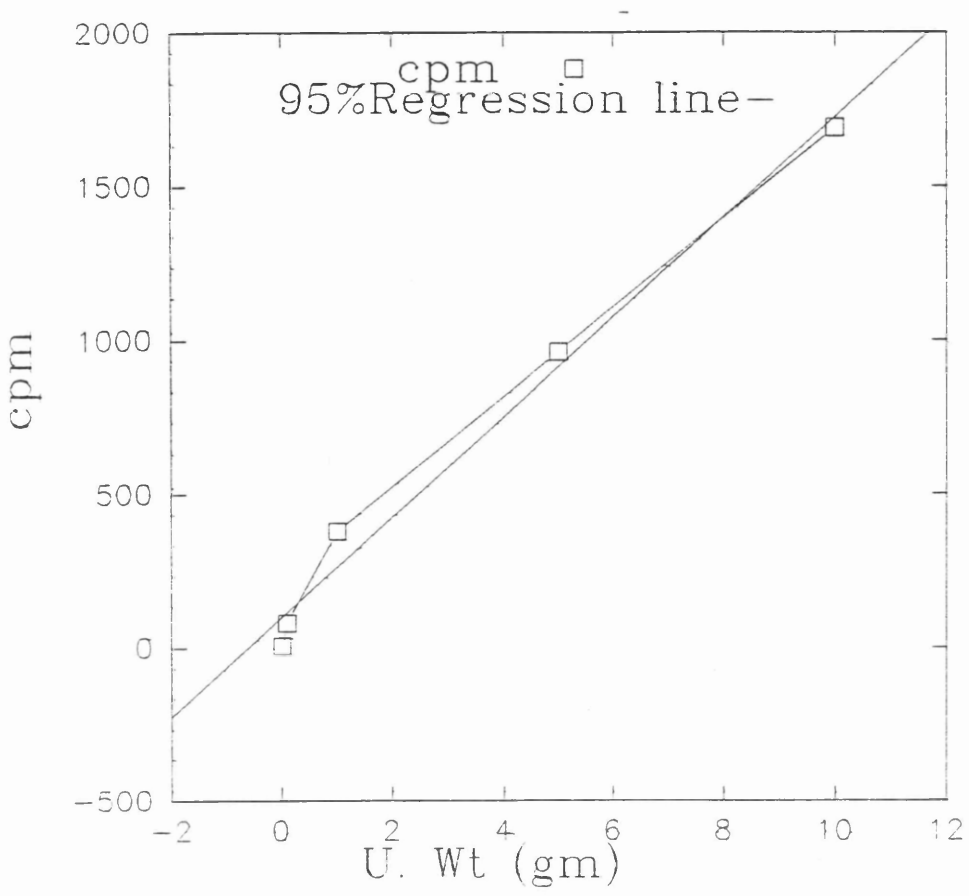

Figure 4.13 Calibration curve of the sensitivity of 80% HPGe-detector using the net count rate versus different Uranium metal weights.

4.2.5 ^{134}Cs and ^{137}Cs BOMAB phantoms

To calibrate for ^{134}Cs and ^{137}Cs, two phantoms previously prepared after the Chernobyl accident (23.11.1988) were used. Details of the phantoms are outlined in Tables 4.11 and 4.12. Column five presents the calculated corrected activities for the recent measurement dates (25.10.1994). The ^{137}Cs could be measured by the two detection systems using different photons as it decayed to the ground state of ^{137}Ba which emitted X-rays at 31, 32 and 36 keV in addition to the high energy gamma-ray at 662 keV as outlined in Table 4.13.

Phantom section	Fraction of total %	Required wt of std.sol (g)	Actual wt of std.sol. (g)	Activity of ^{137}Cs (Bq)	Corrected activity ^{137}Cs(Bq)
Head	5.6	50	50	559	487
Neck	1.5	13	13	149	130
Chest	27.6	249	250	2768	2413
Pelvis	16.5	149	149	1653	1441
Thigh R	10.6	96	97	1071	934
Thigh L	10.6	94	94	1041	907
Leg R	7.0	64	65	719	627
Leg L	7.0	62	62	693	604
Arm R	6.8	61	61	678	591
Arm L	6.8	62	62	689	601
Total				10020	8735

Table 4.11 ^{137}Cs activity values and phantom preparation data.

Phantom section	Fraction of total %	Required wt. of Std.Sol (g)	Actual wt of Std. Sol. (g)	Activity of ^{134}Cs (Bq)	Corrected activity ^{134}Cs(Bq)
Head	5.58	28	28	375	51
Neck	1.49	7	7	96	13
Chest	27.65	138	139	1858	254
Pelvis	16.54	83	83	1108	151
Thigh R	10.69	53	54	726	99
Thigh L	10.41	52	512	693	95
Leg R	7.14	36	36	480	66
Leg L	7.91	35	34	459	63
Arm R	6.82	34	34	455	62
Arm L	6.79	34	34	458	63
Total			502	6708	916

Table 4.12 ^{134}Cs activity values and phantom preparation.

^{137}Cs-Decay	Energy	% Abundance
K_α	31.817	1.99
K_β	32.194	3.68
Gamma-ray	36.5	1.34
Gamma-ray	661.66	85.20

Table 4.13 ^{137}Cs X-and gamma-ray energies and abundance

Firstly, the ^{137}Cs phantom was measured in both scanning and static counting modes using the two detection systems. The scanning sensitivity for the 80% HPGe-detector was calculated to be 1.19×10^{-4} cps Bq^{-1} and using the 662 keV peak a MDA of 35 Bq

was calculated for a counting time of 30 minutes. Also the chest section alone was counted along with the water phantom parts and its sensitivity was calculated to be 7.58×10^{-4} cps Bq^{-1} with a MDA of 20 Bq for a 30 min count. These results compared favourably with the large NaI (Tl) detectors which gave 9.5 cps kBq^{-1} and MDA of 26 Bq. Figure 4.14 shows a typical gamma-ray spectrum of the whole ^{137}Cs phantom in comparison with a K-phantom spectrum counted for 4 hours using one LOAX detector. The low-energy peaks are clearly defined. Figure 4.15 a & b presents the 80% HPGe-detector gamma-ray spectra for ^{137}Cs and ^{134}Cs phantoms. Also the whole phantom was measured using three LOAXs summed and the 80% HPGe-detector followed by a series of measurements, each time removing phantom sections starting with the extremities and counting for 2000 seconds.

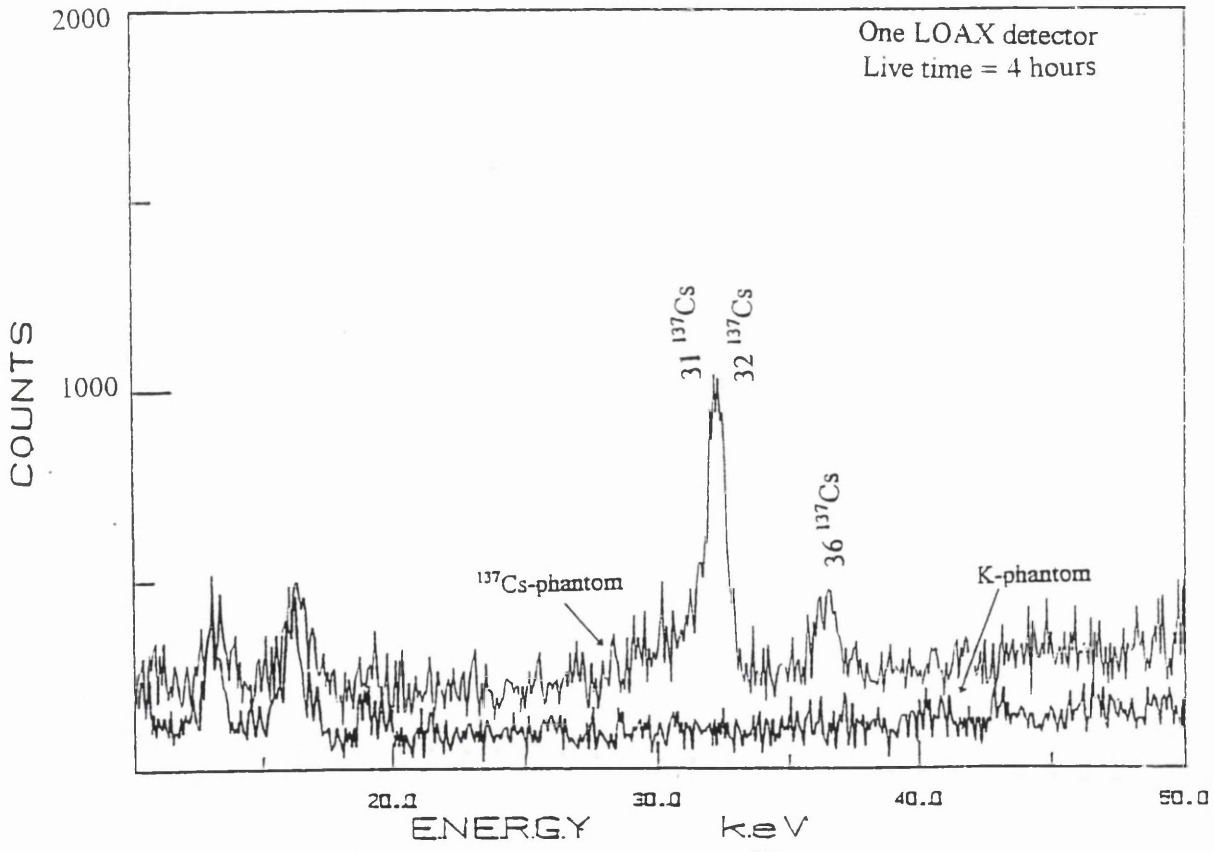

Figure 4.14 A Typical γ-ray spectrum of ^{137}Cs using one LOAX detector in comparison with K-phantom.

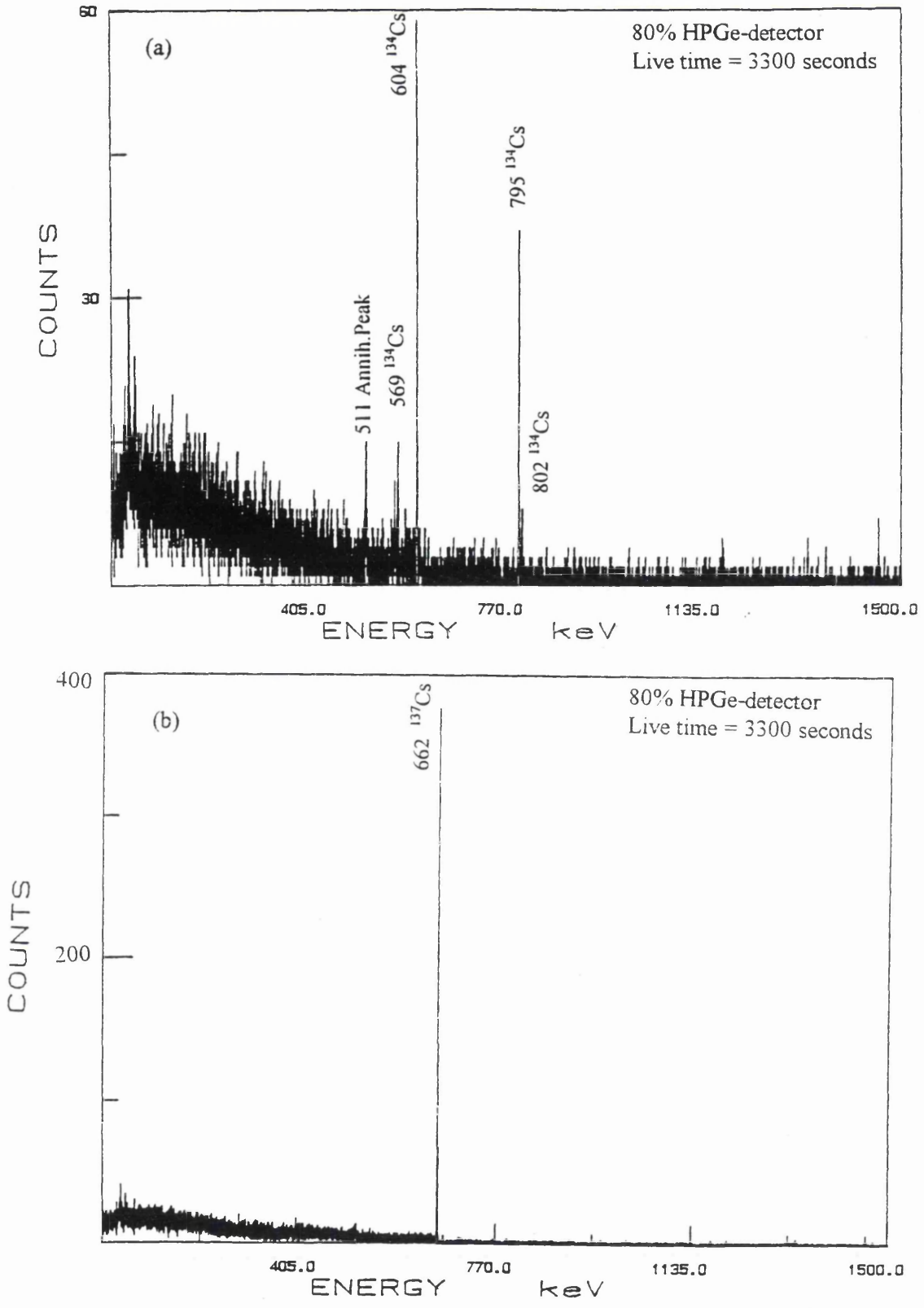

Figure 4.15 Gamma-ray spectra obtain using the 80% HPGe-detector measuring; (a) for ^{134}Cs; (b) for ^{137}Cs.

Tables 4.14 and 4.15 give details of the sensitivities and MDA values for the 80% HPGe- and the LOAX-detectors measuring ^{137}Cs and ^{134}Cs for one hour counts respectively. It could be seen that the three LOAXs were able to detect the ^{137}Ba X-ray. The sensitivity values for the measurement of ^{137}Cs indicate a high degree of uniformity of detection; the normalised sensitivity values in column 4 of Table 4.14 range from 91-114% for the phantom configurations selected. The corresponding measurements with the LOAX detectors showed greater variability with increases up to 34%.

Phantom Sections	^{137}Cs Bq±1%	662keV cpm±1σ	Sensitivity cpm kBq^{-1} (%)*	MDA (Bq)	1462keV cpm±1σ
Complete water phantom	Blank	1.1±0.2	------	----	1.15±0.14
Compete ^{137}Cs-phantom	8735	79±1	9 (100%)	29	1.21±0.14
^{137}Cs-phantom w/o arms	7543	69±1	9 (102%)	28	1.27±0.15
^{137}Cs-phantom-w/o arms & legs	6312	62±1	8 (91%)	32	1.22±0.14
^{137}Cs-Phamtom w/o arms, legs & thighs	4471	46±1	10 (114%)	25	1.24±0.14
^{137}Cs chest and pelvis	3854	37±1	10 (107%)	27	1.20±0.14
^{137}Cs chest only	2413	22±1	9 (102%)	28	1.21±0.14

Table 4.14 Count rate per minute and sensitivities of the main energy peaks for scanning measurements of various parts of the ^{137}Cs-phantom using the 80% HPGe-detector. *Normalised factors in percentage.

Phantom Sections	^{137}Cs Bq	31.82keV cpm±1σ	31.82keV cpm kBq^{-1} (%)*	36.5keV cpm±1σ	36.5keV cpm
Complete water phantom	Blank	0.312±0.07	----	0.316±0.07	-----
Compete ^{137}Cs-phantom	8735	10±0.4	1.11(100%)	5.09±0.32	0.58
^{137}Cs-phantom w/o arms	7543	9±0.4	1.19 (107%)	4.11±0.28	0.55
^{137}Cs-phantom w/o arms & legs	6312	9±0.4	1.42 (128%)	3.42±0.26	0.54
^{137}Cs-Phamtom w/o arms, legs & thighs	4471	6±0.3	1.29 (116%)	3.03±0.25	0.68
^{137}Cs Chest and pelvis	3854	6±0.3	1.48 (133%)	2.46±0.23	0.64
^{137}Cs Chest only	2413	4±0.3	1.49 (134%)	1.03±0.17	0.43

Table 4.15 Count rate per minute of the main energy peaks for scanning measurements of various parts of the ^{137}Cs-phantom using three LOAX-detectors summed. *Normalised factors in percentage.

This is probably due, to the non-optimum position of the LOAX detector array in relation to the standard scanning position and to the inherently limited field of view of the LOAX-detectors. It was also noticed that the background count rates for the peak 93 keV increased up to 10% margin with the increase of ^{137}Cs activity due to the Compton effect while the 1461 keV was not affected at all.

Table 4.16 gives the scanning sensitivity for different counting times, which clearly indicates that the longer the counting time the lower the corresponding MDA due to reductions in standard deviation of the background count rate.

Number of scans	Net counts per minutes	Background 1St.deviation	Sensitivity (cpm Bq^{-1})	2σ MDA Bq
20 (2400sec)	**1.05±0.02**	**0.002**	**$1.19x10^{-4}$**	**35±7**
10 (1600sec)	**1.05±0.02**	**0.003**	**$1.19x10^{-4}$**	**54±16**
4 (700sec)	**0.99±0.02**	**0.005**	**$1.13x10^{-4}$**	**80±28**

Table 4.16 Count rates, calculated sensitivities and MDA for the whole ^{137}Cs phantom scanned using different scanning times by the 80% HPGe-detector.

Secondly, the ^{134}Cs phantom was measured under the same static and scanning geometries and Table 4.17 gives the count rates for the main energies and their calculated sensitivities and MDA for the 80% HPGe-detector. It could be seen that the two main energies used for ^{134}Cs are the 604 and 795 keV with MDA of 61±15 Bq to 70±18 Bq respectively.

Energy keV	Background (cps ± 1σ)	Net cps (cps ± 1σ)	Sensitivity cps Bq^{-1}	2σ MDA Bq
604	$(1.43±0.2)x10^{-2}$	$(8±0.5)x10^{-2}$	$6.51x10^{-5}$	61±15
795	$0.91±0.16)x10^{-2}$	$(5±0.5)x10^{-2}$	$4.56x10^{-5}$	70±18

Table 4.17 Calculated sensitivities and MDA for the ^{134}Cs phantom measurement using the 80% HPGe-detector for 1 hour count.

4.3 Tissue equivalent phantoms (TEP)

4.3.1 Historical background

Theoretically derived calibration values for *in vivo* measurements using Monte Carlo calculation methods have been carried out by a number of researchers (Scott et al, 1977). They involve much simulation and computer calculation data but they do give reliable calibration results. However, with the establishment of the United States Transuranium Registry (USTR) which was considered to be a national centre for the acquisition and dissemination of information about the metabolism of transuranic radionuclides in transuranium workers, a number of entire human bodies of previous accidentally exposed workers containing easily measurable radioactivity were donated. They were measured *inter alia* by body counting methods before tissue chemical analysis so that the detectors could be calibrated in counts per Becquerel (Bq) (Palmer et al., 1984). These donated bodies represent a superior method of detector calibration because the radioactivity exists in its "natural" non-uniform distribution within the body and in the individual organs such as bone, lung, and liver. A whole-body was donated to the USTR containing 5.4 kBq of ^{241}Am and Palmer (Palmer et al., 1985) used the gathered data to prepare a skull calibration phantom containing 672 Bq of ^{241}Am and reported only 0.3% difference in the counting efficiency when it compared to the actual skull content. These measurements confirmed the ability to construct authentic skull phantoms (Cohen, 1984) for use in the assessment of skeletal ^{241}Am (Hickman and Cohen, 1988).

The scientific evidence and data obtained from various measurements of real human cadavers, internally contaminated with transuranic nuclides, were therefore utilized to construct a number of tissue equivalent phantoms for use as human surrogate structures containing known quantities of radioactive nuclides.

Linear scan measurements made over the total body length of an internally contaminated subject, showed that peak deposition activities occur over bone joints and the skull (McInroy et al., 1989). This finding was later supported by the highly sensitive

radiochemical analysis of all the long bones and their joints. Consequently more emphasis was placed on measuring the skull content as a measure of total skeletal content assuming that skull bone constitutes about 15% of the total skeletal bone mass. It had been shown that about 15% of the radionuclide deposited in bone was found to be localised in the skull (Cohen et al., 1977) and (Toohey, 1981).

For this reason the USTR reconstructed a number of skulls for the purpose of producing a calibration structure to be used for determining ^{241}Am and ^{210}Pb skeletal content from *in vivo* measurements. A number of these artificially labelled real skulls were prepared by coating the bone surfaces respectively with ^{241}Am and ^{210}Pb in a pattern representative of natural deposition (Hickman and Cohen, 1988). In one skull the internal surfaces were coated and in the other, the external surfaces were painted with a known amount of ^{214}Am or ^{210}Pb activity. Each skull was covered with the appropriate amount of tissue equivalent material, and the internal cavities were filled with the same material (Toohey et al., 1991). For other parts of the body similar techniques were used to prepare phantoms from real bones in combination with tissue equivalent materials. These include the thoracic region, arms and legs.

4.3.2 Tissue equivalent phantom characteristics

For the purpose of calibrating our detection system a number of tissue equivalent phantoms, namely skulls, labelled externally and internally, thorax, arm, leg and the highly specialized Lawrence Livermore torso (lung) model were available from the National Radiological Protection Board (NRPB). These phantoms were labelled with ^{241}Am, ^{210}Pb and natural uranium and are shown in Figure 4.16. Their activities are listed in Table 4.18. These phantoms, were made of mixtures of polyurethane and $CaCO_3$ material to represent the attenuation and the gamma scattering properties of actual human tissue (Griffith et al., 1984). This tissue equivalent thorax represented that of an average -size Caucasian male and weighted about 40 kg. It consisted of: a complete vertebral column, complete rib cage including cartilage; and sternum scapulae and

clavicles. It contained a total of 9.2 kBq of ^{241}Am which had been applied to these parts including the cervical thorax and lumbar portions of the vertebral column (Palmer et al., 1985).

Phantom description	Activity in kBq labelled	
	Internally	Externally
^{241}Am-head skull	5.08	5.14
^{210}Pb- head skull	4.75	4.86
^{241}Am-thorax	9.2	---------
^{241}Am-left arm	6.53	---------
^{241}Am-left leg	11.93	---------

Table 4.18 Activity content of tissue equivalent phantoms.

To calibrate and determine the sensitivity of the detection systems, the above phantoms were measured separately using the 80% and the two or four LOAX HPGe-detectors in different relevant geometries as outlined in the following sections.

4.3.3 Field of view (FOV) measurements

In order to determine the optimum field of view (FOV) of the detectors, that is the positions where the best counting geometries and the highest sensitivities are obtained, the phantoms were measured at various heights and positions, with the addition of appropriate water phantom sections to simulate the whole body. The sensitivities obtained for the (FOV) of both systems are shown in Figure 4.17. The ^{241}Am thorax was placed on the bed surface at approximately 8cm from the detector surface and moved longitudinally in 5 cm increments. It can be seen that the response for the two LOAX detectors was steady for 20 cm around the centre line and then drops off to more than 50% of its original values at both sides. For the 80% HPGe-detector the relatively constant region only extends to 15 cm and then also drops by 80% on both sides.

The highest sensitivity for each system was found to be 4.05×10^{-4} and 1.12×10^{-4} cps Bq^{-1} ^{241}Am for the LOAX and 80% HPGe-detectors respectively as shown in Figure 4.17. Similar measurements were carried out for the same thorax phantom in a raised position, 5 cm from the detector surfaces. For this arrangement the counting sensitivities increased by 15% and 20% respectively.

Figure 4.16 All the tissue equivalent phantoms that were used for the measurements.

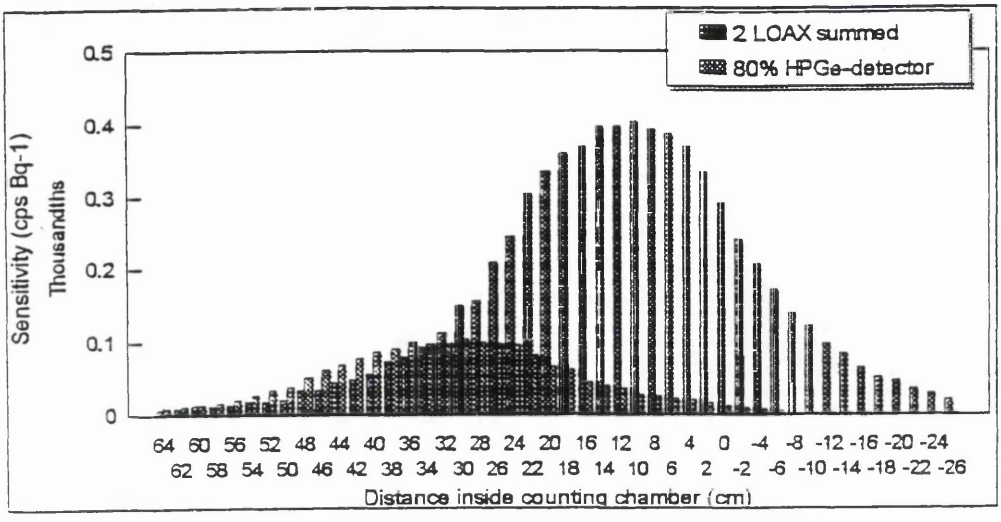

Figure 4.17 Combined field of view of ^{241}Am thorax measured using two LOAX detectors summed and the 80% HPGe-detector.

Also the same field of view measurements were carried out for the skulls labelled with the ^{210}Pb and ^{241}Am. For the ^{210}Pb externally labelled skull, using the two LOAX detectors, the steady sensitivity range of (1.7-1.9)x10^{-4} cps Bq^{-1} for 46.4 keV was found to extend 10 cm only and then start to drop on both sides substantially. For the 80% detector the sensitivity values were one order of magnitude lower than that for the two LOAX detectors of (2.0-2.7)x10^{-5} cps Bq^{-1}. The range extended only 10 cm as shown in Figure 4.18 and it could be clearly seen that the 80% HPGe-detector was not suitable for the measurements of the low-energy ranges. The same field of view ranges were observed for the 59.5 keV of ^{241}Am skull with a higher sensitivity factors of (1.2-2.2)x10^{-3} and (2.2-4.7)x10^{-4} cps Bq^{-1} for the two LOAX and the 80% detectors respectively.

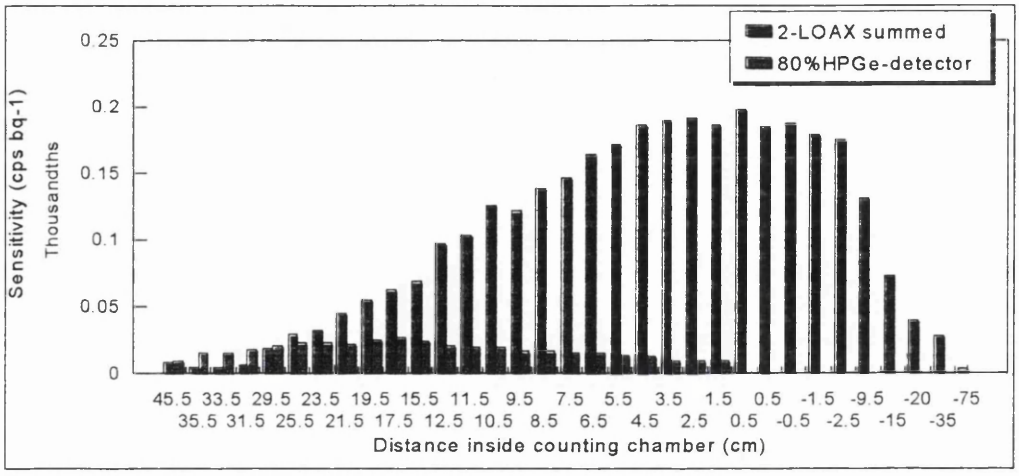

Figure 4.18 Combined field of view of sensitivity for the externally ^{210}Pb skull using the two LOAX and 80% HPGe-detectors.

4.3.4 Static and scanning measurements

Having examined the field of view characteristics of the LOAX and 80% detectors the sensitivities were further measured in static counting mode with the aim of optimising counting conditions for use *in vivo*. Tables 4.19 and 4.20 outline all the sensitivities (cps Bq^{-1}) and the MDA obtained for the 80% and the two LOAX HPGe-detectors respectively using static counting geometries at two selected distances and one hour counting times.

	Phantom to detector distance	
	5 cm	8 cm
Sensitivity(cps Bq^{-1})	1.06×10^{-4}	8.54×10^{-5}
MDA (Bq)	67±13	83±25

Table 4.19 Measured sensitivities (one hour count) in cps Bq^{-1} ^{241}Am thorax measured in static mode using the 80% HPGe-detectors at two different distances.

Phantom descriptio	17 keV cps Bq^{-1}	MDA Bq	26keV cps Bq^{-1}	MDA Bq	59 keV cps Bq^{-1}	MDA Bq
Thorax at 8cm	$1.16x10^{-5}$	526±184	$4.02x10^{-6}$	3734±1494	$1.54x10^{-4}$	41±10
Thorax at 5cm	$1.58x10^{-5}$	386±116	$5.33x10^{-6}$	2816±986	$3.96x10^{-4}$	16±3

Table 4.20 Measured sensitivities cps Bq^{-1} (1hour count) for ^{241}Am-thorax measured using two LOAX HPGe-detectors summed at two different distances from detectors surfaces.

Also, a number of counts were taken on different combinations of phantoms placed simultaneously under detectors at various distances to demonstrate the ability of the detectors to measure these low-energy emitters simultaneously if required and in the presence of higher energy emitters. Figure 4.19 gives a combined gamma-ray spectrum obtained for measurement of ^{241}Am thorax, ^{210}Pb skull and ^{137}Cs pelvis using two LOAX detectors summed. It could be seen that all the relevant peaks are well defined.

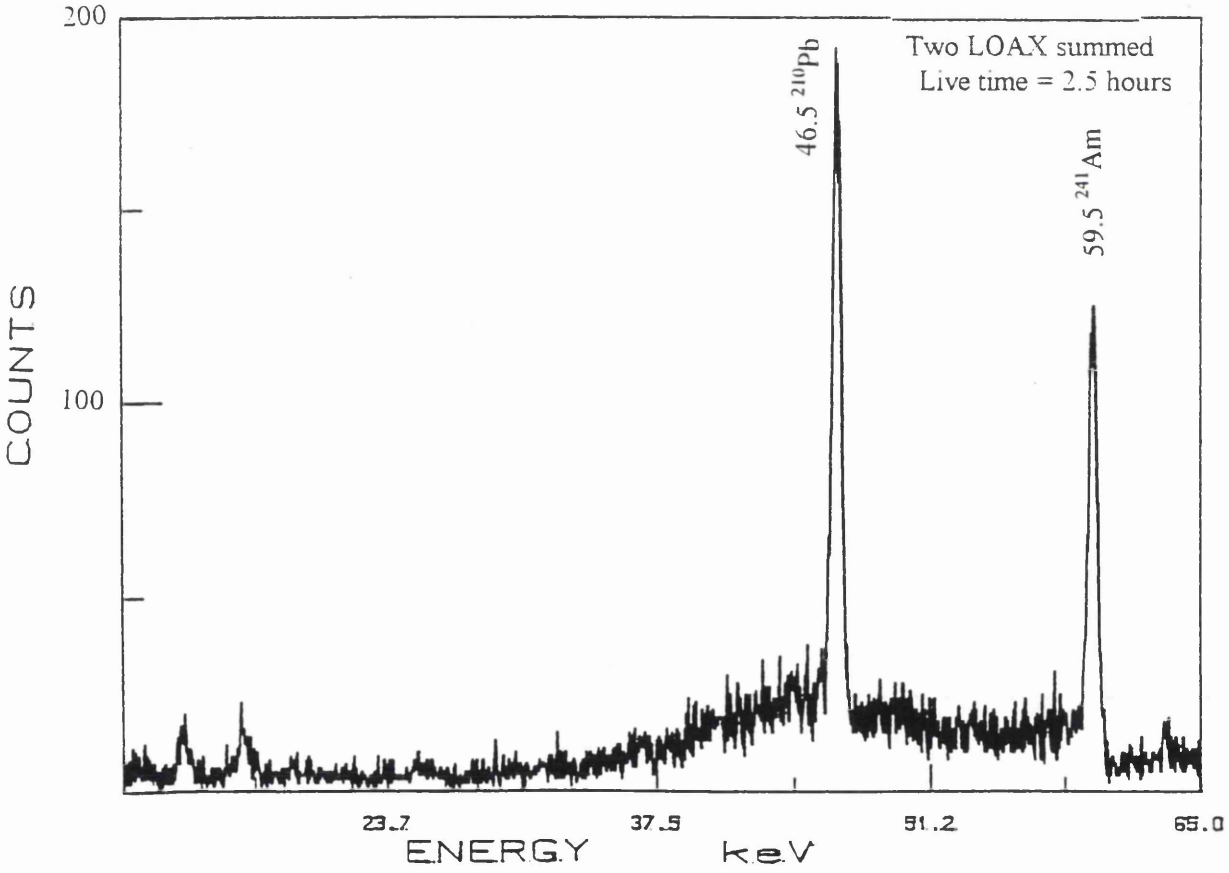

Figure 4.19 Typical gamma-ray spectrum of combined ^{241}Am-thorax, ^{210}Pb-skull and pelvic ^{137}Cs sources using two LOAX detectors summed.

4.3.5 Comparison of static counts between detection systems

Because of the close proximity of the semiconductor detectors (20 cm longitudinal separation), it was possible to carry out simultaneous counts on different parts of the subject. Thus, whilst the LOAX detectors were measuring the head, the 80% was measuring the chest (lungs). In actual measurements of human subjects these geometries proved to be valuable. The relative detection ratio for the thorax being centered directly under the two LOAX detectors, and a second set of data with it directly centered under the 80% detector is also given in Table 4.21. Taking the optimum counting positions for the two LOAX and the 80% HPGe-detector, the relative difference was found to be 45% for the LOAX detectors and about 70% for the 80% HPGe-detectors. These results could be used theoretically to correlate counts when only one count could be carried out on a subject. They could also be used to explain counting contributions from one organ to another during the subject measurements.

4.3.6 The effect of subject-detector distance

The clearance between the detectors and bed was 28 cm. Therefore, it was possible to raise the thorax (20 cm thickness) through 7 cm in 1 cm increments to test the effect on counting sensitivity. Normalised factors were calculated taking the 2 cm distance to be representative of a 100% response factor. From the Table 4.21 it could be seen that the percentage sensitivity drop with the increase of distance was found to be lower for the two LOAX detectors than that of the 80% detector.

The spectra obtained are shown in Figures 4.20 for both detector systems. In Table 4.21, the count rates for the 59.5 keV peak increased for decreasing phantom-detector distance reaching a maximum 0.442 cps kBq^{-1} at 2 cm (an increase of 146%) and then dropped due to the narrowing field of view of the two LOAX. The opposite effect occurred when measured closer to the 80% detector because the sensitivity continued to increase over the last few centimeters. At 8 cm and 5 cm it was found to be 0.0854 cps kBq^{-1} and 0.199 cps kBq^{-1} i.e. an increase of 137%. This continuing increase for the 80%

HPGe-detector could be explained by the fact that the detector's FOV was not effectively collimated as the source-detector distance decreased and therefore, the 59.5 keV peak was detected with higher counting efficiency. The ability to raise and lower the phantoms in this way, was used for the counting of subjects by supporting them with foam material of known thickness depending on body build.

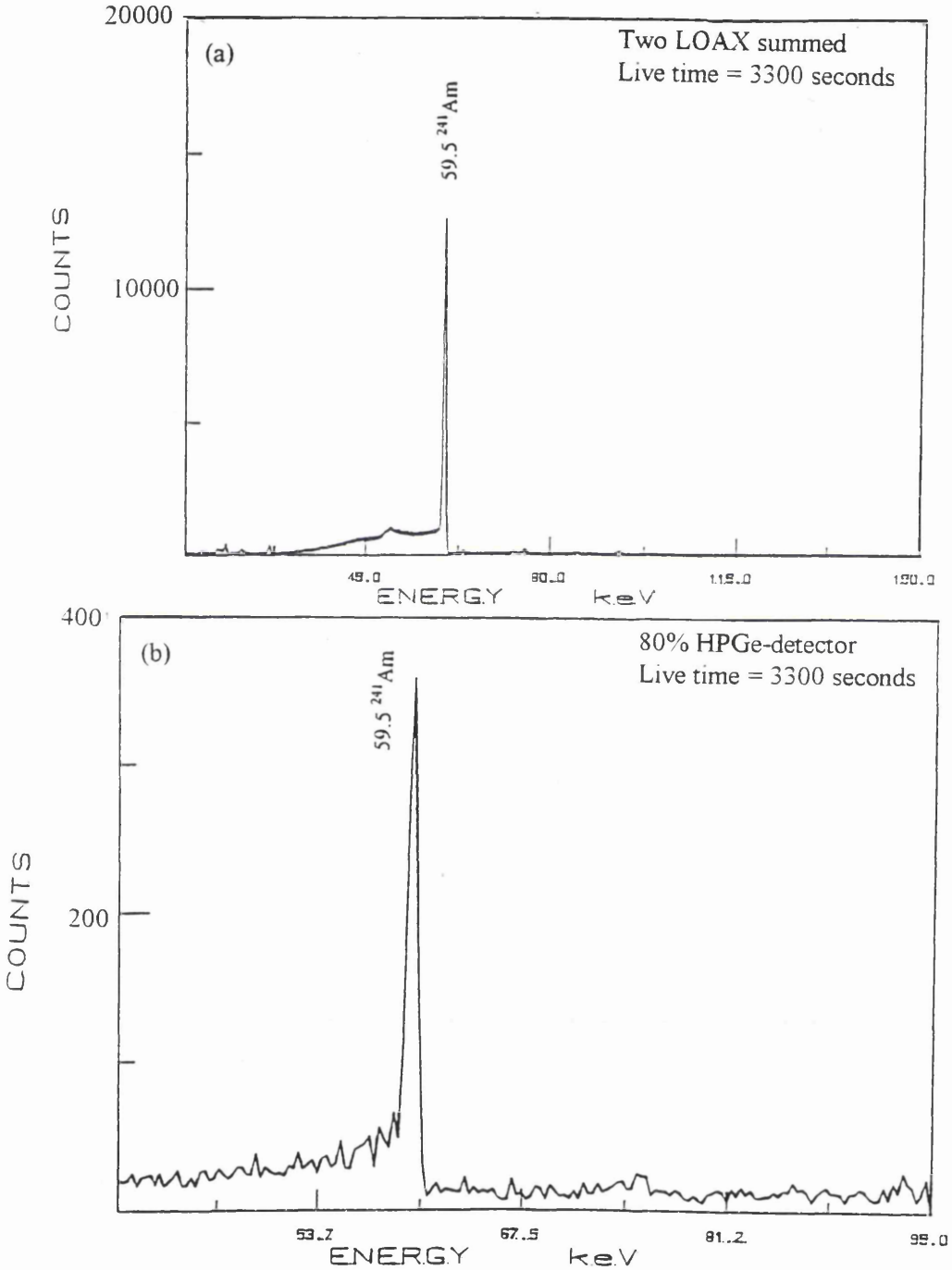

Figure 4.20 Gamma-ray spectra of the ^{241}Am thorax measured using: (a) two LOAX detectors summed; (b) the 80% HPGe-detector.

This enabled a particular organ to be counted as close as possible to the detector to utilise the maximum sensitivity of the counting systems as was given in Table 4.19 & 4.20. Using the count rates at 8 cm and 5 cm from the detectors and taking twice the standard deviations of the background counts, the minimum detectable activities (MDA) were calculated as shown in Tables 4.19 & 4.20. The calculated values corresponding to the higher sensitivities of both detectors were 16 Bq for the two LOAX detectors summed and 67 Bq for the 80% HPGe-detector.

All these measurements were repeated for the scanning geometry. The scanning sensitivities for the two LOAX and the 80% detector were found to be 1.59×10^{-5} and 1.80×10^{-5} cps Bq^{-1} respectively and their corresponding MDA were 82 Bq and 172 Bq for the thorax phantom. It could be clearly noticed that the scanning mode gave lower counting sensitivities mainly because the sources are seen only part of the time by the respective detector. Therefore, it could be concluded that static counts are more useful and provide higher counting sensitivities.

Thorax-det-dis.cm	directly under two LOAX Sens. (cps kBq^{-1}) (%)*		directly under 80%-det Sens.(cps kBq^{-1}) (%)*		% Ratio of relative Sens. (80%/2LOAX)
1	0.401	91%	0.215	69%	54
2	0.442	100%	0.311	100%	70
3	0.409	93%	0.254	81%	62
4	0.388	88%	0.211	68%	54
5	0.358	81%	0.199	64%	56
7	0.302	68%	0.091	29%	30
8	0.274	63%	0.085	27%	31

Table 4.21 Sensitivity factors for measuring the ^{241}Am-thorax directly under the two LOAX detectors compared with the simultaneous response of the 80% detector. *Percentage normalised factors.

4.3.7 Sensitivity for counting ^{241}Am and ^{210}Pb in the head-calibration with phantoms prepared from real skulls

Using the two sets of head phantoms prepared from real skulls as described previously, the counters were calibrated for ^{241}Am and ^{210}Pb in all possible positions. The skulls were labelled both internally and externally, that is, on the inner and outer surfaces of the bone, to permit assessment of gamma ray attenuation. The positions were: both left and right

sides; back; front; and the top. Table 4.22 gives the full detailed sensitivities for the two LOAX and the 80% HPGe-detectors for the various counting geometries for the externally labelled ^{210}Pb skulls. When the same measurements were made on the internally labelled skulls the same pattern of detection was observed but with lower sensitivity factors as expected.

However, Figure 4.21 shows a comparison of the gamma-ray spectra on an expanded scale for the internally and externally labelled ^{241}Am-skulls up to 55 keV mainly to emphasize the low-energy peaks. Table 4.23 outlines the counting sensitivities and the respective MDA for the same skulls obtained using two LOAX detectors summed.

Skull geometry	Two LOAXs Net cps	Sensitivity cps kBq-1	80% HPGe Net cps	Sensitivity cps kBq-1
Supine position,8cm	1.08±0.02	0.221±0.010	0.118±0.006	0.024±0.002
Supine position 3cm	1.51±0.02	0.311±0.020	0.122±0.006	0.025±0.002
Tilted to right side,10cm	0.52±0.01	0.106±0.010	0.117±0.006	0.024±0.002
Tilted to left-side,10cm	0.449±0.011	0.092±0.005	0.096±0.005	0.019±0.002
Standing-up right,4cm	0.924±0.011	0.190±0.010	0.123±0.006	0.025±0.002
Facing down,8cm	0.344±0.009	0.071±.0.004	0.082±0.005	0.017±0.002

Table 4.22 Externally labelled ^{210}Pb-skulls measured count rate and the respective sensitivities for the various counting positions for both detector systems.

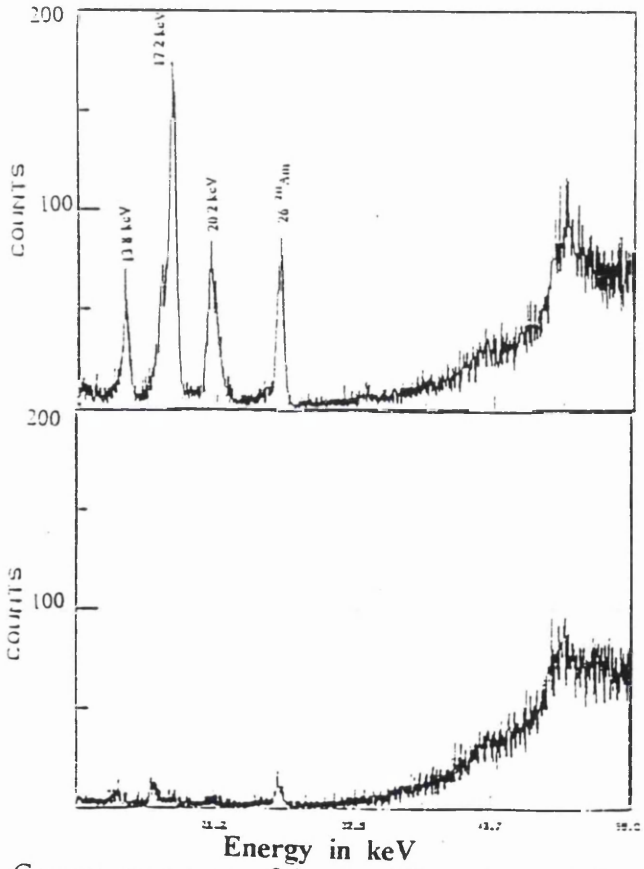

Figure 4.21 Gamma-ray spectra of the two different labelled ^{241}Am skulls measured using two LOAX detectors summed: (a) externally labelled; (b) internally labelled.

The difference in the detection of the low-energy X-rays was clearly apparent between the two measured skulls.

For ^{210}Pb externally labelled, the counting sensitivity for a two LOAX summed combination was found to be $6.73x10^{-4}$ cps Bq^{-1} at a distance of 4 cm from the two LOAX detectors and the respective MDA calculated to be 15±5 Bq. Also the internally labelled skull was measured and found to give $2.94x10^{-4}$ cps Bq^{-1} and a MDA of 34±12 Bq. The same phantoms were measured in scanning mode and their respective sensitivities were found to be $4.05x10^{-5}$ and $2.54x10^{-5}$ cps Bq^{-1} whilst their MDAs were calculated to be 249±87 Bq and 394±138 Bq respectively. It has to be noticed that the data for the 13 keV peak were omitted because of their results were proved to be useless in this case, and the other low energy peaks were included for comparison purpose.

Phantom description	17 keV Bq cps Bq^{-1} 2σMDA	26 keV Bq cps Bq^{-1} 2σMDA	59keV Bq cpsBq^{-1}
Internal skull at 8cm	$6.27x10^{-7}$ 6443±2255	$1.20x10^{-7}$ 50667±25333	$2.14x10^{-4}$ 32±11
Internal skull at 4cm	$4.39x10^{-7}$ 477±143	$1.40x10^{-6}$ 4343±1950	$1.29 x10^{-3}$ 5±2
External skull at 8cm	$1.08x10^{-6}$ 67±20	$3.40x10^{-5}$ 178±62	$1.18 x10^{-3}$ 6±2
External skull at 4cm	$1.16x10^{-4}$ 52±13	$7.28x10^{-5}$ 84±21	$2.26 x10^{-3}$ 3±1

Table 4.23 Measured sensitivities cps Bq^{-1} and MDA (1hour count) for ^{241}Am skulls, measured at two different distances from detectors surfaces using two LOAX -detectors summed.

The sensitivity provided by the 80% HPGe-detector for measurement of all the phantoms was calculated and tabulated in Table 4.24 and 4.25 at 4 cm and 8 cm from the detector surface along with one and two LOAX detectors respectively.

Phantom description	one LOAX-detector (cps Bq^{-1}) 2σ MDA	80%HPGe-detector (cps Bq^{-1}) 2σ MDA
Internal skull at 8cm	$8.06x10^{-5}$ 59±30	$2.65x10^{-5}$ 239±120
Internal skull at 4cm	$1.74x10^{-4}$ 27±11	$5.12x10^{-5}$ 124±50
External skull at 8cm	$3.94x10^{-4}$ 12±3	$4.72x10^{-5}$ 134±40
External skull at 4cm	$5.78x10^{-4}$ 8±2	$1.80x10^{-4}$ 35±7

Table 4.24 Measured sensitivities cps Bq^{-1} (1hour count) for ^{241}Am skulls, measured using one LOAX and the 80% HPGe-detectors at two different distances from detectors surfaces.

Phantom description	Two LOAX detectors (cps Bq^{-1})	2σ MDA (Bq)	80%HPGe-detector (cps Bq^{-1})	2σ MDA(Bq)
Internal skull at 8cm	$5.34x10^{-5}$	120±54	$4.68x10^{-6}$	299±150
Internal skull at 4cm	$9.24x10^{-5}$	65±26	$8.63x10^{-6}$	162±73
External skull at 8cm	$1.67x10^{-4}$	40±12	$1.35x10^{-5}$	104±36
External skull at 4cm	$2.08x10^{-4}$	30±6	$2.03x10^{-5}$	69±21

Table 4.25 Measured sensitivities cps Bq^{-1} (1hour count) and MDA for ^{210}Pb skulls, measured using two LOAX and 80% HPGe-detectors at two different distances from detectors surfaces.

4.3.8 Real arm and leg bone phantoms labelled with ^{241}Am

The arm and leg phantoms were measured at 3 cm and 8.5 cm distance separately. Also they were positioned on the left side of the water phantom by replacing sections and were measured in scanning and static modes. The measured sensitivities and their respective calculated MDA values are presented in Table 4.26 and 4.27 for the LOAX and the 80% HPGe-detectors respectively. It has to be noted that all the above phantoms were measured using both detector systems in order to calibrate them and to further examine their ability for measuring these low energy peaks from ^{241}Am.

Phantom description	17 keV Bq cps Bq^{-1}	2σMDA	26 keV Bq cps Bq^{-1}	2σMDA	59keV Bq cps Bq^{-1}	2σMDA
Arm at 5cm	$4.39x10^{-7}$	9203±3680	$1.22x10^{-5}$	474±237	$6.25 x10^{-4}$	11±3
Leg at 8cm	$1.29x10^{-7}$	31318±14093	$1.12x10^{-6}$	5160±2580	$4.46 x10^{-4}$	15±5
Leg at 5cm	$1.23x10^{-6}$	3285±1314	$7.6 x10^{-6}$	760±304	$8.15 x10^{-4}$	8±2

Table 4.26 Measured sensitivities cps Bq^{-1} and MDA (1hour count) for ^{241}Am, arm and leg measured using two LOAX HPGe-detectors summed at two different distances from detectors surfaces.

Phantom description	4cm of detector (cps Bq^{-1})	MDA (Bq)
^{241}Am- Arm	$1.46x10^{-4}$	49±22
^{241}Am- Leg	$1.07x10^{-4}$	66±30

Table 4.27 Measured sensitivities cps Bq^{-1} and MDA (1hour count) for ^{241}Am, arm and leg measured using 80% HPGe-detectors summed at 4cm distances from detectors surfaces.

4.3.9 The effects of four LOAX detectors summed

In order to check the effects of the extra added detectors for the system's detection capability and to study its advantages, the four LOAX detectors were installed and summed and were used to measure all of the tissue equivalent phantoms separately. Table 4.28 shows all the count rates of the four LOAX detectors summed for the main gamma energies of 46.5 keV and 59.54 keV for ^{210}Pb and ^{241}Am phantoms respectively.

Phantom description	Count rate cps ± 2σ	Sensitivity cps Bq^{-1}	2σ MDA Bq
Water phantom	0.019±(5x10^{-3})	------	---
External ^{241}Am skull	14±0.1	2.65x10^{-3}	2±0.5
Internal ^{241}Am skull	11±0.1	2.19x10^{-3}	2±1
Thorax ^{241}Am	6±0.08	6.88x10^{-4}	7±2
Arm ^{241}Am	7±0.09	1.11x10^{-3}	4±2
Leg ^{241}Am	9±0.1	7.33x10^{-4}	6±3
External *^{210}Pb skull	1±0.1	2.09x10^{-4}	21±5
Internal *^{210}Pb skull	0.439±0.022	9.24x10^{-5}	48±14

Table 4.28 Four LOAX detectors summed count rate, sensitivities and, MDA of the various tissue equivalent phantoms. (one hour counts)

* Note for comparison the 2σ for the 46.5 keV was 4.44x10^{-3} .

Increasing the number of detectors results in more surface area of the object being measured, and this in turn increases the activity seen by the detectors which means a higher detection sensitivity and lower MDA than just having one or two detectors only. It has to be noticed that the background count rate was also increased especially for the detectors positioned on the outer end of the tunnel of the monitor shield. However, the detector arrangement provided the lowest MDA for the measurements of all the tissue equivalent phantoms.

4.4 Measurements of an ^{241}Am disk reference source

A standard large area ^{241}Am source was available and was also used to provide an independent check on the calibrations.

4.4.1 Source description

The standard large area or extended source (Amersham International) contained 3.63 kBq ± 10% of ^{241}Am incorporated in an anodised layer, on 0.3 mm thick aluminum backing. The thickness of the ^{241}Am activated layer was approximately 6 μm. This foil was mounted on a corresponding planchette and the total active dimension of the source was a disk 197 mm in diameter.

4.4.2 Measurement procedure

The source was measured in the static mode using the four LOAX detector system at three source to detector distances with the results outlined in Table 4.29.

Energy Distanc	13 keV cps Bq^{-1}	MDA Bq	17 keV cps Bq^{-1}	MDA Bq	26.3 keV cps Bq^{-1}	MDA Bq	59.54 keV cps Bq^{-1}	MDA Bq
23cm	3.94×10^{-4}	24±12	7.0×10^{-4}	184±60	1.44×10^{-4}	36±12	2.19×10^{-3}	4±2
12cm	9.21×10^{-4}	104±30	1.14×10^{-3}	92±27	2.63×10^{-4}	20±6	4.95×10^{-3}	2±1
6cm	1.58×10^{-3}	60±15	2.75×10^{-3}	46±14	5.12×10^{-4}	10±2	8.87×10^{-3}	1±0.5
3cm	2.21×10^{-3}	42±8	3.04×10^{-3}	42±8	6.88×10^{-4}	7±2	1.22×10^{-3}	8±3

Table 4.29 Measured sensitivities and calculated 2σ MDA for the main energies of ^{241}Am extended circular source using four LOAX detectors summed.

The same source was scanned for an hour on the bed surface without any absorber and also underneath the chest water phantom to simulate scatter and absorption effects. The measured sensitivity for four LOAX detectors summed was found to be 4×10^{-4} cps Bq^{-1} in air and 1.66×10^{-5} cps Bq^{-1} underneath a water chest phantom of thickness approximately 20 cm. It could be seen that the attenuation of about 20 cm of water

results in a reduction in the sensitivity of 24 times. It should be noted that this 20 cm thickness of water simulates the thickness of a subject trunk.

4.4.3 Discussion of results

Looking at the data collected for the static counts presented in Table 4.29, the highest sensitivity obtained for the 59.5 keV peak was found to be $8.87x10^{-3}$±10 % cps Bq^{-1} at 6 cm distance and a respective MDA, 1±0.5 Bq at two standard deviations for the four LOAX detector system. It was noticed when measuring the source at 3 cm from the detector surfaces, the count rate for the 59.5 keV peak dropped because while for the count rate for the low energy peaks increased. This fact was mainly due higher penetration ability of the 59.5 keV in comparison with the other low energy peaks and also to the fact the view of the four detectors i.e. their solid angle did not cover the total active area of the active circular source. To further examine this criterion the circular source was measured at further away distances, the measured count rate for all energies was found to drop appreciably more for the low energies due to the inverse square law and absorption in air especially for energies lower than 59.5 keV. Therefore, care has to be taken when optimising the counting geometry to obtain the best counting sensitivity according to the sizes and configuration of the source-detector geometries and the main energy of interest.

It must be emphasized that the higher sensitivities and the lower MDA values gained by the measurements of this source were unique and compared very well with the measurements of the ^{241}Am skull. The best counting sensitivity for the 59.5keV where found at 6 cm distance which corresponded to a one Bq MDA, were at 3 cm distance the best counting sensitivity produced a 42±8 Bq for 13 & 17 keV energies. For the 80% detector, the best sensitivity was found to be $4.49x10^{-3}$ cps Bq^{-1} and a corresponding MDA of 6±2 Bq in the static mode at 6cm for the 59.5 keV. It could be seen the sensitivity of the four LOAX detectors summed gave twice the sensitivity of the 80% HPGe-detector. It has to be noted that the uncertainty of the measured MDA was in the range of 15-20% for both types of detectors.

4.5 The Lawrence Livermore National Laboratory (LLNL) tissue equivalent phantom measurements and data analysis

Plastic and BOBAB phantoms are deficient in representing the human tissue attenuation properties. This was brought out by an experiment sponsored by the International Atomic Energy Agency (IAEA) in 1972. Three male subjects of small, medium, and large build inhaled a $^{103}Pd/^{51}Cr$ mixture, and visited 14 laboratories, each having its own preferred method of determining the amount of ^{103}Pd present. The final results showed that only one laboratory could estimate the ^{103}Pd present with better than 20% error and this result was only possible because they had attempted to use previously obtained tissue correction factors for ^{103}Pd. This finding led to the proposal for the construction of a realistic thorax phantom as the best solution to inter-calibration problems. The design criteria for the phantom were developed by an inter-calibration committee for low-energy emitters, composed of representatives from the laboratories involved in low-energy photon *in vivo* measurements (Dean et al., 1976). A prototype tissue equivalent human torso phantom was constructed at the Lawrence Livermore National Laboratory and circulated to other laboratories for inter-calibration purposes. Subsequently a number of these phantoms were constructed and made available for laboratories over the world that were interested in low-energy photon *in vivo* measurements. One of these phantoms was used to calibrate the present system. The construction of the phantom, with its four chest overlays, is shown in Figure 4.22. The phantom was supplied with lungs labelled with natural uranium and four over layers of 50/50 fat to muscle equivalent material.

Table 4.30 outlines the measured densities of the tissue equivalent (TE) material obtained by Computerized Axial Topography (CAT) compared to the actual densities of human tissue of the reference man (Griffith et al., 1979 b).

	Reference man Tissue	TE-polyurethane of LL-ph.
Muscle	1.06 g cm^{-3}	1.09 g cm^{-3}
87%adipose,13%muscle	---	1.01 --
Adipose tissue	0.92 --	--
Lung	0.31 --	0.28 --

Table 4.30 Densities of tissue and tissue equivalent plastic material measured by a computerized axial tomograhic scanner.

When assessing the sensitivity for lung burden measurement for low-level, low-energy transuranium radionuclides, such as ^{239}Pu, ^{241}Pu, ^{241}Am and natural U, a phantom must be anatomically realistic and its relevant organs and tissues must attenuate the low-energy X-and gamma-ray photons correctly.

Clearly, different organs must also be labelled with uniform high purity radionuclides as required, in this context the most important organs being the liver, lymph nodes, and lungs. Perhaps the most important factor was the accurate measurement of the thickness of the chest wall so as to correct for the severe attenuation of low-energy X-and gamma-ray photons. The Livermore phantom was designed to provide data on these various aspects. This phantom is considered the *de facto* standard for calibration of lung measurement geometries (Griffith et al., 1979 a & b) and was on loan from Atomic Weapons Establishment (AWE) at Aldermaston.

4.5. 1 Details of the Lawrence Livermore Phantom design

The LLNL phantom was designed to simulate an average sized adult American male thorax, between the 5^{th} cervical and 4^{th} lumbar vertebrae, and consists primarily of a polyurethane based material mixed with varying percentage to simulate muscle and fat (Griffith et al., 1979 a & b). Its relevant organs and tissues are made of polyurethane loaded with various proportions of calcium carbonate [$CaCO_3$] necessary to attenuate uranium L X-rays correctly and to simulate the tissue scattering properties of bone, cartilage, muscle and fat. The principal internal structure of lungs, mediasternum, liver and surrounding tissue are contained in a shell of muscle-equivalent material (MEM),

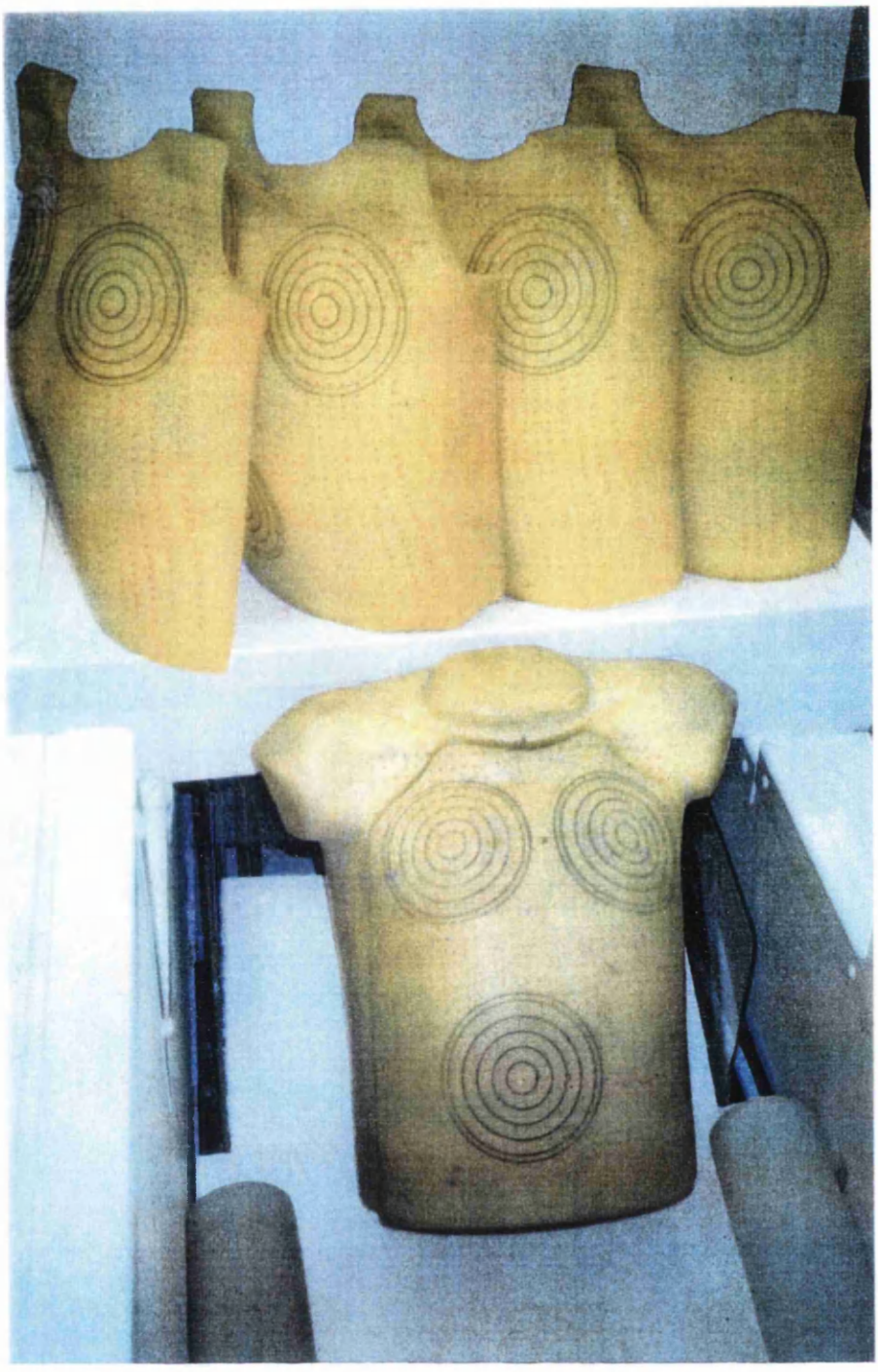

Figure 4.22 The Lawrence Livermore Torso Phantom with its chest layer plates.

incorporating a simulated sternum, rib cage and vertebrae, to represent the chest wall (Griffith et al., 1979 b). The phantom was provided with the rib cage embedded in "basic" chest overlay (10 mm) in order to produce realistic photon scattering conditions. The extra added feature of this thorax phantom was the provision of a set of chest overlay "plates" which were placed over the basic chest cover to increase the chest tissue thickness. These three sets were made with different chest wall thickness and muscle to fat ratios. The three sets have the following muscle to fat proportions as follows:

- Set one: contained 87% fat, and 13% muscle. The material gave the same attenuation as a 13/87 mixture of muscle and adipose tissue, which was referred to as 87A
- Set two: contained 50% fat and 50% muscle. The material gave the same attenuation as a 50/50 mixture of muscle and adipose tissue and was referred to as 50A.
- Set three: contained 100% muscle with appropriate attenuation.

In addition, each set above was made of four thicknesses allowing the chest wall to be varied from 16 mm to approximately 41 mm as described below. The composition used for this research study was the 50% fat to 50% muscle material, and the thicknesses available were 6 mm, 12.5 mm, 17.5 mm, and 25 mm. The LL- phantom, with its chest overlays is shown in Figure 4.22. The following measurements were made:

1- The LL- phantom with non active lungs for background determination.
2- The active lung phantoms labelled with 17.3 kBq natural uranium without any chest covering - "open counting arrangement ".
3- The active lungs with the "basic" cover.
4- A series of counts with the four different thicknesses of overlay.

The range of thickness available covered the variation in about 95% of male radiation workers (Griffith et al., 1984 a). Table 4.31 presents the comparative values of the volumes of the various organs between human (reference man) and the LL-phantom (Griffith et al., 1979b). The phantom used for this research work was supplied with a lung set containing homogeneously distributed natural uranium - 9 kBq ^{238}U in the right

lung and 11 kBq in the left lung, which gave total activity of 17.3 kBq equivalent to 1.394 g of natural uranium.

Organs	*Reference Man Volume (cm^{-3})*	*LL-phantom Volume (cm^{-3})*
Lungs		
left	1762	1689
Right	2153	2180
Total	3915	3869
Heart	742	748
Liver	1700	2050
Kidney	149	170
Spleen	171	155

Table 4.31 Comparative values of organs volumes between reference man and LL-phantoms.

4.5.2 Chest wall thickness studies by other workers

The relationship between chest wall thickness and low energy photon attenuation was studied by Rundo at Argonne National Laboratory (Rundo et al., 1969). He used ^{103}Pd (half-life = 17 days) which emits X-rays similar to the uranium L alpha X-rays at 20.2 and 22.8 keV. Seven male volunteers of different body sizes inhaled an aerosol of 5 μm-diameter polystyrene ^{103}Pd microspheres. The results of *in vivo* measurements were used to derive a function called the Effective Soft-Tissue Thickness (ESTT). It was defined as the thickness of tissue that reduces the counting rate from a point source to that observed from the same amount of activity *in vivo* count.

The ESTT was related to the chest wall thickness (CWT) of the subject by the equation;

$$ESTT = 0.9CWT + 30 \quad \ldots\ldots\ldots\ldots\ldots\ldots \quad 4.1$$

Where all dimensions are in mm.

However, the ultrasound measurements of chest wall thickness of 19 male subjects showed that the CWT is related to anthropomorphic factors by the equation:

$$CWT = 1.53\ (W/H) - 10C - 35.5 \quad \ldots\ldots\ldots 4.2$$

Where; W = The subject's mass in kg
H = The height in meters
C = The chest circumference in meters

The two equations combined to yield :

$$ESTT = 1.38\ (W/H) - 9.0\,C - 2 \quad \ldots\ldots\ldots\ldots\ldots 4.3$$

This expression provided a simple practical means of determining chest wall thickness.

4.5. 3 Mapping of LL-phantom activity

The phantom, with the active lungs in proper position, was placed on the bed surface at 8 cm from the detector surface with other parts of water phantom sections. The phantom was covered by its basic overlay only having thickness of 1.6 cm. Starting with thorax outside of detector's view at a reference point taken as the Cu-edge of the right side roof of the monitor, the phantom was moved by increments of 0.5 cm / 2 cm towards the detector field. A series of 1200 second counts were taken underneath and beyond the paired two LOAX detectors and the 80% HPGe-detectors, viewing the anterior surface of the upper thorax area. The resultant detection sensitivity for the activity profile distribution position for the main energy peaks relative to two LOAX detectors is shown in Figure 4.23 and for the 80% detector in Figure 4.24.

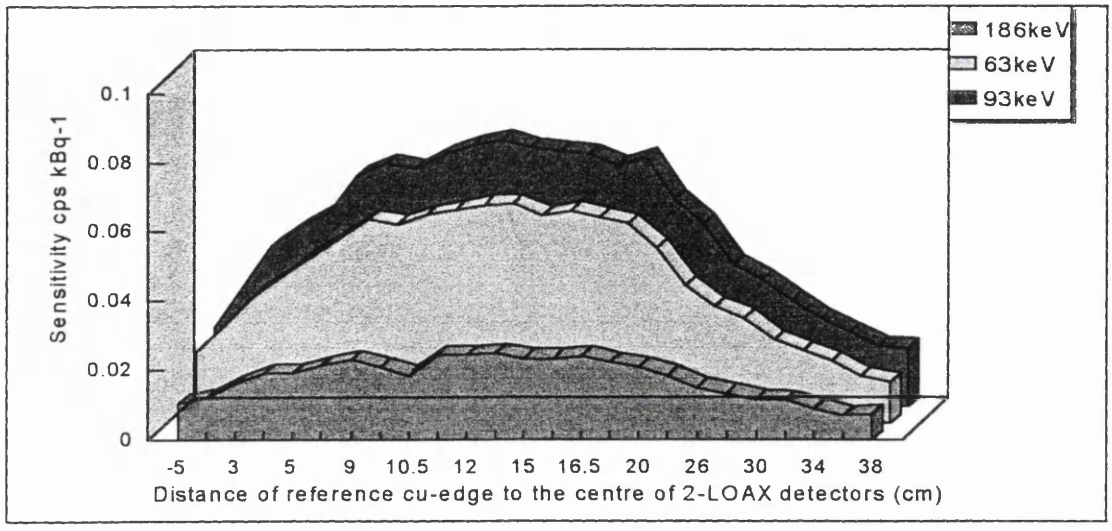

Figure 4.23 A profile of field-of-view of the LL-phantom of the 63 and 93 keV energy peaks using the two LOAX detectors summed.

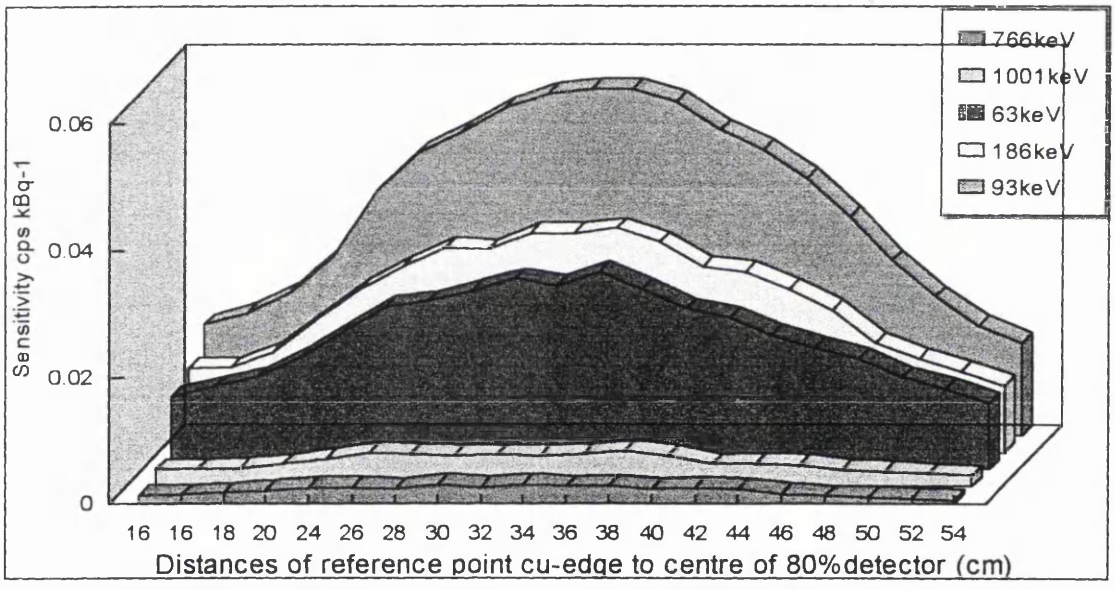

Figure 4.24 A profile of the field-of-view for the LL-phantom for the main energies measured using the 80% HPGe-detector.

As can be seen the highest detected sensitivity was 0.055 cps kBq^{-1} for the 93 keV peak in the 80% detector and 0.075 cps kBq^{-1} for the two LOAX detectors. These positions correlate to the mid centre of the lungs at the mid upper chest region at about 2.5 cm

from the clavicle as marked in Figure 4.25. It was noted that the activity profile decreased on both sides symmetrically for the 80% detector and showed a higher decline at the inner position of the two LOAX detectors due to the steel plate collimation of the signal on that side.

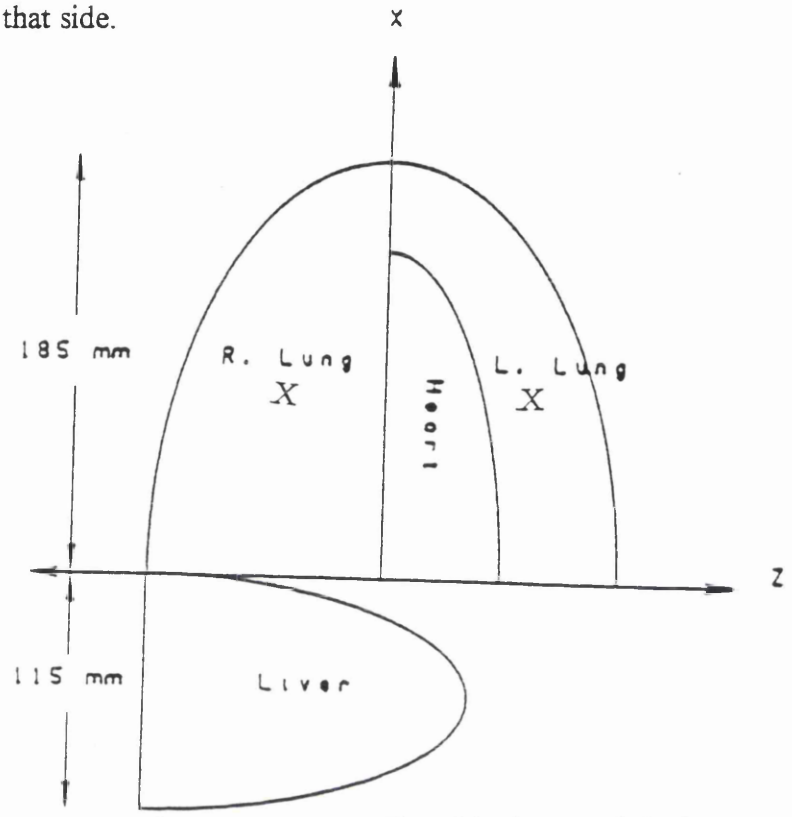

Figure 4.25 A profile of the lung and the heart models in an anterior coronal plane.

4.5. 4 Muscle equivalent versus count rates

Taking the highest geometrical count rate position, determined from the mapping profile of the whole torso under each detector field of view, as the ideal counting geometry a series of measurements were carried out using the 80% HPGe-detector and the two LOAXs: (a) separately connected to the MCA; (b) summed and; (c) four LOAXs summed to the MCA. Tables 4.32 & 4.33 present the sensitivity factors for the main energy peaks of ^{238}U at 63 and 93 keV for the three combinations of LOAX detectors respectively.

Phantom geometry	LOAX-1 cps kBq^{-1}	LOAX-4 cps kBq^{-1}	2 LOAXs cps kBq^{-1}	2 LOAXs cps kBq^{-1}	4 LOAXs cps kBq^{-1}
Thorax w/o rib cover	3.00×10^{-2}	3.59×10^{-2}	7.11×10^{-2}	6.65×10^{-2}	1.10×10^{-1}
Rib cover only	1.83×10^{-2}	2.53×10^{-2}	4.53×10^{-2}	4.24×10^{-2}	7.46×10^{-1}
Rib cover +1st layer	1.76×10^{-2}	2.01×10^{-2}	6.06×10^{-2}	3.46×10^{-2}	6.47×10^{-1}
Rib cover +2nd layer	1.34×10^{-2}	1.90×10^{-2}	4.94×10^{-2}	2.92×10^{-2}	5.22×10^{-1}
Rib cover +3rd layer	1.24×10^{-2}	1.50×10^{-2}	4.56×10^{-2}	2.42×10^{-2}	4.80×10^{-1}
Rib cover +4th layer	1.01×10^{-2}	1.35×10^{-2}	3.66×10^{-2}	2.23×10^{-2}	3.64×10^{-1}

Table 4.32 Sensitivity factors for 63 keV of the LL-phantom single and summed LOAX detectors.

Phantom geometry	LOAX-1 cps kBq^{-1}	LOAX-4 cps kBq^{-1}	2 LOAXs cps kBq^{-1}	2 LOAXs cps kBq^{-1}	4LOAXs cps kBq^{-1}
Thorax w/o rib cover	3.95×10^{-2}	5.06×10^{-2}	8.84×10^{-2}	8.27×10^{-2}	1.47×10^{-1}
Rib cover only	2.68×10^{-2}	3.52×10^{-2}	5.86×10^{-2}	5.98×10^{-2}	9.54×10^{-1}
Rib cover +1st layer	2.31×10^{-2}	2.98×10^{-2}	7.92×10^{-2}	5.20×10^{-2}	7.92×10^{-1}
Rib cover +2nd layer	1.80×10^{-2}	2.45×10^{-2}	6.82×10^{-2}	4.42×10^{-2}	7.80×10^{-1}
Rib cover +3rd layer	1.65×10^{-2}	2.00×10^{-2}	6.13×10^{-2}	3.58×10^{-2}	6.47×10^{-1}
Rib cover +4th layer	1.34×10^{-2}	1.71×10^{-2}	4.98×10^{-2}	3.18×10^{-2}	6.24×10^{-1}

Table 4.33 Measured sensitivity factors for the 93 keV using single and summed signal of LOAX-detectors measuring the LL-phantom.

The increased sensitivity of the summed detector arrangement where the detectors view most of the lung activities is clear. It must be noted that when using single LOAX detector, each detector was assumed to be counting the respective lung it is covering. However when using two LOAX detectors summed both are to be covering each lung such as shown in column 4 & 5 in Tables 4.32 & 4.33 for the same detectors, a comparable result were measured for both energies. From the same Tables, it was inferred that the increase in sensitivity between two and four LOAX summed is in the range of 45%. This limitation in maximizing sensitivity of four LOAX detectors could be attributed to the fact that much of the active detector area did not cover the whole active area of the lung, as well as the increase in background count rates. The active

volumes of both lungs was 3869 cm^3 and by comparison, the volume covered using different combination of LOAX-detectors was 38.8, 78 and 155 cm^3 for one, two and four LOAX detectors respectively.

This fact had been supported by the small difference in count rates between two LOAX summed and a single detector. Table 4.34 gives the highest measured sensitivities for the main energy peaks of the 80% HPGe-detector namely the 63, 93, 186, 766 and 1001 keV with a 20% uncertainty.

All these measurements were carried out in a static counting mode with: no cover over (open arrangement count); and then subsequently placing the basic cover; followed by the other four different layers using a similar counting time of one hour duration. The main aim of these measurement to characterize the attenuation effects of the various thickness on the counting sensitivity of the detection systems therefore no MDA were calculated.

Phantom Geometry	63keV Cps kBq^{-1}	93keV Cps kBq^{-1}	186keV Cps kBq^{-1}	766keV Cps kBq^{-1}	1001keV Cps kBq^{-1}
Open thorax	0.0199	0.0538	0.0405	0.0027	0.0058
Rib cover only	0.0102	0.0343	0.0314	0.0024	0.0049
Rib-cover+1st layer	0.0087	0.0300	0.0255	0.0020	0.0045
Rib-cover+2nd layer	0.0086	0.0254	0.0223	0.0018	0.0041
Rib cover +3rd layer	0.0079	0.0217	0.0218	0.0015	0.0015
Rib-cover+4th layer	0.0065	0.0196	0.0184	0.0011	0.0009

Table 4.34 Measured sensitivity of the main energy peaks of the 80% HPGe-detector measuring the LL-phantom with its various chest overlays.

As can be seen from the above tables, the count rates and calculated sensitivities dropped slowly with the addition of various layers as expected. The percentage drop was calculated by the normalizing factors for each layer. It could be seen that more than 50% drop of sensitivity was calculated by the sequential addition of the various layers. The reduction was mainly attributed to the thickness and composition of the each layer because the distance between detector and lungs stayed the same during the counting procedure. Due to the thickness of the whole phantom it was not possible to raise it any closer to the detection arrangement as the space available did not allow for that.

Also another set of experimental counts were taken by removing the basic cover and just having an open count and then placing the four layers only on top of the torso. The observed counts are presented in Table 4.35. The reason for this was to get the overall reduction factor for each layer with a higher count from the active lungs.

Phantom Geometry	Thorax under two LOAX Sensitivity cps kBq^{-1}		Thorax under 80% HPGe Sensitivity cps kBq^{-1}		% Relative Sensitivity	
	63keV (%)*	93keV (%)*	63keV (%)*	93keV (%)*	63keV	93keV
Open thorax	0.0711 157	0.0884 151	0.0179 163	0.0254 158	25	29
Rib cover only	0.0453 100	0.0586 100	0.0110 100	0.0161 100	24	28
Rib-cover+1st layer	0.0381 84	0.0507 87	0.0093 85	0.0126 78	24	25
Rib cover+2nd layer	0.0331 73	0.0410 70	0.0080 73	0.0106 66	24	26
Rib cover +3rd layer	0.0276 61	0.0377 64	0.0084 76	0.0118 73	31	31
Rib cover+4th layer	0.0242 53	0.0318 54	0.0049 45	0.0115 71	20	36

Table 4.35 Count rates of the main energy peaks for the LL-phantom with its different chest thickness layers measured using the two LOAX summed under two counting geometries. *Normalised factors in percentage.

Another set of results was taken for both detection systems to find the count rates of the 80% HPGe-detector while the lungs were positioned for the optimum counts under the two LOAX detectors and vice versa. From these collected count rates, Table 4.36 showing relative percentage count rates between the two optimum positions was constructed. The overall measurement uncertainty for this phantom was 15% for two LOAX detectors and 20% for the 80% HPGe-detector.

Also two other counts were taken on the LL-phantom after being turned up-side down to check the detection possibility on a real subject lying in a prone position and an average sensitivity for the 93 keV peak of a single LOAX-detector of 0.05 cps kBq^{-1} was found.

Phantom Geometry	Thorax under 80% HPGe Sensitivity Cps kBq^{-1}		Thorax under two LOAX Sensitivity. Cps kBq^{-1}		%Relative Sensitivity	
	63keV (%)*	93 keV (%)*	63keV(%)*	93 keV(%)*	63keV	93keV
Open thorax	0.199 175	0.0536 170	0.0031	0.0092	16	17
Rib cover only	0.114 100	0.0316 100	0.0024	0.0056	21	18
Rib cover+1st layer	0.087 76	0.0300 95	0.0021	0.0048	24	16
Rib cover+2nd layer	0.086 75	0.0254 80	0.0018	0.0048	20	19
Rib cover +3rd layer	0.079 69	0.0217 69	0.0011	0.0041	14	19
Rib cover+4th layer	0.065 57	0.0196 62	0.0009	0.0035	14	18

Table 4.36 Relative percentage count rates of the LL-phantom measured using the 80 % HPGe-detector under two counting geometries. *Normalised factors in percentage.

4.. 5. 5 Scanning counts of the LL-phantom

The phantom was placed on the bed surface among the other water phantom parts and scanned having no cover as an open arrangement and with different thicknesses of tissue. Table 4.37 presents the collected scanning count rates and the calculated sensitivities as well.

Phantom Geometry	Two LOAX-HPGe Sensitivity cps kBq^{-1}		80% HPGe Sensitivity cps kBq^{-1}	
	63 keV	93 keV	63 keV	93 keV
Open thorax	$1.24x10^{-5}$	$1.54x10^{-5}$	$2.43x10^{-6}$	$8.32x10^{-6}$
Rib cover only	$7.63x10^{-6}$	$8.91x10^{-6}$	$1.50x10^{-6}$	$4.39x10^{-6}$

Table 4.37 Measured sensitivities for scanning counts of the LL-phantom using both two LOAX and the 80% HPGe-detectors.

Also, to study the effect of low-energy peak identification when scanning subjects in the presence of multiple nuclide contamination, other tissue equivalent phantoms, such as the ^{241}Am and ^{210}Pb skull and the, ^{137}Cs and K/U pelvis section were placed alongside the LL-phantom and were scanned simultaneously. It could be seen that the low energy peaks may be detected in the presence of the high energy gamma-rays but with lower sensitivity factors. The general decrease of sensitivity was calculated to be in the range of ten fold lower than a similar static count. This fact indicates that a short static count gives better reliability of detection of low-energy and low-level deposited activity than a scanning count. These measurements have been carried out to investigate the detection capability and the effect of Compton continuum increase for both detection systems when measuring multi-radionuclide sources. Two typical gamma-ray spectra of these measurements are shown in Figures 4.26 & 4.27. They show the main low-energy peaks of ^{210}Pb skull (46.5 keV) and the two ^{234}Th (63 &93 keV) of the LL-phantom while at the same time measuring the pelvis of ^{137}Cs-phantom simultaneously using the 80% HPGe-detector and the two LOAX detectors. The two spectra are shown in an expanded mode with a limited regions not extending to cover 661.5 keV from ^{137}Cs phantom.

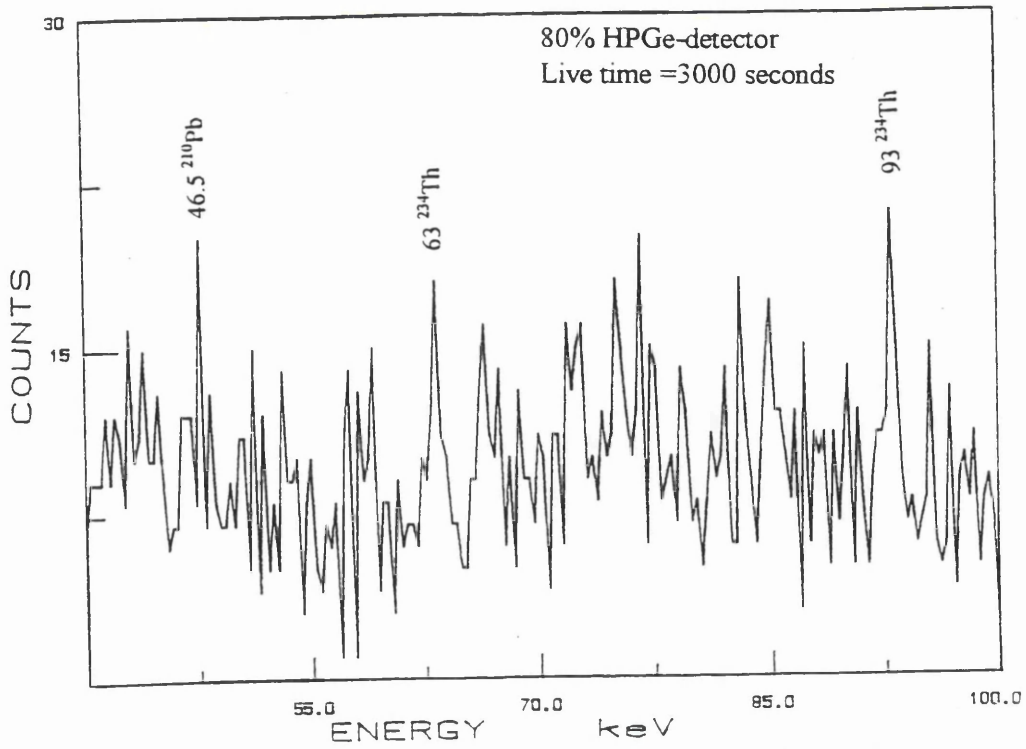

Figure 4.26 Typical gamma-ray spectrum of LL-phantom and ^{210}Pb skull phantom simultaneously with ^{137}Cs-pelvis phantom using the 80% HPGe-detector.

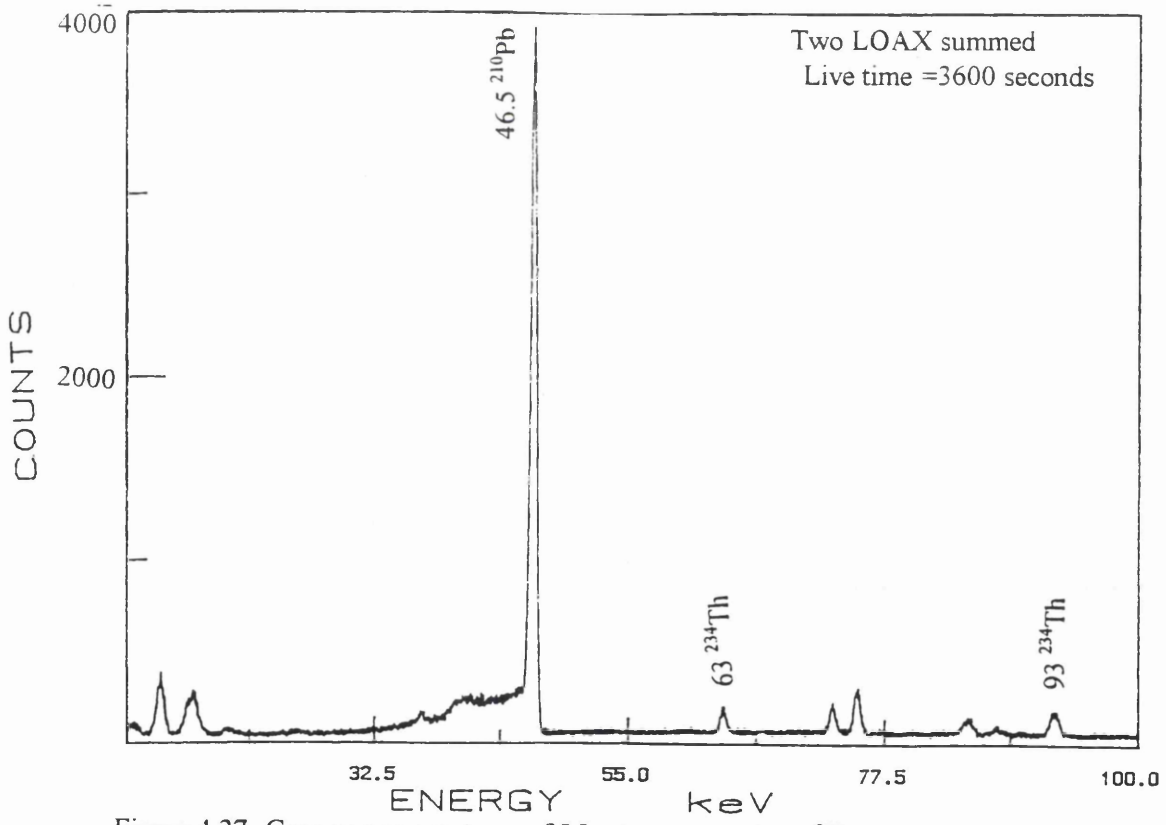

Figure 4.27 Gamma-ray spectrum of LL-phantom and the ^{210}Pb-skull simultaneously with ^{137}Cs-pelvis phantom using two LOAX HPGe detectors summed.

4.5. 6 Calibration graphs and equations

The calculated sensitivity factors and the measured count rates of the various chest wall thickness of the 50/50 percentage adipose and muscle tissue were analyzed statistically and regression plots were obtained. A number of regression graphs are presented for the 80% HPGe-detector in Figure 4.28, and for single and multiple LOAX detectors summed in Figure 4.29. The prediction equation and the regression factors are obtained with 95% confidence limits. Even though the gamma-ray attenuation is known to be exponential, the set of collected data for LL-phantom was found to follow more of linear relationship.

Each of these plots was found to fit a straight line equation for the 63 and 93 keV energy peaks of natural uranium. The calculated regression equations were found to be linear fits in the form of cps (count rate) = a + bx , where (a) and (b) are constants and (x) is the chest thickness in millimeters. From these regression plots half-value layers (HVL) for the chest thickness were calculated for both detection systems; an average value of 25±2 mm for 63 keV and 23±2 mm for 93 keV were found.

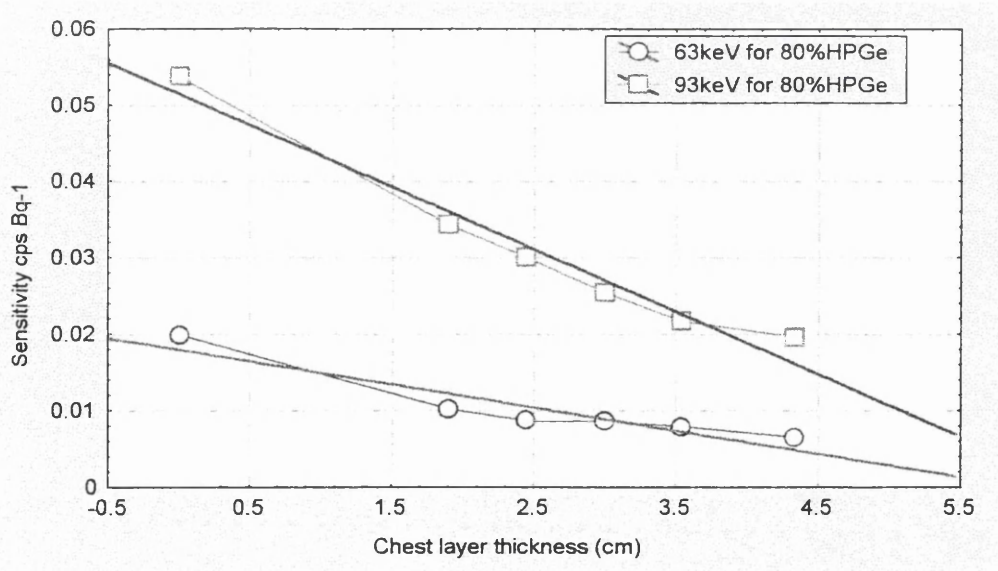

Figure 4.28 Sensitivity calibration for the 63 and 93 keV of LL-phantom measured in static mode using the 80% HPGe-detector.

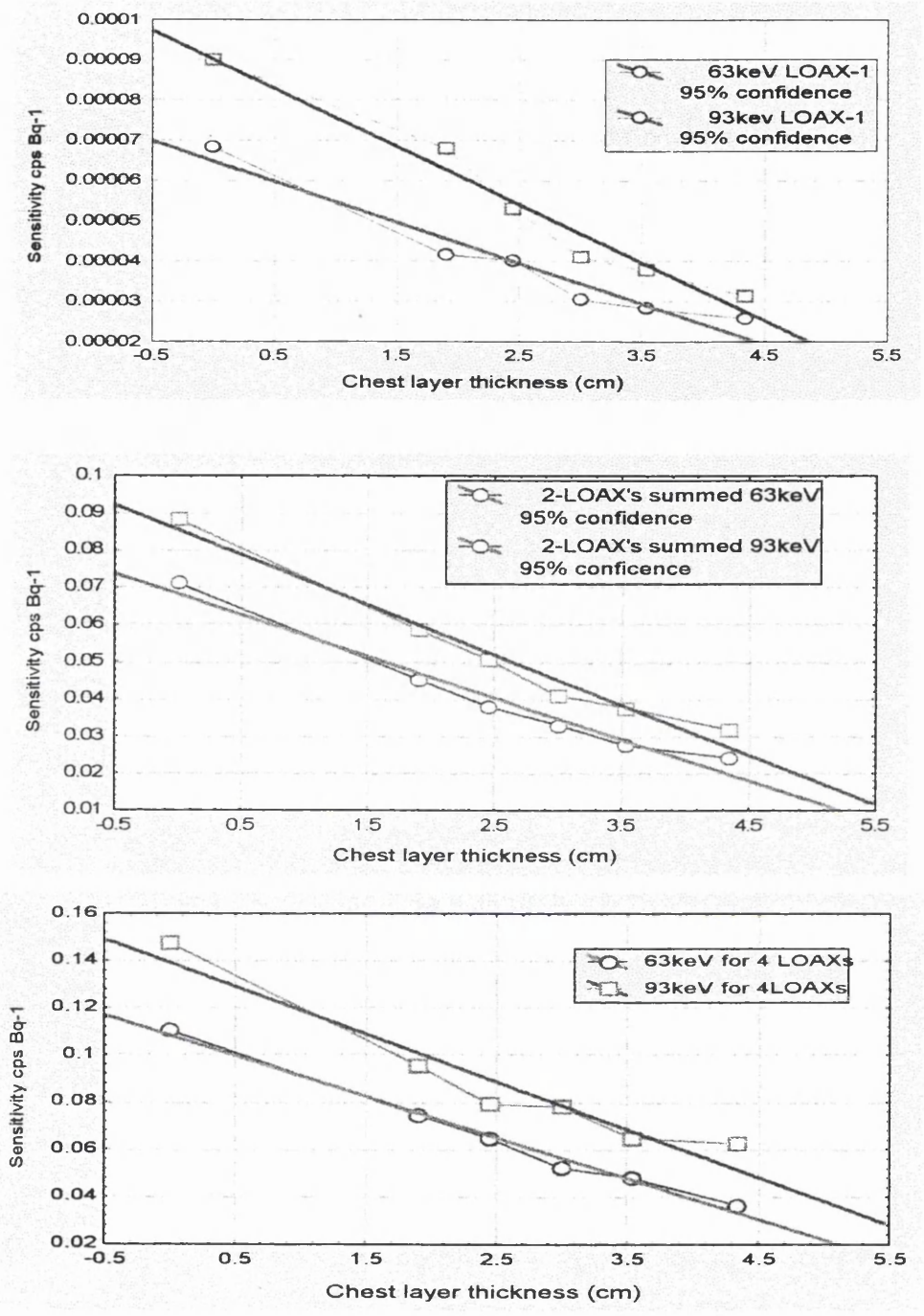

Figure 4.29 Regression graphs for the main energy peaks 63 and 93 keV of LL-phantom measurements counts using: (a) one LOAX detector; (b) two LOAX detectors summed; (c) four LOAX detectors summed.

4.6 The Inter-comparison study of *In vivo* Systems in Europe

As part of the comprehensive calibration and checking procedure for the final stages of the SURRC hybrid whole-body monitor, an opportunity arose to participate in a European Inter-comparison study. The study was called "Inter-comparison of *in vivo* Monitoring Systems in Europe" and was coordinated by the Bundesamt fur Strahlenschutz in Munich. The main purpose of the study was to examine the detection ability and to check the calibration methods of the various types of whole-body monitors which are in use for *in vivo* monitoring throughout Europe in relation to the standardisation of dosimetry measurements on radiation workers for the implementation of international regulations. Further, these laboratories could be designated as the counting centers for *in vivo* monitoring in the event of a nuclear emergency which might occur in the future, in Europe.

Firstly, the study involved the measurement of a specially made phantom called Ego labelled with particular radionuclides in which the identity and activity were known only to the organizers of the inter-calibration study. Secondly, the determination of the total body potassium (^{40}K content) of the study coordinator had to be made and thirdly, measurements of mock thyroid ampoules containing ^{131}I and ^{125}I, prepared on the day of the whole-body measurements had to be completed. These measured activities of iodine nuclides were compared with the results obtained by the study coordinator using a standard instrument for activity assessment. The complete set of results which was made on the unknown phantom, the study coordinator and the mock thyroids (^{125}I and ^{131}I), was submitted as the official results of the SURRC study. A comprehensive report was to be published by the organizers of the study outlining all the various results obtained from all the different participating European laboratories.

4. 6.1 Measurements and results

Figure 4.30 a & b shows a side and frontal view of the configuration of the unknown phantom configuration and the relative position of the detectors. According to the measurement protocol set by the organizers, the phantom was counted in a supine position on the scanning mode as required by the study procedures for a 45 minute count. All three detector systems: the two NaI-detectors; 80% HPGe-detector; and the two LOAX HPGe-detectors were used. The results indicated that the phantom appeared to contain a mixture of high and low-energy emitting radionuclides. The radionuclides ^{57}Co, ^{60}Co, ^{137}Cs and ^{40}K were clearly detected from the 45 minute scanning count as shown in Figure 4.31 a & b for both detection systems. The estimated activities were calculated using sensitivity factors for all HPGe-detectors which had been determined previously using tissue equivalent phantoms. Table 4.38 presents the measured phantom and the subject results obtained using all three types of detectors system.

Nuclide & Energy	80%HPGe-det.	2-LOAX summed	2-NaI-detectors
^{57}Co- 122 keV (Ego)	1733±200 Bq	1595±150 Bq	----
^{137}Cs- 661 keV (Ego)	1000±100 Bq	Out of energy range	970 ±50 Bq
^{60}Co- 1332 keV(Ego)	2293±230 Bq	- - - - -	2480±100 Bq
^{40}K- 1461 keV(Ego)	4210±400 Bq (132±8g)	- - - - -	3872±224Bq (121±7g)
^{40}K-1461keV(subject)	2496±250 Bq (78±4g)	- - - - -	2525±146Bq (78.9±5g)

Table 4.38 The activities (Bq) for the unknown (Ego) phantom and the K of the subject (study coordinator) measured at SURRC using "hybrid" whole-body monitor using the three detection systems.

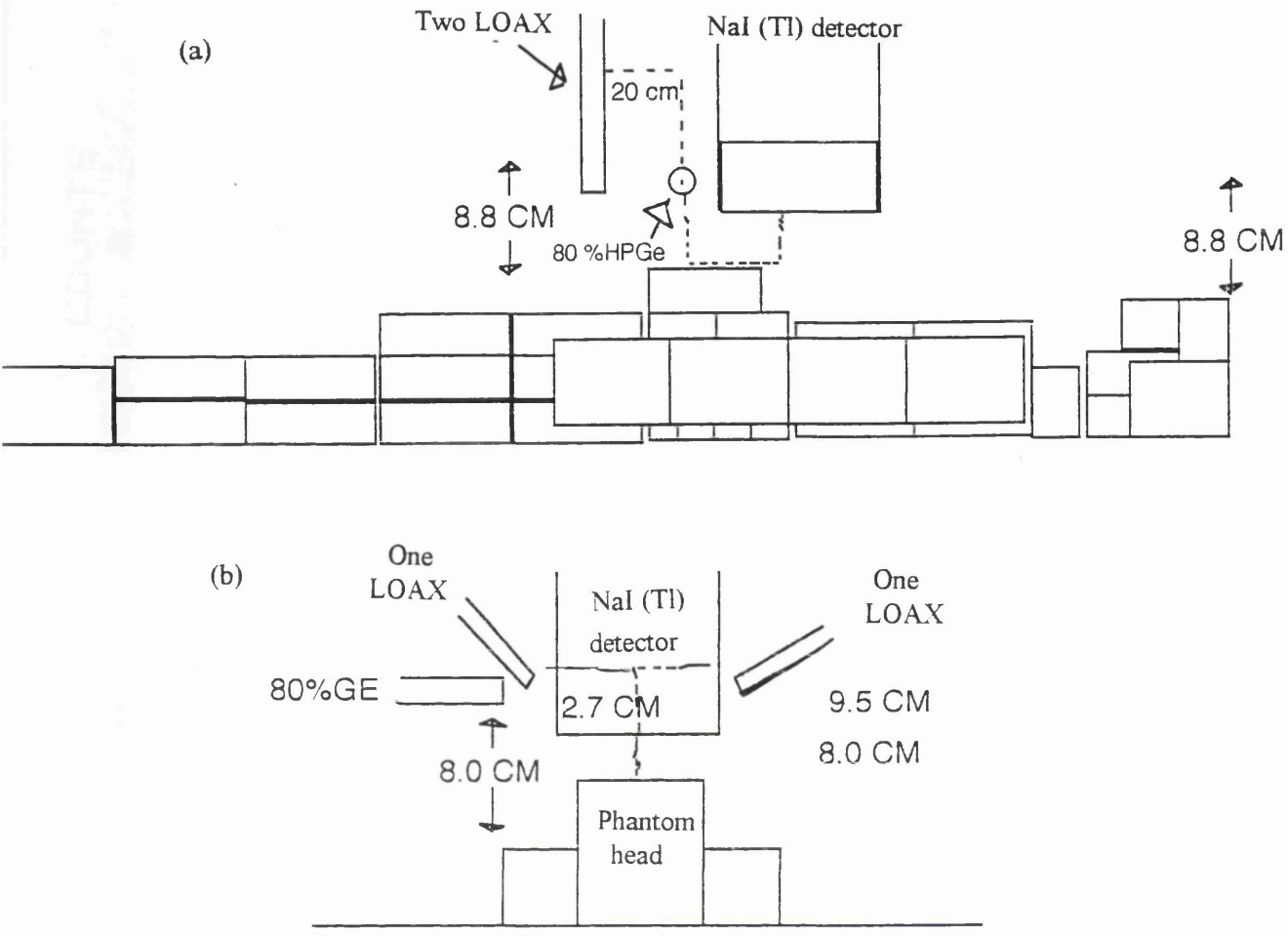

Figure 4.30 The Ego phantom in relation to three detection system geometry showing: (a) side view and; (b) frontal view.

It was the intention of the German coordinators to publish the comprehensive results of the comparison study as a final report in the summer of 1997. However, a preliminary report containing all the results of the participating laboratories in a coded form was made available prior to this. The results were given in graphical form showing the ratios of the measured activities to the known activities for each radionuclide separately on the day of measurement. Two representative graphs showing the results of this laboratory labelled as (CJ) in comparison with other participant laboratories are given in Figure 4.32 a & b.

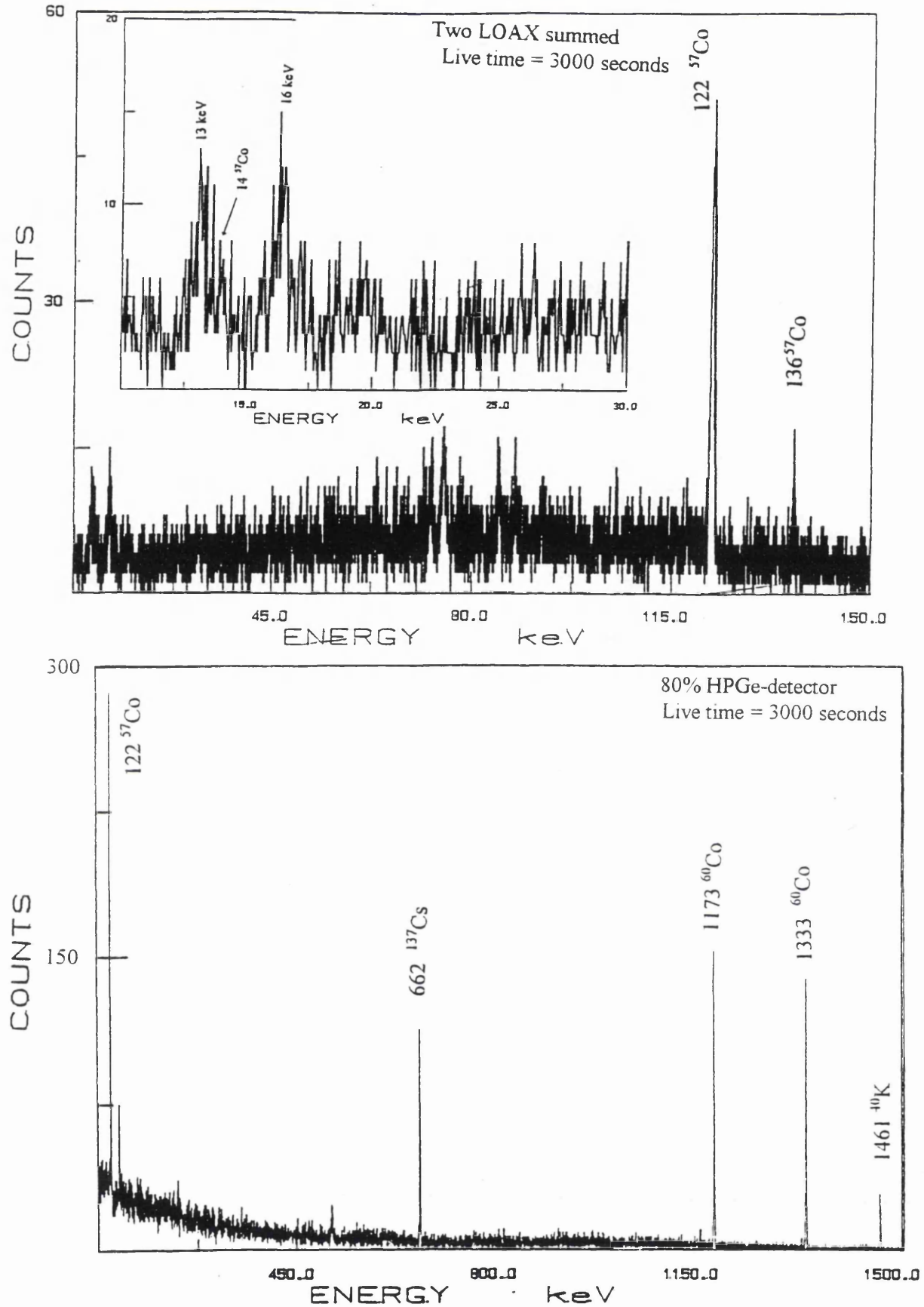

Figure 4.31 Gamma-ray spectrum of the multi-nuclides detected in the Ego phantom (a) two LOAX detectors and (b) 80% HPGe-detector.

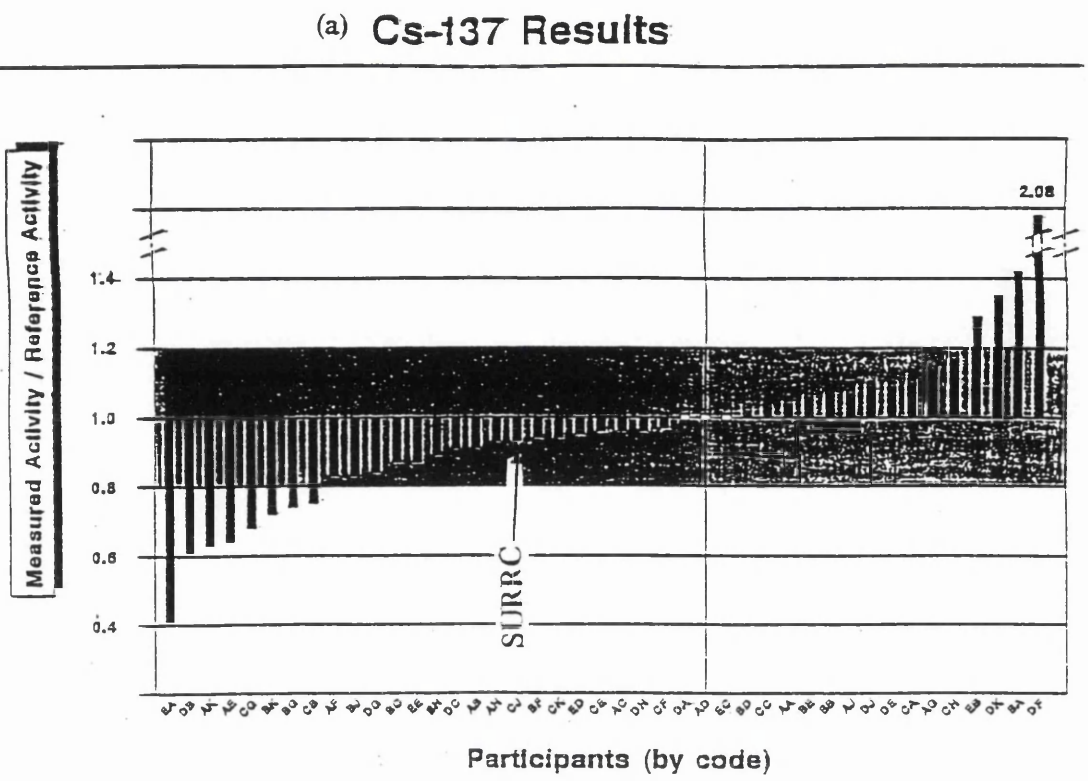

Figure 4.32 Two representative graphs depicting the final results of all participating laboratories for the radionuclides: (a) ^{137}Cs and (b) ^{40}K.

No exact values were given for the actual activities of each radionuclide. SURRC reported results were all within the 0.2 ratio limit (shaded area of Figure 4.32), accept for ^{60}Co which was slightly above the ratio of 1.2. These excellent results confirmed the precision and accuracy which could be achieved with the " hybrid " whole-body monitor detection system operating at the SURRC. A list of all the participating laboratories involved in the study describing the types and number of detection systems used for these measurements, was sent to all the participants. Upon examining the list, it was clear that the SURRC "hybrid" monitor detection system is unique and could be highly rated in its versatility. In addition its performance compared favourably with most other laboratories in the study. The types of detectors used in the hybrid monitor provide practical means whereby a wide range, both in the energy of the photon emission and the levels of the radioactivity present, of measurements can be made.

4.7 Important relationships in *in vivo* measurement

One important aspect of *in vivo* measurements of any internally deposited radionuclide is the estimation of the Intake Retention Functions (IRF). Because of the complexity of the internal deposition process of radionuclides in the body, the IRF is used for the estimation of the internal radiation dose distribution in the body over any appropriate time interval. For any measurement to provide the sensitivity and accuracy needed to ensure adequate detection capability of the monitoring system, the Minimum Detectable Activity (MDA) had to be outlined and well known. Using these two criteria the Minimum Detectable Intake (MDI) which represents the intake expected to be present in the measured subject at certain times after the intake could be determined using the following relationship:

$$\mathbf{MDI = MDA / IRF} \quad \textbf{.....Equation 4.4}$$

4.8 Summary and conclusion

This chapter outlined the large amount of research data obtained using the final shadow-shield whole-body monitor to measure anthropomorphic phantoms containing different low-energy radionuclides namely ^{241}Am and ^{210}Pb. In addition to that, a number of different radionuclide sources of different shapes and geometries were measured under different counting geometries. The measured sensitivity factors and calculated MDA values for the various radionuclides were tabulated and certain calibration graphs were plotted for both detection systems. The utilisation of high purity semiconductor detectors (HPGe-detectors) in this type of shadow-shield arrangement has provided workable sensitivities and adequate limits of detection which encouraged their uses for human *in vivo* measurements, as can be seen in the next chapter. The large amount of count rates data collected from measuring different phantoms were further used to calculate the sensitivity and efficiency of the HPGe-detectors which enables the interpretation of *in vivo* results for the low-energy photon emitting radionuclides. The results presented in this chapter are the first documentation of the variability associated with the use of HPGe-detectors in *in vivo* measurements in the shadow-shield whole-body monitor.

It has been pointed out that for the optimum counting efficiency with the lowest uncertainty and the best MDA, a number of factors need to be taken into account, such as detector positioning, detector configuration relative to the phantom source distribution, and the ultimate number of detectors used for the measurements. These factors proved to have an inter-dependence and multiplicative effect on the sensitivity and final MDA of the detection system. Definitive values for the various phantom geometries were given in a number of tables as well as plotted as graphs.

CHAPTER 5

Practical measurements of human subjects *in vivo* and of organs from dead animals

5.1 Introduction

Having calibrated and optimised the HPGe detectors in the shadow shield whole body monitor which already accommodated two large volume NaI(Tl) detectors, the capability of the overall system was considerably enhanced. The three types of detectors widened the monitor versatility so that low, medium and high energy gammas could be measured at either, high resolution with lower sensitivity or low-resolution with high sensitivity. Thus the monitor could be regarded as a " hybrid " system which could be used for measurements of various shapes of sources in different counting modes. The monitor was used to make whole-body measurements of subjects in scanning and static modes and also to measure whole animals or separated organs which were positioned on the bed. In the following sections, details of various *in vivo* studies will be described to assess the counter's performance for the detection of low-level low-energy emitting radionuclides which was the principal aim.

5.2 Preliminary whole body *in vivo* measurements

Forty five subjects consisting of adult males and females, were measured in the "hybrid" body monitor using all three types of detector and static and scanning modes with particular emphasis on searching for low-energy gamma emitters, either from the background or from man-made radionuclides such as ^{241}Am. The subjects were a group of normal individuals; a group of patients being followed-up clinically for their potassium levels by the ^{40}K method; and a group of normals who had previously been monitored on many occasions.

In addition to the above subjects, four selected individuals who had been exposed intentionally or voluntarily, to certain small levels of internal radioactivity were measured. These subjects along with details of their exposure and their collected results are described fully in the following sections. These four cases are labelled A, B, C and D corresponding to the order in which they were examined and measured.

5.2.1 Scanning counts

Twenty patients, were scanned using the NaI(Tl) detectors simultaneously with the 80% HPGe-detectors and the LOAX-detectors. The counting times were short (30 min) because most of the subjects in this group were elderly patients who could not tolerate long counting times. Another group of 10 healthy subjects were also measured in scanning counting mode under similar conditions and their average count rates for the main gamma peaks were added and their errors were calculated. A third group of 15 normal subjects who had been measured on frequent occasions previously, was also scanned.

The collected average gross and net count rates are shown in Tables 5.1 and 5.2 for the main gamma peaks for the LOAX and the 80% HPGe-detectors respectively. Typical gamma-ray spectra for a subject are shown in Figures 5.1 and 5.2 a & b, for single and summed spectra of both detection systems used. From the summed spectrum it could be clearly seen that the low count rate peaks became well recognized and more pronounced. From these added spectra the collective dose equivalent may be calculated.

In order to search for low-energy, low-level activities, the spectra within each group were added and the summed spectra were inspected and analysed. The critical limit ($L_C = 2.33\sigma_B$) was calculated for the energies of interest as presented in both tables.

	Gross counts		Net counts	
Energy keV	cps±2σ	*$L_C=2.33\sigma_B$	cps±2σ	*$L_C=2.33\sigma_B$
13 U x-rays	0.064±0.03	0.07	0.031±0.02	0.05
17 U x-rays	0.065±0.03	0.07	0.038±0.02	0.05
46.5 ^{210}Pb	0.032±0.02	0.05	0.007±0.004	0.009
59.5 ^{241}Am	0.037±0.02	0.05	0.006±0.004	0.009
63 ^{234}Th	0.051±0.03	0.07	0.028±0.02	0.05
93 ^{234}Th	0.057±0.03	0.07	0.033±0.02	0.05
186 U/Ra	0.028±0.02	0.05	0.013±0.01	0.02

Table 5.1 Average count rates of gross and net count rates of the scanning measurements of subject using the two LOAX HPGe-detectors. *L_C= in cps units

Energy	Gross counts		Net counts	
keV	cps±2σ	*$L_C=2.33\sigma_B$	cps±2σ	$L_C=2.33\sigma_B$
46.5 ^{210}Pb	0.056±0.02	0.05	0.005±0.003	0.007
59.5 ^{241}Am	0.051±0.02	0.047	0.002±0.001	0.002
63 ^{234}Th	0.044±0.02	0.003	0.004±.002	0.005
93 ^{234}Th	0.051±0.02	0.035	0.009±.005	0.012
662 ^{137}Cs	0.021±0.002	0.005	0.012±0.001	0.002
1461 ^{40}K	0.052±0.004	0.009	0.046±0.003	0.007

Table 5.2 Average count rates for gross and net counts of scanning subject for the main energy peaks using the 80% HPGe-detector.

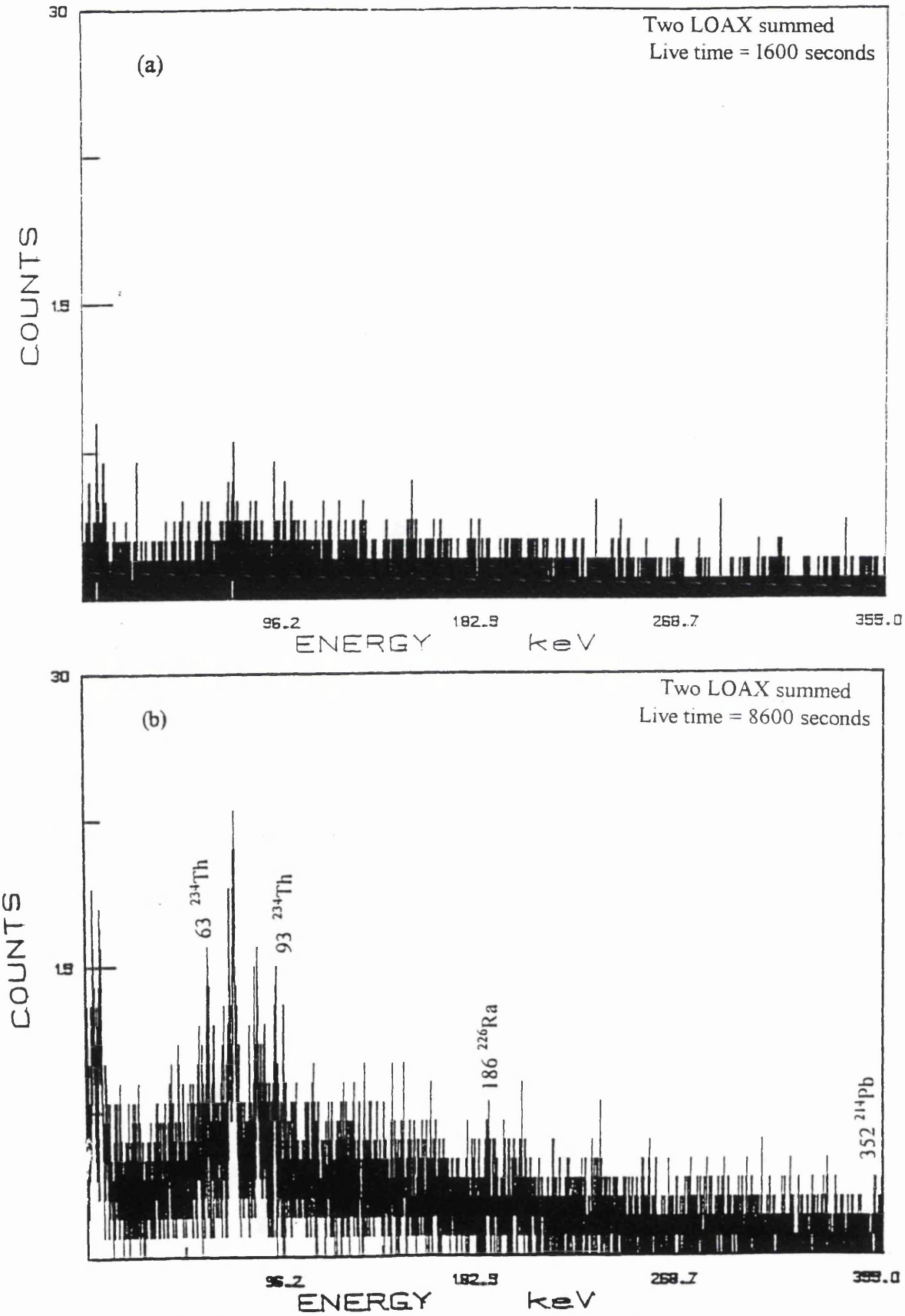

Figure 5.1 Typical gamma-ray spectrum of subject scanning count using two LOAX detectors: (a) single spectrum and; (b) 10 summed spectra.

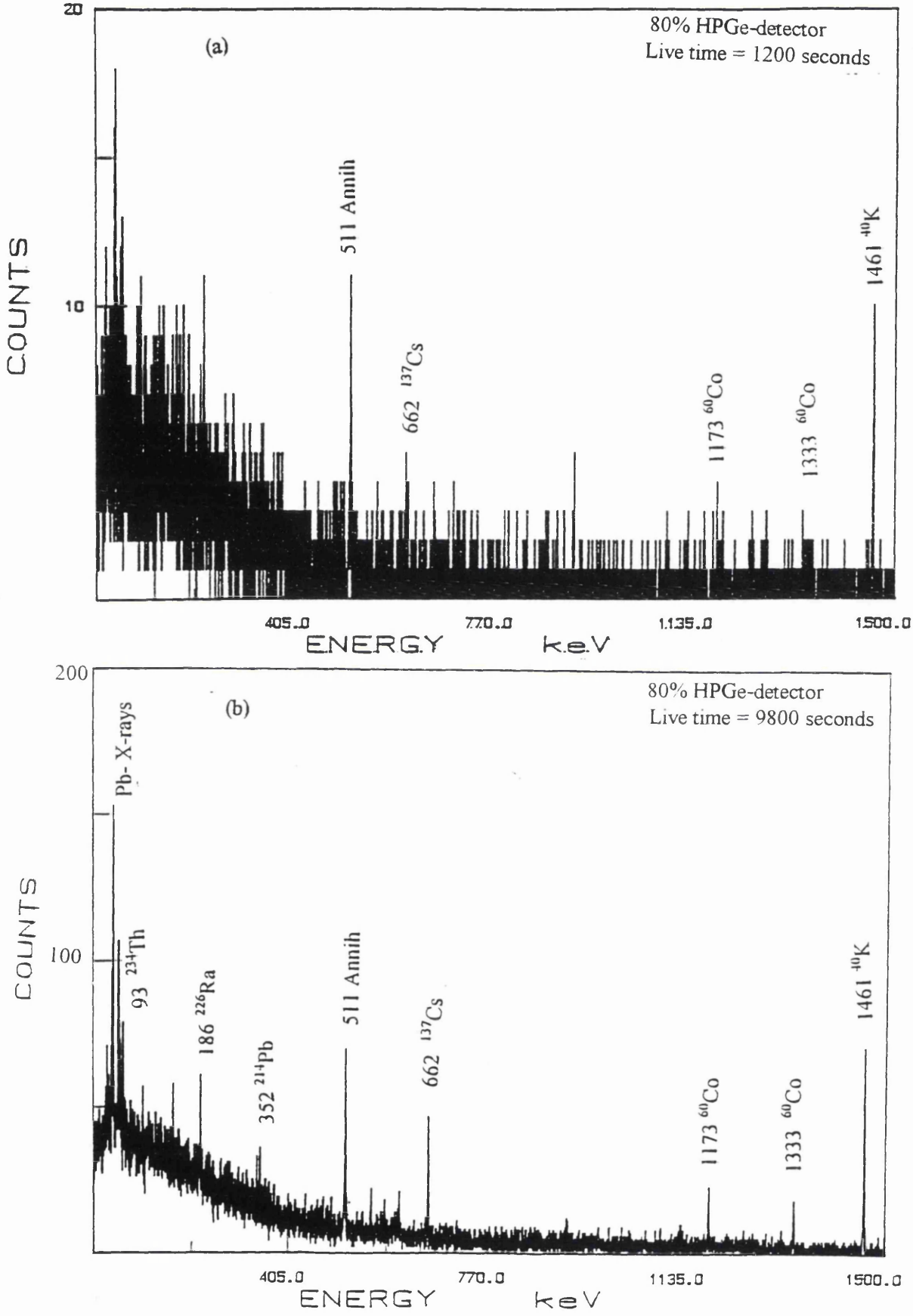

Figure 5.2 Typical gamma-ray spectrum of subject scanning count using the 80% HPGe-detector: (a) single spectrum and; (b) 8 summed spectra.

5.2.2 Static counts of subjects

Eight healthy normal subjects were measured in static mode for a counting time of one hour having the two or four LOAX-detectors either positioned over the head or the area of the lungs. The results of the summed data are given in Table 5.3. Table 5.4 presents all data for the 80% detector for a water phantom; K-chest phantom; K/U-chest phantoms and subjects. The statistical analysis of the main energies of interest is shown in columns 3 and 5 of Table 5.3 as well as column 3 of Table 5.4b. The mean, gross and net count rates which represent the normal background ranges for each energy peak provide the natural background levels of the measured subjects since they are known to be free from internal exposures. These recorded count rates for both detectors would be considered as the base line for the main energy peaks to be compared with other future measurements suspected of internal exposure. Any net (or gross) count rates of the same energy peaks that exceed these ranges with statistical significance, will be considered as a positive indication of the presence of activity. Typical gamma-ray spectra both single and summed, of subject static counts using both detection systems are presented in Figures 5.3 a & b and 5.4 a & b.

Energy keV	Gross counts cps ± 2σ	$L_C=2.33\sigma_B$ cps	Net counts cps ± 2σ	$L_C=2.33\sigma_B$ cps
12.5-13.5	0.049±0.02	0.05	0.027±0.015	0.035
15.5-17.5	0.059±0.02	0.05	0.023±0.012	0.028
25.3-26.5	0.023±0.01	0.02	0.004±0.003	0.007
45.5-47.5	0.031±0.01	0.02	0.002±0.001	0.002
58.5-60.3	0.039±0.02	0.05	0.003±0.002	0.005
62.2-64.2	0.053±0.03	0.07	0.015±0.011	0.026
92.3-93.6	0.059±0.03	0.07	0.025±0.015	0.035
184.5-186.5	0.036±0.02	0.05	0.005±0.003	0.007

Table 5.3 Statistical analysis of detected count rates for the main energy peaks of subject static counts using two LOAX detectors.

5.2.3 Discussion of the subjects measured data

One of the main aims of this research work was to establish bases for the *in vivo* counting of natural and man-made radioactivity in the general population. Therefore, a number of non classified subjects i.e. none radiation workers were measured using both counting systems in the static and scanning modes. Peaks from naturally occurring activity were clearly apparent as usual but were not enhanced by the subjects as might have been expected. This fact was supported theoretically because the measured net count rates were below the (severe) critical limits of the detectors. In more detail, it was interesting to note

Energy keV nuclide	Water-chest cps ± 2σ	K-chest cps ± 2σ	Subjects counts cps ± 2σ	K/U chest cps ± 2σ
46.5 ^{210}Pb	0.035±0.02	0.047±0.03	0.038±0.02	0.058±0.03
63 ^{234}Th	0.047±0.02	0.063±0.04	0.050±0.03	0.116±0.05
93 ^{234}Th	0.058±0.03	0.083±0.05	0.060±0.03	0.199±0.08
238 ^{212}Pb	0.039±0.02	0.051±0.03	0.043±0.03	0.053±0.02
295 ^{214}Pb	0.031±0.02	0.040±0.02	0.034±0.02	0.044±0.02
352 ^{214}Pb	0.028±0.01	0.035±0.02	0.027±0.01	0.033±0.01
583 ^{208}Tl	0.013±0.01	0.020±0.01	0.016±0.01	0.019±0.01
609 ^{214}Bi	0.019±0.01	0.020±0.01	0.017±0.01	0.022±0.01
662 ^{137}Cs	0.015±0.01	0.024±0.01	0.021±0.009	0.023±0.01
766 ^{234}Pa	0.008±0.005	0.015±0.01	0.008±0.004	0.020±0.01
1001 ^{234m}Pa	0.005±0.003	0.013±0.01	0.006±0.003	0.031±0.01
1172 ^{60}Co	0.016±0.01	0.025±0.02	0.022±0.009	0.014±0.01
1461 ^{40}K	0.014±0.008	0.355±0.2	0.105±0.002	0.368±0.2

Table 5.4a Statistical analysis of the measured subjects static counts of the main energy peaks using the 80% HPGe-detector.

Energy keV nuclide	Subjects counts cps ± 2σ	$L_C=2.33\sigma_b$ cps
46.5 ^{210}Pb	0.038±0.02	0.05
63 ^{234}Th	0.050±0.03	0.07
93 ^{234}Th	0.060±0.03	0.07
238 ^{212}Pb	0.043±0.03	0.07
295 ^{214}Pb	0.034±0.02	0.05
352 ^{214}Pb	0.027±0.02	0.05
583 ^{208}Tl	0.016±0.01	0.02
609 ^{214}Bi	0.017±0.01	0.02
662 ^{137}Cs	0.021±0.009	0.02
766 ^{234}Pa	0.008±0.004	0.009
1001 ^{234m}Pa	0.006±0.003	0.007
1172 ^{60}Co	0.022±0.009	0.021
1461 ^{40}K	0.105±0.002	0.005

Table 5.4b Statistical analysis of the subject measured static counts of the main energy peaks using the 80% HPGe-detector.

MDA for ^{238}U using the two LOAX detectors summed was in the range of 6-8 mg, which is equivalent to 70-100 Bq. The radioactive burden of these subjects, using the previously calculated sensitivities, was found to be in the range of 1- 3 mg for ^{238}U, 44 Bq for ^{137}Cs and 135- 145 gm of ^{40}K. If the collected spectra of these subjects Figures 5.3 &5.4, whose uranium burdens were below the detection limit are taken and summed by computation, the resulting spectra show most of the peaks. When the average contents of these individuals are found however they are to be below the MDA. In spite of this, the technique would certainly have extensive application in radiation protection in the study of such groups as uranium mill workers and miners. It would also be useful in monitoring the as low as reasonably achievable (ALARA) principle in radiation protection.

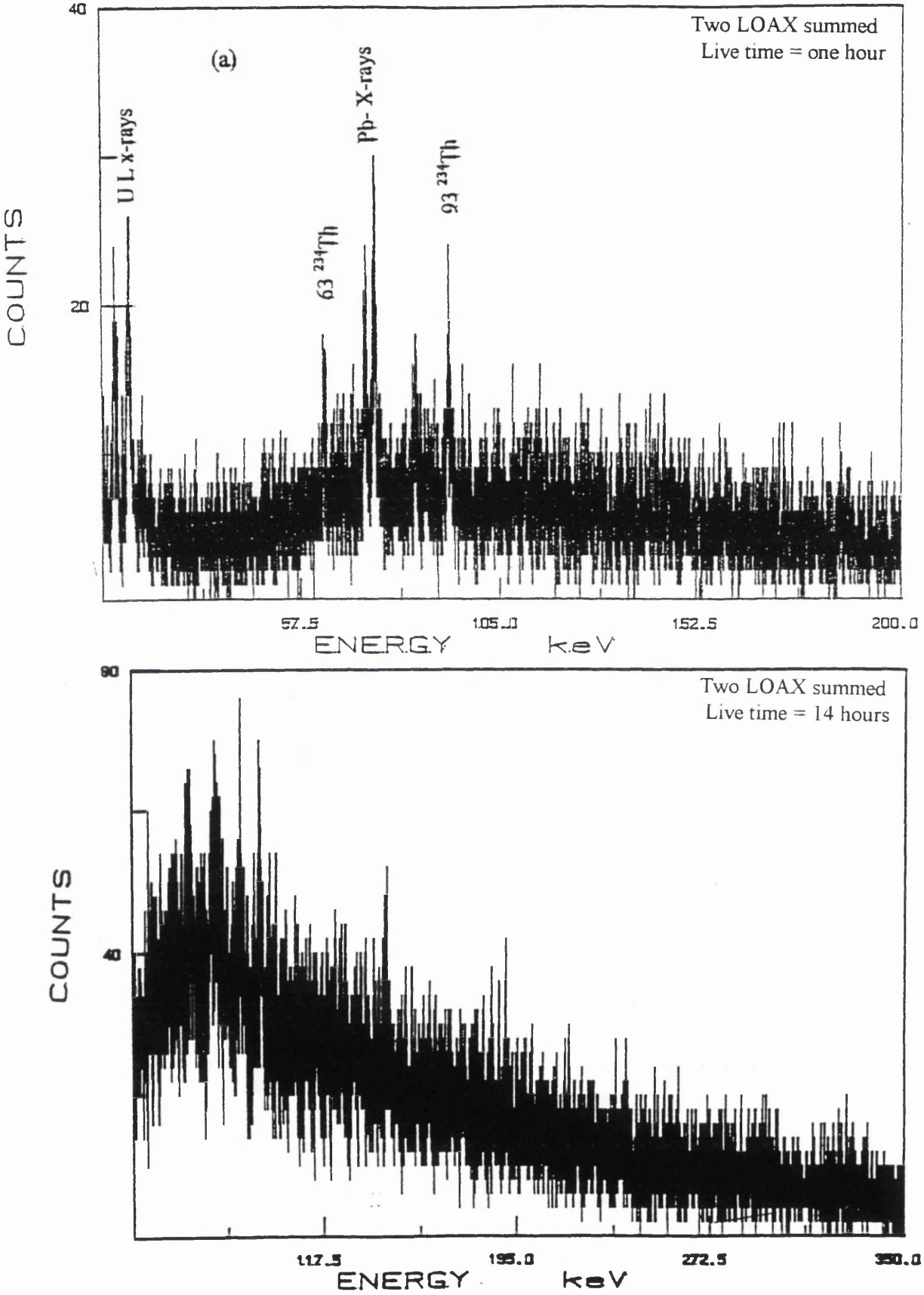

Figure 5.3 Typical gamma-ray spectra of subject static counts using two LOAX detectors: (a) single and (b) summed spectra.

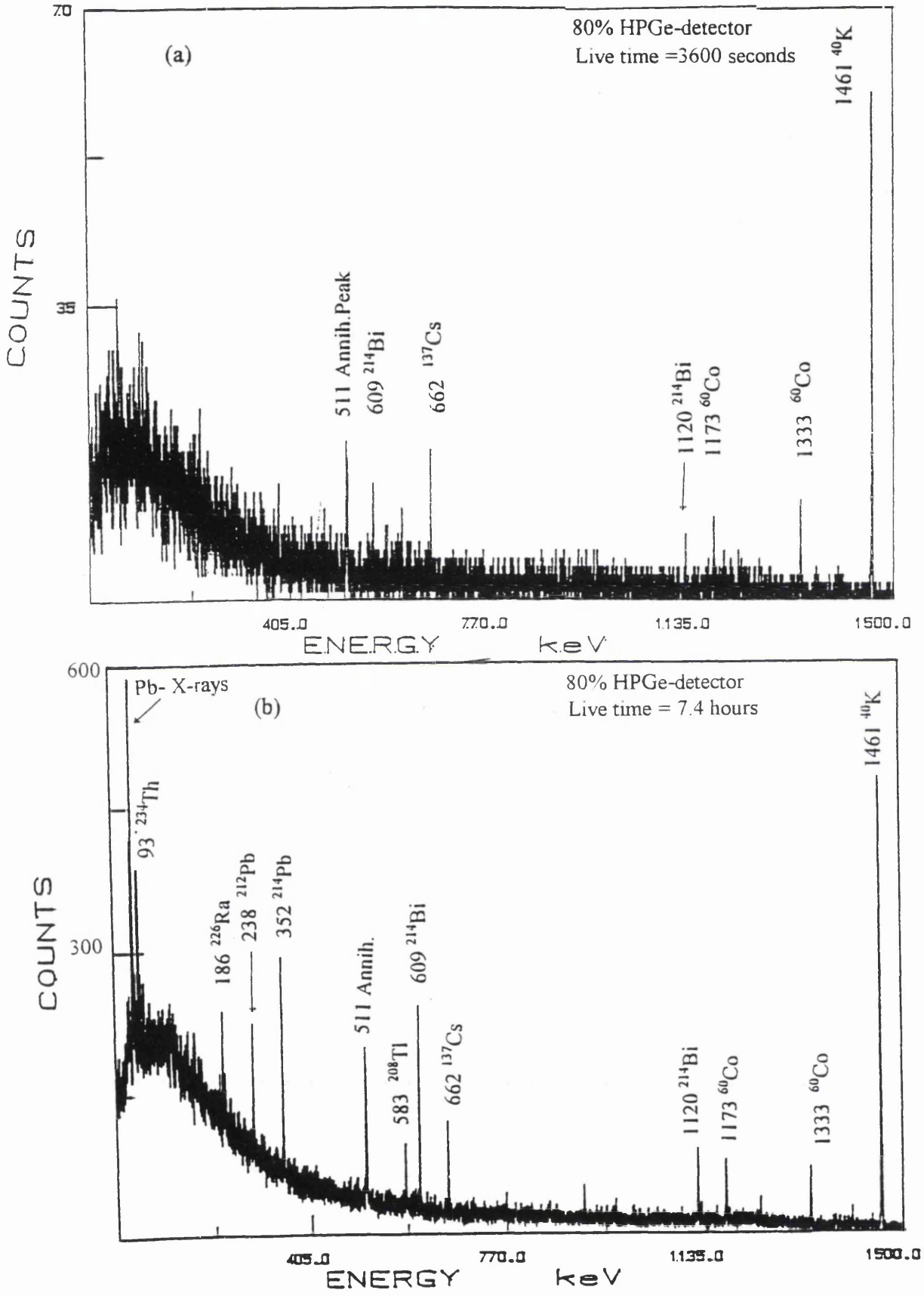

Figure 5.4 Typical gamma-ray spectra of subjects static counts using the 80% HPGe-detector: (a) single and; (b) summed spectra.

5.3 *In vivo* identification and calibration with injected ^{237}Pu

5.3.1 Introduction

Two of the n-type HPGe LOAX detectors were used to measure a healthy male subject A, injected intravenously with a monomeric solution of ^{237}Pu (IV) citrate, as a part of an AEA Technology (Harwell) absorption experiment. The subject under study was a healthy volunteer and the injected radionuclide was 19.42 kBq of ^{237}Pu (IV) inter-cubitally (Newton, 1994). ^{237}Pu is an electron capture radionuclide with a half-life of (45.73 ± 2.7 day) (Talbot et al., 1993), and the injection was highly purified to remove ^{239}Pu and traces of other plutonium radionuclides (Demitriev, 1993). This was done to ensure that the committed effective radiation dose was minimized to an acceptably low level. It is known that 100 kBq could deliver a committed effective dose (CED) of 100 μSv (ICRP, 1991). Further, ^{237}Pu decays by two $K_{\alpha 2}$ X-rays at 97.1 and $K_{\alpha 1}$ X-rays at 101.1 keV; gamma-rays of energy 59.6 keV; it also emits X-rays of $K_{\beta 1}$ 113.3; 114.2 combined and $K_{\beta 2}$ 117 keV and other less abundant lines at lower energies (ICRP 38, 1983). Details of these principal emission are shown in Table 5.5.

Energy (keV)	Decay probability dis. s^{-1}
59.6	0.00241
97.1	0.1210
101.08	0.1940
113.3	0.0240
114.2	0.0455
117.7	0.0241

Table 5.5 Main energy peaks of ^{237}Pu and their decay probability (ICRP 38).

5.3.2 Measurement procedures

The opportunity to make these measurements at SURRC arose at an early stage in the setting-up of the new semiconductor shadow-shield whole-body counter. The monitor was used in the static mode and the subject was positioned to give the closest arrangement between subject abdomen surface and detectors by adjusting the height with packing on the monitor bed. The LOAXs could be positioned close to each other because of the small Dewars and could therefore cover a significant area of the liver, which was the organ of interest. Three counts, ranging from 33-38 minutes in duration were initially taken consecutively; the first with both LOAX detectors positioned vertically over the liver.

A second count was taken with one detector placed beside the subject under the shield and positioned in contact with the right side of the subject's body. The other detector was placed at the top of the subject's head, also inside the turret. To obtain the appropriate background counts, a water phantom was measured in the same geometries. Both detectors were calibrated for energy using ^{241}Am, ^{133}Ba and ^{57}Co point standard sources at 25 cm distance. The gamma-ray spectra obtained from the three measurements on the subject along with water phantom counts are shown in Figure 5.5 a & b and 5.6 a & b.

5.3.4 Results and discussion

The measurements of the subject were carried out on the 31st day after injection of the ^{237}Pu, which meant approximately 37% of the injected activity had decayed. The total residual activity which remained in the subject was calculated to be 12.2±2.6 kBq. Plutonium compounds entering the circulation are known to accumulate mainly in two sites: approximately 45% in the skeleton; and 45% in the liver (ICRP, 1997 a). For this reason, the subject's measurements were carried out on these two key deposition sites, with the skull being chosen to be representative of the skeleton. Therefore, the estimated activities deposited in the liver, skeleton and the head (15% of skeletal mass) on the measured data are presented in Table 5.6. Figure 5.5a. shows the recorded spectrum of one of the detectors, which gave higher counts because it was positioned (vertically) directly above the area of the liver. From the count rates listed in Table 5.7 it could be seen that the other LOAX detector (No 2) was probably positioned slightly further from the centre of the liver. However, the count rates were approximately identical for these two detectors, which meant the deposited activity was uniformly distributed in the liver. Figure 5.5b shows the collected spectrum with the single detector beside the subject. Twice the counts were observed from the side count because the detector was positioned closer to the body. The spectrum recorded from the top of the head, along with that of the water phantom, is shown in Figure 5.6 a & b. A lower level of scattering can be seen, probably due to there being less soft tissue in this part of the body, and also a lower count rate was recorded. For completeness, the observed counting rates for all the ^{237}Pu peaks are given in Table 5.8.

Organ	^{237}Pu activity kBq
Liver	5.5 ±2.4
Whole skeleton	5.5 ±2.4
Head	0.82±0.44

Table 5.6 Calculated deposited ^{237}Pu activity in liver, skeleton and head.

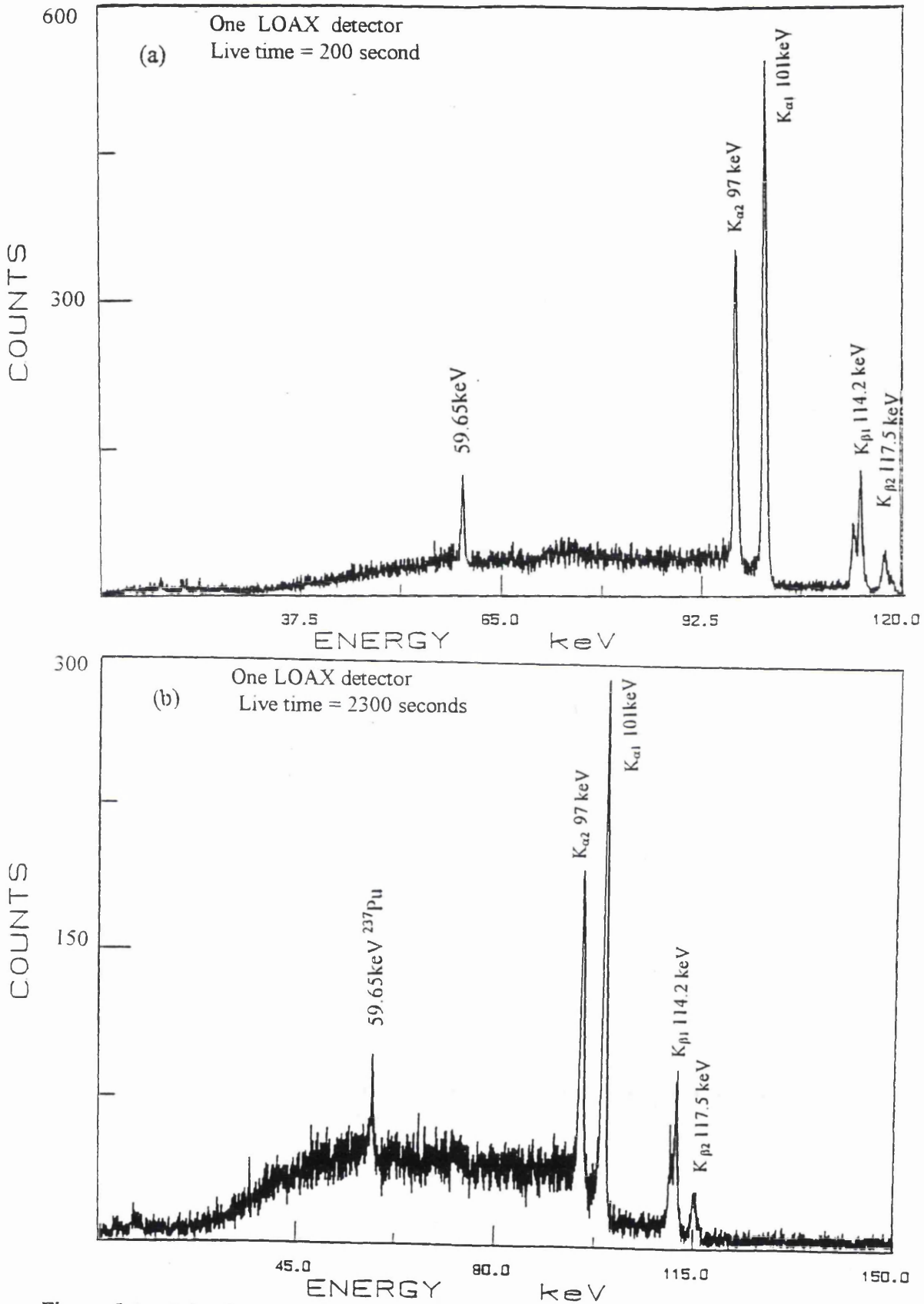

Figure 5.5 a & b Gamma-ray spectra of subject A injected with ^{237}Pu measured using two single LOAX-detectors: (a) vertical liver count; (b) liver side count.

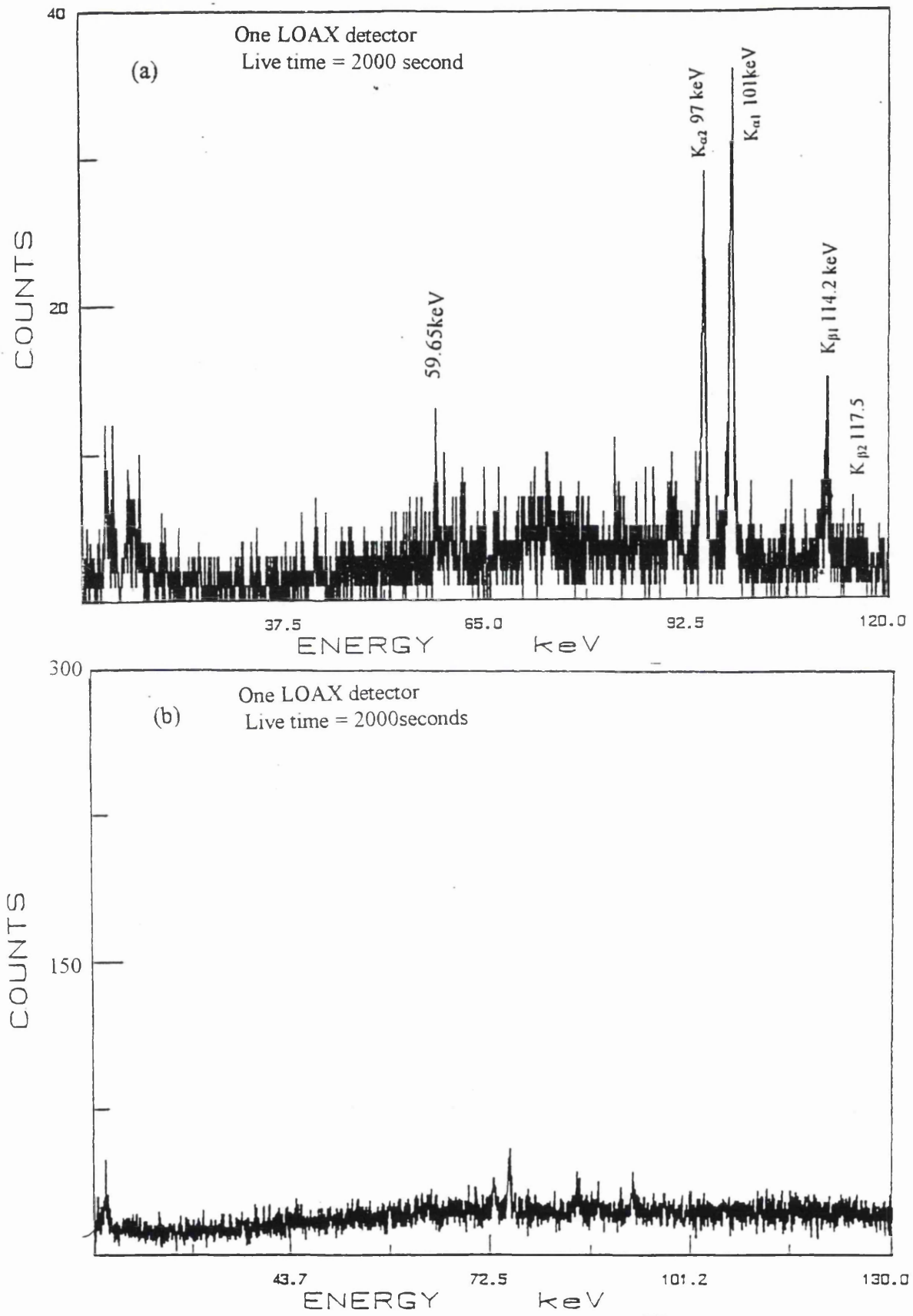

Figure 5.6 Gamma-ray spectra of subject A injected with ^{237}Pu measured using two different single LOAX-detectors: (a) head count (b) water phantom.

Energy		Vertical liver counts LOAX # 1	LOAX # 2	Beside liver LOAX # 1	Head count LOAX # 2
Observed count rates in cps for the main x & γ-peaks	59.6keV	0.129±0.01	0.104 ± 0.01	0.31±0.01	0.012±0.01
	97.2keV	1.001± 0.02	0.90 ± 0.02	1.75±0.02	0.121±0.01
	101keV	1.682 ±0.02	1.43 ± 0.02	2.91±0.03	0.181±0.01
Efficiency in cps Bq^{-1}	59.6keV	2.36×10^{-5}	1.90×10^{-5}	5.67×10^{-5}	1.46×10^{-5}
	97.2keV	1.83×10^{-4}	1.65×10^{-4}	3.20×10^{-4}	1.47×10^{-4}
	101keV	3.08×10^{-4}	2.62×10^{-4}	5.32×10^{-4}	2.20×10^{-4}

Table 5.7 Measured *in vivo* sensitivities for two LOAX detectors counting ^{237}Pu in subject A.

Energy keV	1st Vertical position cps±1σ	2nd Vertical position cps±1σ	Beside body cps±1σ	Head count cps±1σ
59.6	0.129±0.01	0.104±0.01	0.31±0.01	0.012±0.002
97.1	1.00±0.02	0.90±0.02	1.75±0.02	0.121±0.006
101.1	1.68±0.02	1.43±0.02	2.91±0.03	0.181±0.007
113.3	0.21±0.02	0.17±0.01	0.35±0.01	0.035±0.003
114.2	0.37±0.01	0.31±0.02	0.64±0.02	-----
117.7	0.18±0.01	0.18±0.01	0.26±0.01	-----

Table 5.8 Net counts per second of the various measurements carried out on the subject A (^{237}Pu) using the two LOAX detectors.

As a cross-check on the above results, approximate calibration for the two detectors were obtained using two standard point sources of 427 kBq ^{241}Am and 25 kBq ^{57}Co. These were placed 10 cm from the detectors and counted without any phantom arrangements in order to minimise scattering effects. The efficiency calibration curve obtained is shown in Figure 5.7 with the calculated efficiency factors presented in Table 5.9.

Energy keV	Efficiency of LOAX No.1 cps Bq^{-1} ±5%	Efficiency of LOAX No.2 cps Bq^{-1} ±5%
14	0.00263	0.00234
26.3	0.00341	0.00335
59.5	0.00422	0.00412
122	0.00444	0.00423
136	0.00411	0.00378

Table 5.9 Measured efficiency for both LOAX detectors using ^{241}Am and ^{57}Co standard point sources.

The efficiency values obtained were found to be approximately 100 times those for the *in vivo* measurements. However, this was explicable by the fact that the sources were point sources and therefore did not simulate the distribution in the subject at all well. Taking this into consideration, the result was regarded as being satisfactory and as independent standardisation of counting sensitivity.

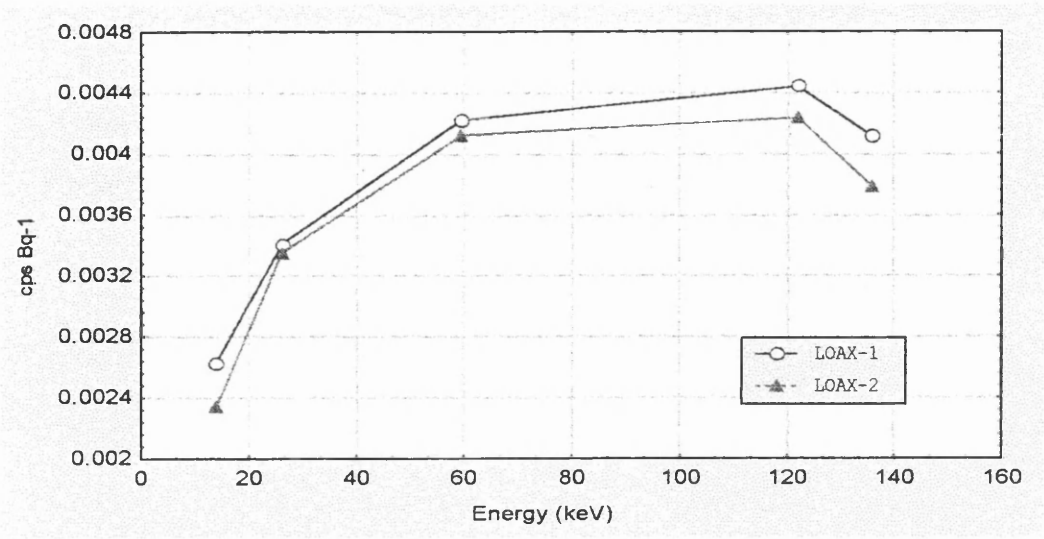

Figure 5.7 Efficiency calibration curves for both LOAX detectors connected separately using ^{241}Am and ^{57}Co.

5.3.5 Conclusion

The opportunity to measure ^{237}Pu *in vivo* provided an ideal calibration experiment for the low-energy photon detector set up. Whilst phantoms can be constructed in an attempt to simulate the body, the best method of calibration is always to make *in vivo* measurements if possible. Because of the short half-life and relatively low dose emissions of ^{237}Pu, and the fact that it could be obtained with high purity, it was an ideal material for calibration. All of the photon energies of ^{237}Pu could be identified clearly. The *in vivo* calibration sensitivity for the principal peaks of 97 and 101 keV was found to be in the range of 1.7-5.3x10^{-4} cps Bq^{-1} for the various geometries. From the results, the best counting arrangement for a subject contaminated with Pu would be to have the detector beside the liver, which gave the highest response for the *in vivo* experiment. Care would be required when positioning the detector however to maintain adequate reproducibility. It was much easier to maintain reproducibility when positioning a detector over the top of the head, although a lower sensitivity was obtained in this geometry. However, a measurement of the skull provided data on the skeletal content assuming uniform distribution through the skeleton. The sensitivity factors for measuring the 59.5 keV peak of ^{241}Am could be compared to that of 59.6 keV of ^{237}Pu *in vivo* i.e. calculated efficiencies in the range of (1.5-5.3)x10^{-5} cps Bq^{-1}. This lower sensitivity was mainly attributed to the high attenuation by the body tissue. The measured MDA values of the *in vivo* counting for ^{237}Pu were found to be: 88 Bq for the 59.6 keV; 9 Bq for 97 keV; and 6 Bq for the 101 keV; for one LOAX detector and a 50 minute count.

5.4 Attempts to measure radon via its daughters by body counting

5.4.1 Radioactivity background in mines

Underground uranium gives rise to radiation exposure both directly and from radon and thoron decay products in the air. The deposited activity in miners' lungs and the associated airborne concentrations of ^{220}Rn and ^{222}Rn have been studied in a number of mining sites over the world. As described in Chapter 3, Figure 3.2, uranium-238 and thorium-232 are the parents of two naturally occurring radioactive chains which give rise to ^{220}Rn and ^{222}Rn respectively. These two radioactive noble gases migrate from the walls and the ground into the mine atmosphere by diffusion and other transport mechanisms. Due to the low ventilation rates inside mines, the short-lived decay products of ^{222}Rn (^{218}Po, ^{214}Pb, ^{214}Bi, ^{214}Po and ^{210}Pb) and also those of ^{220}Rn (^{212}Pb, ^{212}Bi, ^{212}Po, and ^{208}Tl) build up in mine air and become of considerable importance in internal dosimetry and are the probable cause of heightened incidence of lung cancer among miners (Cohen et al., 1992). Several of these daughters emit gamma rays, which could be detectable by body monitoring provided this was possible soon after exposure had occurred. Also, ^{210}Pb from ^{222}Rn is more persistent with a half-life of 22 years and because it is known to accumulate in the bones, could provide a retrospective measure of uranium/radon exposure if detectable. It was therefore of interest to examine suitable subjects to establish the feasibility of body counting for this purpose. The following section describes the measurement of an individual known to have been exposed to underground radon.

5.4.2 Description of subject exposed to underground radon

An ideal subject, who regularly visited old mines in Devon and Cornwall, was found. She was an amateur uranium prospector, 162 cm in height and weighing 61 kg. The subject frequently visited mining sites at St.Terras and Tolgarrick where the recorded levels of radon concentration measured using portable radiation instruments were found to be approximately 2.1 MBq m^{-3}. Other sites which she regularly visited were Bushdown, Nuns Cross Tunnel and Eylesbarrow where the recorded concentrations of radon were approximately 7.1 kBq m^{-3}. This subject was measured twice; firstly, in September 1994 and secondly during September. 1995. The following description is a detailed account of both the measurements and the data analysis for each count.

5.4.3 The first examination of subject B

For whole-body monitoring, the subject was invited to attend for two days immediately following one of her usual visits to a number of the above mentioned mines. She was asked to follow basic instructions which included taking a shower the night before the measurements and cleaning her nails thoroughly to avoid any possibility of external contamination. In order to obtain the required data, a comprehensive measurement programme was carried out on her as detailed in Table 5.10. To provide a control, and to be certain about the measured activities, a non-exposed subject was sought for comparison. A female volunteer with comparable body measurements in terms of weight and height was measured soon after completion of the measurements on subject B. It was not possible to carry out all the measurements on the control subject, therefore the volunteer was only measured for a one-hour scanning count and two static counts using the same geometry as for subject B. A comparison of the static counts rates (cps) of subject B, the volunteer and the K/U chest phantom is presented in Table 5.11. Table 5.12 outlines the static count rates of subject B during the first and second day counts along with the water phantom for both detection systems. It was evident that the various count rates obtained on the first day for subject B were higher than those for the second day, and both were higher than the volunteer and the water phantom count rates for most of the main peak energies. Two separate and summed gamma-ray spectra representing the first and second days of counting of subject B are given in Appendix A.

Counting geometry	Counting time	Tow/four LOAX-HPGe position	80%HPGe-Detector	NaI(Tl) Detector
Scanning at 8 cm dist.	**60 minute**	**Whole body**	**W-body**	**W-body**
Static at 8 cm distance	**80 minute**	**Over chest**	**Abdomen**	**L-Abdomen**
Static at 4 cm distance	**60 minute**	**Over head**	**Chest**	**Abdomen**
Static at 4 cm distance	**50 minute**	**Over liver**	**L-Abdomen**	**Thighs**
Static at 4 cm distance	**50 minute**	**Over kneecap**	**Chest**	**Abdomen**
Static at 4 cm distance	**90 minute**	**Over chest**	**Abdomen**	**L-Abdomen**
Scanning at 8 cm dist.	**50 minute**	**Whole-body**	**W-body**	**W-body**
Static at 4 cm distance	**50 minute**	**Over chest**	**Abdomen**	**L-Abdomen**
Static at 4 cm distance	**50 minute**	**Over chest**	**Abdomen**	**L-Abdomen**

Table 5.10 The measurement protocol for static and scanning counts carried out on subject (B) using the three detectors over various parts of the body.

The count rates for the main energy peaks of the gamma-ray spectra obtained from the 80% HPGe-semiconductor detector systems for the various subject B measurements and the control subject are presented in Figure 5.8 along with their respective water phantom spectra. They show the differences between the water phantom, the control subject (volunteer) [labelled as Sub] and, subject B single and summed spectra of the first [labelled in the figure as Sum1.Sub B] and second day [labelled in the figure as Sum2.Sub B] counts. The results suggested: that the subject had some residual activity from short-lived radon daughter products which decreased during the second day's measurement; or it might be an indication of the first day's counts were detecting some external contamination of the subject's body. This fact could be seen in Figure 5.8 which depicts some of the various levels for a number of gamma peaks of the separate counts on the control subject and subject B single and summed spectra for all the first and second day measurements. The actual gamma-ray spectra of subject B are shown in Figures 5.9 a & b and 5.10 a & b compared with volunteer counts of comparable body physique using both of detection systems.

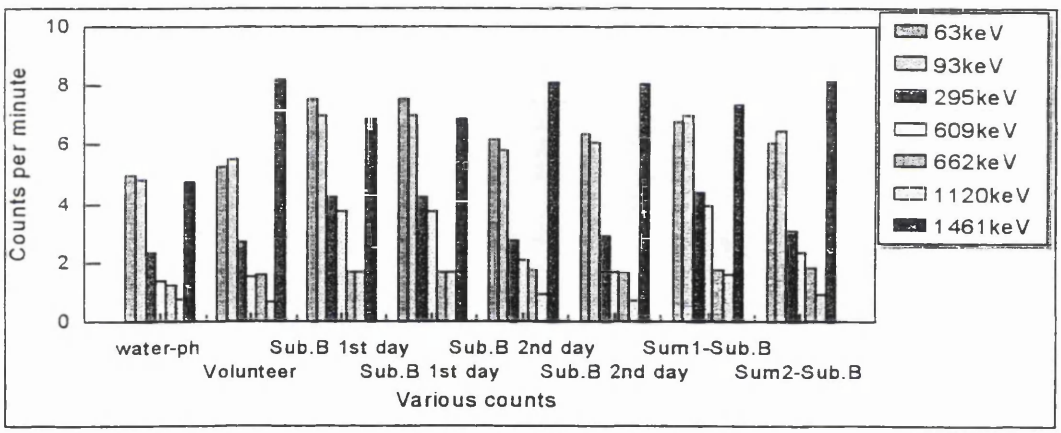

Figure 5.8 Comparison of the count rates for the main gamma-energy peaks of single and summed spectra obtained measuring subject B and control subject.

Also Table 5.11 presents the static count rates for both days for the chest and the difference in count rate compared with the volunteer using the 80% HPGe-detector. Similar data are given for the abdomen.

Taking the count rates for the main energy peaks namely 63 and 93 keV to calculate the uranium concentrations in her body the values came out to be (10±4 mg) and (15±5 mg), which was conceivable for such a subject with her prospecting history extending over more than twenty years. However, the method could not distinguish whether the activity was internal or external and it had to be assumed that external activity was negligible,

because, as mentioned, the subject was asked to take precautions to eliminate external contamination. All the other counts of the head and knee caps also showed higher count rates than the water phantom but no comparable counts for the volunteer were possible. Subject B was very cooperative and showed much patience during the various long static counts which enabled all the outlined data to be collected.

Energy keV	Complete water-phantom Cpm±1σ	Subject B 1st day chest cpm±1σ	Subject B 2nd day Chest cpm±1σ	Volunteer Chest cpm±1σ	K/U-chest raised& inv. Cpm±1σ
U X-ray 13	9.0±0.4	9.9±0.4	9.4±0.3	8.1±0.4	18.6±0.5
- 16	12.0±0.4	12.4±0.4	10.8±0.4	11.4±0.4	27.6±0.6
- 20	3.0±0.2	7.1±0.3	4.8±0.2	4.9±0.3	12.6±0.4
- 25	4.5±0.2	4.6±0.2	3.3±0.2	3.8±0.3	7.6±0.3
^{133}Ba 31	3.5±0.2	5.5±0.3	5.0±0.2	3.7±0.3	7.4±0.3
- 36	4.0±0.2	5.2±0.3	4.1±0.2	3.5±0.2	7.5±0.3
^{210}Pb 46	5.0±0.2	7.01±0.3	5.3±0.2	4.6±0.3	10.9±0.4
^{234}Th 63	12±0.4	17.0±0.5	13.0±0.4	11.5±0.4	46.4±0.7
PbX-ray75	14.1±0.4	17.3±0.5	11.7±0.4	10.8±0.4	21.0±0.5
^{234}Th 93	15.0±0.4	18.4±0.5	15.5±0.4	11.6±0.4	47.3±0.7
^{226}Ra 186	8.8±0.3	9.6±0.4	6.7±0.3	5.4± 0.3	13.1±0.4
^{214}Pb 238	3.8±0.2	5.1±0.3	3.7±0.2	2.7±0.2	4.2±0.2
- 295	2.6±0.2	4.1±0.2	2.3±0.2	2.2±0.2	3.0±0.2

Table 5.11 Count rates of the various static measurements of: water phantom; subject B chest region; the volunteer; and the K/U phantom chest raised and inverted using the four LOAX HPGe-detectors as one summed signal.

Energy keV	Water-phantom cpm±1σ	Subject B 1st day chest cpm±1σ	Volunteer for B cpm±1σ	Difference Sub.-Vol. cpm±1σ	Subject B 1st day Abdo. Cpm±1σ	Subject B 2nd day Abdo. cpm±1σ
^{133m}Ba	2.8±0.2	3.2±0.2	2.5±0.2	0.7±0.3	2.6±0.2	2.7±0.2
- 32	2.9±0.2	3.8±0.3	2.3±0.2	1.5±0.3	2.9±0.2	2.2±0.2
- 36	2.5±0.2	2.6±0.2	2.4±0.2	0.2±0.3	2.2±0.2	2.8±0.2
^{210}Pb 46	2.3±0.2	3.2±0.2	2.8±0.2	0.3±0.5	2.6±0.2	2.6±0.2
^{234}Th 63	6.0±0.3	7.6±0.4	5.5±0.3	2.0±0.3	6.5±0.3	4.1±0.3
- 93	5.8±0.3	9.0±0.4	6.2±0.3	2.7±0.5	6.7±0.3	6.1±0.3
^{226}Ra 186	4.7±0.3	5.4±0.3	4.4±0.3	1.1±0.4	5.1±0.3	4.7±0.3
^{214}Pb 238	3.7±0.3	4.5±0.3	3.6±0.3	0.9±0.4	3.9±.3	3.4±0.2
- 295	2.6±0.2	4.5±0.3	2.4±0.2	2.1±0.3	4.9±0.3	3.2±0.2
- 352	2.0±0.2	4.9±0.3	2.3±0.2	2.6±0.3	4.3±0.3	3.2±0.2
^{214}Bi 609	1.5±0.2	4.0±0.3	1.6±0.2	2.4±0.6	4.3±0.3	2.3±0.2
^{137}Cs 662	1.3±0.2	1.8±0.2	1.7±0.2	0.2±0.2	1.7±0.2	1.6±0.2
^{214}Bi 766	0.6±0.1	1.0±0.1	0.7±0.1	0.3±0.2	0.7±0.1	0.6±0.1
- 1001	0.7±0.1	1.6±0.2	0.5±0.1	1.2±0.2	1.5±0.2	0.9±0.1
^{60}Co 1172	0.8±0.1	0.9±0.1	0.9±0.1	—	1.2±0.1	1.3±0.2
^{40}K 1461	4.6±0.1	6.9±0.1	7.1±0.3	—	8.5±.4	8.0±0.4

Table 5.12 Comparison of static count rates (cpm) between subject B and volunteer for the main energy counts of chest and abdomen regions using the 80% HPGe- detector.

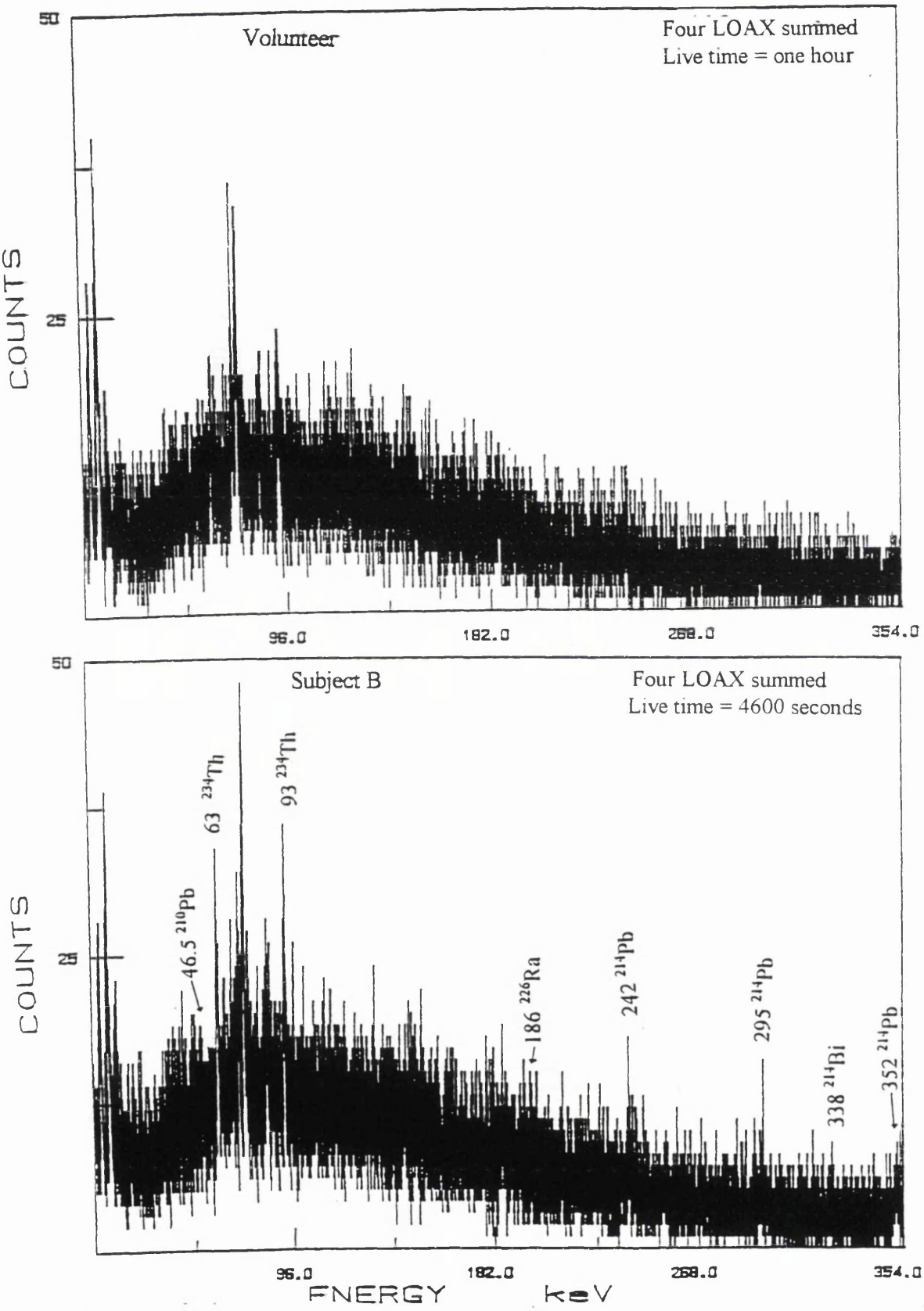

Figure 5.9 Typical gamma-ray spectra from static measurements using the four LOAX detectors to monitor the chest (lungs) region: (a) Volunteer; (b) Subject B.

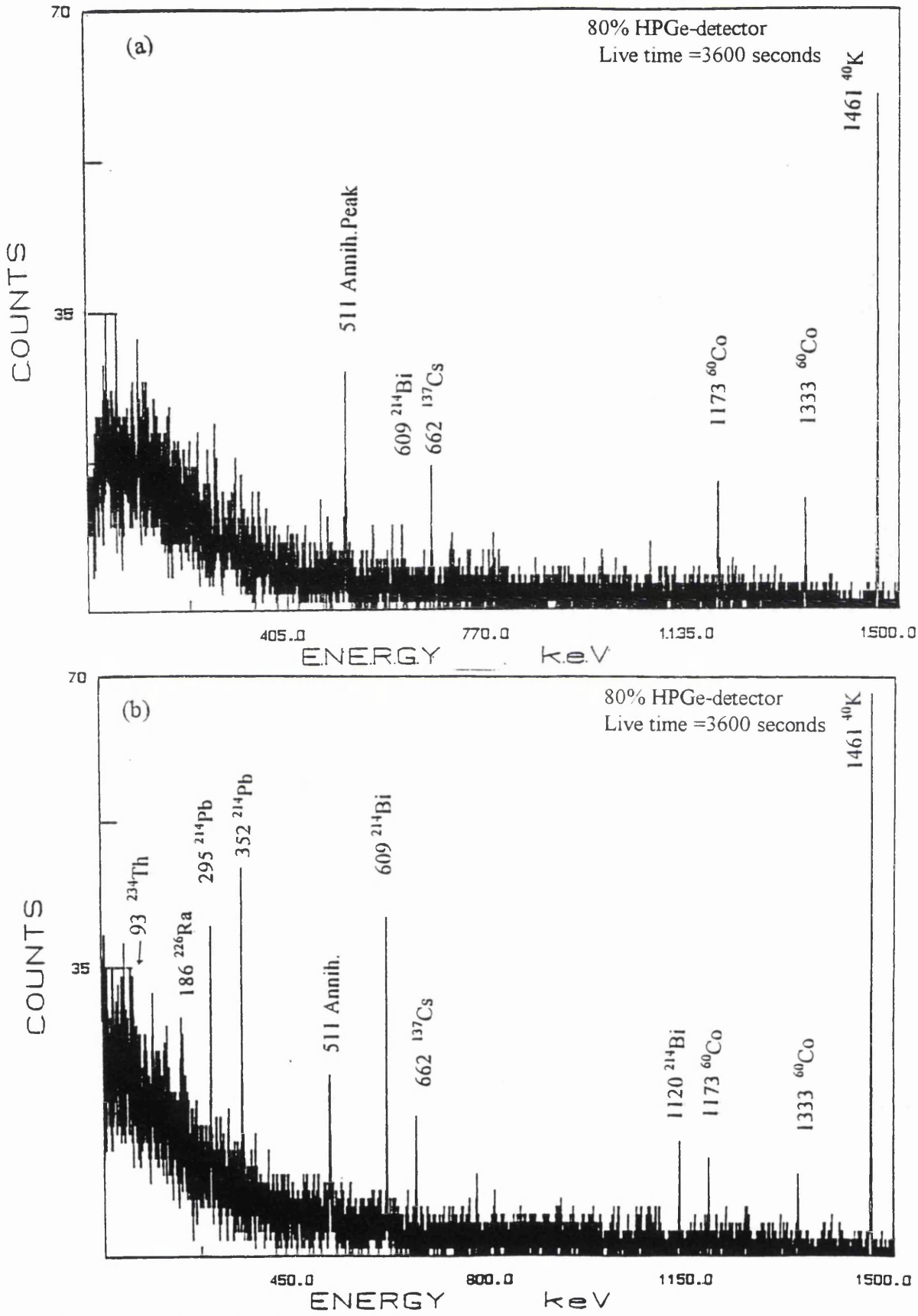

Figure 5.10 Typical gamma-ray spectra from static measurements using the 80% HPGe-detector to monitor the chest (lungs) region: (a) Volunteer; (b) Subject B.

The same trend of decrease in activity was also observed for the scanning measurements with both systems which showed a drop on the second day by the same margin for all of the main peaks shown in Figure 5.11 and as presented in Table 5.13 for the four LOAX detector in comparison with water phantom background count and the control subject's count.

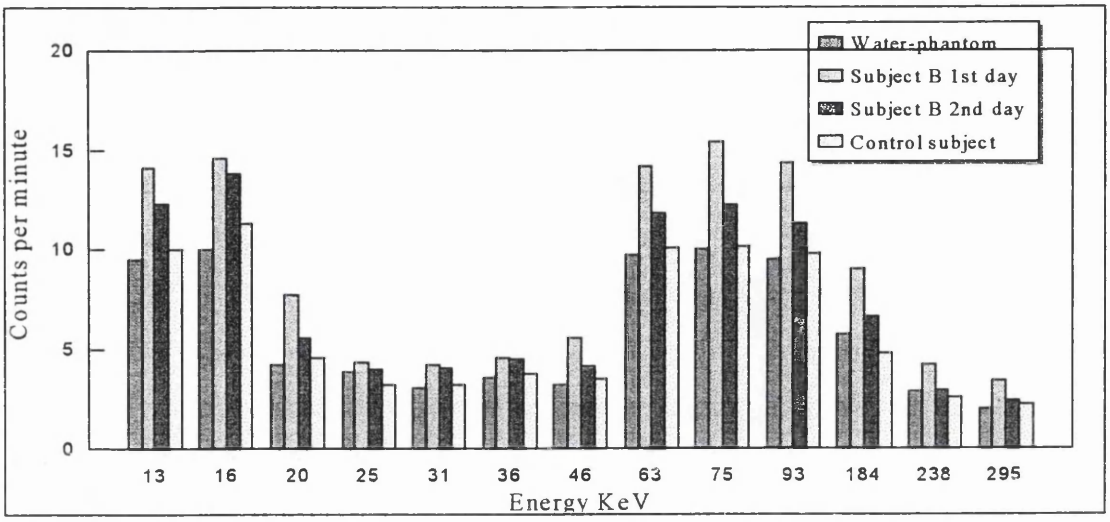

Figure 5.11 Scanning count of the subject B on both days in comparison with water phantom background and the control subject's count using the four LOAX-detectors.

Energy Nucl. keV	4-LOAX Water-phant. cpm ±1σ	4-LOAX Sub.B 1st day cpm±1σ	4-LOAX Sub.B 2nd day cpm±1σ	80%Det water-phant. cpm±1σ	80%Det Sub.B1st cpm±1σ	80%Det Sub.B 2nd day cpm±1σ
U-x-ray 13	9.5±**0.4**	14.1±**0.5**	12.3±**0.5**	*ND	*ND	*ND
- 16	10.0±**0.4**	14.6±**0.5**	13.8±**0.5**	-	-	-
^{133}Ba 36	3.6±**0.3**	4.6±**0.3**	4.5±**0.3**	2.6±**0.2**	2.9±**0.2**	2.7±**0.2**
^{210}Pb 46	4.0±**0.3**	5.6±**0.3**	4.1±**0.3**	2.3±**0.2**	2.7±**0.2**	2.2±**0.2**
^{234}Th 63	9.7±**0.4**	14.2±**0.5**	11.8±**0.4**	4.5±**0.3**	6.2±**0.3**	5.9±**0.3**
- 93	10.1±**0.4**	15.4±**0.5**	11.3±**0.4**	5.1±**0.3**	6.7±**0.3**	5.1±**0.3**
^{226}Ra 186	5.8±**0.3**	9.0±**0.4**	6.7±**0.3**	3.6±**0.3**	4.6±**0.3**	4.1±**0.3**
^{214}Pb 238	2.9±**0.2**	4.2±**0.3**	4.0±**0.3**	3.4±**0.3**	4.3±**0.3**	3.5±**0.3**
- 295	2.0±**0.2**	3.5±**0.2**	2.4±**0.2**	2.1±**0.2**	3.7±**0.3**	2.2±**0.2**
- 352	*ND	*ND	*ND	1.8±**0.2**	4.2±**0.3**	1.9±**0.2**
^{214}Bi 609	-	-	-	1.5±**0.2**	3.3±**0.2**	1.7±**0.2**
^{137}Cs 662	-	-	-	1.2±**0.1**	1.4±**0.2**	1.3±**0.1**
^{214}Bi 766	-	-	-	0.6±**0.1**	0.6±**0.1**	0.7±**0.1**
- 1001	-	-	-	0.4±**0.1**	0.6±**0.1**	0.5±**0.1**
- 1120	-	-	-	0.4±**0.1**	1.0±**0.2**	0.7±**0.1**
^{40}K 1461	-	-	-	2.1±**0.2**	4.8±**0.3**	4.3±**0.3**

Table 5.13 Scanning count rates of both detection system four LOAX and the 80% HPGe-detectors for the first and second counts along with the respective water phantoms measurements.

(* Not detected because out of detector's energy range).

5.4.4 Second examination of Subject B

5.4.4.1 *In vivo* measurement procedures

One year later, the detector systems having been calibrated with the tissue equivalent phantoms, subject B was contacted again for a second investigation. The subject came to the laboratory two days after visiting some of the mines stated earlier and was asked to observe the same precautions regarding external contamination. Almost the same measurement protocol was carried out on her except that more attention was paid to the liver and the lower abdomen area where more activity was measurable. However, this time the subject showed a completely different pattern of radioactivity in her body. The whole complex gamma-ray spectra obtained using the two LOAX and the 80% detectors are shown in Figure 5.12 and Figure 5.13 for static counts over the abdomen (liver area). The complete detailed analysis of the spectra is shown in Appendix A under the same figure numbers respectively. The analysis of these spectra showed clearly the presence of fission and activation products consisting of the following radionuclides; ^{241}Am, ^{133}Ba, ^{60}Co, ^{137}Cs, $^{152\ \&\ 154}$Eu and the U-Th series radionuclides. These peaks showed different levels of activities in the chest and lower abdomen. The highest count rates were encountered during the second static count when the 80% detector was positioned over her lower abdomen and the two LOAX detectors were over the liver area. Figures 5.14 & 5.15 graphically depict a comparison between her two lower abdomen and water phantom counts for the two detection systems separately. To be certain that the detected count rates for the main peaks genuinely originated from the measured subject, a water phantom background count was taken immediately whenever the subject was out of the counter for rest or other breaks and overnight using the same counting geometry. Typical gamma-ray spectra of these background counts are presented along with the subject liver static counts in Figure 5.16 and Figure 5.17 for the two detection systems. Expanded and complete sections of the detailed peaks in the spectrum are shown in Appendix A for the two lower abdomen counts. The main peaks of a number of activation and fission products could be clearly seen in most of the obtained gamma-ray spectra. A graphical representation of the low- and upper abdomen counts of subject B using the 80% HPGe-detector is depicted in Figure 5.18.

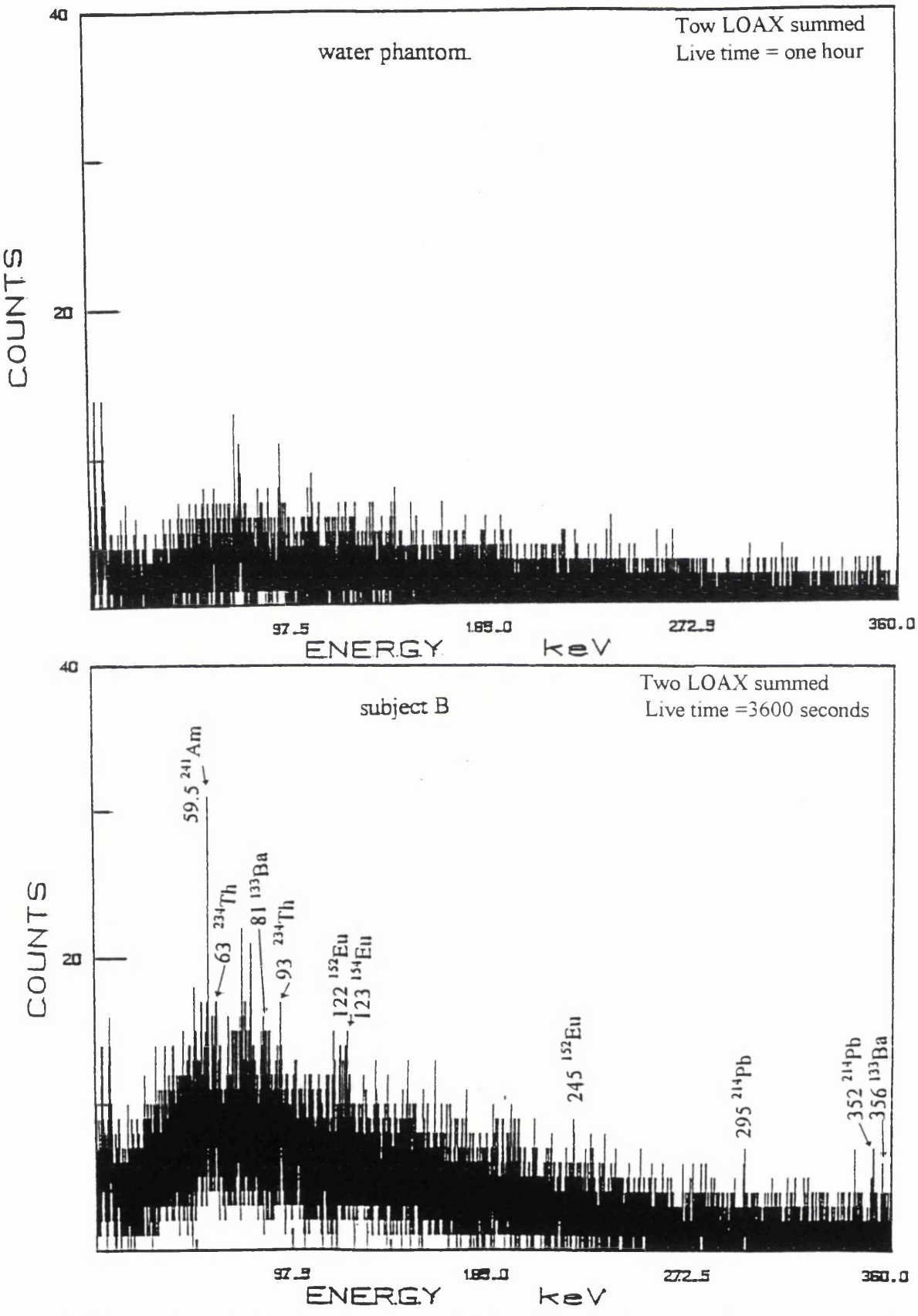

Figure 5.12 a & b Gamma-ray spectra of the subject B liver second static count using two LOAX detectors in comparison with water phantom count of similar geometry.

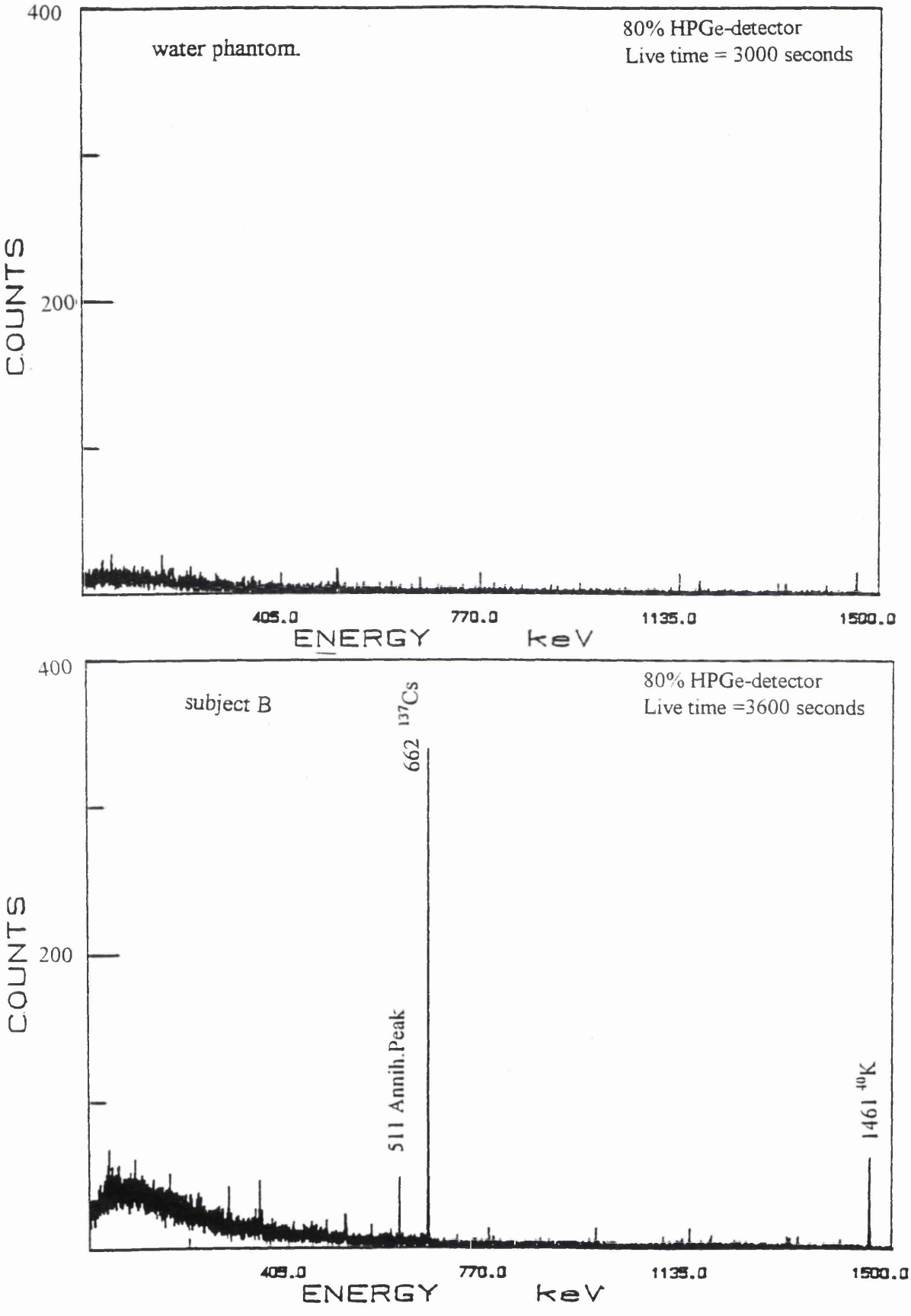

Figure 5.13 a & b Gamma-ray spectrum of subject B second count of lower abdomen using the 80% HPGe-detector in comparison with the water phantom.

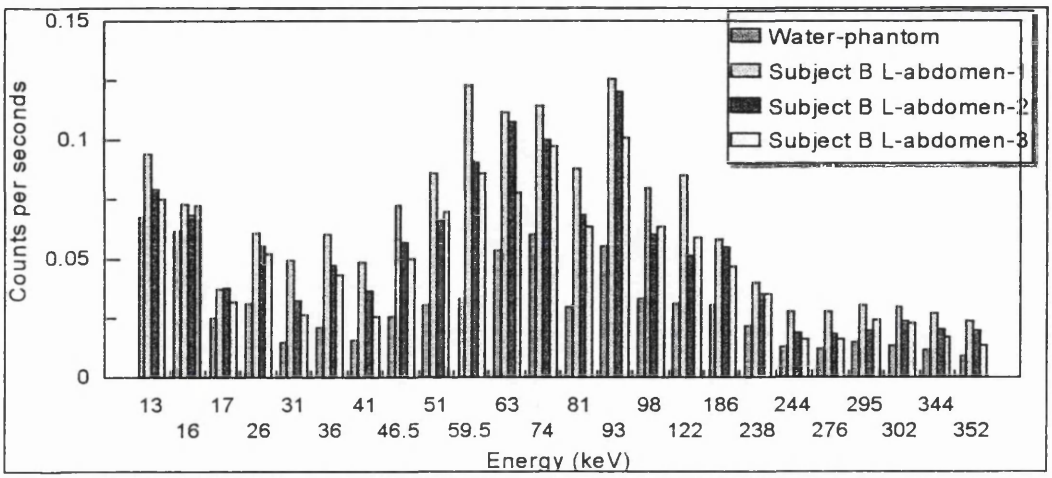

Figure 5.14 Count rates per second of the main peaks of two LOAX detectors measurements of three lower abdomen counts of subject B along the water phantom.

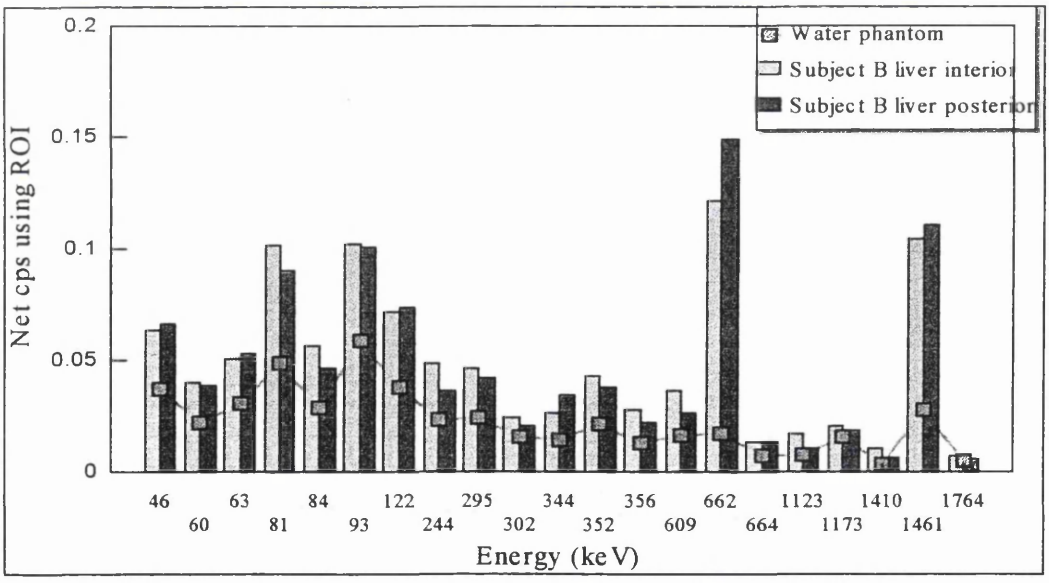

Figure 5.15 Count rates (cps) of the main peaks of both liver counts posterior and anterior of subject B in comparison with water phantom count using the 80% HPGe-detector.

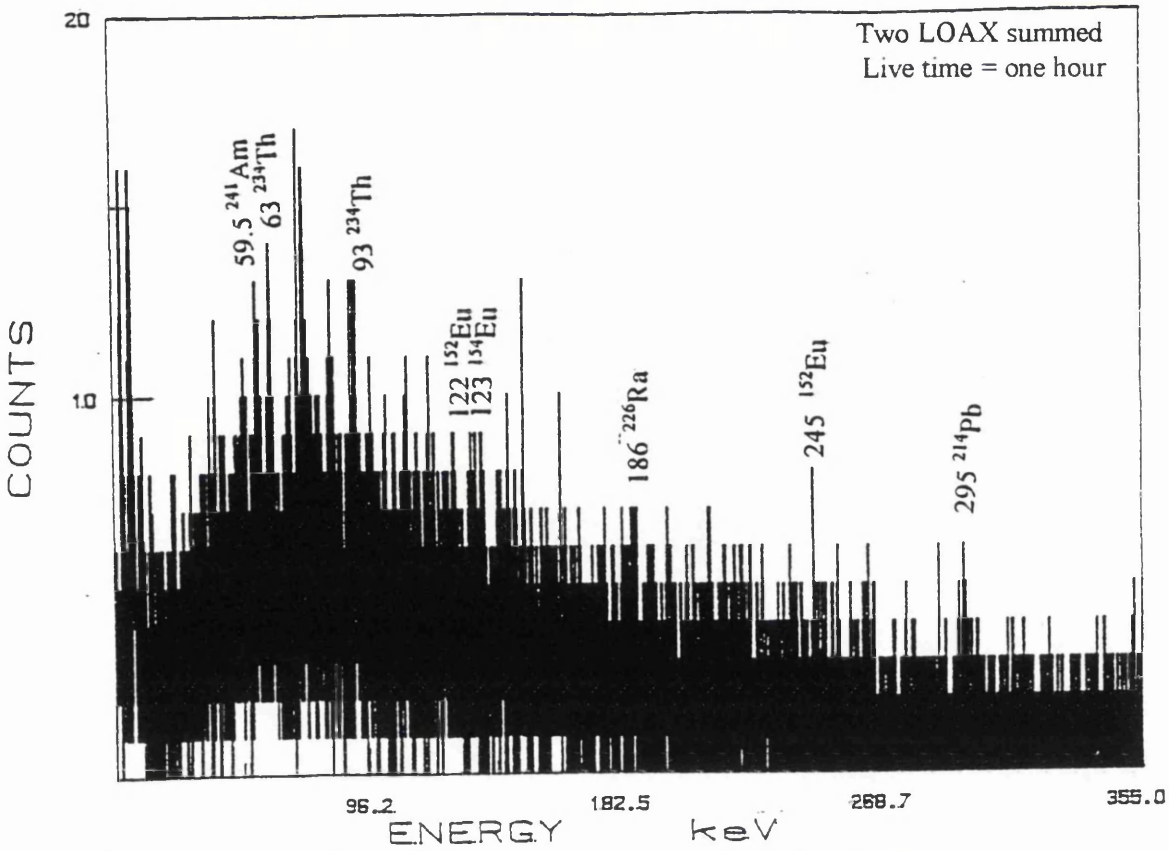

Figure 5.16 Typical gamma-ray spectra of the subject B liver static count using two LOAX detector.

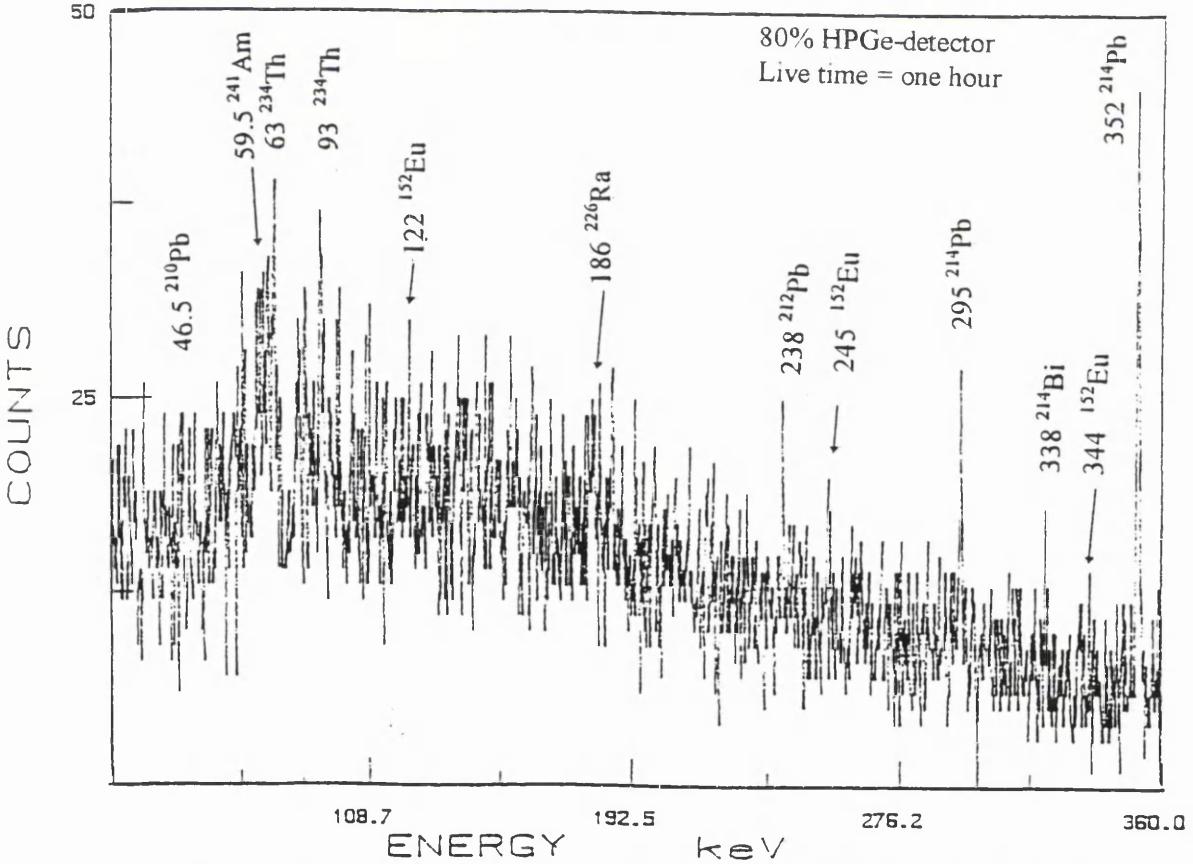

Figure 5.17 A typical gamma-ray spectrum of the 80% HPGe-detector measuring the liver of subject B.

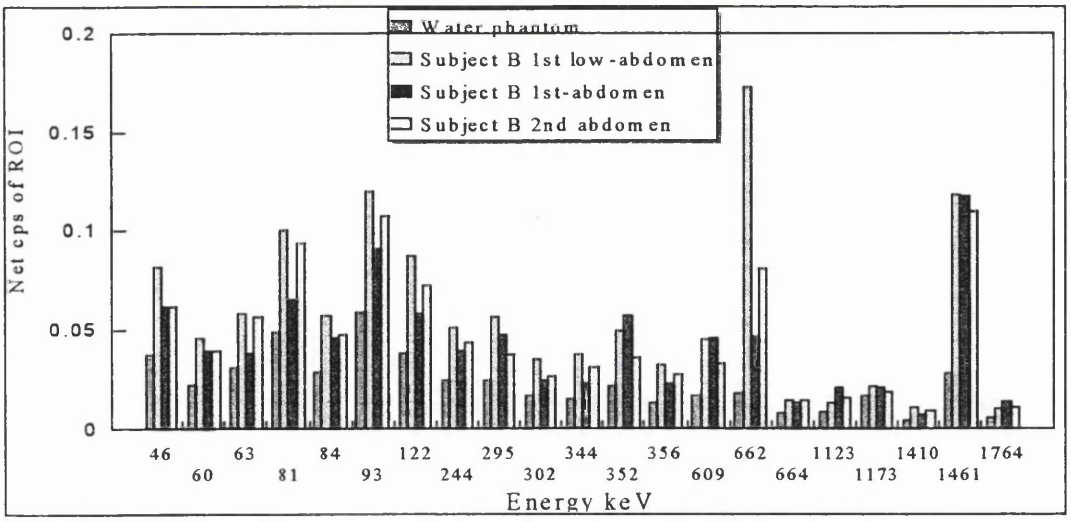

Figure 5.18 Comparison of net count rates between: water phantom; low-abdomen; two upper abdomen; for static count on subject B using the 80% HPGe-detector.

In order to analyze the gamma-ray data, the net count rates were calculated using the Minigam programme and the detailed trapezium method taking ROIs above and below the peaks (as described in chapter 3). These calculated values of the net count rates for all the detected radionuclides for the liver and lower abdomen static counts are presented in Table 5.14.

Nuclides keV	1st day Liver cps±1σ	2nd day Liver cps±1σ	1st day*L-abd. cps±1σ	2nd day L-abd cps±1σ	3rd day L-abd cps±1σ
^{241}Am					
59.5	$(5.8\pm4.0)\times10^{-3}$	$(1.0\pm1.0)\times10^{-3}$	$(1.8\pm1.2)\times10^{-2}$	$(2.7\pm1.5)\times10^{-3}$	---
^{133}Ba					
81	$(1.7\pm1.0)\times10^{-3}$	$(8.3\pm5.0)\times10^{-3}$	$(3.2\pm2.0)\times10^{-3}$	$(1.3\pm1.0)\times10^{-2}$	$(1.2\pm1.0)\times10^{-2}$
276	------	----	----	$(8.7\pm5.0)\times10^{-3}$	$(8.5\pm5.0)\times10^{-2}$
302	------	----	----	$(3.2\pm2.0)\times10^{-3}$	$(3.0\pm2.0)\times10^{-2}$
^{152}Eu					
122	$(8.8\pm5.0)\times10^{-3}$	$(5.6\pm4.0)\times10^{-3}$	$(6.0\pm4.0)\times10^{-3}$	$(8.1\pm5.0)\times10^{-3}$	$(7.9\pm5.0)\times10^{-2}$
344	------		$(7.2\pm5.0)\times10^{-4}$	$(2.3\pm2.0)\times10^{-4}$	$(2.3\pm2.0)\times10^{-2}$
U-Th					
63	$(1.8\pm1.0)\times10^{-2}$	$(2.8\pm1.5)\times10^{-2}$	$(2.6\pm1.5)\times10^{-2}$	$(7.3\pm1.0)\times10^{-3}$	$(7.1\pm1.0)\times10^{-2}$
93	$(3.8\pm2.0)\times10^{-2}$	$(5.0\pm3.0)\times10^{-2}$	$(3.0\pm1.5)\times10^{-2}$	$(3.7\pm5.0)\times10^{-2}$	$(3.7\pm2.0)\times10^{-2}$
186	$(2.0\pm2.0)\times10^{-2}$	$(2.6\pm2.0)\times10^{-2}$	$(1.2\pm1.0)\times10^{-2}$	$(1.5\pm1.0)\times10^{-2}$	$(1.5\pm1.0)\times10^{-2}$

Table 5.14 Net count rates (cps) of *in vivo* subject B calculated using the trapezium method for the main peaks using the two LOAX HPGe detectors, taking one hour count.

Using the previously measured sensitivity factors from the tissue equivalent phantoms, K/U and ^{137}Cs phantom for both detection systems, the measured count rates of the low-abdomen count for the main detected gamma peaks were converted into activities in Becquerels. These calculated activities for the main radionuclides are presented in Table 5.15.

^{241}Am 59keV	80±24 Bq
^{133}Ba 81keV	42±13 Bq
^{133}Ba 356keV	53±16 Bq
^{152}Eu 122keV	60±18Bq
^{152}Eu 244keV	45±14Bq
^{234}Th 63keV	12±4 mg
^{234}Th 93keV	17±5mg
^{137}Cs 662keV	430-850 Bq

Table 5.15 Calculated activities (Bq) for the main energies of the net count rates of subject B of Table 5.14.

5.4.4.2 Conclusion and discussion of *in vivo* results

The *in vivo* counting of the subject using both detection systems revealed unexpected data. Whole summed spectra for all the various counts are shown in Figures 5.19 and 5.20 for both detection systems and the detailed spectra analysis is presented in Appendix A. The gamma-ray spectra obtained showed a number of fission and activation products which was unusual for such a prospecting subject who had encountered mine environments. The radionuclides of interest and expected were those belonging to the natural decay series. But the observations were puzzling because it was not clear how the subject could have come in contact with fission and activation products typical of nuclear processing facilities. However, after presenting and discussing these results with the subject and questioning her about the possibility of her coming into contact with man-made radioactive materials, she admitted that she had been in contact with other higher than background man made radioactive materials in the form of contaminated coarse soil which she had kept buried for some time at her own premises. It seemed that these contaminating activities were internal because, external contamination had being ruled out as she had taken baths and changed into clean gowns before being measured. For comparison purposes she agreed to send us some samples of the soil which she had been handling before she presented for whole-body counting. The main purpose of our measurement programme was to check the ability of the detection system to measure naturally occurring radionuclides and so these additional activities were considered interesting as much as a complication.

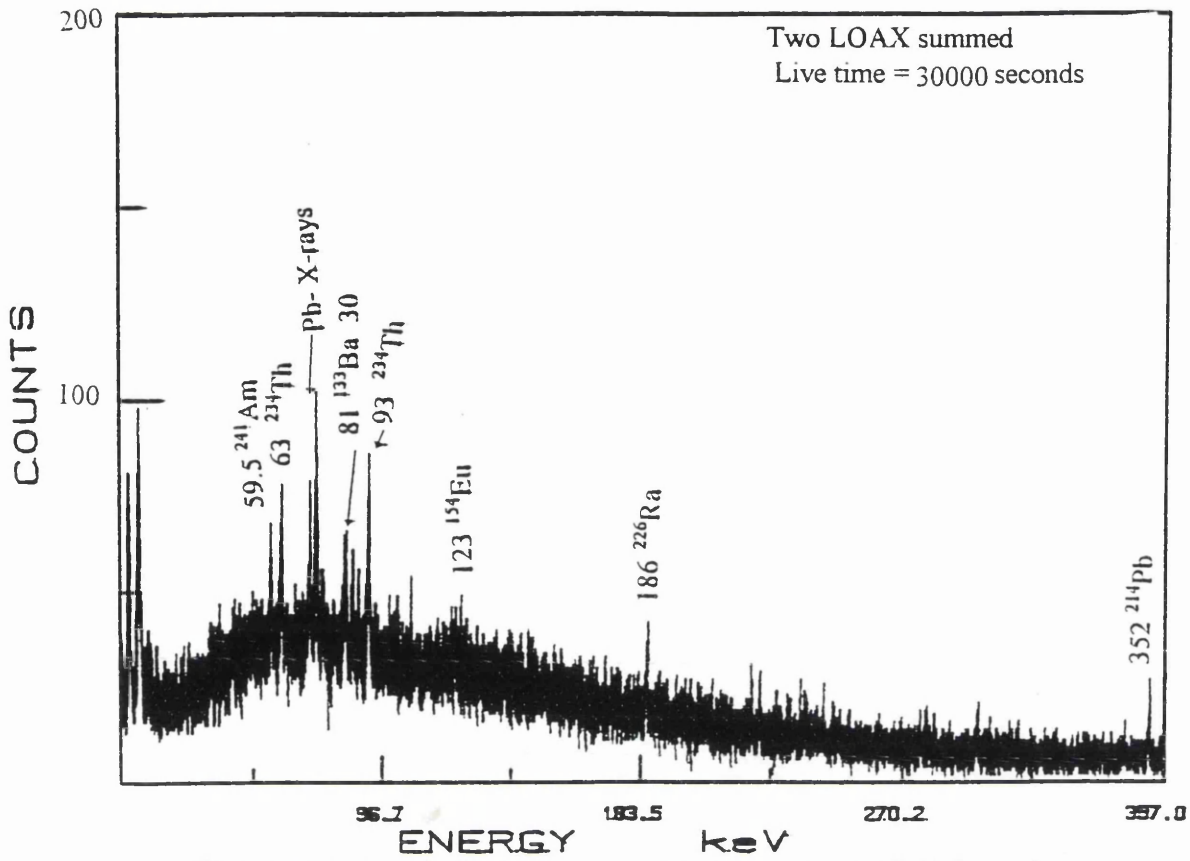

Figure 5.19 A typical gamma-ray summed spectrum of all the various counts of subject B using two LOAX detectors.

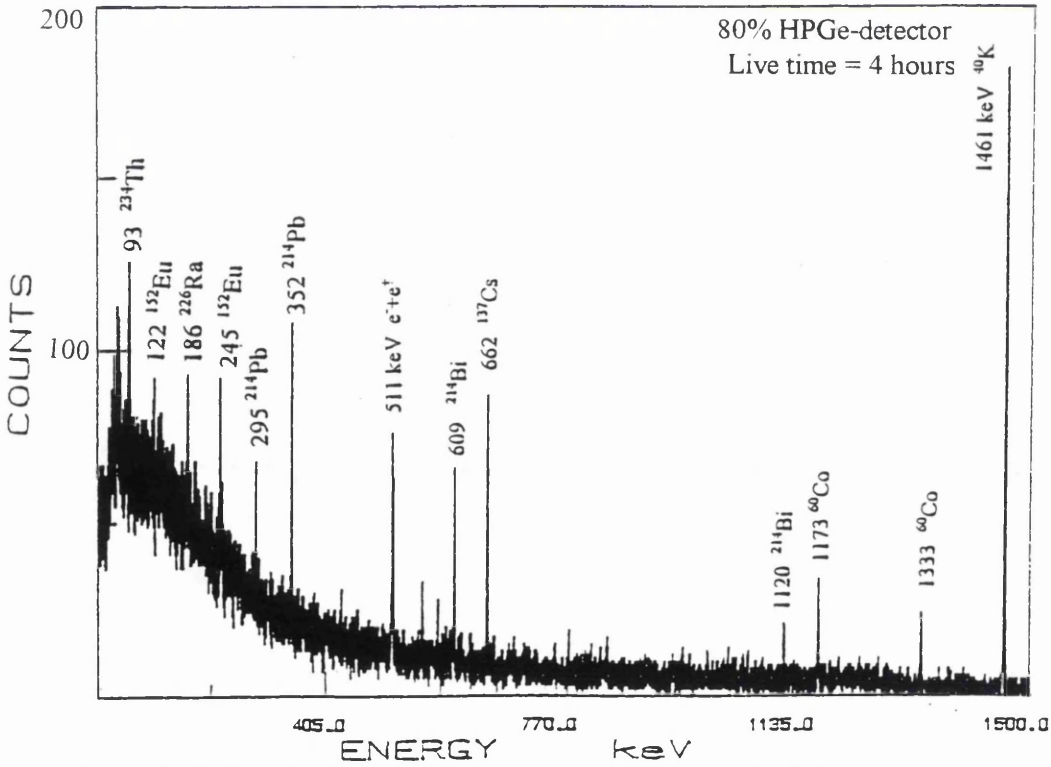

Figure 5.20 A typical gamma-ray summed spectrum of all the various counts of subject B using the 80% HPGe-detector.

5.4.4.3 Soil sample associated with subject B

A week following the subject B's measurements a sample was sent to us in the form of soil and small pieces of rock weighing 30 g. The whole sample was placed in three plastic bags to prevent it from contaminating the detectors. The bag was placed at about 3 cm from the detector surface and counted in static mode using the two LOAX detectors and then positioned under the 80% detector. The sample was counted several times using different counting times, first for one hour and then for a longer counts of 31 and 15 hour counts at the 3 cm position using both detection system respectively. The gamma-ray spectra of both detectors are shown in Figures 5.21 for the two LOAX detectors and Figure 5.22 for the 80% detector. For the whole spectrum analysis, expanded ranges of the complete spectra for both detection systems, which show all the labelled energy peaks, are presented in Appendix A.

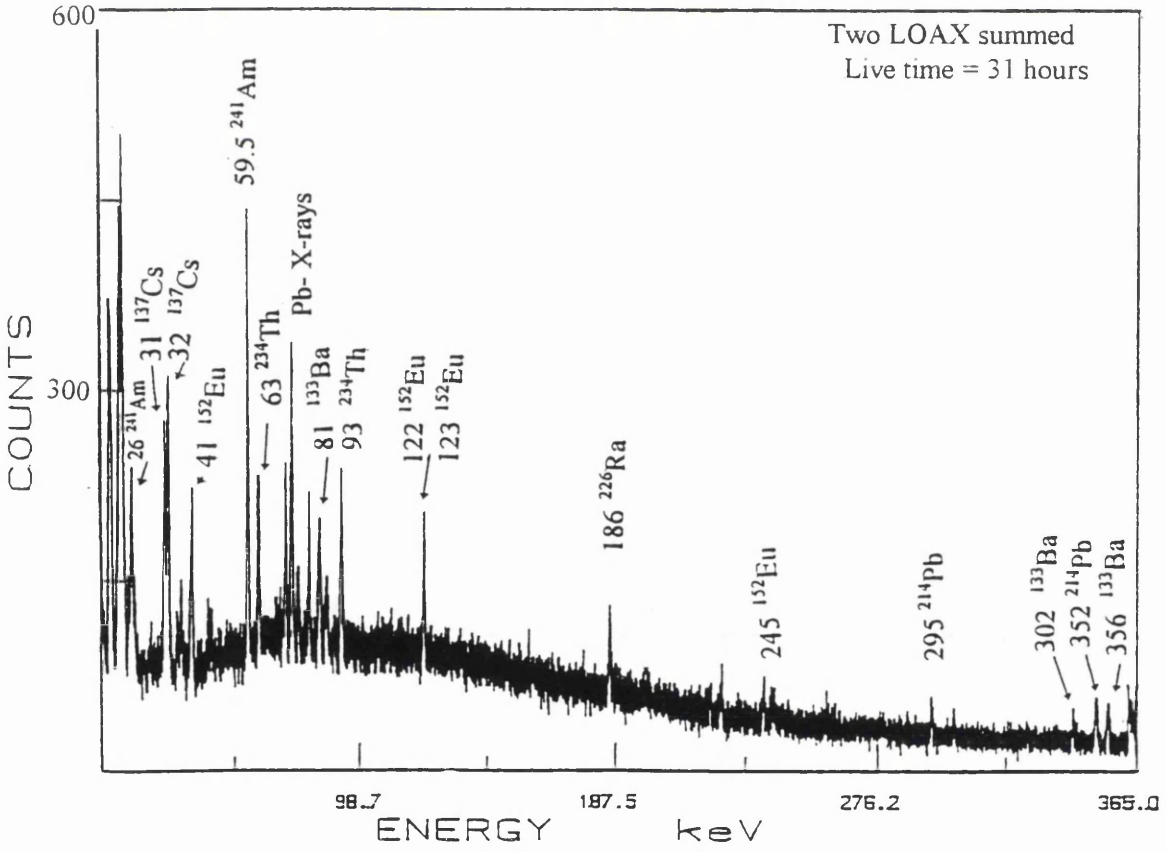

Figure 5.21 A typical gamma-ray spectrum of subject B soil sample measured using two LOAX detectors summed.

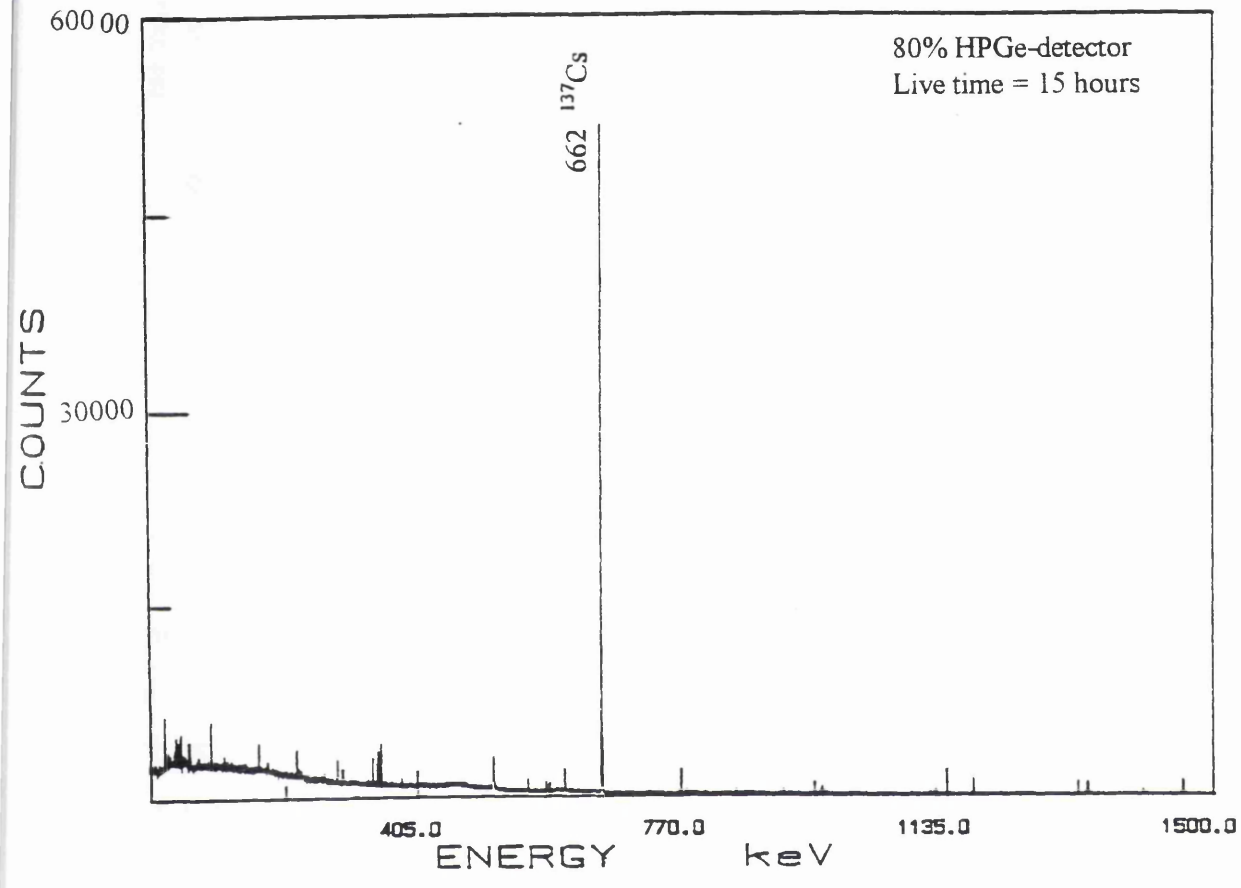

Figure 5.22 A typical gamma-ray spectrum of subject B soil sample measured using 80% HPGe-detector.

In addition, the sample was measured at certain distances from both detectors and placed under a water chest phantom to simulate being measured internally. The net count rates of the soil sample measurements: first being close to both detector surfaces, positioned at 3 cm from detectors in air, positioned at 10 cm and 20 cm underneath the chest water phantom section; are presented in Figure 5.23. For completeness and comparison purposes, the resultant soil net count rates were lower than the net count rate of the lower abdomen count rate. This means the detected count rates of the subject are genuinely measure from the within subject.

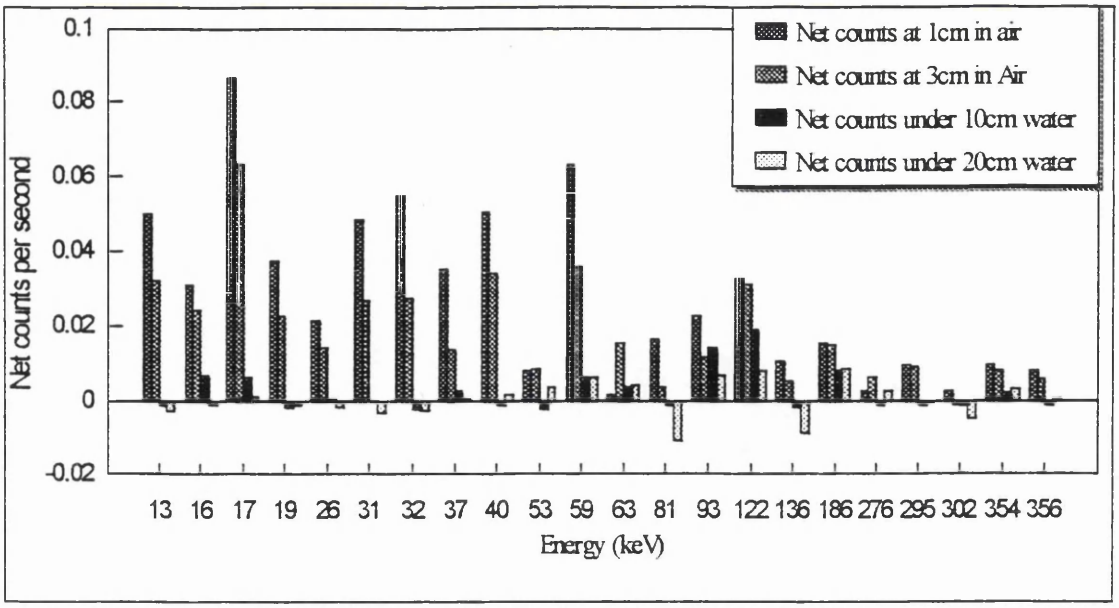

Figure 5.23 Net count rates for soil sample using different geometries with two LOAX detectors summed.

To study further the relationship between subject B and the soil sample and to determine their relative levels, the count rate obtained for the soil sample counted on the bed surface at 32 cm from the two LOAX detectors was subtracted from subject B's lower abdomen count. The resultant net count rate was graphed along with a similar water phantom count for comparison purposes as shown in Figure 5.24. It could be seen that the net count showed residual activity of all the main detected gamma in both the subject and the soil sample. The main U-Th energy (63 & 93 keV) and the ^{210}Pb peaks were also evident which indicated a detectable residual activity in the subject. When calculated this corresponded to approximately 5-10 mg of natural uranium. This measured activity corresponded to the first count done on the same subject a year before.

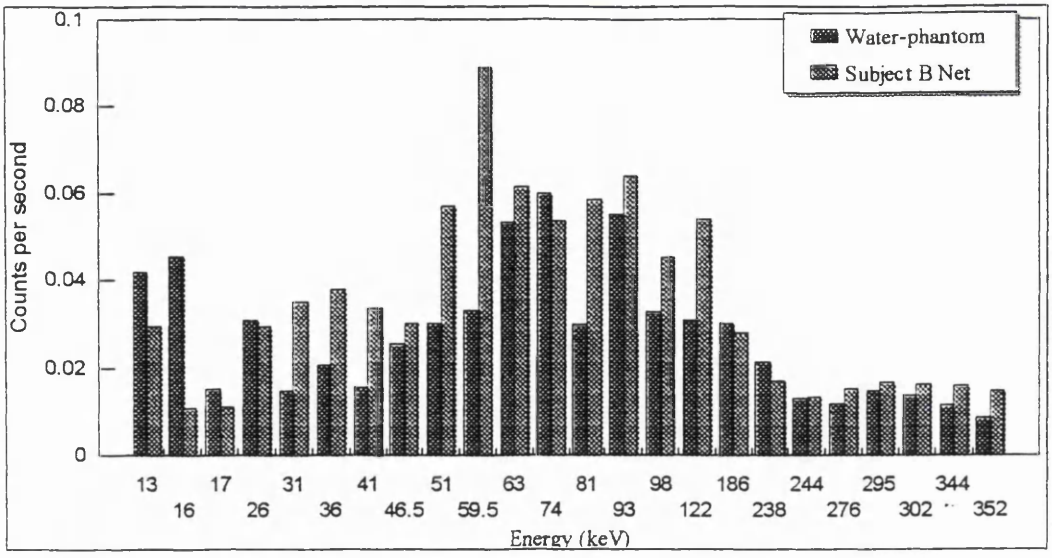

Figure 5.24 Comparison of count rates between water phantom and subject B subtracted count of soil sample count.

Overall, the gamma-ray spectra showed the same pattern of peaks to that found in subject B. They were characterized by pronounced high levels of the same fission nuclides and nuclear activation products. After the careful examination of all the obtained data for subject B and the associated soil sample measurements, two possible explanations were considered to account for the different measurements of this subject. The first was that the contamination was genuinely internal and that the subject had become contaminated while she was handling the soil samples. The second was that the subject had purposely brought some of this sample along with her and was placing it at different positions around the lower abdominal area during the various counts which gave the different measured levels. Both of the above assumptions were discussed with the subject but she denied that she had purposely done anything to affect the counting results. This means that the recorded spectra of the subject showed a genuine internal activity and that the subject was actually internally contaminated to a certain extent with these activities.

In conclusion, the main object of the measurement of subject B was to check the detection system's capability for low-level low-energy measurements and to investigate their sensitivities for measuring any previous natural uranium deposition and whether over a short time interval, residual activity due to radon daughters was detectable. Overall, it was found that a general increase in her activity was discernible and this was attributed to her continual exposure to radioactive mine environments.

5.4.4.4 Sellafield Soil sample comparison

In order to further investigate the possible source of the soil associated with subject B, a soil sample from the Sellafield area which was known to contain contamination from liquid waste was measured using the same geometry. This soil sample was found to contain natural U-Th series in addition to ^{241}Am and ^{137}Cs radionuclides from Sellafield discharges. For comparison purposes the gamma-ray spectra obtained using both detection systems are shown in Figure 5.25 and 5.26 respectively. The soil sample was measured at certain distance in air i.e. without any absorbers and in other geometries with the sample being positioned under certain thickness of water phantoms and bottles. These results proved that the detection systems of the monitor were sufficiently sensitive to permit the detection of low-levels of activity even for samples containing mixed multiple radionuclides.

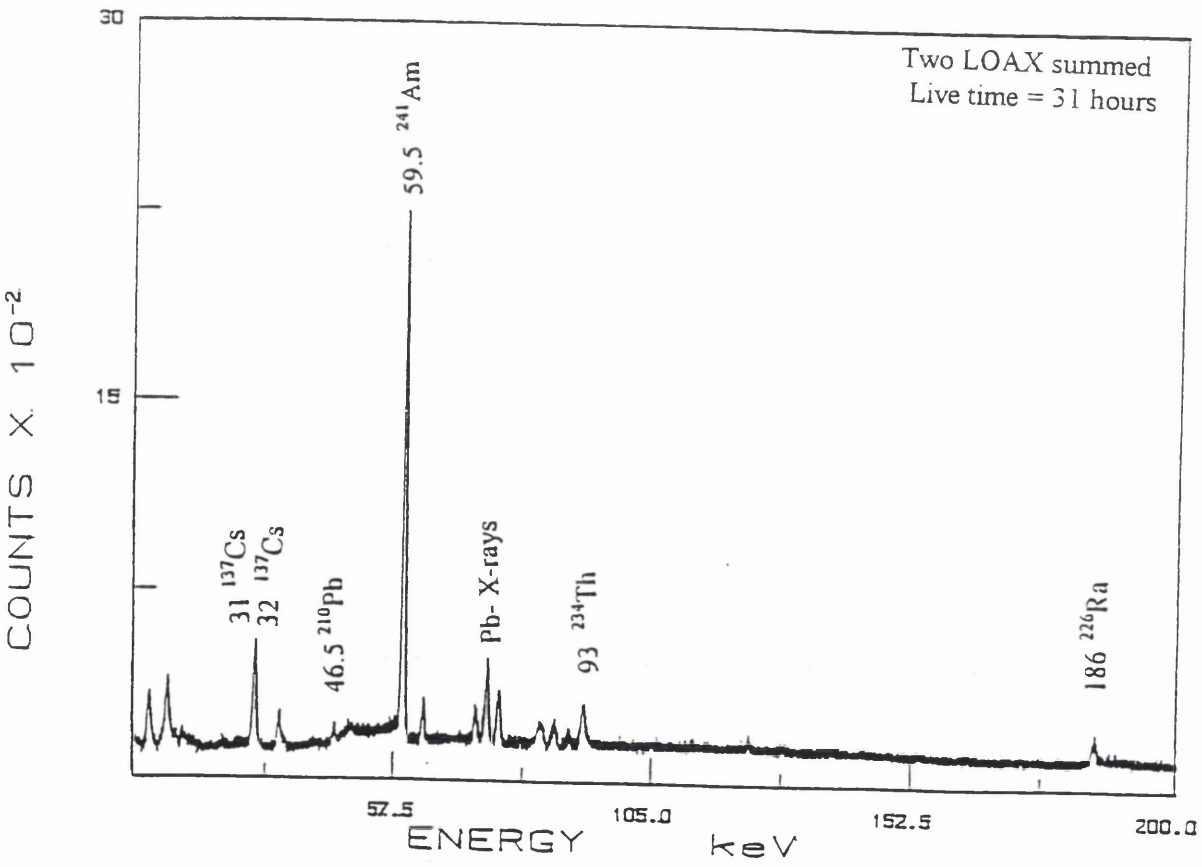

Figure 5.25 Typical gamma-ray spectrum for the Sellafield soil sample using the two LOAX detectors summed.

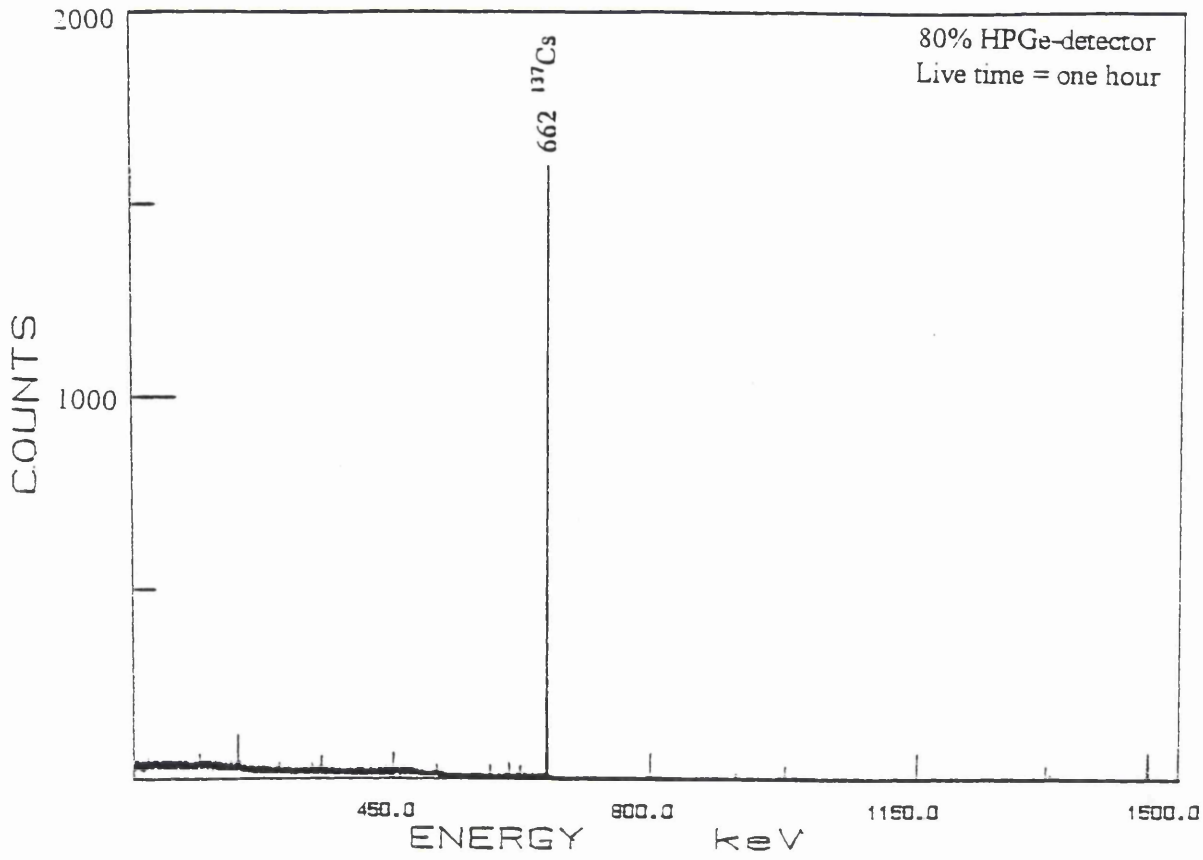

Figure 5.26 Typical gamma-ray spectrum for the Sellafield soil sample using the 80% HPGe-detector.

5.5 Heather honey ingestion (subject C)

Heather honey is produced by bees that feed on the wild flowers of the heather (*Calluna vulgaris*) found in South West Scotland, which is known to concentrate higher radiocaesium activity with respect to other plants (Jackson, 1989). SW Scotland was known to contain Chernobyl-derived radiocaesium (^{137}Cs) and it was shown that this was transferred to honey (Fisk, 1994). To demonstrate that this could be a route of caesium intake, a volunteer agreed to ingest a small amount of contaminated honey (200 gm) which contained 92 Bq of ^{137}Cs in order to measure body uptake. This amount of activity gave only a negligible total radiation body dose of 2-4 μSv. The subject ingested the honey over three days. He was scanned one day prior to the ingestion when his body content of ^{137}Cs was estimated to be below the detection limit of 26 Bq by two NaI (Tl) detectors and about 34 Bq using the 80% HPGe-detector. He was then monitored for the two days following the honey intake, and then twice every month for the following nine months as shown in the Table 5.16. The subject's body content of ^{137}Cs showed a pattern of increasing activity immediately after the ingestion of the honey up to 150±23 Bq which then started to change slowly for the following three months. After this time the

level started to decrease due to the natural body elimination mechanism and the biological half-life. It is known that ^{137}Cs has a biological half-life ($T_{1/2B}$) of 110 days in the adults. Typical gamma-ray spectra of the highest measured activities recorded using the 80% HPGe, the four LOAX detection system and the two NaI detectors are shown in Figure 5.27 a, b & c respectively. The total body potassium (TBK) calculated by the parameter formula taking the height and weight of the measured subject was also given in column 3 of Table 5.16 for comparison purposes.

Days-after intake days	Body wt. kg	TBK g	NaI(Tl)-det. Activity of ^{137}Cs Bq	NaI(Tl)-det. Specific Act. Bq g^{-1} ^{40}K	80% HPGe-detector ^{137}Cs Bq
Before intake	69.0	133.1	< D.L*	-	34±5
2	69.0	139.0	103±10	0.74	119±18
4	69.2	128.1	114±11	0.89	140±21
5	69.4	128.5	106±11	0.82	150±23
17	69.6	129.6	93±9	0.72	145±22
34	69.7	130.3	88±9	0.68	143±21
60	70.5	129.9	108±11	0.83	150±23
96	69.8	129.4	66±7	0.51	100±15
151	71.0	132.6	74±7	0.56	80±12
206	70.9	128.7	52±5	0.40	60±9
268	70.5	124.6	27±3	0.22	47±7
371	69.4	129.0	<D.L.	-	30±5

Table 5.16 Measured ^{137}Cs activities of volunteer using the two NaI(Tl) and 80% HPGe-detector during one year following the intake of the 92 Bq of ^{137}Cs.

* Detection Limit of the NaI(Tl)-detectors for ^{137}Cs (total body) = 26 Bq and 20 Bq for the 80% HPGe-detector.

This follow-up counting experiment using the 80% HPGe-detector in conjunction with the two NaI(Tl) detectors showed clearly that the low-level intake and release could be detected using both systems. It has to be noted that up to a period of two months from the first intake, the decrease of subject activity appeared to be statistically insignificant. However, after that period a decreasing trend in the net count rates was observed which was expected.

It has to be noted that different numbers of LOAX detectors were used throughout the measurement period which made it difficult to gain a comprehensive picture of their capability to follow-up all the changes of the measured counts.

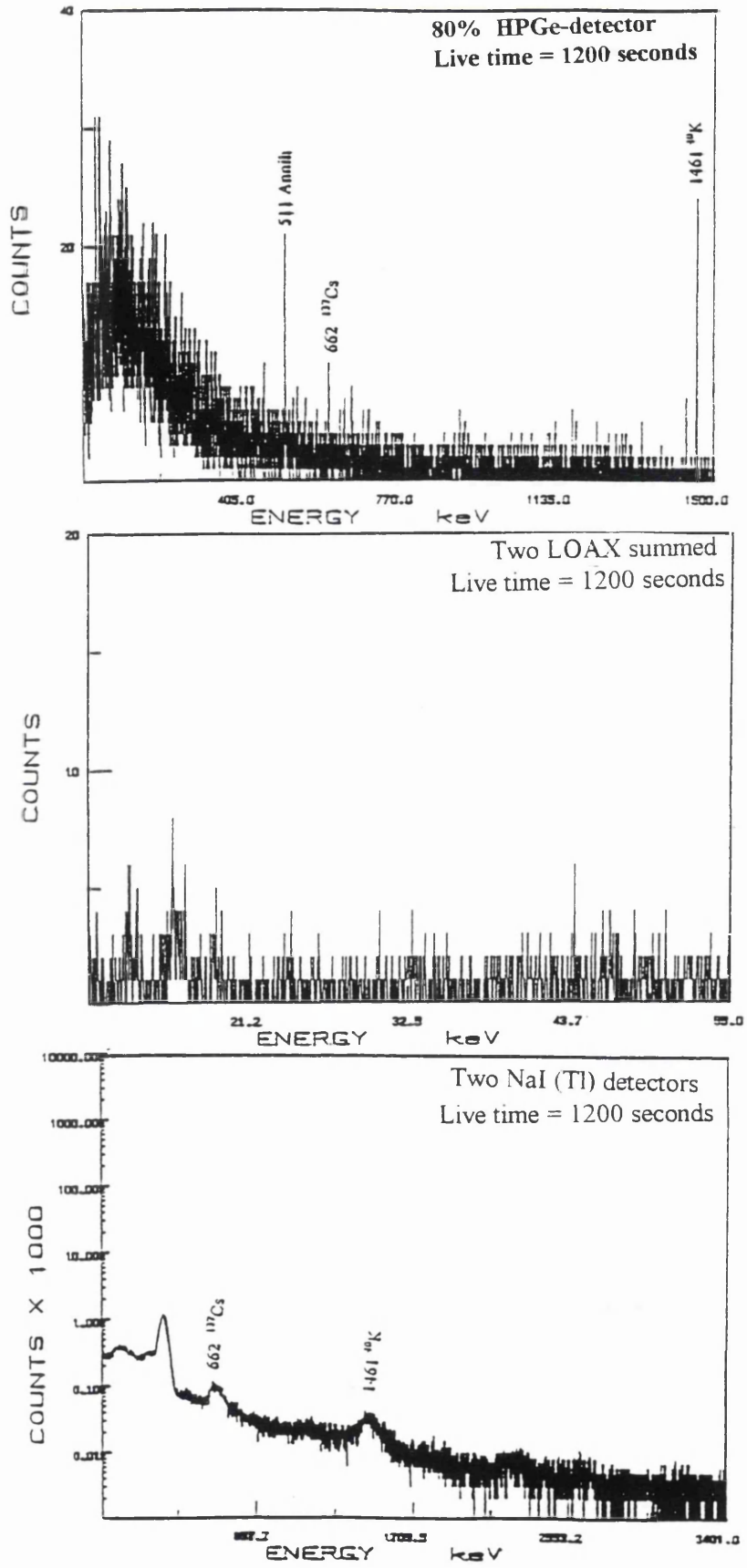

Figure 5.27 Gamma-ray spectrum of the subject using: (a) the 80% HPGe-detector; (b) two LOAX detectors summed and (c) two NaI(Tl) detectors.

5.6 The ^{241}Am-Test Phantom samples

5.6.1 Preparation of the Test Phantoms

Following the setting-up of the monitor and the completion of the measurements of the tissue equivalent phantoms as described in section 4.3, further tests were carried out to provide an independent check on the sensitivity of the counter for ^{241}Am. Six 5 l test phantoms were therefore prepared by another worker from an ^{241}Am stock solution containing 6000 Bq ml^{-1} and 3.6 ml 1000 mg l^{-1} ($La(NO_3)$ solution in 5% HNO_3. A suitably dilute solution of specific activity 1.2 Bq ml^{-1} was prepared by further dilution to 500 ml. A known volume of this solution was added to five polyethylene containers and made up to 5000 ml with water. The subsequent analyses were carried out blind, without any knowledge of the radioactive content of the test phantoms.

5.6.2 Measurement procedures

Several one hour counts were taken of the six labelled test-phantoms at a distance of 4 cm from the two LOAX detector system. The counts obtained were converted to Becquerels using the sensitivities found from the internally labelled tissue equivalent phantoms. Computer analysis was done as before, utilizing the Minigam programme to obtain the first set of results. The second set was obtained by a manual calculation method whereby the spectrum was inspected and the counts in each channel totalled over the appropriate energy range (58.5-60.5 keV). The net activities were calculated by subtracting the corresponding quantities for a water phantom and then dividing by the sensitivity determined using the internally labelled ^{241}Am tissue equivalent phantom. Although this calculation procedure was tedious it gave very accurate and reliable results in a situation of low-level counts for which the computer software was not designed and where the peak was only just observable above the background. The final set of results was calculated using the other method of synthesized spectra analysis described for *in vivo* work in section 2.8 of chapter 2. Here, taking the internally labelled standard tissue equivalent ^{241}Am skull phantom, a number of spectra were synthesized by the subtraction of a certain fraction of the skull spectrum and adding it to the water phantom spectrum. A number of spectra with different activity levels ranging from 3 Bq to 130 Bq were produced. These synthesized spectra were plotted and compared to the collected and plotted spectra for the test phantoms. Figure 5.28 shows the comparison of the blank water phantom with three test-phantom spectra.

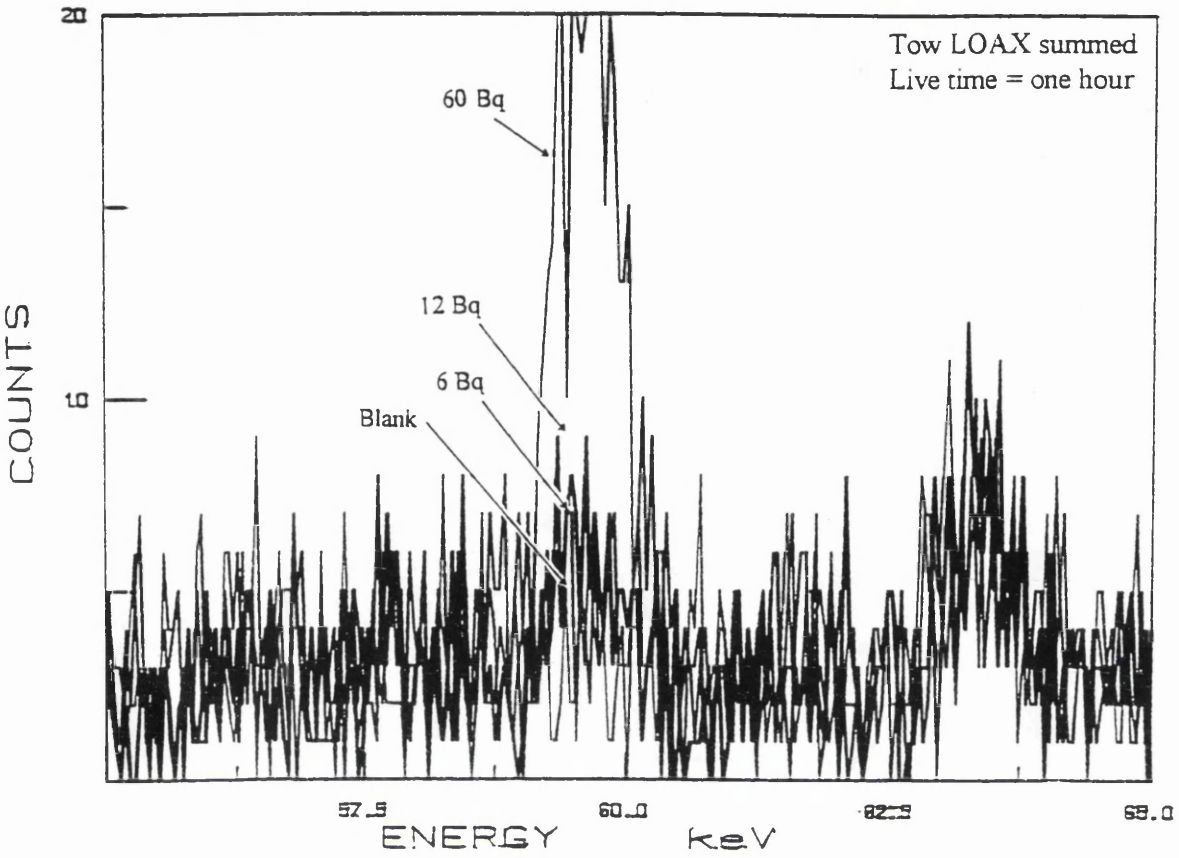

Figure 5.28 A comparison of the gamma-ray spectra of blank water phantom with three ^{241}Am test-phantoms.

The results are given in Table 5.17 where: column 2 gives ^{241}Am activity added; column 3 the measured activities obtained by computer analysis of the spectrum; column 4 activities obtained by manual calculation; and column 5 gives activities deduced from the synthesized spectra.

5.6.3 Results and Discussion

Comparing the three results for each phantom it can be seen that the measured values are in reasonable agreement with the actual values, the highest difference being about 35% for sample Z and the remainder of the samples differing from the actual value by less than 20%. It could be clearly seen that these differences are not statistically different which provides more evidence of the application of the syntheses methods of spectra evaluation.

Phantom label	Added Activity Bq ± σ	Measured activity 1 Bq ± σ	Measured activity 2 Bq ± σ	Synthesized activity Bq
V	zero	Blank	Blank	Blank
W	6±1	8±3	8±3	7±1
X	60±6	72±5	64±4	69±10
Y	120±12	132±6	122±7	124±18
Z	12±2	8±3	9±3	13±2

Table 5.17 ^{241}Am test phantom activities compared with the measured values using three methods: (a) net cps of report files; (b) channel by channel and; (c) spectrum synthesis.

From the above results the two LOAX detection system was shown to be giving reliable results for the range of phantom sizes tested. For an activity of 12 Bq, a one hour count gave an error of approximately 35%. Previously, the limit of detection had been found to be in the region of 4-6 Bq and therefore this result was in keeping with this trend.

5.7 The study of radioactivity in sheep samples from South West Scotland

The main source of radioactive waste in the United Kingdom is the British Nuclear Fuel Ltd. reprocessing plant at Sellafield, Cumbria which is, in fact considered to be the largest source of nuclear waste on a worldwide basis at present. Its annual discharges of ^{241}Am and ^{241}Pu have ranged from $2x10^{12}$ to $1x10^{14}$ Bq and $3x10^{14}$ to $3x10^{15}$ Bq respectively in the last 30 years with maximum discharges occurring in the early nineteen seventies (Gray et al., 1995). The waste discharges from Sellafield arise from the reprocessing of spent reactor fuel; it is known that for each tonne of fuel reprocessed $5m^3$ of high activity liquid waste is produced. The majority of high and medium solid and liquid waste is concentrated and stored in safe storage facilities. However, low activity liquid waste containing ^{241}Pu and ^{241}Am, after being stored for some time, is discharged into the Irish sea according to strict rules and authorized limits set by the Environmental Agency (EA). Some of these actinide elements, discharged into the Irish Sea, have accumulated in sediment close to the Cumbrian coast. Resuspension of this sediment maintains measurable actinide concentrations in the near-shore areas, despite large decreases in radionuclide discharges in recent years (McKay and Walker, 1990). The transfer of these nuclides to land from the sea and sea sediment has been observed along the Cumbrian coast and other coastlines of the Irish Sea (McKay, 1990). Therefore it was of interest to study the possible uptake of activity in animals that graze in farms adjoining these coastal areas.

The amount of these nuclides discharged during the years 1989-1994 from Sellafield are presented in Table 5.18 (Cambray, 1982; B.N.F.L. , 1989-1994).

Radionuclide	*1989*	*1990*	*1991*	*1992*	*1993*	*1994*
Americum-241	1.06	0.75	0.744	0.542	0.873	0.381
Plutonium-241	30.24	31.61	29.5	25.3	37.5	14.4
Plutonium alpha	1.21	1.14	1.08	0.935	1.33	0.663
Cerium-144	3.78	2.01	1.73	1.73	2.51	0.836
Caesium-137	28.60	23.46	15.6	15.2	21.9	13.8
Caesium-134	1.73	1.15	0.765	0.834	1.19	0.611
Strontium-90	9.17	4.22	4.09	4.14	17.1	28.9

Table 5.18 Discharged levels of various radionuclides in liquid waste (TBq) from the Sellafield reprocessing plant during 1989-1994.

An important mechanism in the plutonium wastes is that ^{241}Am " grows in " from the beta emitting ^{241}Pu as indicated in Figure 5.29. In this Figure ^{241}Pu (half-life 14.4 years) is continuously produced in nuclear reactors by neutron bombardment, as well as ^{239}Pu, and the subsequent growth of the ^{241}Am daughter can be seen. This provides a method of monitoring for ^{239}Pu since the ^{241}Am is readily detected by means of its photon emission of 59.5 keV. For the detection of the low-energy X-rays at 17.2 keV of plutonium in the presence of americium X-rays at 17.6 keV, requires a detector with an average resolution of less than 0.5 keV.

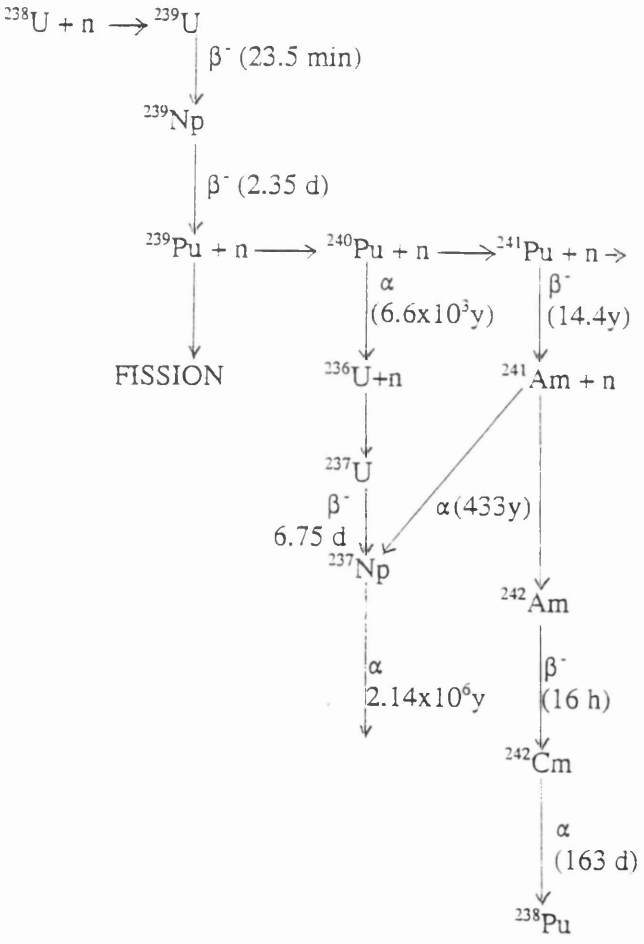

Figure 5.29 Transuranic production of ^{241}Pu by the neutron irradiation of uranium.

The areas surrounding Sellafield, including the merses (salt marshes), which have accumulated appreciable activity from past discharges of low level radioactivity, have been under continuous survey and measurement. The SURRC radiochemical laboratories have carried out a number of investigations regarding sediment radionuclide concentration profiles which provided a record of Sellafield waste deposition since the 1960s (MacKenzie et al., 1994). Also, SURRC aerial surveys have identified considerable activities of a number of nuclides in the coastal and estuarine environments around the Irish sea; salt marsh sites in West Cumbria; the North Wales coast, the Ribble and inner Solway estuaries; and, in lower concentrations, in the Firth of Clyde (Sanderson et al., 1994). The measurements on samples of farm livestock and recovered carcasses from the area to search for the possible contamination or uptake of ^{241}Am are now described.

5.7.1 Measurements of a whole sheep

One of the main animals farmed in the area is sheep. A sheep weighting 12 kg and eight months old, collected from a farm in the Dumfries area, was sacrificed and its internal organs: stomach; liver; lungs; and kidneys etc. were removed. The remainder of the sheep, including the head, legs and fleece, was put in an appropriate plastic bag for cleanliness and for accurate positioning in the body monitor. A series of measurements was firstly taken on the sheep carcass using the two LOAX detector system and the 80% HPGe-detector at 15 cm intervals along the length of the body. Based on the findings, counting was then concentrated on two main areas i.e. the head and the abdominal area of the animal. The two detection systems were used simultaneously for counting by the careful positioning of the sheep's head under the two LOAX detectors while the position of the 80% detector corresponded to the abdominal area (20 cm separation). The counting sensitivity was maximized by supporting the body of the sheep 1-2 cm from the detectors. The sheep was kept frozen and only slight thawing occurred during the counting periods. Between counts, the water phantom was measured using the same counting geometry. Also, a number of scanning counts were carried out on the whole body of the sheep along with water phantom sections.

At a later stage the sheep was left out of the freezer overnight to allow it to thaw and, the fleece (skin) was removed taking care to avoid cross-contamination by working in clean and controlled conditions. At the same time the head, lower legs and hooves and the fleece were removed and put separately into plastic bags for counting individually. A number of counts were taken of the fleece, legs, the head and the skinned body in order to determine the location of the activity on and within the body. Also the internal organs - the liver, lungs and kidneys were measured separately using static counting geometries. The calculated activities were obtained using the detection sensitivity 3.98×10^{-4} cps Bq^{-1} ^{241}Am for the two LOAX detectors and 1.0×10^{-4} cps Bq^{-1} ^{241}Am for the 80% detector, these having been determined using the ^{241}Am-thorax phantom (9200 Bq), which was comparable in size with the body of the whole sheep. The activity of internal organs and the fleece, which was wrapped to approximate the dimensions of a skull, was based on a sensitivity of 1.48×10^{-3} cps Bq^{-1} ^{241}Am for two LOAX detectors obtained with the internally labelled skull.

5.7.1.1 Results and discussion

The gamma-ray spectrum of the whole sheep with its fleece is shown in Figure 5.30. The main radionuclides detected were ^{241}Am and a slight suggestion of ^{210}Pb with peaks at 59.54 keV and 46.5 keV respectively. The highest activity of the whole sheep measurements of ^{241}Am was found in the body with the fleece and was 24±9 Bq. The liver was measured separately by positioning it immediately under two LOAX-detectors and was found to contain 8 ± 5 Bq of ^{241}Am. Figure 5.31 presents the spectrum of the count on the of fleece alone. In the sheep skin alone, after being dissected from the body of the sheep, the highest detected activity was 50 ± 7 Bq of ^{241}Am and 45 ± 8 Bq of ^{210}Pb as outlined in Table 5.19. The fleece was gathered together inside a plastic bag, the size of which was similar to that of that skull which gave the best efficiency. It was found that, the lungs and kidneys were below the limit of detection of 6 Bq.

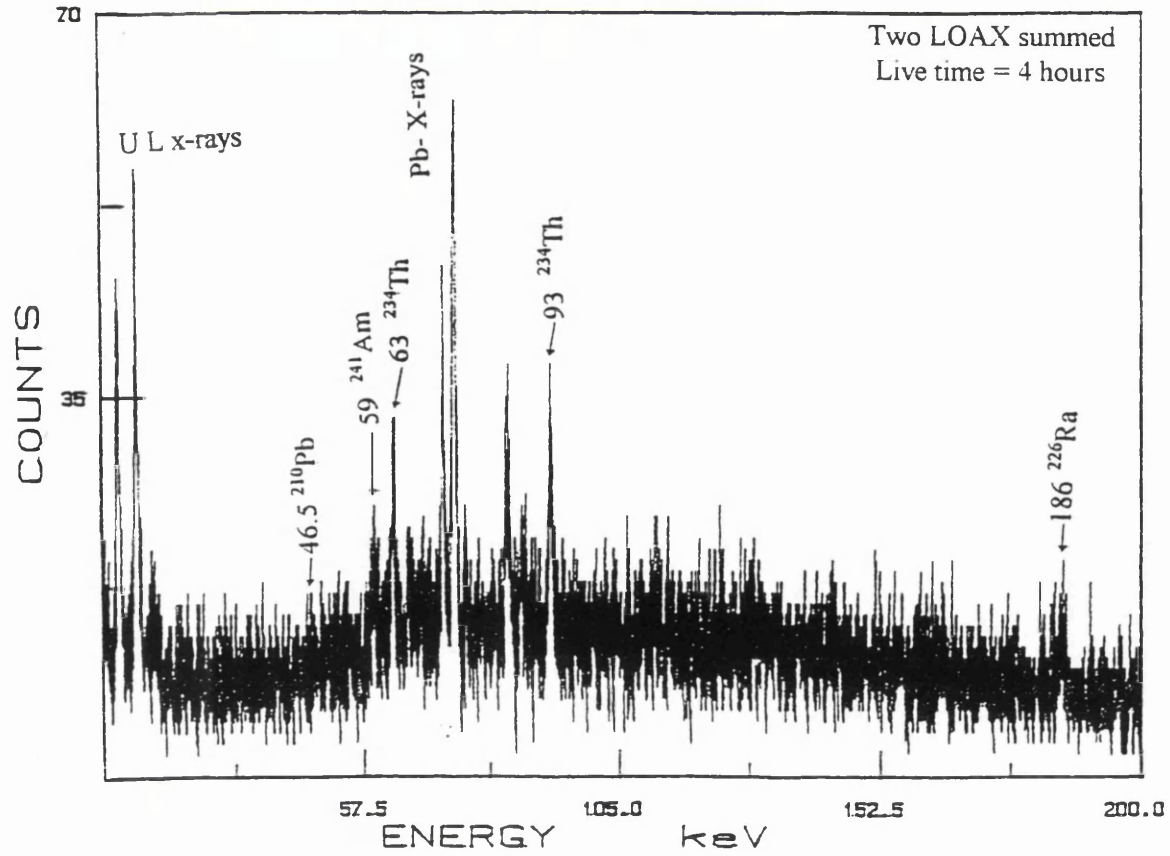

Figure 5.30 Gamma-ray spectrum of the whole sheep counted at 2 cm of two LOAX detectors summed over the liver region.

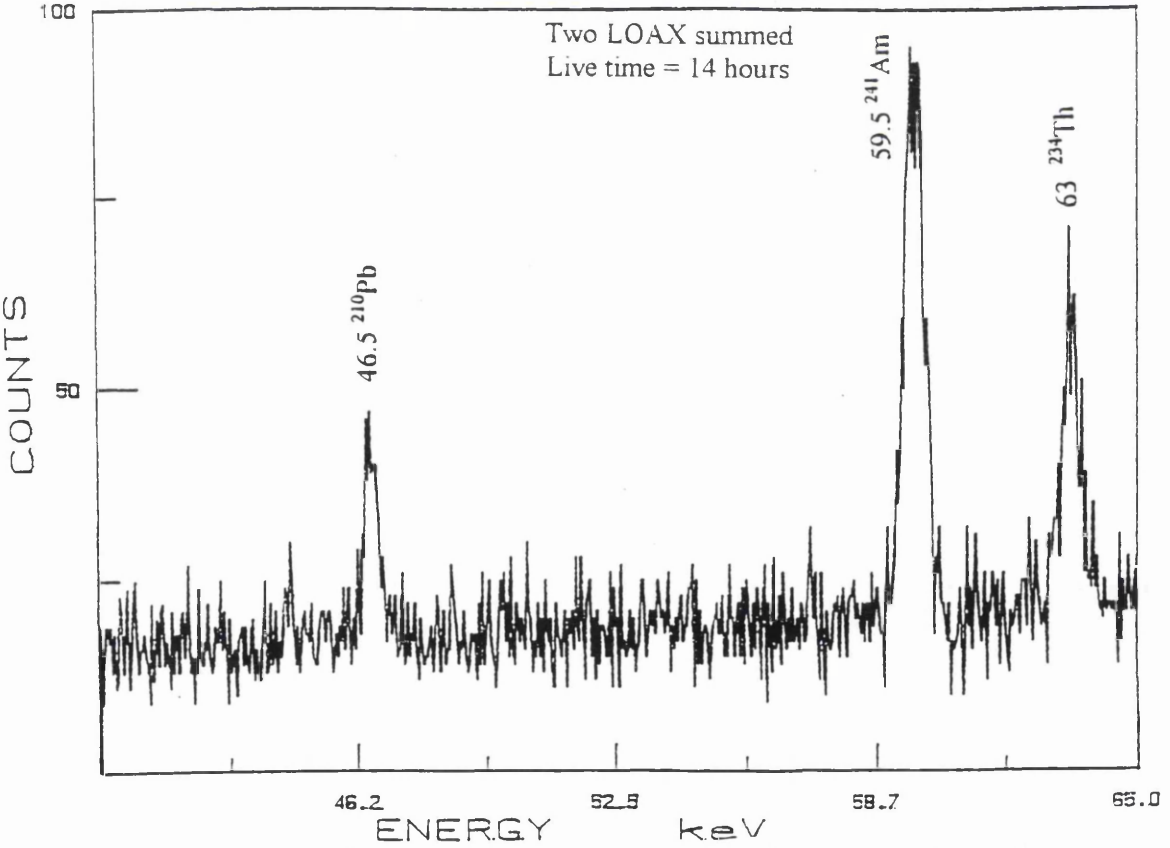

Figure 5.31 Gamma-ray spectrum of the fleece counted at a distance of 2 cm from the two LOAX detectors summed.

Organ description	Two LOAX-summed ^{241}Am	^{210}Pb	80%-HPGe-det ^{241}Am
Whole-sheep (12 kg)	22±4	30±6	13±3
Whole-fleece (0.578)	50±10	45±9	60±12
Whole-body (8.91kg)	5±1	<6	<8
Hooves (0.590)	14±3	10±2	<8
Liver (0.305kg)	8±2	<6	<8
Kidney	<6	<6	<8
Lung	<6	<6	<8

Table 5.19 The measured activities of the main radionuclides of the sheep and its separate organs counted using the two LOAX-detectors summed and the 80% HPGe-detector.

Where the 80% HPGe-detector was also used for the sheep and its organs, the observed activity gave somewhat similar results for most of the counts taken by the two LOAX-detectors, as shown in Table 5.19. For the whole sheep, activities were found to be 13 ± 3 Bq and in the fleece 60±12 Bq. Also 200 ± 20 Bq ^{137}Cs was detected in the whole sheep. Figure 5.32 represents the gamma-ray spectrum of the whole sheep counted directly under the 80% HPGe-detector showing the range of energy up to 1500 keV which included the main low-energy peaks detected.

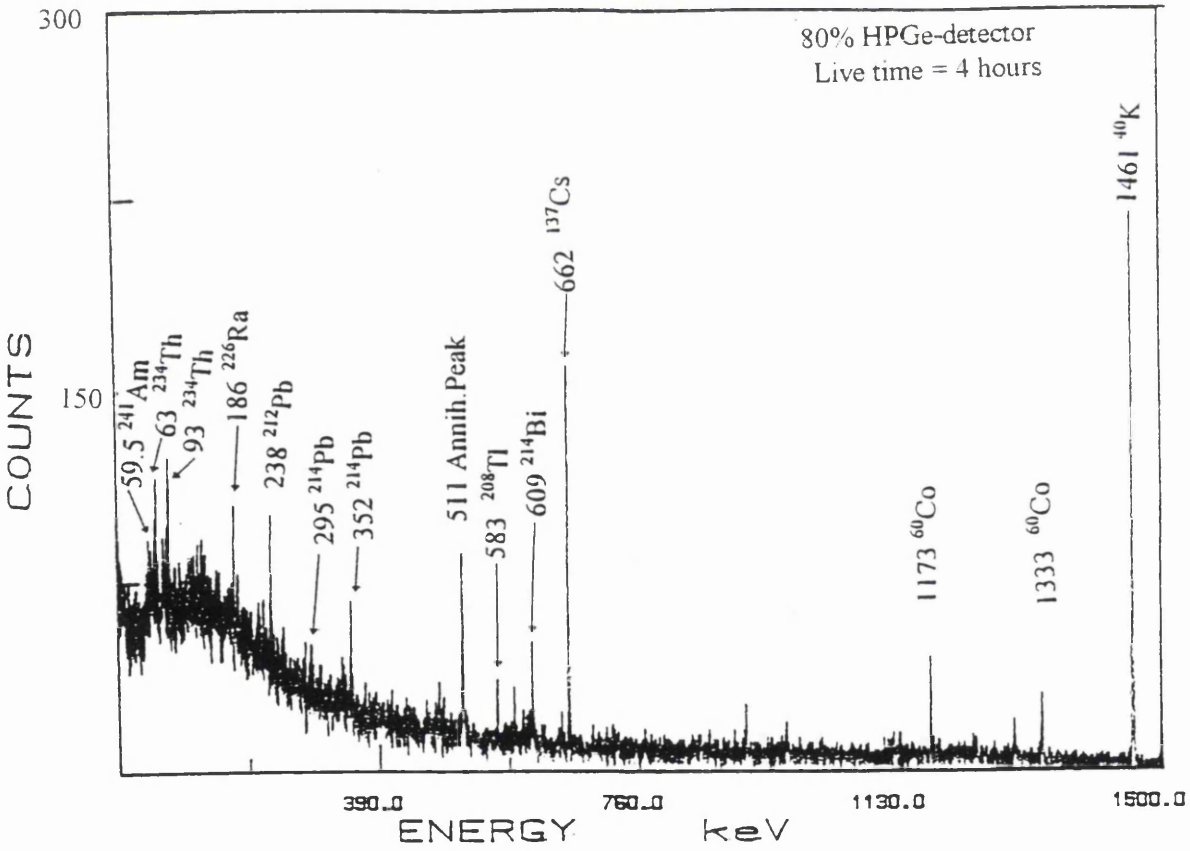

Figure 5.32 Gamma-ray spectrum of the whole sheep counted directly under the 80% HPGe-detector.

The discrepancy between the LOAX and 80% detectors for the total activity in the animal when measuring parts of the body separately was difficult to explain but could have clearly been dependent upon the calibration methods and factors taken. Based on the above results and the detailed values in Table 5.19, the highest activity of ^{241}Am was detected in the fleece of the animal, while there appeared to be traces of activity in the liver and the whole body after removing the fleece. Another finding was that the hooves of the animal showed the presence of ^{241}Am and ^{210}Pb. These results definitely indicated the presence of ^{241}Am activity around the farm where the animal had been grazing. Most of the measured activity appeared to be external contamination rather than internal deposition in the animal. Lead-210, on the animal's hooves and fleece was consistent with pickup from the surroundings also, although the levels observed were somewhat high. The ^{241}Am contamination could have resulted from the sheep grazing on farm land having a generalized level of contamination, or alternatively farm land having 'hot spot' areas.

To investigate the degree of ^{241}Am-contamination spread in the farms around these areas additional animals from the same area need to be studied more extensively to compare their activities. The extent of americium contamination needs to be determined and studied further using other methods of survey, as well as more samples being measured using this method. Since it has been found that the highest activity was on the fleece, probably because the ^{241}Am radionuclides stick to mud and dust which in turn gets into the wool, and are not easily removed, the relevance of this source of potential contamination in the wool industry merits further consideration. Also, the human consumption of lamb meat from animals from these areas does not appear to present any problems currently but probably needs to be kept under review because of the evident persistence of materials such as ^{241}Am in the environment.

5.7.2 Measurement of sheep bones

Animals are sometimes lost or washed up on the beaches in the Dumfries area and in addition to the measurements of sacrificed sheep i.e. recently grazing on the area, a complete skeleton of a decayed male sheep found in such circumstances was collected for measurement and analysis. All the bones of the skeleton of the decayed animal, including the skull, were found in some Dumfries farms. These measurements were considered to be a useful indication of contamination levels of live stock animals affected by radionuclides in the surrounding area arising from the discharges from the Sellafield

nuclear reprocessing plant in Cumbria. Any measured radioactivity could have arisen from bone uptake following ingestion during the animal's lifetime or from subsequent contamination after death from the surroundings.

5.7.2.1 Methods of Bone Measurement

Initially, all the collected bones, contained in one plastic bag, were measured using the 80% HPGe detector and two LOAX detectors connected separately for a series of static measurements for one hour and for 14 hours overnight. The spectra obtained from the two detectors are shown in Figure 5.33 a & b, and Figure 5.34 for the 80% HPGe-detector. The bones were then segregated according to their type in separate plastic bags as follows: skull; long bones of legs and shafts; large surface area bones of the scapula and the hips; rib cage bones and back bones of the spine. All samples of bones were labelled, weighed and measured separately for one and four hours under similar counting geometries. The bones in plastic bags were positioned about 3 cm from the LOAX detectors. However, due to the loose packing of the pieces of bone inside the bags, the geometry was not entirely reproducible and it was not possible necessarily to measure exactly the same surface of the bones in different counts.

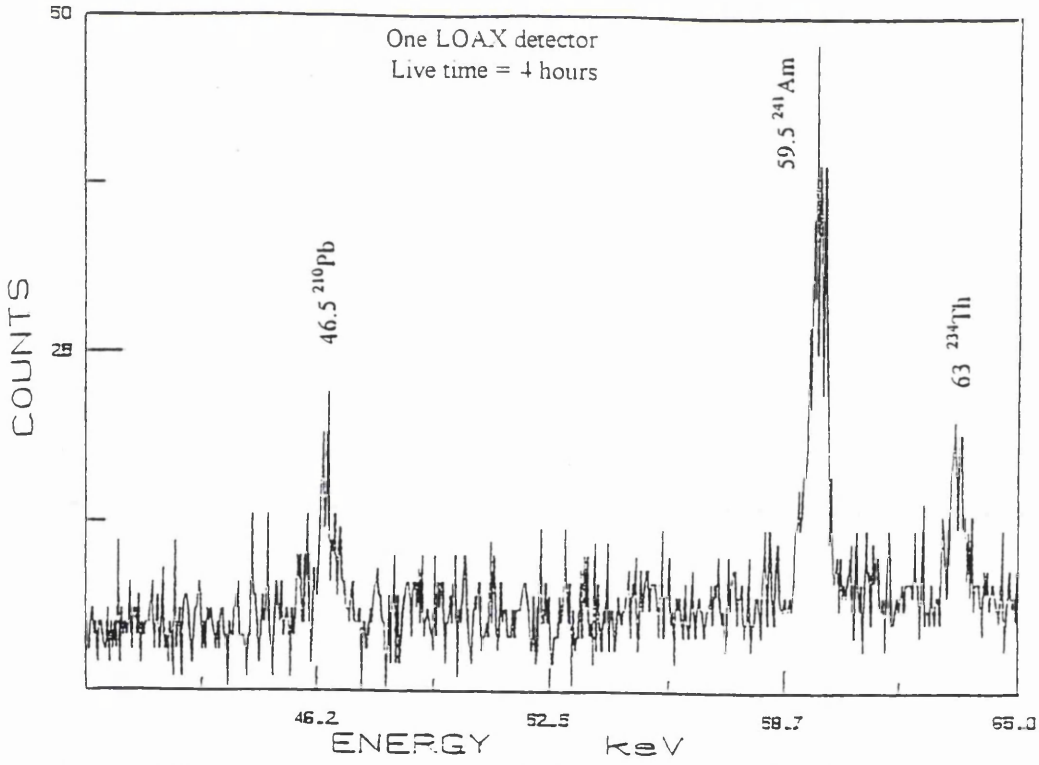

Figure 5.33 Gamma-ray spectrum obtained using a single LOAX detector for the measurement of the complete collection of sheep bones.

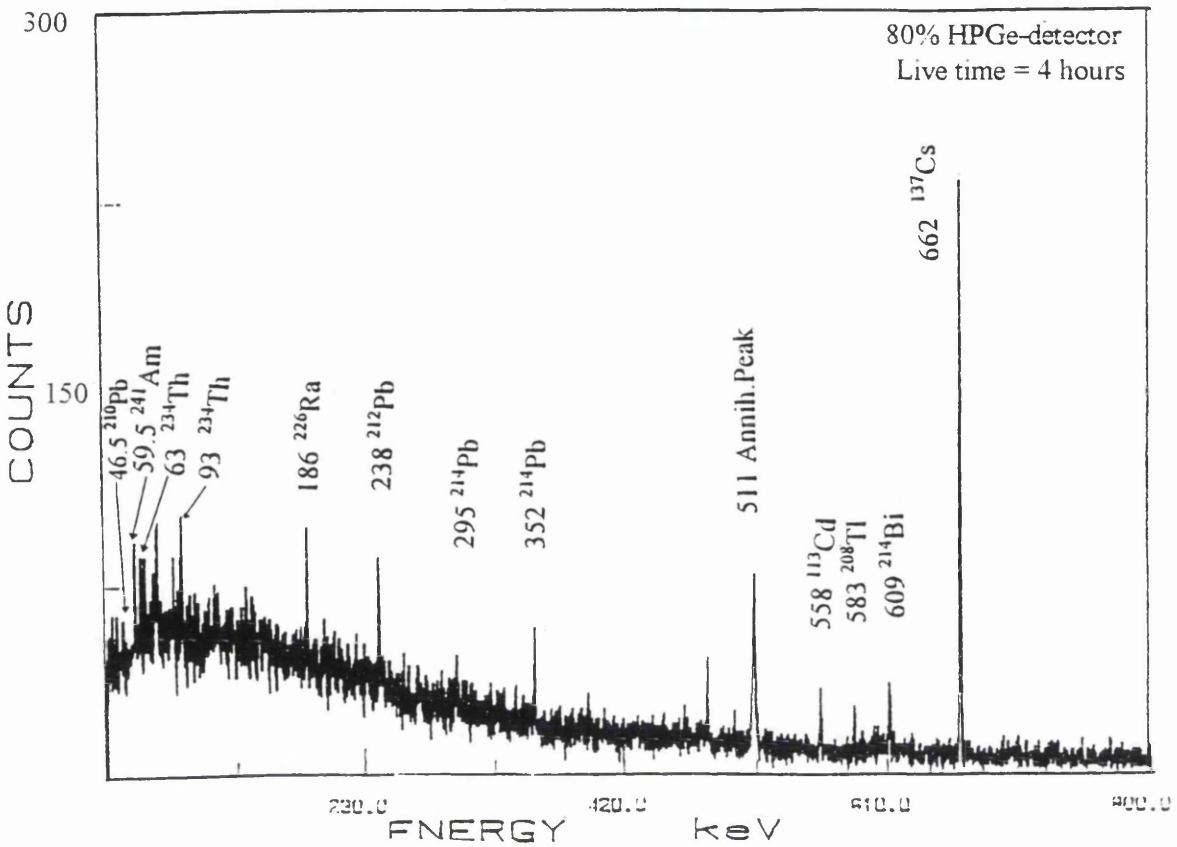

Figure 5.34 Gamma-ray spectrum of the complete collection of bones using the 80% HPGe-detector.

To investigate whether the activities were deposited within the bone and not simply due to contamination by mud and external dirt on the external surfaces, the bones were immersed in water for some time and then cleaned with water and chemical detergent using a brush to rub the surface of the bones thoroughly. After they were rinsed with clean water and dried with tissues and the use of heat lamp, the bones were recounted. The water used for cleaning and the residue collected from the bones was retained and also measured. A scanning count of one hour was made on the skull along with the other water phantom sections. The skull was positioned alongside the water phantom instead of the head section to ensure that the counting geometry was consistent with the calibration studies in which the tissue equivalent skull phantom labelled with ^{241}Am and ^{210}Pb radionuclides had been used.

5.7.2.2 Bone measurement results

All the measurements carried out on the bones showed considerable measurable activities of both ^{241}Am and ^{210}Pb radionuclides, as shown in Figure 5.33 & 34. Different levels of the americium and lead radionuclides were observed in the separate groups of bones. The highest activities were found in the skull, which had about twice the amount of activity found in other bone types. The gamma-ray spectra obtained for the top and the base of the skull are shown in Figure 5.35 a & b respectively. Using the measured calibration sensitivity factors for both detectors separately and taking the net count rates of the measurements for all the bone samples, their activities have been calculated and presented in Table 5.20. It presents the activities observed with the two LOAX detectors. These activities were based on the net count rates and sensitivities of these detectors using the internally labelled ^{241}Am and ^{210}Pb tissue equivalent phantom skulls, taking the two main energies 59.54 keV and 46.5 keV respectively. It was found that almost all of the activities were deposited in the bones and the minimum detectable activity was approximately 4 Bq for ^{241}Am and 6 Bq for ^{210}Pb. The results for some bones and the collected residue (washing water) gave values which were less than the detection limit.

Bone type & description	LOAX No.3		LOAX No.4	
	^{210}Pb(Bq)	^{241}Am(Bq)	^{210}Pb(Bq)	^{241}Am(Bq)
Water residue (5 l)	≤6	≤4	≤6	≤4
Top skull surface(0.382 kg)	34±4	30±3	50±5	17±4
Base skull surface(0.382 kg)		13±2	108±10	25±3
Surface bones(0.578 kg)	35±4	4±1.0	37±4	6±1
Long bones(0.999 kg)	40±5	≤4	48±5	5±2
Back bone(0.647 kg)	16±3	≤4	≤6	≤4
Rib cage bones(0.417 kg)	≤6	≤4	≤6	≤4
All bones +skull(3.023 kg)	60±6	9±3	63±6	12±2
All bones - skull(2.641 kg)	30±3	6±1	38±4	10±2

Table 5.20 Detailed data analysis of activity of ^{210}Pb and ^{241}Am for the various sheep bones measured using the two LOAX detectors.

These findings proved the fact, that the americium and lead radionuclides had been deposited uniformly in the bones. The low levels of activity in the washing residues underlined the assumption that had been made in this measurement procedure that the

detected activities of both nuclides were effectively non-transportable (non-soluble). The highest activities, found by the three methods of calculation, were from the top of the skull surface and were approximately 108±10 Bq of ^{210}Pb and 25±3 Bq of ^{241}Am. The lowest activity was found in the rib cage bones and the other samples had activities in a descending order as follows: high surface area bones; joints of the long bones; back bones; and finally the rib cage bones. Although the bones were washed, it could not be concluded for certain that the measured activities of the bones had been deposited as ingested material or inhaled radionuclides during the animal's life time or whether the carcass had been exposed to radionuclides as an external environmental contaminant during the decaying process.

However, the results were suggestive of radionuclide uptake. In order to obtain further evidence, measurements could be carried out using other detection methods and procedures such as auto-radiography, alpha spectrometry, mass spectrometry and ICP-MS after some chemical treatment. These types of measurement, which were not possible here, might have given more conclusive evidence about the range and type of dispersion of these radionuclides in the bone matrix and the extent of bone penetration. At the same time, more bones were ideally needed in order to investigate the degree of distribution of these nuclides in the surrounding area. All of these factors would clearly give further evidence of the causes and the source of the activity and the extent of the radionuclide dispersion.

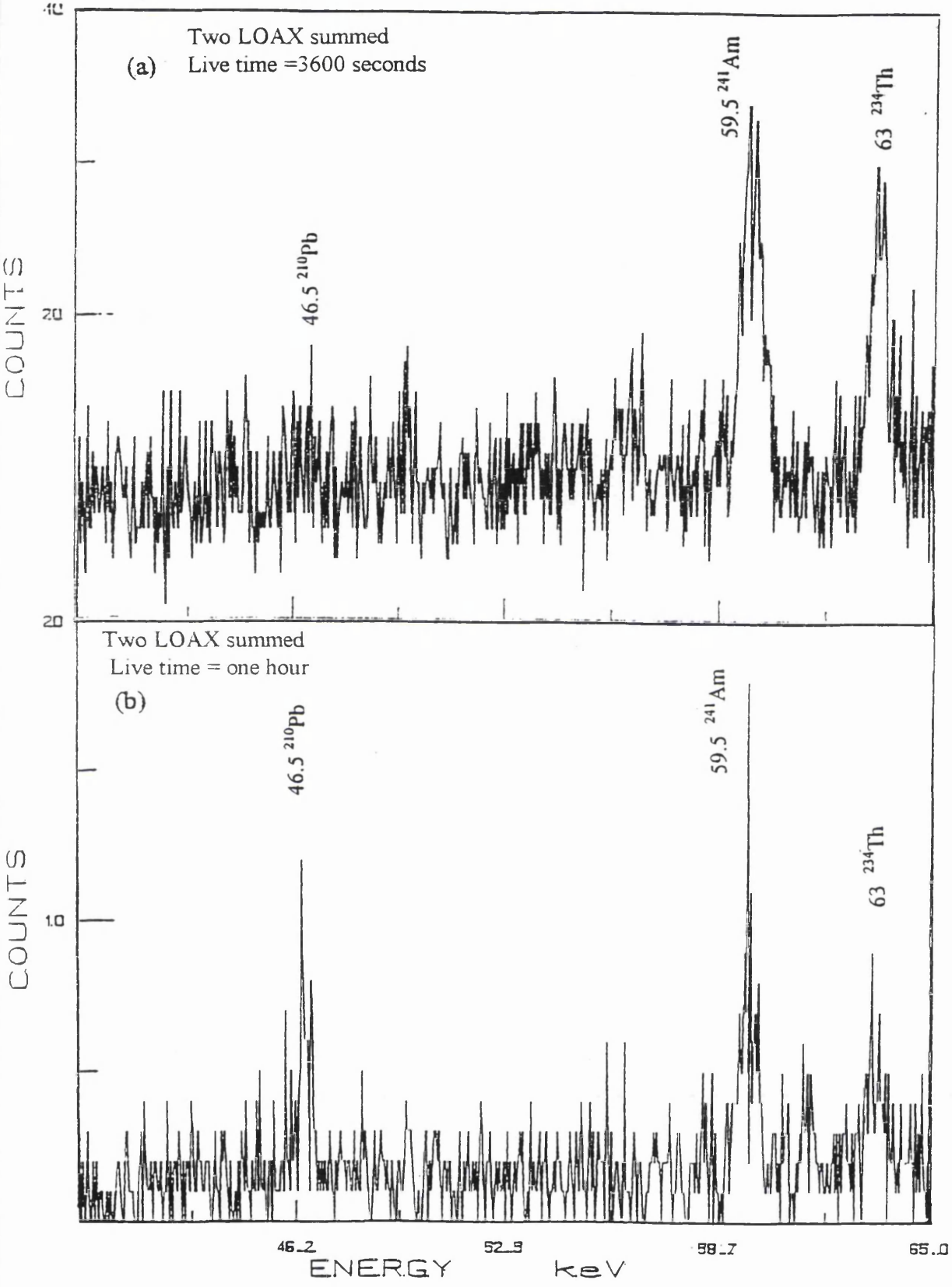

Figure 5.35 Gamma-ray spectra of two LOAX-detectors summed measuring the skull at 2 cm distance: (a) top surface; (b) base surface.

5.7.3. Measurement of sheep wool

5.7.3.1 Methods and results

Two complete fleeces of wool sheered from sheep from the Dumfries area were brought to the laboratory for measurement. Each fleece was placed in a separate bag (A and B), and compressed manually to shape it as closely as possible to the shape of the thorax phantom. A series of static counts from different sides were taken using the two LOAX detectors connected separately. The main peaks which appeared prominently in all of the obtained spectra for both fleeces were again, the ^{241}Am and ^{210}Pb as shown in Figure 5.36 a & b. The average activity of both wool sets was in the range of 50-100 Bq of ^{241}Am and about 100-170 Bq of ^{210}Pb as presented in Table 5.21.

Detector Number	Fleece A		Fleece B	
	^{210}Pb (Bq)	^{241}Am(Bq)	^{210}Pb (Bq)	^{241}Am(Bq)
LOAX-3	111±10	32±3	94±10	68±7
LOAX-4	170±17	45±5	121±12	86±9

Table 5.21 Measured activities of ^{241}Am and ^{210}Pb for both wool sets using two-LOAX detectors connected separately.

Details of the location, age of the animals and the time of grazing were not available for theses samples. However, the detection of ^{241}Am showed that this material from Sellafield can find its way onto sheep. The average value for fleece A was 39 Bq and for fleece B was 77 Bq. Compared with the ALI of 300 Bq, these are significant activities and if a worker was sheering one hundred sheep he could easily be handling several times this quantity. In terms of external radiation hazard, this would probably be of little significance but depending upon conditions there could be the possibility of uptake by inhalation of dusty material during the process. One obvious step would be to count a worker involved with sheering before and after the operation to see if there were any uptake.

Compared with the previous fleece measurement the values obtained here are almost the same so that the results are consistent and probably provide a good indication of the levels of activity in other sheep in the Dumfries area.

Regarding ^{210}Pb, significant activities were also observed on the fleeces. The rocks in parts of this geographical area consist of granite intrusions with uranium veins which would account for the notable presence of this radionuclide in the environment. The values obtained can be compared with the ALI of 10^4 Bq.

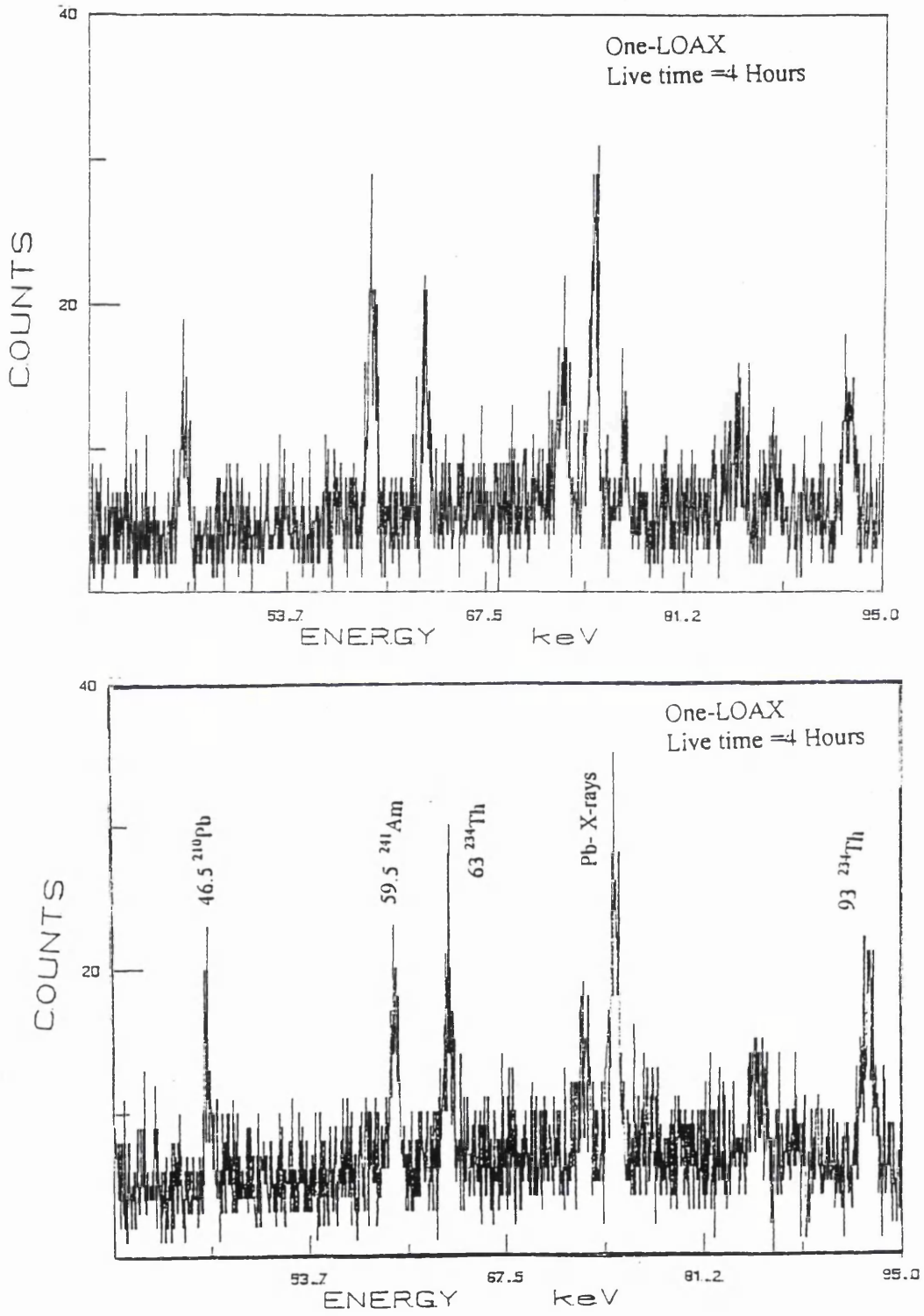

Figure 5.36 a & b Gamma-ray spectrum of the complete two sets of fleeces (wool) of sheep counted using single LOAX-detector.

5.8 *In vivo* calibration and measurements of ^{241}Am

The assessment of human radioactivity exposure due to the Sellafield discharges was of paramount interest. Following the findings of traces of ^{241}Am in a number of samples of whole-sheep and some bones collected from farming areas in South West Scotland (as discussed and presented in the previous section 5.7) a programme was set-up to organize the measurement of a number of human subjects by whole-body monitoring. As a start to this programme, one subject was measured in considerable detail. This subject labelled (D) was chosen because he was considered to be representative of the members of the rural farming population in that his life-style activities interacted closely with the natural environment. This made him a very good candidate for possible internal contamination with ^{241}Am resulting from the likely influence of Sellafield discharges on his farming area.

5.8.1 Calibration Procedures

Two LOAX detectors were used as described previously, for the measurements. In order to provide calibration factors and cross-check previous calibrations for ^{214}Am, nine specially prepared plastic-backed paper strips, labelled with a known amount of ^{241}Am activity, were counted. The strips were made from 1.5 cm wide and 58 cm long pieces of "Benchkote". They were spiked with a stock solution of ^{241}Am having a concentration of 59.99 Bq ml^{-1} as presented in Table 5.22. The activity was distributed evenly over the whole length of the paper and was contained using transparent adhesive tape applied to both sides of the labelled strip after drying. The strips were first counted individually in a 4 cm diameter coil in front of one LOAX detector with the results for net counts presented in Table 5.22. A calibration curve was constructed for 59.5 keV as shown in Figure 5.37.

Sample number	**Volume ml**	**Labelled Activity** ^{241}Am (Bq)	**Measured (59.5keV)** cps±1σ	Sen.(cps Bq^{-1})
1	0	Blank	0.1±0.01	---
2	0.02	1.2±0.1	1.9±0.2	1.58
3	0.08	4.8±0.4	6.9±0.5	1.54
4	0.17	10.2±1.0	16.2±0.9	1.59
5	0.3	18±1	30±1	1.67
6	0.6	36±2	62±2	1.52
7	1.0	60±3	104±3	1.63
8	3.0	180±9	282±4	1.57
9	5.0	300±15	473±5	1.58

Table 5.22 Results for the ^{241}Am strips measured at 59.5 keV using LOAX-4 positioned in a closed lead shield arrangement.

Due to the very close geometry, and because the arrangement had not been calibrated for efficiency, these counts were only used to check for proportionality of the activities in the set of spiked strip. A calibration curve was constructed using these values as shown in Figure 5.37.

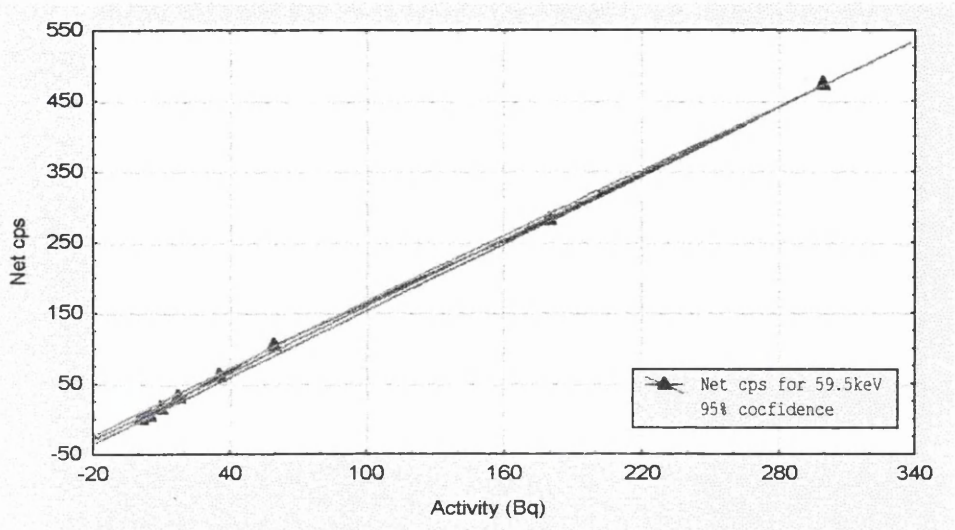

Figure 5.37 Calibration curve for the ^{241}Am strips measured in the closed lead shield arrangement.

In order to carry out the simulated *in vivo* calibration, the same strips were attached circumferentially to the water head phantom and positioned at a distance of about 4 cm from both LOAX detectors in the whole-body monitor shield. The measured net count rates for the three low X-ray energies (13, 17 and 26 keV) and for the main gamma peak at 59.5 keV, are presented in Table 5.23 for LOAX-1, and Table 5.24 for LOAX-4 for a counting period of one hour. Two calibration curves were constructed using the above data as shown in Figure 5.38 and Figure 5.39 for LOAX-1 and LOAX-4 detectors respectively.

Activity Bq ± 1σ	13 keV cps ± 1σ	17 keV cps ± 1σ	26 keV cps ± 1σ	59.54 keV cps ± 1σ
Blank	0.013±0.002	0.020±0.002	0.007±0.001	0.003±0.001
1.2±0.6	0.005±0.002	0.001±0.002	0.001±0.001	0.012±0.002
4.8±0.4	0.069±0.005	0.009±0.003	0.002±0.001	0.013±0.002
10±0.5	0.009±0.003	0.009±0.003	0.009±0.002	0.009±0.002
18±0.9	0.009±0.003	0.029±0.004	0.057±0.002	0.033±0.003
36±2	0.022±0.003	0.052±0.004	0.012±0.002	0.077±0.005
60±3	0.025±0.004	0.043±0.004	0.004±0.001	0.120±0.006
180±9	0.068±0.004	0.133±0.006	0.024±0.002	0.310±0.010
300±15	0.088±0.005	0.190±0.008	0.016±0.002	0.450±0.011

Table 5.23 Background count rates and net count rates (cps) for all energies of LOAX-1 measuring ^{241}Am strips placed around the water head phantom.

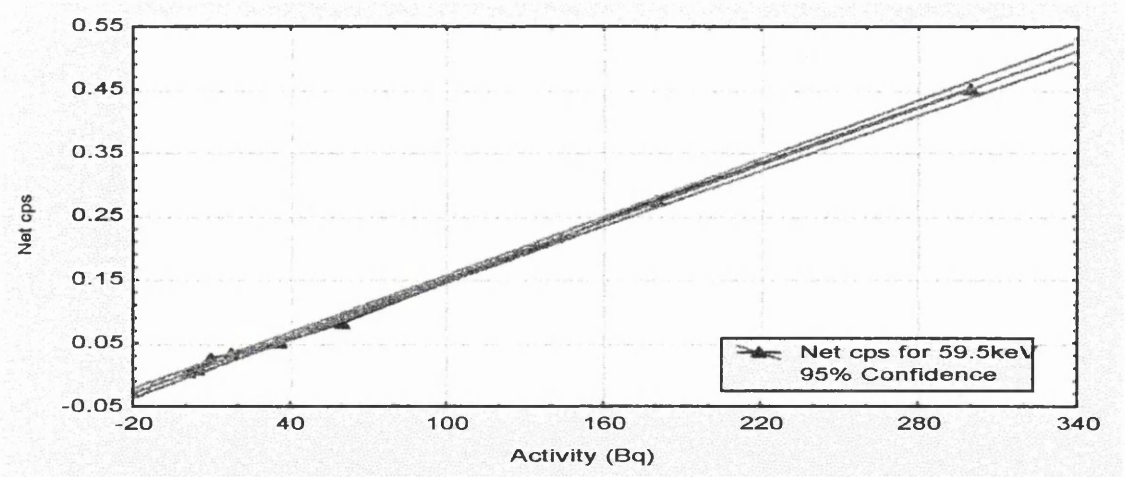

Figure 5.38 Calibration of LOAX-1 using ^{241}Am strips wrapped around the head section of the water phantom in the WBM-shield.

Activity Bq ± 1σ	**13keV** cps ± 1σ	**17keV** cps ± 1σ	**26keV** cps ± 1σ	**59.54keV** cps ± 1σ
Blank	**0.015±0.002**	**0.022±0.003**	**0.0082±0.002**	**0.002±0.001**
1.2±0.1	**0.005±0.003**	**0.002±0.003**	**0.0001±0.002**	**0.003±0.001**
4.8±0.3	**0.001±0.002**	**0.007±0.003**	**0.0001±0.002**	**0.008±0.002**
10±0.5	**0.005±0.002**	**0.004±0.003**	**0.0055±0.002**	**0.025±0.003**
18±0.9	**0.002±0.002**	**0.015±0.004**	**0.0011±0.002**	**0.034±0.003**
36±2	**0.016±0.003**	**0.026±0.004**	**0.0088±0.003**	**0.051±0.004**
60±3	**0.018±0.003**	**0.033±0.004**	**0.0006±0.002**	**0.082±0.005**
180±9	**0.055±0.004**	**0.087±0.006**	**0.0155±0.003**	**0.274±0.008**
300±15	**0.105±0.006**	**0.141±0.007**	**0.0222±0.003**	**0.452±0.011**

Table 5.24 Background count rates and the net count rates (cps) of LOAX-4 measuring ^{241}Am strips placed around the water head phantom.

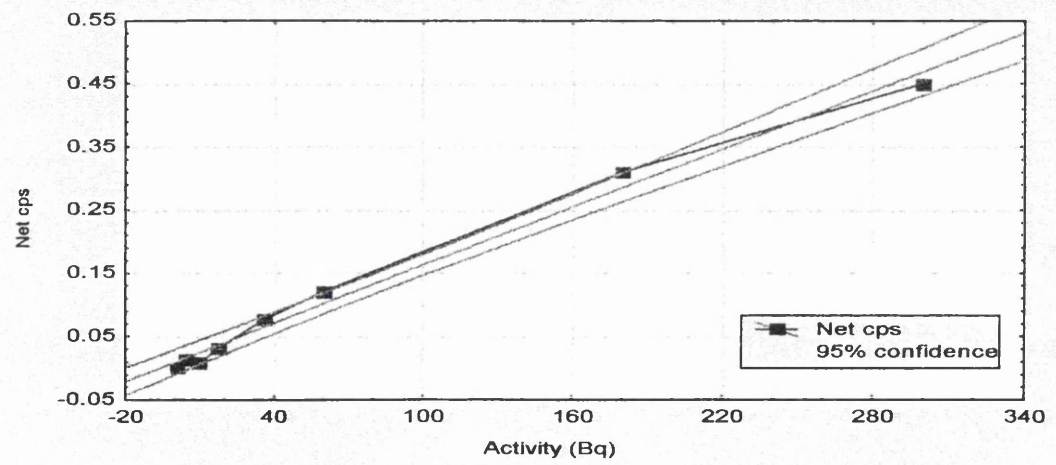

Figure 5.39 Calibration data for the LOAX-4 using ^{241}Am strips wrapped around the head section of the water phantom in the WBM-shield.

In order to assess the effects of background, scattering and attenuation effects in the examination of a human subject *in vivo* measurements were carried out on a volunteer wearing a number of the above ^{241}Am labelled strips around the head was monitored. Strips containing 4, 10, 18, 36 and 60 Bq were measured in this manner, each for a counting time of 30 minutes. Also, one count was taken having the two 60 Bq strips wrapped around the knee. The collected count rates for the 59.5 keV peak are tabulated in Table 5.25 for both detectors.

Calibration Strips of ^{241}Am Activity (Bq)	LOAX-1 over subject's head Net cps±1σ	Sen. cps Bq^{-1}	LOAX-4 over subject's head Net cps±σ	Sen. cps Bq^{-1}
Blank strip	0.0094±0.0023	----	0.002±0.001	-----
4 Bq around head	0.008±0.003	0.0019	0.009±0.002	0.0022
10 Bq around head	0.009±0.003	0.0009	0.022±0.004	0.0022
18 Bq around head	0.033±0.005	0.0019	0.047±0.005	0.0026
36 Bq around head	0.063±0.006	0.0017	0.099±0.007	0.0028
60 Bq around head	0.075±0.007	0.0013	0.119±0.008	0.0019
60 Bq -folded head	0.221±0.01	0.0037	0.249±0.012	0.0042
60 Bq around Knee	0.637±0.02	0.0106	0.973±0.023	0.0162

Table 5.25 *In vivo* blank and net count rates for the main energy 59.5 keV measuring the ^{241}Am-strips around the subject head using both LOAX-detectors for 1800 seconds counts.

The subject's skin dose was calculated for the highest activity of 60 Bq during the half-hour count and was considered to be negligible. A calibration curve was constructed using the above data as shown in Figure 5.40 and 5.41 for both detectors.

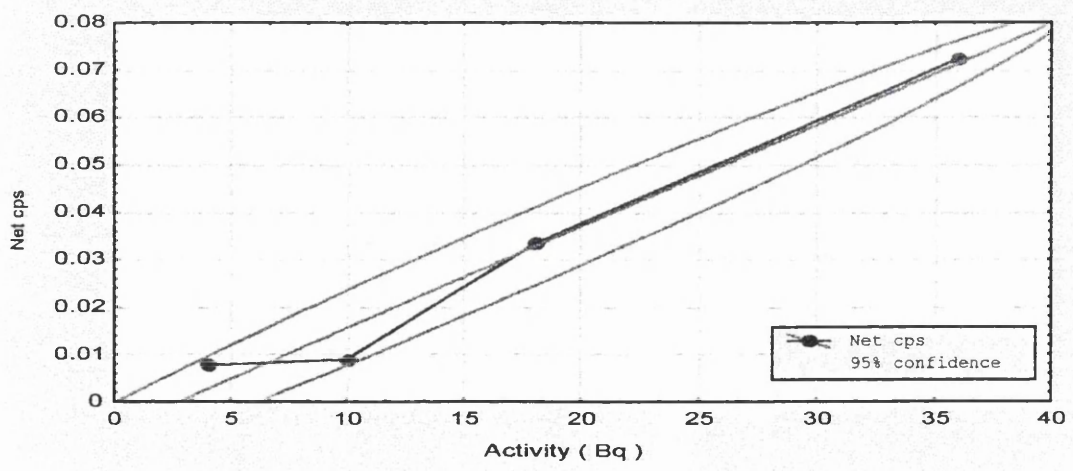

Figure 5.40 *In vivo* calibration curve for LOAX-1 obtained by counting ^{241}Am strips placed around subject's head.

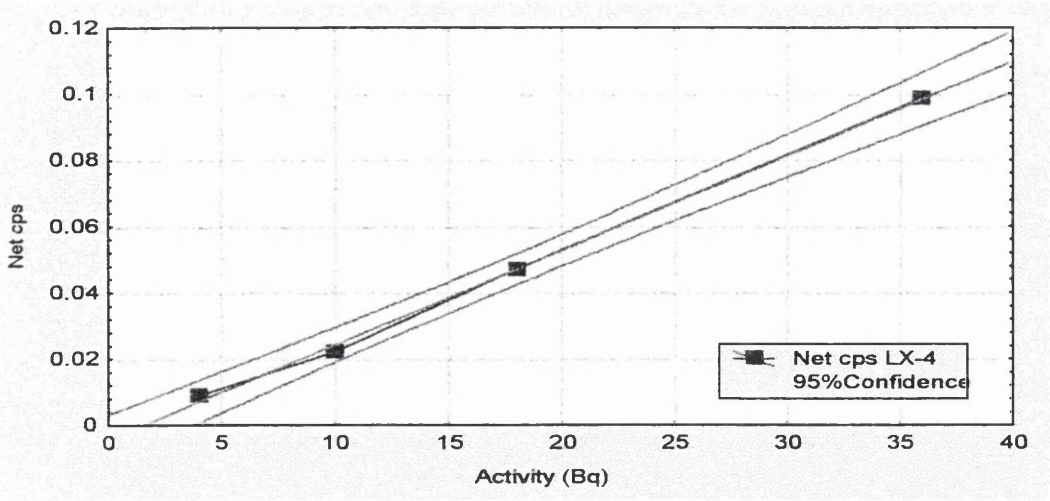

Figure 5.41 *In vivo* calibration curve for LOAX-4 obtained by counting ^{241}Am strips placed around subject's head.

5.8.2 Results and discussion

As could be deduced from the above data and the constructed calibration curves for both detectors, shown in Figures 5.38-5.39, that the calibration procedure with the water phantom and for the single detectors in the small lead shield, gave straight line curves for the set of labelled strips. However, this did not seem to be the case for the *in vivo* studies where the strips formed a band around the subject's head. The count rates for lower activity strips were affected by the ^{40}K background contribution. The experimental *in vivo* sensitivity calibration factors for both detectors using the various ^{241}Am-strrips over the water phantom, were calculated from the measured values plotted in Figures 5.40 & 5.41 to be 1.49×10^{-3} cps Bq^{-1} and 1.62×10^{-3} cps Bq^{-1} for the 59.5 keV gamma peaks. Taking two standard deviation of the background, the MDA values were calculated to be 3 Bq and 2.5 Bq for LOAX No. 1 and No.4 respectively. These data compare very well with the previously calculated values.

However, when the same strips were measured around the volunteer's head, the calibration curves produced (shown in Figure 5.40. and 5.41) and the sensitivity factors were found to be; 1.98×10^{-3} cps.Bq^{-1} and 2.53×10^{-3} cps Bq^{-1} for LOAX-1 and LOAX-4 respectively. The calculated MDAs using two standard deviations of the background were 2 and 1.7 Bq for the two detectors respectively. These values of MDA were supported by the plots of the various gamma-ray spectra of the different activity labelled strips when

compared with the blank strip as shown in Figure 5.42. There was a problem with the 60 Bq strip when it was counted with the volunteer and therefore it was omitted from the consideration of the results.

To check further on the effects of geometry and activity distribution, the ^{241}Am strips were folded into one third of their length and positioned along the forehead of the volunteer and counted for 30 minutes.

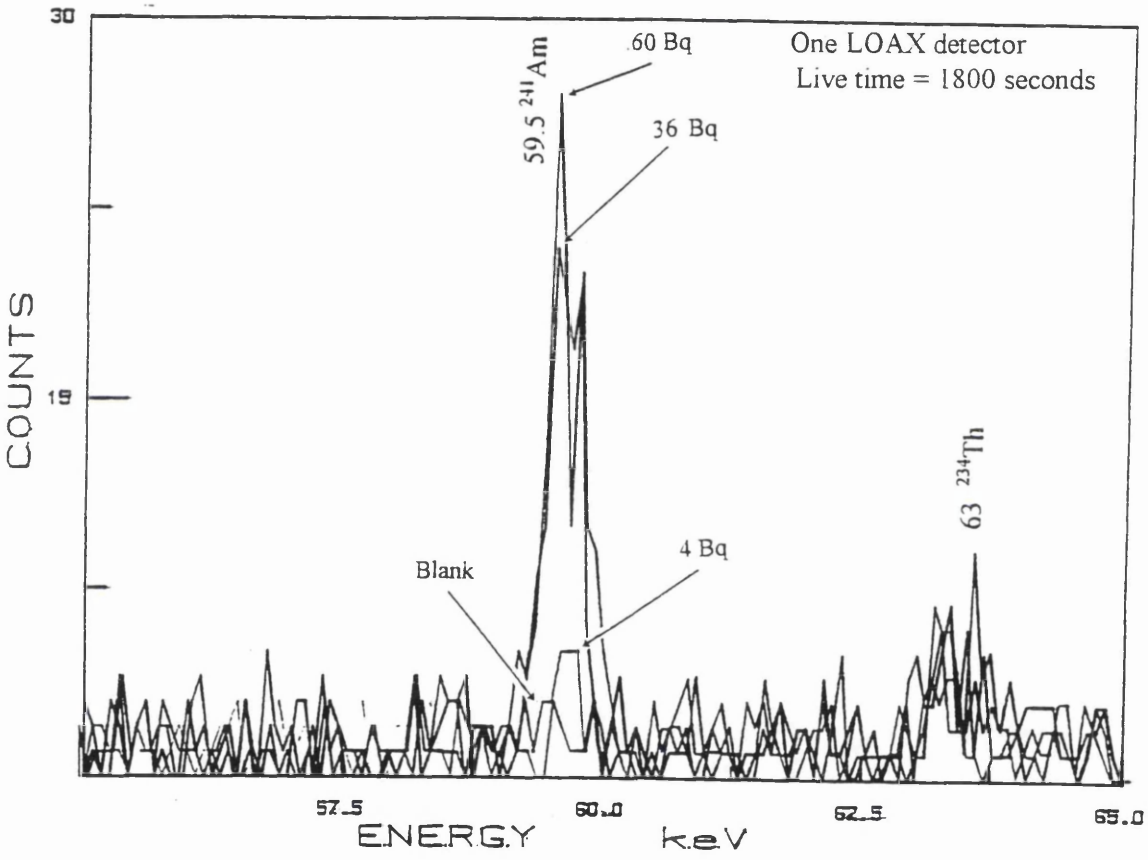

Figure 5.42 Gamma-ray spectrum of the *in vivo* calibration of LOAX detectors using the various activity ^{241}Am labelled strips.

As expected, this count gave approximately three times the count rate compared with the source completely around the head. This fact indicated that some of the ^{241}Am activity was not seen by the LOAX-detectors because of skull attenuation of the 59.5 keV radiation, and that the effective depth of the field of view was quite limited. Also, the two strips of 60 Bq activity were wrapped around each knee of the volunteer and measured directly under the LOAX-detectors. It was found that this count was more sensitive than

the head due to low bone matrix of the knee and improved geometry. Also each detector was measuring a contribution from the adjacent strip which could account for the higher count rates. According to Palmer (Palmer et al., 1984) the skull, the knees and the ankles are the main sites where americium concentrates i.e. at the large bone joints. This, therefore, was the reason for our interest in obtaining counting sensitivity factors for the volunteer at these particular sites.

For completeness, the low-energy peaks were plotted and sensitivity and MDA factors were calculated and presented in Table 5.26. It could be seen that these low-energy peaks were very difficult to measure with a high standard of accuracy and certainty. Their counting sensitivities are low and MDAs are higher as can be seen from Table 5.26.

Detector	13keV		17keV		59.5keV	
	Sensitivity cps Bq^{-1}	MDA Bq	Sensitivity cps Bq^{-1}	MDA Bq	Sensitivity cps Bq^{-1}	MDA Bq
LOAX-1	$3.33x10^{-4}$	18±3	5.32x10-4	11±2	$1.49x10^{-3}$	4±1
LOAX-4	$3.29x10^{-4}$	18±3	$7.05x10^{-4}$	9±2	$1.62x10^{-3}$	5±1

Table 5.26. Sensitivity factors for the low-energy peaks of ^{241}Am-strips measured using single LOAX detectors.

Following this calibration work, subject D was measured using the two LOAX detectors in a number of static configurations as follows: two separate counts with the head area directly under the two LOAX detectors at a distance of about 4 cm; one count with the detectors over the liver / lower-abdomen area; finally, one count with the detectors over the knees. All the counts were taken for half-hour periods between which the subject was allowed to sit up and relax for short breaks. The collected spectra recorded for each detector were summed and corrected for background contributions. Typical *in vivo* summed gamma-ray spectra of the subject D for one LOAX-detector in comparison with similar summed spectra of two unexposed volunteers measured using the same counting geometries are shown in Figure 5.43 a & b for LOAX-1.

Using the subtraction programme of the computer software the above two spectra subtracted from each other and the resulted net gamma-ray spectrum of subject D clearly shows a residual ^{241}Am activity at the gamma-ray peak of 59.5 keV. Unfortunately, due to electronic problem, LOAX-4 detector showed a temporary energy calibration peak

detectors over the liver / lower-abdomen area; finally, one count with the detectors over the knees. All the counts were taken for half-hour periods between which the subject was allowed to sit up and relax for short breaks. The collected spectra recorded for each detector were summed and corrected for background contributions. Typical *in vivo* summed gamma-ray spectra of the subject D for one LOAX-detector in comparison with similar summed spectra of two unexposed volunteers measured using the same counting geometries are shown in Figure 5.43 a & b for LOAX-1.

Using the subtraction programme of the computer software the above two spectra subtracted from each other and the resulted net gamma-ray spectrum of subject D clearly shows a residual ^{241}Am activity at the gamma-ray peak of 59.5 keV. Unfortunately, due to electronic problem, LOAX-4 detector showed a temporary energy calibration peak drift which degraded the resolution during these *in vivo* measurements. Because of this, no peaks could be observed so that the data from the first detector could not be supported. Therefore, the results of the measurements and analysis proved to be inconclusive due to the very low number of counts observed in the 59.5 keV ^{241}Am region-of-interest. By close inspection of the gamma-ray spectra very small peaks were discerned in the spectra collected for the head and knees with LOAX-1, but when these counts were analyzed statistically they were found to be insignificant.

The 80% detector was also used simultaneously with the LOAX detectors. The spectra showed considerable ^{137}Cs activity and some other natural peaks present in the background as shown in Figure 5.44. The measured ^{137}Cs activity was calculated to be 150±10 Bq, which was higher than other recently measured subjects in Scotland which is below 50±5 Bq. Other naturally occurring nuclides could also be identified as labelled in the spectrum.

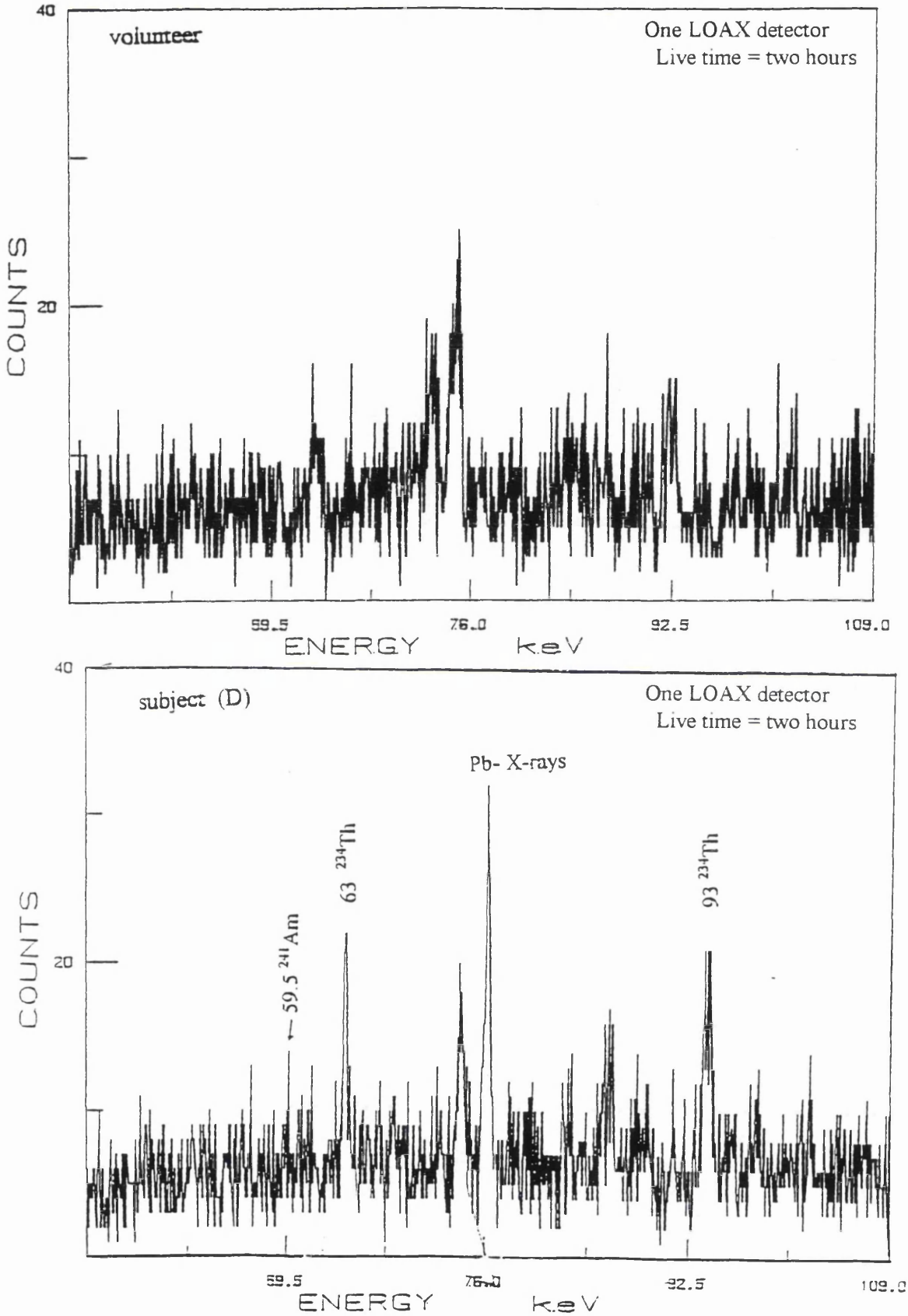

Figure 5.43 Gamma-ray spectra for *In vivo* measurement using one LOAX detector: (a) volunteer; (b) subject D.

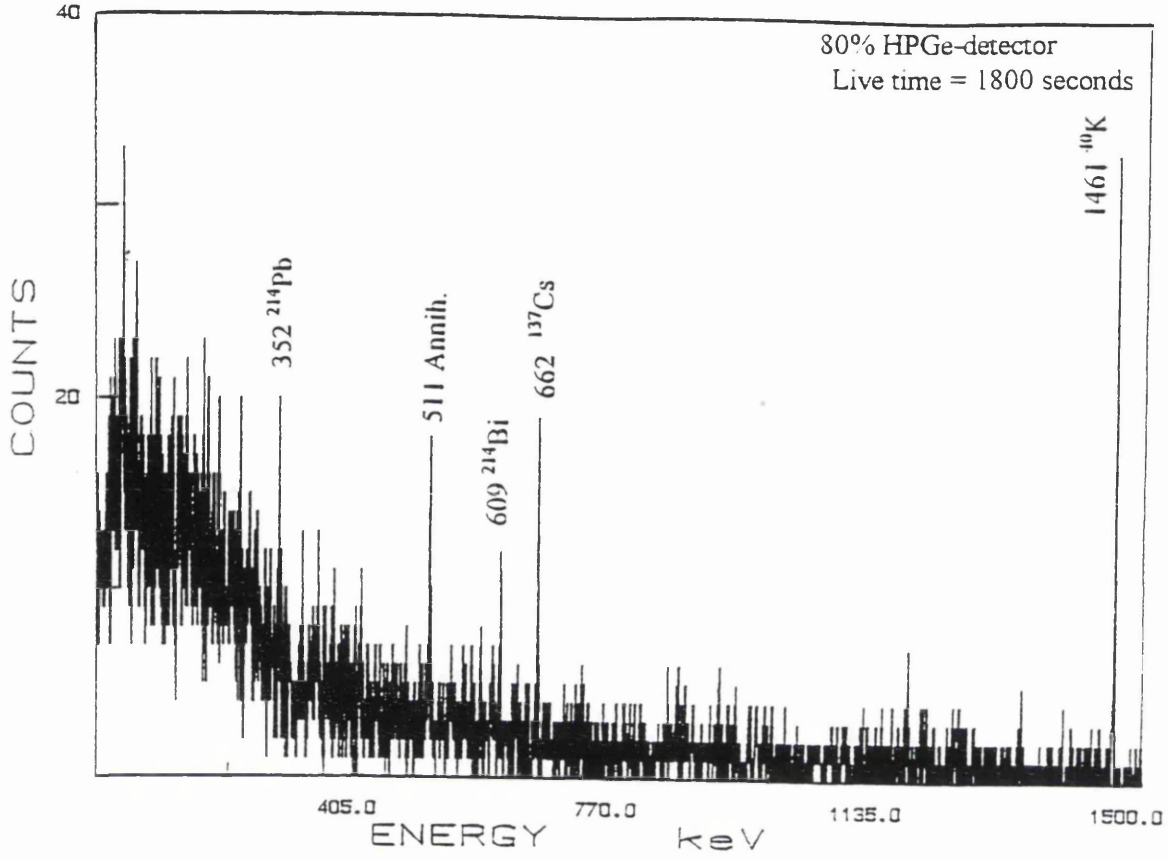

Figure 5.44 Gamma-ray spectrum obtained for measurement of subject D using the 80% HPGe-detector.

The LOAX 1 spectra for subject D were summed: two head counts; one liver count ; and one knee count. From this total spectrum the summed background from two control subjects, counted under the same conditions, was subtracted giving the resultant stripped spectrum shown in Figure 5.45. Close inspection of this spectrum certainly suggests the presence of a trace of ^{214}Am at 59.5 keV. Similarly, there may be residual activity at 63 keV corresponding to ^{234}Th and an unidentifiable peak at approximately 51 keV, although these suggested peaks do not appear to be as significant.

The conclusion that could be drawn from these measurements, is that the measured ^{241}Am activity was below 4 Bq. These observations provide evidence that there was certainly no appreciable internal contamination in the measured subject. These initial

observations point to the need for further measurements on suitable subjects from the area in order to confirm or otherwise reject, the suggestion that americium can be taken up in trace quantities. It is not unreasonable that trace quantities of this radionuclide could find their way into the body in persons who work on the land with animals which become slightly contaminated.

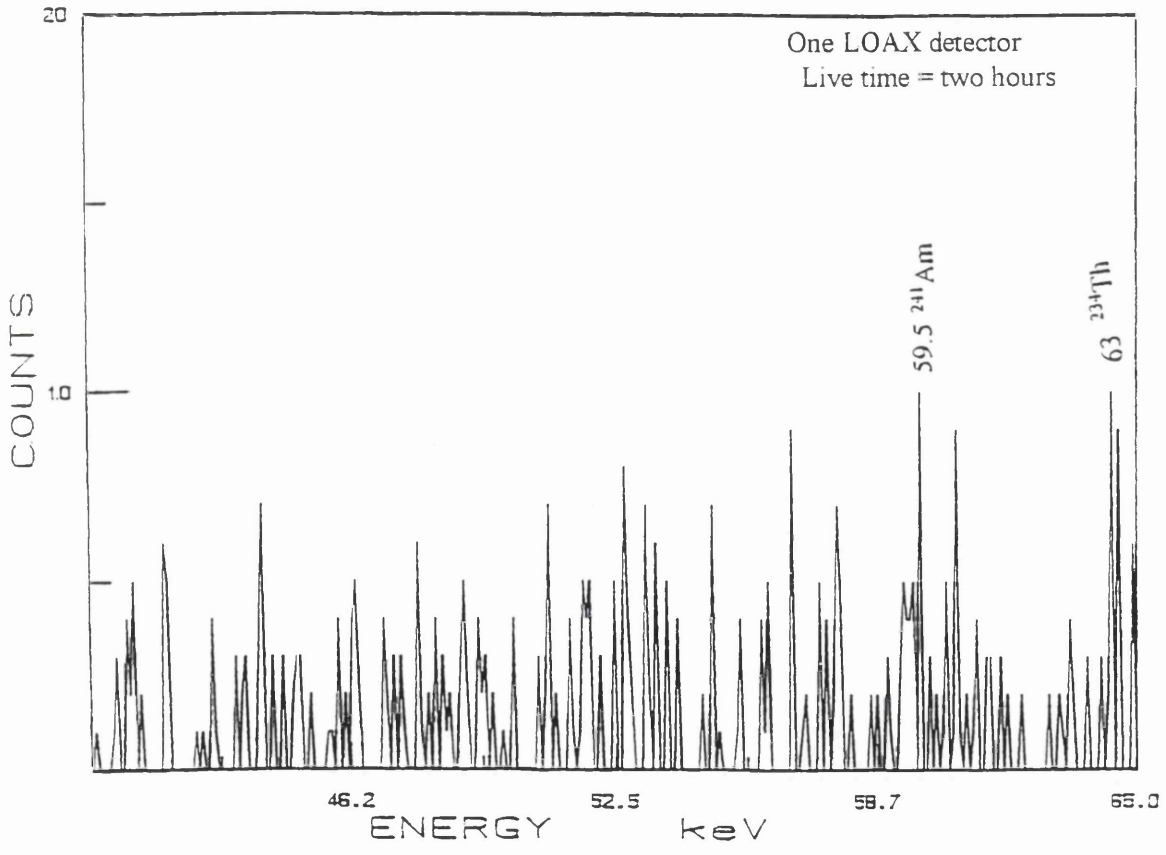

Figure 5.45 Summed and stripped gamma-ray spectrum of subject D.
(showing a suggestion of the residual activity at the 59.5 keV gamma-ray peak)

Chapter 6

Summary, conclusion and recommendations

6.1 Introduction

Following recommendations made in recent years for the need to monitor members of the population, particularly those living near nuclear installations, the ability to measure the low-energy photon emissions which come from such radionuclides as Pu and Am in addition to the high energy emission from radiocaesium and other fission products now has a renewed emphasis. Therefore the requirements for both low-energy and high energy photon monitoring had been thoroughly studied and investigated in this research work. Because of increased of availability of Germanium detectors which offer high resolution gamma-ray spectrometry, partial and whole-body counting techniques are steadily changing to their use either as an adjunct to or a replacement for NaI or "phoswich" detectors.

In this research work substantial data on the measurements and the appraisal of typical shadow-shield monitoring facilities have been gathered in order to investigate the feasibility of the measurement of actinides in human subjects. The detection capabilities, particularly the sensitivity and minimum detectable activity of germanium semiconductor detectors for actinides and the various associated calibration procedures with tissue equivalent phantoms have formed an integral part of the study. When completed, the system was dubbed " hybrid " because of the mixture of detector technologies used, which gave a versatility for gamma-ray measurements from very low energy with the LOAX detectors to relatively high energy with the 80% and NaI(Tl) detectors.

An important aspect has been the positive and interesting results of *in vivo* measurements carried out on a number of individuals, some of whom were special cases where internal actinides were thought to have been deposited. In addition, the finding of traces of ^{241}Am and ^{210}Pb on sheep and in sheep organs originating from

the South West of Scotland (Dumfries area) has enabled the system to be checked and also provided interesting and sometimes unexpected results. In this final chapter, the principal aspects of the work are summarised, conclusions are drawn and some recommendations are made.

6.2 The construction, optimisation and calibration of the detection system

The shield housing the previously built NaI whole-body monitor at SURRC, has been reconfigured to accommodate a single p-type Coaxial 80% HPGe-detector and up to four n-type low-energy photon detectors (LOAX). The four LOAX's have been installed close to each other in a rectangle, this arrangement has made it possible to measure the head while the 80%-detector is simultaneously measuring the upper thorax with the subject in a supine static position. Using the moving bed the subject can also be scanned under the detectors.

When constructing the new monitor, the approach was to the have the detection systems so that the subject-to-detector solid angles were large to give an invariant response and to accommodate bulk samples. This was successfully arranged for the additional semi-conductor detectors by studying various geometries in order to determine the optimum to be used to gain the highest counting sensitivity. In order to increase sensitivity, it was found that subject-to-detector distance geometry should be minimum and for the shadow-shield arrangement the subjects were raised up using a special low background foam bed support, to an amenable distance from the detector surfaces to achieve this. The adjusted geometry proved to give the highest sensitivities, especially for the low-energy photon emitting radionuclides as has been described earlier in the results sections. The other geometrical approach used was to have the measured subject or phantom as far away as possible (bed surface to detector surface 29 cm) without any bed support. This method was mainly used for high energy gammas and allowed the photon emission from the organ(s) to have

approximately equal path length into the detector, and was not therefore influenced by the solid angle and nuclide distribution to the same degree. This counting geometry was mainly used for the scanning counting mode where the clearance between the subject and the detector had to be sufficient for safety.

Another detection variable studied in the case of the LOAXs, was the number of the detectors used. By increasing the number of the detectors viewing an organ the area covered is larger so that the sensitivity is increased. For our present system this could be attained by summing up to four LOAX HPGe-detectors with the results shown in Table 6.1. With this arrangement, the detectors covered approximately 70% of the lungs. Another method of increasing the sensitivity of the detection tried was the summing of a number of spectra using a specially written computer programme. The summing effect on the peaks was noticeable on a number of added spectra shown in chapter 5. The main requirement for the spectra to be summed in this way was that their energy calibration had to be exactly the same and remain so during measurements. When using commercially available sources for calibration, the main factor that had the greatest effect was the source configuration. There was a general effect whereby the calibration factor improved from point sources to: the circular disk sources: to the parts of body phantoms: to the whole phantoms, so that the accuracy of measurement presumably improved. The 80% HPGe-detector showed the least variation with this factor.

It was realised that the counting sensitivity would be dependent upon the particular parts of the body being examined and so the detectors were calibrated using tissue equivalent phantoms and geometry-specific sensitivity factors were derived. The tissue equivalent phantoms used for the calibration of the detection system are specifically constructed for calibrating systems used to measure transuranic radionuclides in the whole body, or partial body counting for lung, liver and head. Because they are made of real bones and matching tissue equivalent material, in addition to the method of labelling them with different transuranic radionuclides, they

proved to be adequate and very useful for the calibration of whole-body counter. It had been previously shown that head measurements can be used for the measurements of bone seeking radionuclides in the body, because it contains approximately 15% of the total bone mass, and approximately 15% of the radionuclides get deposited in the skull. In addition it was found that, for the low-energy X-ray and gamma-emitters total body counting is not adequate because of background effects, whereas the head could be measured in a lower background because it is easier to be positioned and to be shielded from the rest of the body tissue under a specific counting geometry.

In addition, a number of calibration graphs were obtained using the more specialized phantom known as the Lawrence Livermore phantom described in chapter 4, which allows for differing chest wall thicknesses. The validity and the usefulness of the utilisation of these phantom configurations in detector calibration and their representation of the absorption qualities of the human body for gamma-rays, has been demonstrated by comparison of the calibration factors collected in this research work with those in a number of other laboratories throughout the world.

As has been outlined in the five chapters, the detection capabilities, including the background, the detection sensitivities, and their MDAs were appraised in order to investigate the low-level detection capability. In particular, the limits of 3 Bq for ^{241}Am and 8 Bq for ^{210}Pb using two LOAX detectors summed for one hour counts are considered to be low enough when compared with other whole-body counters as demonstrated in Table 6.1, or when compared with the ALI for these radionuclides of 200 Bq and 8000 Bq respectively.

Radionuclide Energy	SURRC WBM 4-LOAX	*PNL WBM 4/8-LOAX
^{241}Am 59.5 keV	3-6 Bq	1-7 Bq
^{210}Pb 46.5 keV	5-8 Bq	4-6 Bq
^{238}U- 63 keV	6-10 mg	---
93 keV	3-5 mg	5.6 mg

Table 6.1 Minimum detectable activity of different whole-body monitoring facilities for the nuclides of interest.

*Pacific North West Laboratory using an array of four to eight LOAX high purity germanium detectors inside a complete steel room shield.

6.3 Calculation methods for low activity peaks

6.3.1 Data analysis

The low-level whole body counting described in this research work requires delicate spectrum analysis, especially for the low-count peaks. There were a number of methods that could be used in the investigation of the different peaks in the collected spectra either from the LOAX or the 80% HPGe-detectors.

The methods of background determination and the actual peak count rates have been discussed thoroughly in this research work and the main problem faced was the determination of the net count rates of low intensity peaks and the associated uncertainty. Among other methods, the manual trapezium method of calculation and analysis was selected because it could be applied consistently along with visual inspection of the region of interest.

6.3.2 Spectrum synthesis

Another method of data analysis employed in this study for low count rate peaks was that of spectrum syntheses for comparison purposes. This method proved to be very useful, but it had one main drawback which was the requirement for exactly repeatable measurement geometries for the synthesised spectrum to be used for comparison proposes.

The uncertainty of the analysis and the percentage of error was carried out on a number of the synthesized spectra using ^{210}Pb and ^{241}Am externally labelled skull phantoms with activity of 4860 Bq and 5140 Bq added to an *in vivo* subject background spectrum. By taking a strip factor which is a percentage of the skull phantom activities and adding it to the unexposed *in vivo* spectrum. This showed the point at which the activity was becoming higher than the background, which corresponded to the detection limit as can be seen in Table 6.2 and 6.3 for ^{210}Pb and ^{210}Am externally labelled skulls respectively.

Strip-factor	Activity Bq	Net cps	Estimated %error
0.002	**9.72**	**0.0017±0.0036**	**210%**
0.0025	**12.15**	**0.0025±0.0036**	**144%**
0.004	**19.44**	**0.0045±0.0037**	**82%**
0.006	**29.16**	**0.0081±0.0046**	**57%**

Table 6.2 Synthesized spectra of ^{210}Pb-externally labelled skulls: data and error propagation factors.

Strip-factor	Activity Bq	Net cps	Estimated %error
0.0004	**2.1**	**0.0039±0.0046**	**118%**
0.0008	**4.1**	**0.0078±0.0047**	**60%**
0.0010	**5.1**	**0.0092±0.0047**	**52%**
0.0004	**20.6**	**0.039±0.006**	**14%**

Table 6.3 Synthesized spectra of ^{241}Am externally labelled skulls: data and error propagation factors.

6.4 Applications

In the area of internal dosimetry, whole-body counters have been widely used for operational monitoring of radiation workers at nuclear facilities either as a routine or in cases of a suspected accidental intake of radionuclides. These measurements are used to identify and determine the magnitude of the uptake and the retention pattern of the radionuclides in the body. In this study the emphasis has been on members of the public and what has been interesting are the measurements carried out on a number of subjects and farm animal samples where actinides and or their daughters were likely to have been deposited.

The subjects measured in the search and calibration for actinides all gave positive indications of internal activity. In particular, the subject (B) who had frequented mines in Cornwall, demonstrated in her first measurements that she had been in contact with ^{222}Rn decay products, while her second measurement showed a

completely different pattern of radioactivity. It transpired, in this latter measurement, that the subject had handled a highly radioactive soil sample which it was presumed had led to further internal contamination. Substantial data analysis work was carried out to ascertain the source and the amount of the radionuclides detected in these latter *in vivo* measurements. The measured activity levels of the radionuclides were tabulated in Table 5.15, calculated for the main detected radionuclides using the net count rates of the main energy peaks and internal phantom calibration factors.

In addition to the above measurements, environmental samples could be easily positioned inside the monitor under either the LOAX or the 80% HPGe-detectors. An example of environmental evidence of the presence of actinide contamination was the positive detection of traces of ^{241}Am together with ^{210}Pb on sheep and in sheep organs from the South West of Scotland (Dumfries area). These measurements provided a good basis for further research work on similar samples from different sites in order to ascertain the level of the contamination spread. The considerably higher levels of wool concentration of radioactivity-man-made and natural - measured in available wool samples should trigger further measurements and research on their possible route to the general public.

A subject from the farming community was also measured and the borderline results provided a challenging and a controversial basis for further measurements. Maybe further examinations could be carried out on him and other subjects to obtain more details.

The success of the low-level counting of these various subjects, and the measured cases of contaminated sheep and environmental samples confirmed the applicability of the system for low-level photon emitters and pointed to its usefulness for future measurements, despite the difficulties.

Due to the high attenuation factors of tissue materials (human or animal) for the low energy photons (X-rays) of ^{239}Pu, this radionuclide could not be measured directly. However, due further to the fact that all plutonium, including that from fallout from nuclear weapon testing, contains some ^{241}Pu, which in turn decays to ^{241}Am that emits a 59.54 keV gamma-ray which can be easily measured, this daughter can act as a sensitive indicator for the presence of ^{239}Pu. For this to be applicable, the isotopic composition of the measured material must be known or verified by other means of analysis. It has to be concluded that, the present sensitivity and calculated MDA for these low-energy X-rays and photons is not useful, even when compared to the ALI for ^{239}Pu of 200 Bq. For these reasons the task of whole-body counting of low-energy radionuclides in radiation workers and general public still remains formidable and there is still much room for research and improvement.

6.5 Recommendations

As a result of the experience gained from this work, various recommendations can be made regarding improvements to materials, construction, phantoms for better calibration, inter-laboratory calibration and further research.

In order to reduce the background and make optimum use of the shadow shield arrangement, the lead bricks that were the source of the traces of ^{60}Co and ^{137}Cs should be replaced and efforts made to eliminate these contaminants totally. Also, the roof of the left side of the counting chamber could be extended to improve the shielding of the "outer" two LOAXs which showed an elevated background when added to the detector array because of a reduction in effective shielding.

Because the LOAX detectors were delicate and fragile, experience showed that they would not tolerate much handling and that it was preferable to leave them in one counting geometry as much as possible. Over the years they gave a number of problems such as loss of vacuum and resolution deterioration in addition to their

constant requirement of liquid nitrogen. Because of these problems, other types of detectors could be investigated such as silicon detectors which are known to give excellent energy resolution especially for the low-energy x-rays. This particular feature makes them more useful for the measurements of very low-energy ranges 13-20 keV for the ^{239}Pu measurements. However, their main drawbacks is their small size making them still unsuitable to be utilized in a whole-body arrangement. Another possibility is the addition of "phoswich" detectors, much like NaI units, which require less attention and are more rugged providing that the associated pulse-shape processing electronics is available.

The availability of a number of tissue equivalent phantoms to preserve the continuity of calibration procedures for the various detector arrangements over a long-term working plan would be an advantage.

After the successful participation in the European inter-comparison study coordinated by the German authority, the whole-body monitor laboratory should attempt to participate in more inter-comparison studies to maintain accuracy and maybe gain further recognition nationally and internationally.

As the production of high purity germanium detectors continues to improve and detectors become cheaper and more reliable, it is clear that they are likely to eventually supersede conventional NaI systems for *in vivo* measurements. At the present time, 150% relative efficiency crystals are available and although expensive, could provide a body counting facility entirely analogous to the early counters of the 1960's which used a single 76 mm x 76 mm NaI(Tl)- detector.

Further measurements of different critical groups of the general public should be made especially from those areas known to be affected by certain radionuclide discharges such that of Sellafield and Dounreay. Specific groups should be measured such as the farmers caring for different animals especially during shearing season for sheep. At the same time more live animals and different organs from animals collected from the affected areas should be counted to characterize further the pattern and levels of radionuclides contamination.

REFERENCES

Berger, C.D and Lane, B.H. (1981). Detection of ^{210}Pb in the lungs of smokers by *in vivo* gamma-spectrometry. Oak Ridge National Laboratory ORNL/TM-8454.

Bertrand, A. Brill; Adelstein, S. James; Sarnger, L. Eugene; and Webster, W. Edward. (1983). " Low-level radiation effects: A Fact Book. The Society of nuclear medicine, ISBN 0-932004-14-8.

Black, D. (1984). Investigation of the possible increased incidence of cancer in West Cumbria. Report of the independent advisory group. London: HMSO.

BNFL 1971-1990 Annual reports on radioactive discharges and monitoring of the environment published annually, Warrington: British Nuclear Fuels Limited, Risley, UK.

BNFL 1989-1994. Annual reports on radioactive discharges and monitoring of the environment published annually, Warrington: British Nuclear Fuels Limited, Risley,UK.

Boecker, B.B (1991). Current status of bioassay procedures to detect and quantify previous exposure to radioactive materials. *Health. Phys.* **60**,(suppl.1), 45-100.

Boddy, K.; (1966). A mobile shadow-shield whole-body monitor for medical research. *Health. Phys. Pergamon press*, **12**, 1148-1149.

Boddy, K.; Robertson, I.; Mahaffy, M.E.; Hollowy, I. (1975). A high sensitivity dual-detector shadow-shield whole-body counter with invariant responce for total body in vivo neutron activation analysis. *Phys.Med.Biol.* **20**, No 20, 296-304.

Brodsky, A. (1986). Accuracy and detection limits for bioassay measurements in radiation protection-statistical consideration. Nuclear Regulatory Commission, NUREG-1156.

Bunl, K.; Kracke,W.; Petrayev, E.P. and Ruchlja, A. (1993). Plutonium in lungs and livers of persons from Chernobyl fallout affected areas in Byelorussia. *J. Radioanal. Nucl.Chem., letters* **176** (1) .11-20. 1993.

Burns, P.A.; Copper, M.B.; Johnston, P.N.; Martin, L.J. and Williams, G.A. (1994). Determination of the ratios of ^{239}Pu and ^{240}Pu to ^{241}Am for nuclear weapons test sites in Australia. *Health. Phys.* **67**, No.3, 226-232.

Cambray, R.S (1982). Annual discharges of certain long-lived radionuclides to the sea and to the atmosphere from the Sellafield Works, Cumbria 1957-1981. UKAEA Harwell Report AERE-M-3283. HMSO, London.

Cohen, N. (1981-1984). *In vivo* measurements of bone seeking radionuclides, progress report. DOE/EV/04326-6.

Cohen, N. ; Spitz, H.B and Wrenn, M. E. (1977). Estimation of skeletal burden of "bone-seeking " radionuclides in man from *in vivo* scintillation measurements of the head. *Health. Phys.* **33**, 431-441.

Cohen, N. ; Laurer, G.R.; Pomroy, C.; Morse, R. S.; Hickman, D.P.; Estrada, J. S. and Neton, J.W. (1992). Long-term retention of ^{210}Pb in man: A unique case of internal contamination. *Health. Phys.* **62**, NO.6.

Committee on Medical Aspects of Radiation in the Environment (COMARE). (1986) First Report: The implication of the new data on the release from Sellafield in the 1950s for the conclusions of the report on the investigation of the possible increased incidence of cancer in West Cumbria (London: HMSO).

Committee on Medical Aspects of Radiation in the Environment (COMARE). (1988) Second Report: Investigation of the possible increased incidence of leukemia in young people near the Dounreay Nuclear Establishment, Caittness, Scotland (London: HMSO).

Committee on Medical Aspects of Radiation in the Environment and Radioactive Waste management Advisory Committee. (1995) Potential health effects and possible sources of radioactive particles found in the vicinity of the Dounreay Nuclear Establishment, Caittness, Scotland (London: HMSO).

Currie, LA. (1968). Limit for quantitative detectors and quantitative determination. *Analytical Chemistry*, **3** , 586-693.

Dean, P. N; Griffith, R. V. and Anderson, A. L. (1976). Design criteria for phantoms for calibration of external detectors for the *in vivo* assay of plutonium. In: Diagnosis and treatment of incorporated radionuclides, 265-276. Vienna, IAEA.

Debertin, K. and Helmer, R.G. (1988). Gamma-ray and X-ray spectrometry with semiconductor detectors. Elsevier Science Publishers B.V, Amsterdam, The Netherlands. 399 pages.

Dmitriev, S. N; Oganessian, Yu. Ts.; Buklanov, G.V.; Kharitinov, Yu. P.; Novgorodov, A.F.; Salamatin, L.I.; Starodub, G. Ya.; Shishkin, S.V.; Yushkevich, Yu. V. and Newton, D. (1993). Production of ^{237}Pu with high radiochemical purity. *Appl. Radiat. Isot.* **44**, 1097-1100.

Droughi, N.D; (1992). Design criteria for high resolution gamma-ray body counting system. M.Sc. Thesis, Glasgow university.

East, B.W and Robertson, I. (1988). Measurement of radioactivity from Chernobyl in population groups in Scotland. Doe Report: DoE/RW/88.103.

EG&G ORTEC Catalog (1993/1994). Instruments & Systems for Nuclear Spectrumetry. EG&G ORTEC, 100 Midland Road, Oak Ridge, TN,USA.

Falk, R.B; Tyree, W.H; Wood, C.B and Lagerquist, C. R. (1979). A system of high purity germanium detectors for the detection and measurement of inhaled radionuclides. In: Advances in radiation protection monitoring. Proc.Symp. Stockholm, IAEA. Vienna, 445.

Falk, R. B. and Tyree, W. H; (1984). A system of high purity germanium detectors for the detection and measurement of inhaled radionuclide in: Assessment of radioactive contamination in man 1984. Proceedings of an IAEA symposium held in France ISBN 92-0-020085, 445-378.

Fisk, S. (1994). An investigation into the take-up of Chernobyl-derived caesium by heather honey from south west Scotland. SURRC Report.

Fry, F.A (1980) Low-level measurements of transuranic nuclides. *Radiological protection Bull.*, NRPB, No. **35**, 20-23.

Gardner, M. J; and Winter, P.O. (1984). Mortality in Cumberland during 1959-78 with reference to cancer in young people round Windscale. *The Lancet, Vol no.* **I**, 216-217.

Gardner, M. J; Snee, M.P; Hall, A.J; Powell, C; Downes,S.; and Terrell, J.D. (1990). Results of case control study of leukaemia and lymphoma among young people near Sellafield nuclear plant in West Cumbria. *Br. Med. J.* **300**, 423-429.

Gray, J.; Jones, S.R; and Smith, A.D. (1995). Discharges to the environment from the Sellafield site,1951-1992. *J. Radiol. Prot.* **15** No 2, 99-131.

Griffith, R.V; Dean, P.N and Anderson, A.L. (1979 a). " Fabrication of a tissue equivalent phantom for inter-calibration of *in vivo* transuranic nuclide counting facilities" In: IAEA international symposium on advances in radiation protection monitoring held in Stockholm, Sweeden-Jun1978. International Atomic Energy Agency. *IAEA-SM*-229/56, Vienna. 1979:493-504.

Griffith, R.V; Dean, P.N; and Anderson, A.L. (1979 b). A tissue-equivalent torso phantom for Inter-calibration of *in vivo* transuranic nuclide counting facilities. In: IAEA International symposium on advances in radiation protection monitoring held in Stockholm, Sweeden-Jun1978. International Atomic Energy Agency. *IAEA-SM*-229/56, Vienna.

Griffith, R.V; Anderson, A.L. and Alderson, S.W. (1984). Fabrication of a set of realistic torso phantoms for calibration of transuranic nuclide lung counting facilities. In: *Proceedings of the Sixth International Congress of the International Radiation Protection Association.* **3.**

Hickman, D.P. and Cohen, N. (1988). Reconstruction of a human calibration phantom using bone sections from an ^{241}Am exposure case. *Health. Phys.*, **55**.

Hickman, D.P. (1994). *In vivo* measurements Chapter 17 of Internal radiation dosimetry by: Raabe, G. D. (1994). First edition Vol. one. Medical Physics Publishing, Madison, Wisconsin.

IAEA 1970. Directory of whole-body radioactivity monitors. International atomic energy agency, Vienna.

IAEA (1984). Assessment of radioactive contamination in man. Proceedings of a symposium, Paris, organized by the International Atomic Energy Agency, Vienna.

International Commission on Radiological Protection and Measurements. (1975): Reference Amn: Anatomical, Physiological and Metabolic Characteristics. *ICRP Publication* **23**. Pergamon Press, Oxford.

International Commission on Radiological Protection. (1983). Radionuclide Transformation, Energy and intensity of Emissions, *ICRP Publicalication*-**38**, Pergamon Press.

International Commission on Radiological Protection (1988). Individual Monitoring for Intake of Radionuclides by Workers: Design and Interpretation, *ICRP Publication*-**54**, Pergamon Press.

International Commission Radiological Protection (ICRP,1991): Annual limits on intake from intake of radionuclides by workers based on radiological protection. ICRP Publication 61. Ann. ICRP 21(4) Oxford: Pergamon Press.

International Commission Radiological Protection (ICRP,1994). Human respiratory tract model for radiological protection. ICRP Publication 66. *Oxford: Pergamon. Ann. ICRP* **24**(1-3).

International Commission on Radiological Protection (1997a): Limits of intakes of radionuclides by workers. *Ann. ICRP* **30**, No 3/4.

International Commission on Radiological Protection (1997b): Limits of intakes of radionuclides by workers. *Ann. ICRP* **30**, *Ann. ICRP* **2**, No. 3/4 .

Jackson, D (1989) Chernobyl-derived ^{137}Cs and ^{134}Cs in Heather plants in North West England. *Health Phys;* No. **57**: 485-489.

Johnson, J. R. (1989). Internal dosimetry, past and future. Pacific Northwest Laboratory, PNL-SA-16761, Richland, Washington.

Knoll, G.F. (1994). Radiation Detection and Measurement. 2nd edition ed. *J.Wiley and Sons, New York.* 670 pages.

Kozhevrov,V.P. (1991). Unique whole-body counting system for measuring Sr-90, the main issues of long-term investigation. USSR-Japan joint meeting, Chelyabinsk.

Lane, R.C., McCormick, W.B., Jefferies, S.J and Danyluk P. (1985): Use of Six-Element Array of Hyperpure Germanium Detectors in Monitoring for Internal Actinide Contamination: In Assessment of Radioactivity in Man- 1984 IAEA, Vienna,79-91.

McKay, W.A. and Walker, M.I. (1990). Plutonium and americium behaviour in Cumbrian near -shore waters. *J.Environ. Radioactivity,* **12**, 276-283.

MacKenzie, A.B and Scott, R.D. (1993). Sellafield waste radionuclides in Irish sea intertidal and Salt March Sediments. *Environmental Geochemistry and Health* **Vol.15** No 2/3.

MacKenzie, A.B; Scott, R.D; Allan, R.L; Ben Shaban,Y.A; Cook,G.T and Pulford, I.D. (1994) Sediment radionuclide profiles: Implication for mechanisms of Sellafield waste dispersal in the Irish Sea. *J. Environ. Radioactivity* **23**. 39-69.

Mariscotti, M.A. 1967 A method for automatic identification of peaks in the presence of background and its application to spectrum analysis. *Nucl.Inst. Meth.* **50**, 309-320.

McInroy, J. F; Boyd, H.A; Eutsler, B.C. and Romero, D. (1985). The U. S. Transuranium Registry Report on the ^{241}Am content of a whole body, Part IV: Preparation and Analysis of tissues and bones. Health.Phys. 49, 587-621.

Ministry of Agriculture, Fisheries and Food (MAFF) 1989-1992. Radioactivity in surface and coastal waters of the British Isles. Report published annually by the Ministry of Agriculture, Food and Fishery.

McInroy, J.F.; Kathren, R.L. and Swint, M.J. (1989). Distribution of plutonium and americium in whole bodies donated to the United States Transuranium Registry. *Rad. Prot. Dos.* **26**, 151-158.

Mole, R. H (1987). Childhood leukaemia and nuclear establishments. *Br. Med. J.* **294**, 835.

National Council on Radiation Protection and Measurements (NCRP). (1985). A handbook of radioactivity measurements procedures. 2nd ed. Bethesda, MD: NCRP Publications; *NCRP report* No. **58.**

Neton, J. W. (1988). A method for the *in vivo* measurement of ^{241}Am at long times post-exposure. Ph.D. Thesis. New York University.

Newton, D.; Taylor, B.T. and Anderson, A.L. (1978). X-ray counting efficiencies for plutonium in lungs, derived from studies with inhaled palladium-103. *Health Phys.* **34**, 573-585.

Newton, D.; Campbell, G.W.; Anderson, A.L. and Fisher, J.C. (1981). Inter-laboratory comparison of techniques for measuring lung burdens of low-energy photon-emitters. *Health Phys.* **40**, 748-753.

Newton, D.; Wells, A.C.; Toohey, R.E.; Sha, J.Y.; Jones, R.; Jefferies, H.E; Palmer, H.E and Rieksts, G.A. (1984): The Livermore phantom as a calibration standard in the assessment of plutonium in lungs In: Assessment of radioactive contamination in man 1984. Proceedings of an IAEA symposium held in France ISBN 92-0-020085, 183-200.

Newton, D. (1994) Private communication.

Palmer, H.E.; Breitenstein, B.D.; Durbin, P.W.; Heid, K.R. and McInroy, J.F. (1984). "Calibration of whole-body counters for Transuranic radionuclides by using total-body donations to the United States transuranium registry" In: Assessment of radioactive contamination in Man 1984. Proceedings of an IAEA symposium held in France ISBN 92-0-020085, 201-212.

Palmer, H.E. and Rieksts, G.A. (1984). High-purity planar germanium detectors for *In vivo* measurement of uranium and transuranic radionuclides in: Assessment of radioactive contamination in Man 1984. Proceedings of IAEA symposium held in Paris, France 1984. ISBN 92-0-020085, 93-106.

Palmer, H. E.; Spitz, H.B. and Rieksts,G.A. (1985). Gamma-ray measurements. Special issue on the the U.S. Transuranium Registry report on the ^{241}Am content of a whole body. *Health. Phys.* **49**:577-586.

Palmer, H.E.; Rieksts, G.A; Brim, C. P. and Rhoads, M. C. (1988). Hanford whole-body counting manual. Richland, WA:Battelle Pacific Northwest Laboratories; **PNL-6198.**

Palmer, H. E. and Rhoads, M.C. (1989). Determining the ratio of ^{239}Pu to ^{241}Am in wounds by measuring the L_γ X-rays with a Si(Li) detector. *Health. Phys.* **56**, No 2 249-252.

Palmer, H. E.; Rieksts,G.A. and Lynch, T. P. (1991). Performance of an array of large-volume germanium detectors for whole-body counting. *Health.Phys.* **61**, No 5, 595-600.

Pomroy, C and Malm, H (1984a). High-purity germanium detectors for *In vivo* measurements of uranium and thorium in: Assessment of radioactive contamination in man 1984. Proceedings of an IAEA symposium held in France ISBN 92-0-020085, pp. 69-78.

Pomroy,C. and Malm, H .(1984b). Use of six-element arrays of hyper-pure germanium detectors in monitoring for internal actinide contamination In: Assessment of radioactive contamination in man 1984. Proceedings of an IAEA symposium held in France ISBN 92-0-020085, pp.79-92.

Pushparaja, T.K; Haridasan, C.O; Gohel, T.S.; Sharma, R.C and Iyer, M.R. (1992). Estimation of thoron inhalation dose using a sensitive whole-body counter. *Rad.Pro.Dos.* **42** No. 4, 307-312. Nuclear technology publishing.

Raabe,G.d. (1994). Internal radiation dosimetry. First edition ed. Vol. one. Medical Physics Publishing, Madison, Wisconsin.

Rahola, T.; Suomela, M. and Hentela, J.O. (1984). Advantages of using a semiconductor detector for *in vivo* measurement of uranium and transuranic radionuclides. In: assessment of radioactive contamination in Man 1984. Proceedings of an IAEA symposium held in France ISBN 92-0-020085, pp. 107-114.

Roman, E; Beral, V; Carpenter, L; Watson, A; Barton,C; Ryder, H and Aston, D. (1987). Childhood leukaemia in the West Berkshire and Basingstoke and North Hampshire District Health Authorities in relation to nuclear establishment in the vicinity. *Br.Med.J.* **294**, 597-602.

Rundo, J.; Taylor, B.T; Booker, D.V; Newton, D.; and Scargill, D. (1969). Attenuation in the chest-wall of 20 keV X-rays from an inhaled radioactive aerosol. *Nature* **217**. 642.

Sanderson, D.C.W.; Allyson, J.D; Martin, E; tyler, A.N and Scott, E.M. (1990). An airborne gamma-ray survey of the three Ayrshire districts. SURRC. Report.

Sanderson, D.C.W.; Allyson, J.D.; Niriai, S.; Gorden, G; Murphy, S. and Fisk, S. (1994). An aerial gamma-ray survey of Torness nuclear power station in 27-30 . SURRC report.

Scott, L. M.; Warner, G.G. and Poston, J.W. (1977). Theoretical evaluation of optimum detector size and positioning for low-energy *in vivo* gamma spectrometry. *Health.Phys.* **33**, 583-593.

Seymour, R. S.; Paulus,T.J.; Keyser,R.M.; Twomey, T.R; Mulvenon, N.A. and Knight, K.C. (1989). Current trends in nuclear instruments and gamma spectroscopy. EG&G ORTEC, Oak Ridge, Tennessee.

Sharma, R.C.; Surendran,T.; Haridasan, T.K. and Sunta, C.M. (1989) *In vivo* measurements of low-energy photon (LEP) emitters. *Bull. Rad. Prot.* **12**. No4.

Sharma, R.C.; Somasundaram, S.; Kotrappa,P.; Haridasan, T.K.; Surendran, T.; Kapur, D. and Krishnamachari, G., (1976). Assessment of chest burden of plutonium", in Diagnosis and treatment of incorporated radionuclides, pp. 177-201. Vienna : IAEA.

Storm, D. and Stansbury, P. (1992). Minimum detectable activity when background is counted longer than the sample. *Health. Phys.* **63**. 360-361.

Spitz, H.B., Buschbon, R.L.; Rieksts, G.A. and Palmer, H.E. (1983). A new method for analysing high resolution spectra from whole body counter in *in vivo* measurements. *Health.Phys.* **49**. 1085-1096.

Smith, J.R.H; March, J.W; Etherington,G; Shutt, A.L and Youngman, M.J. (1994). Evaluation of high purity germanium detector body monitor. National Radiological protection Board, Chilton, Didcot, Oxon.

Summerling, T.J.; Darby, S.C. (1981). Statistical aspect of the interpretation of counting experiments designed to detect low levels of radioactivity. Chilton, NRPB-R113.

Summerling, T.J.; McClure, D.R. and Massey, D.K. (1985). Measurement of total body activity: The procedures Used at the Board. Chilton. NRPB-R188 NRPB.

Swinth, K.L; Dean, P.N; Rundo , J; and Tomlinson, F.K. (1978). Status and trends in the external counting of inhaled heavy elements deposited *in vivo*. *Health Physics* **37**, 641-657.

Talbot, R.J. and Newton, D. (1994). Blood retention and renal clearance of ^{237}Pu in man.

Talbot, R.J.; Newton, D. and Warner, A.J. (1993). Metabolism of plutonium in two healthy men. *Health Phys.* **65**, 41-46.

Toohey, R.E. (1976). The use of ^{103}Pd as a calibration source for the determination of ^{239}Pu *in vivo*", in : Proceedings of workshop on measurements of heavy elements *in vivo*, Battelle Pacific Northwest Laboratory rep. BNWL-2088, 53-62.

Toohey, R. E. (1981). The distribution of ^{241}Am in the human body as determined by external counting. In: Actinides in man and animals. *Salt Lake City: J. W. Press*; 242-252.

Toohey, R. E; Newton, D.; Moiseev, A. and Bianco, A. (1991). International calibration of detector systems for the measurement of low-energy photon emitters *in vivo*. Final report of a co-ordinated research programme, 1986-1988, Vienna, IAEA.

United Nations: United Nations Scientific Committee on the Effect of Atomic Radiation. (UNSCEAR, 1994). Sources, Effects and risks of ionizing radiation. United Nations.

United Nation Scientific Committee on the Effects of Atomic Radiation UNSCEAR(1990): Sources and biological effects. New York: United Nations.

Watson, W.S and Sumner, D.J. (1996). The measurement of radioactivity in people living near the Dounreay Establishment, Caithness, Scotland. *Int. J. Radiat. Biol.* **70**, No 2, 117-130.

Watson, W.S. (1988). Human $^{134}Cs/^{137}Cs$ levels in Scotland after Chernobyl. *Nature*, **323**, 763-764.

APPENDIX A

The following figures are a number of full and expanded regions of the main gamma-ray spectra obtained using the two detection systems namely the LOAX- array and the 80% HPGe-detector. These are the spectra that showed a number of peaks which were identified using the respective energy calibration of the detectors utilized for the measurement. At first the whole (full) spectrum are shown on top of the pages, then a number of expanded sections representing the main energy peaks are displayed as much as it was feasible.

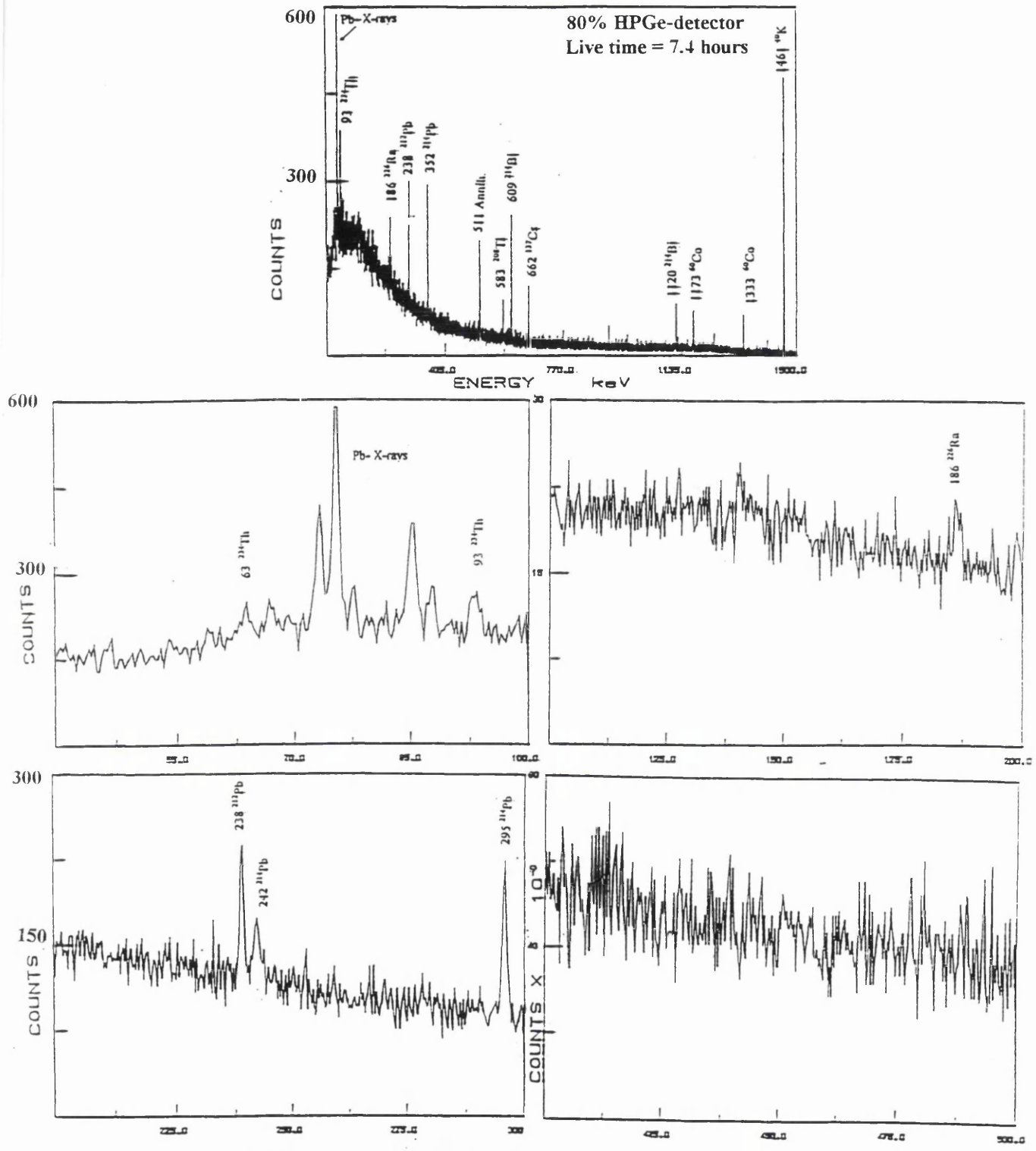

Figure A1 Summed Gamma-ray spectra of all the counts on subject B first count using the 80% HPGe-detector.

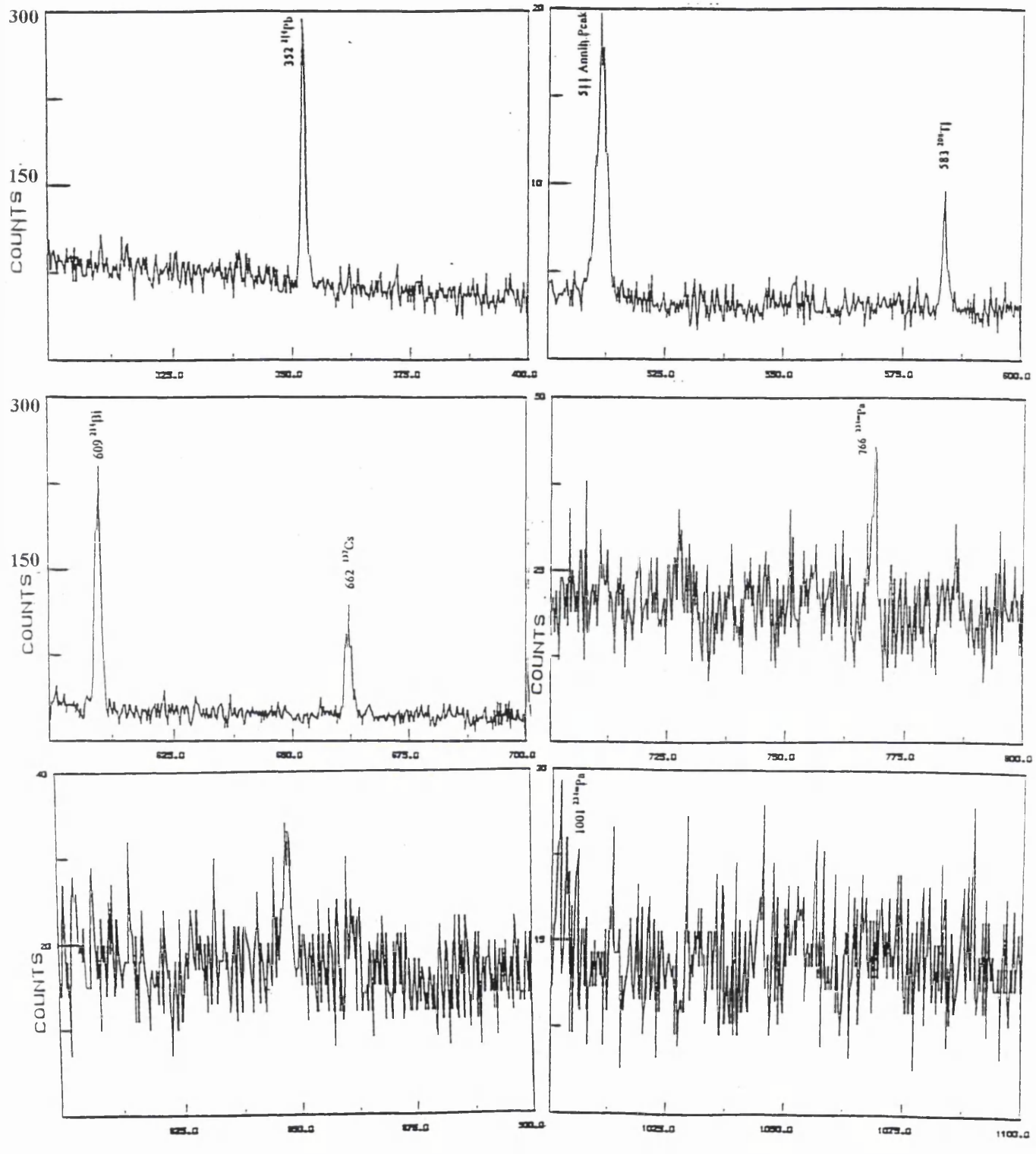
300
150
COUNTS
352 211Pb
511 Annih Peak
583 208Tl
609 214Bi
662 137Cs
769 214Bi
1001 234mPa

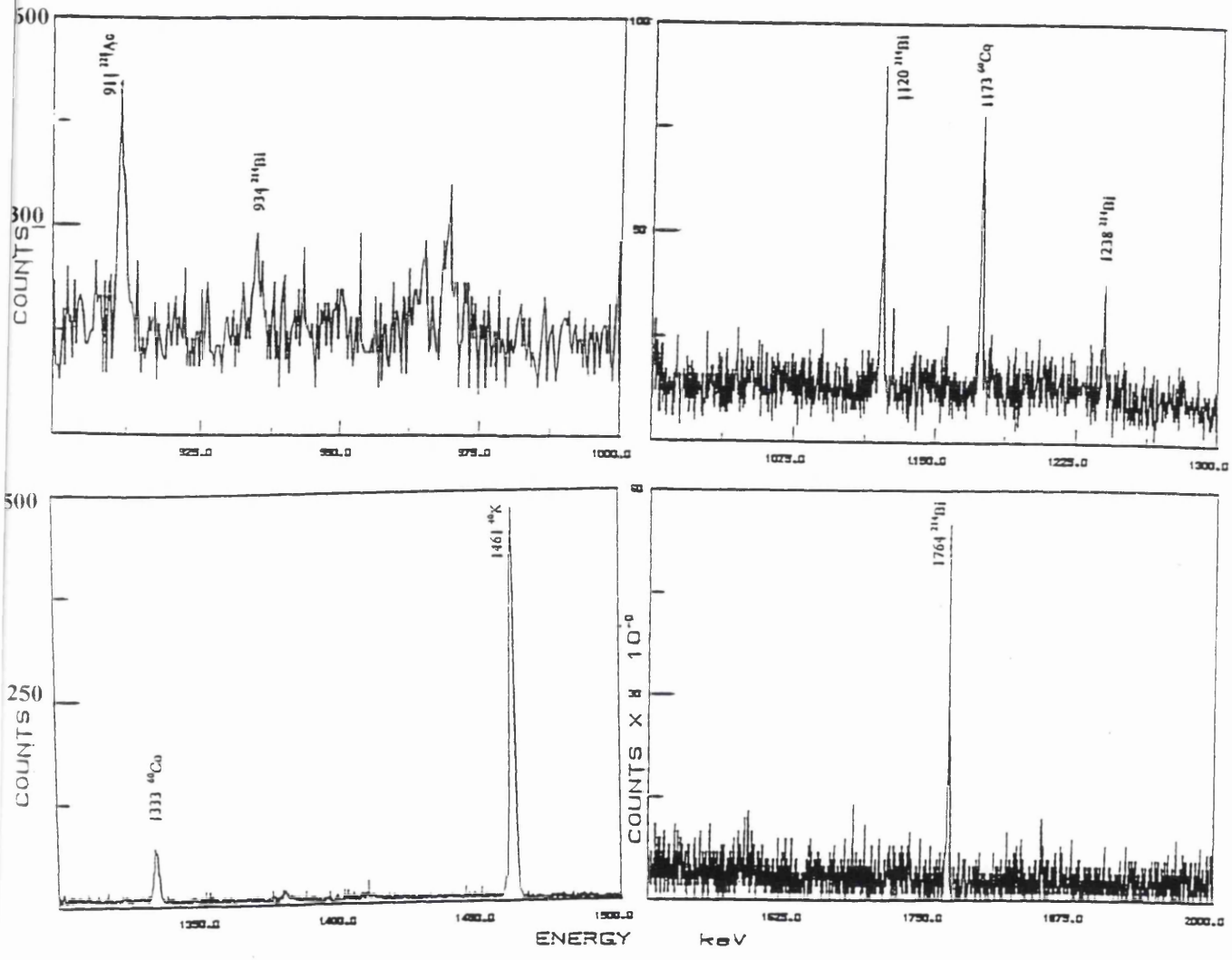
500
300
COUNTS
911 ^{111}Ag
934 ^{111}In
925.0
950.0
975.0
1000.0
100
50
1120 ^{111}In
1173 ^{60}Co
1238 ^{111}In
1075.0
1150.0
1225.0
1300.0
500
250
COUNTS
1333 ^{60}Co
1461 ^{40}K
1350.0
1400.0
1450.0
1500.0
ENERGY
COUNTS X 10^{-0}
1764 ^{214}Bi
1625.0
1750.0
1875.0
2000.0
keV

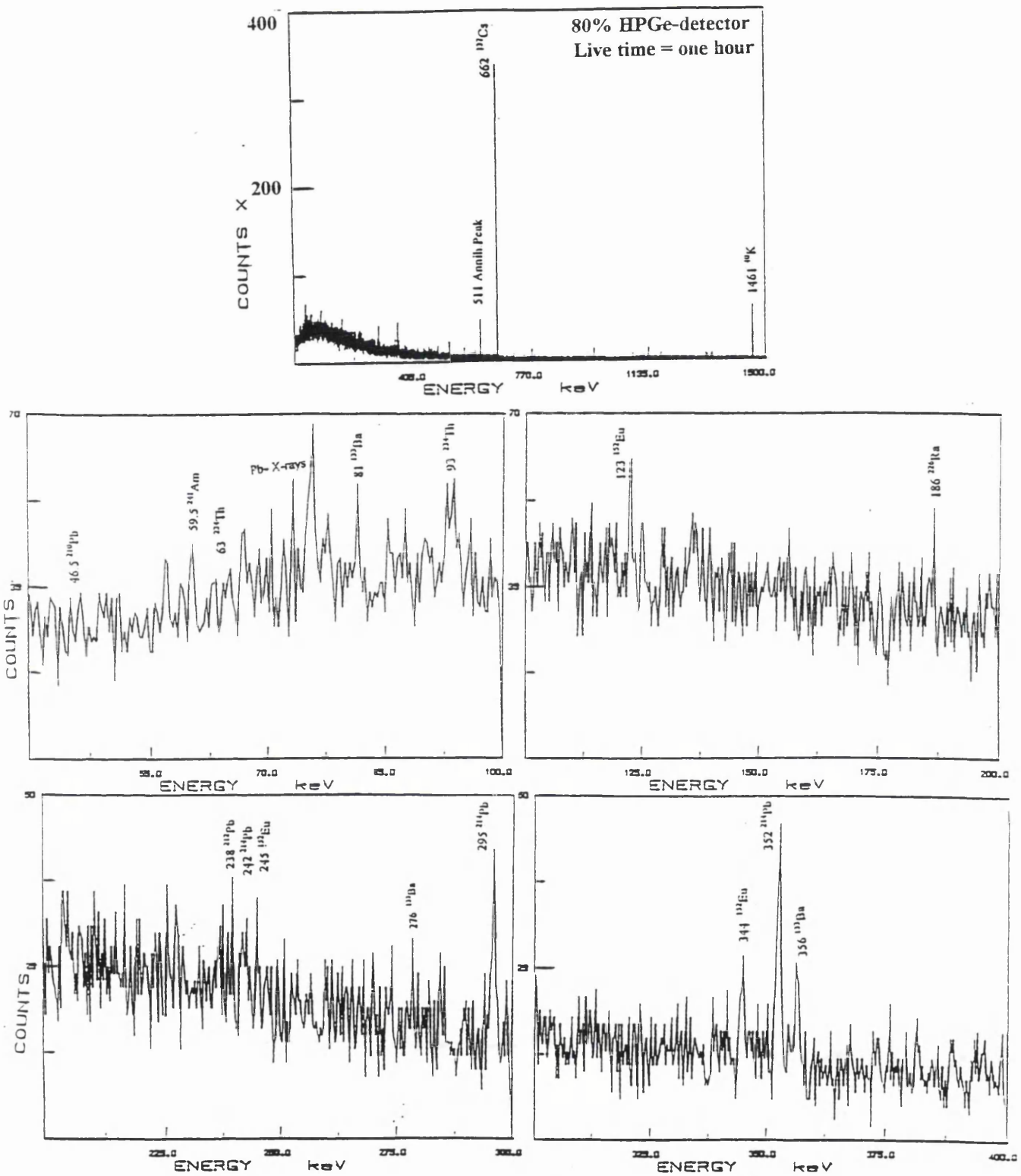

Figure A2 The gamma-ray spectra of the lower abdomen count of subject B using the 80%HPGe-detectors during the second count.

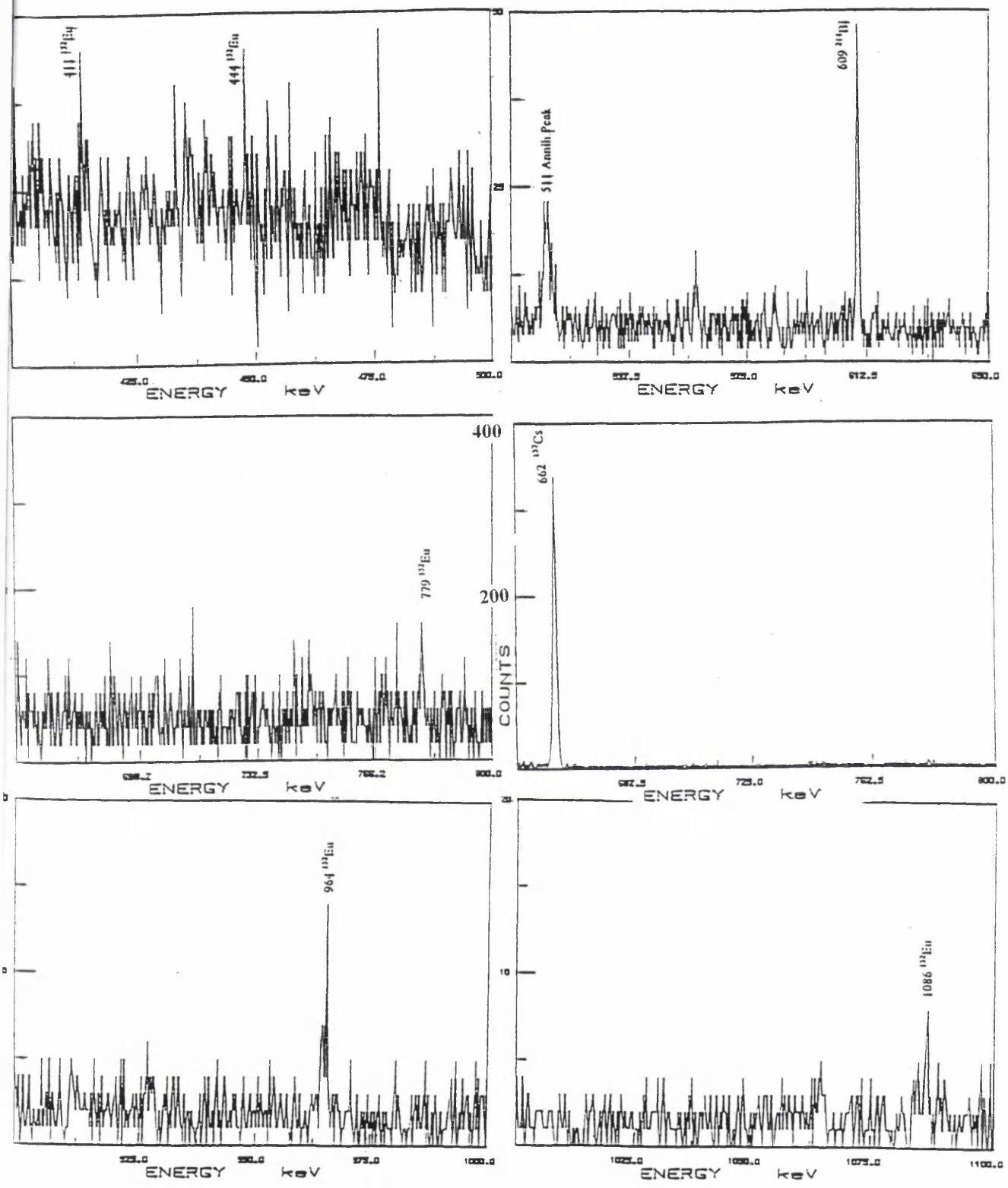
411 ^{152}Eu
444 ^{152}Eu
511 Annih Peak
609 ^{211}Bi
779 ^{152}Eu
662 ^{137}Cs
964 ^{152}Eu
1086 ^{152}Eu
400
200
COUNTS
ENERGY keV

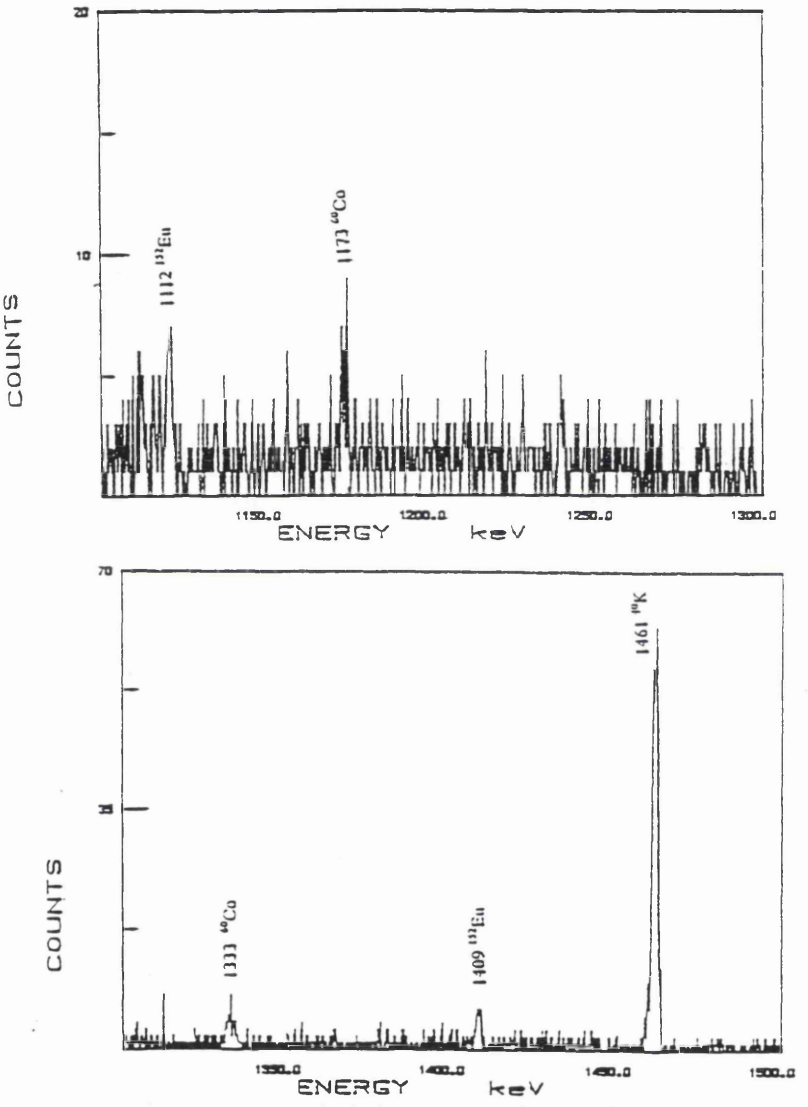
COUNTS
1112 ^{152}Eu
1173 ^{60}Co
1150.0
1200.0
1250.0
1300.0
ENERGY keV
COUNTS
1333 ^{60}Co
1409 ^{152}Eu
1461 ^{40}K
1350.0
1400.0
1450.0
1500.0
ENERGY keV

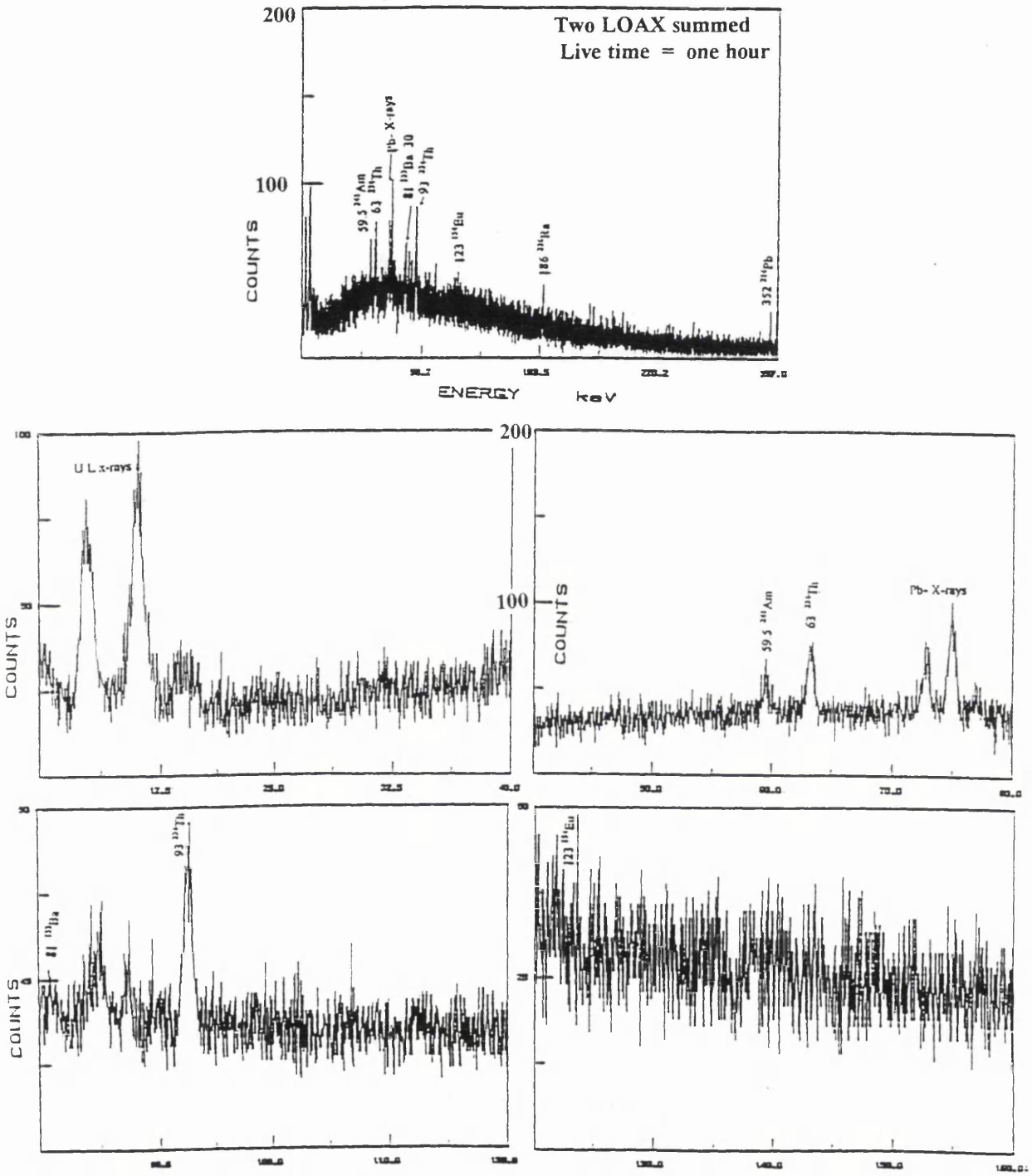

Figure A3 Summed Gamma-ray spectra of all the measurements of subject B second count using the 2LOAX HPGe-detector.

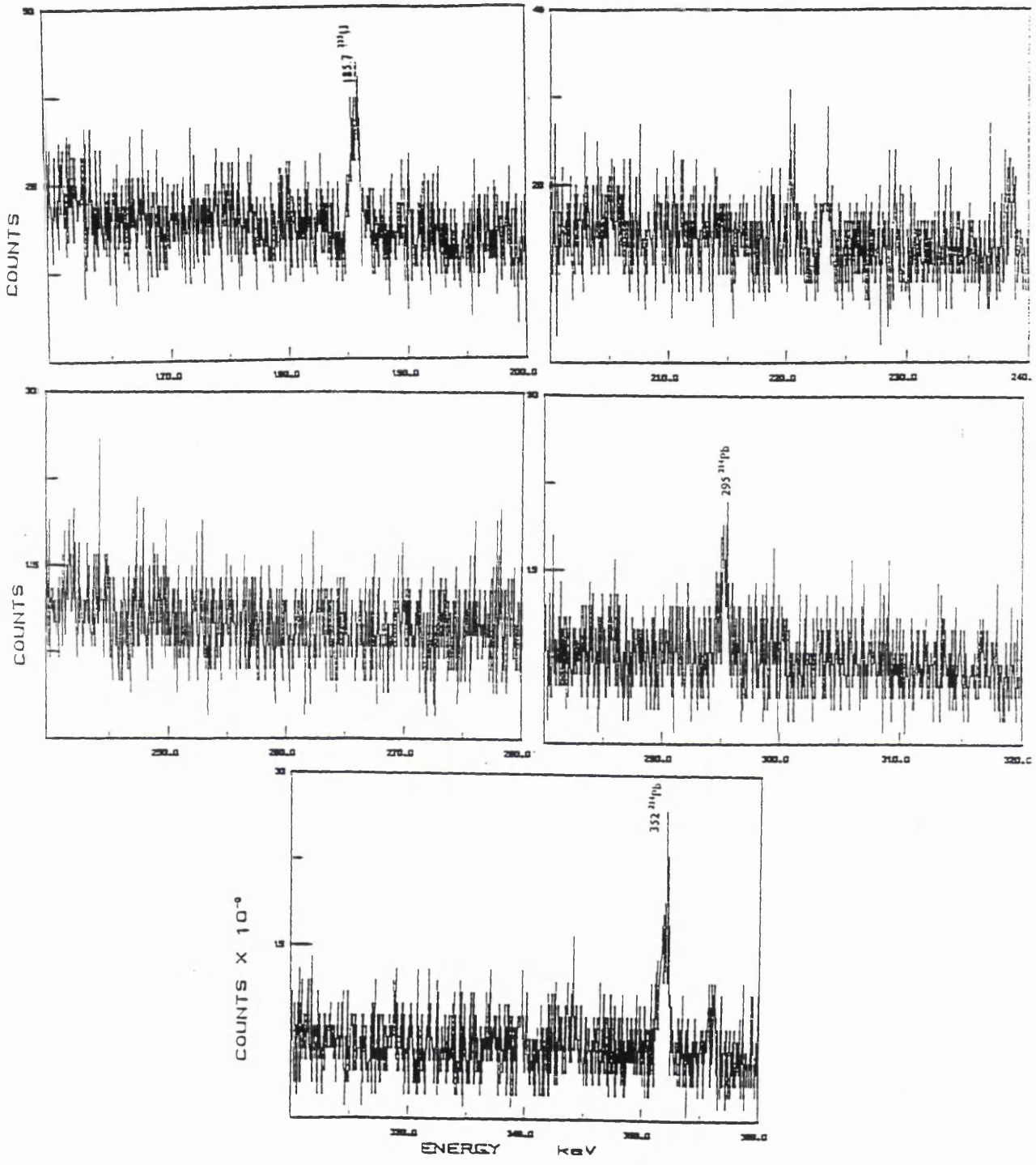
COUNTS
COUNTS
COUNTS X 10⁻⁹
ENERGY
KeV

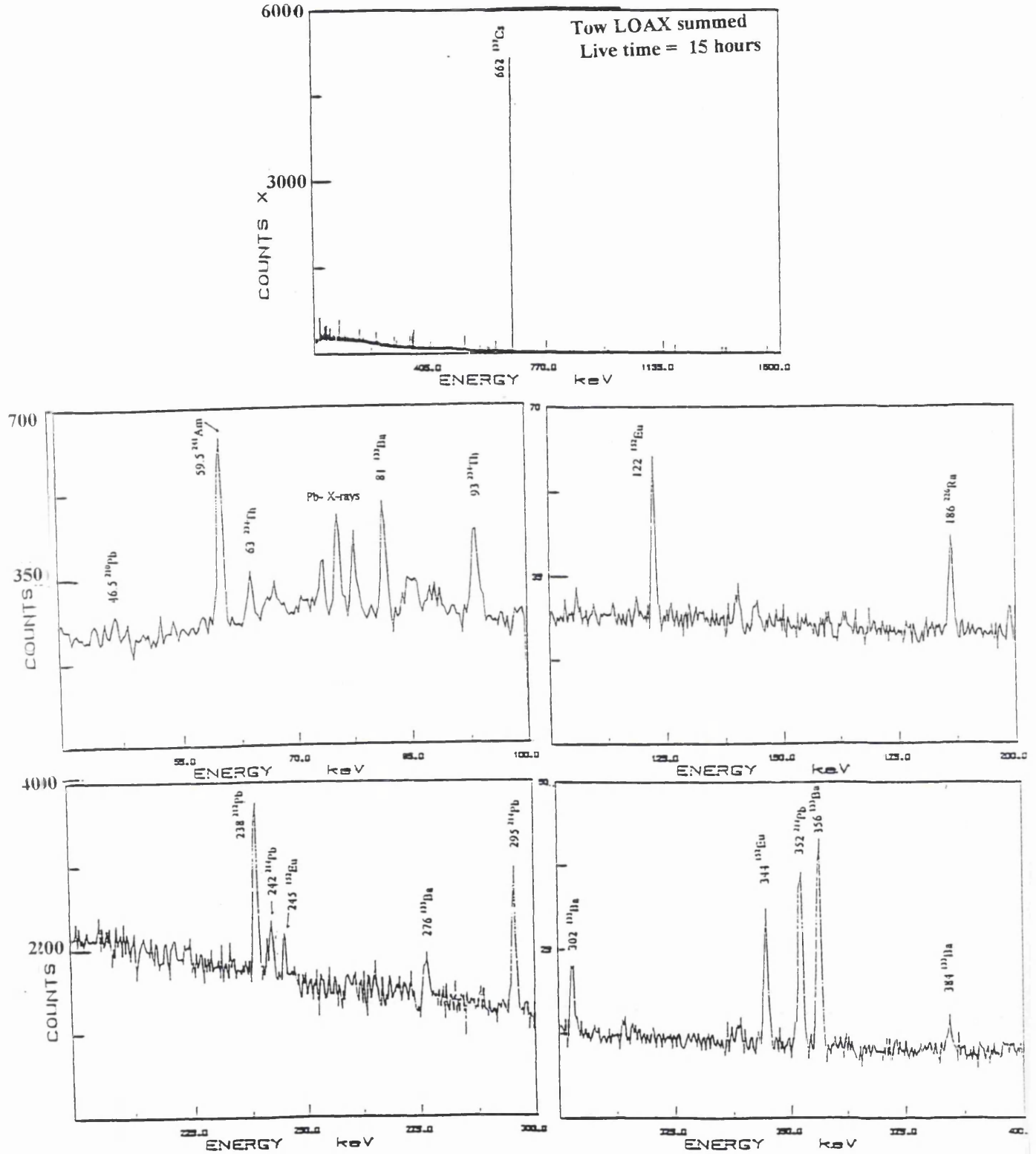

Figure A4 Long count of subject associated soil sample measured using the 80%HPGe-detector.

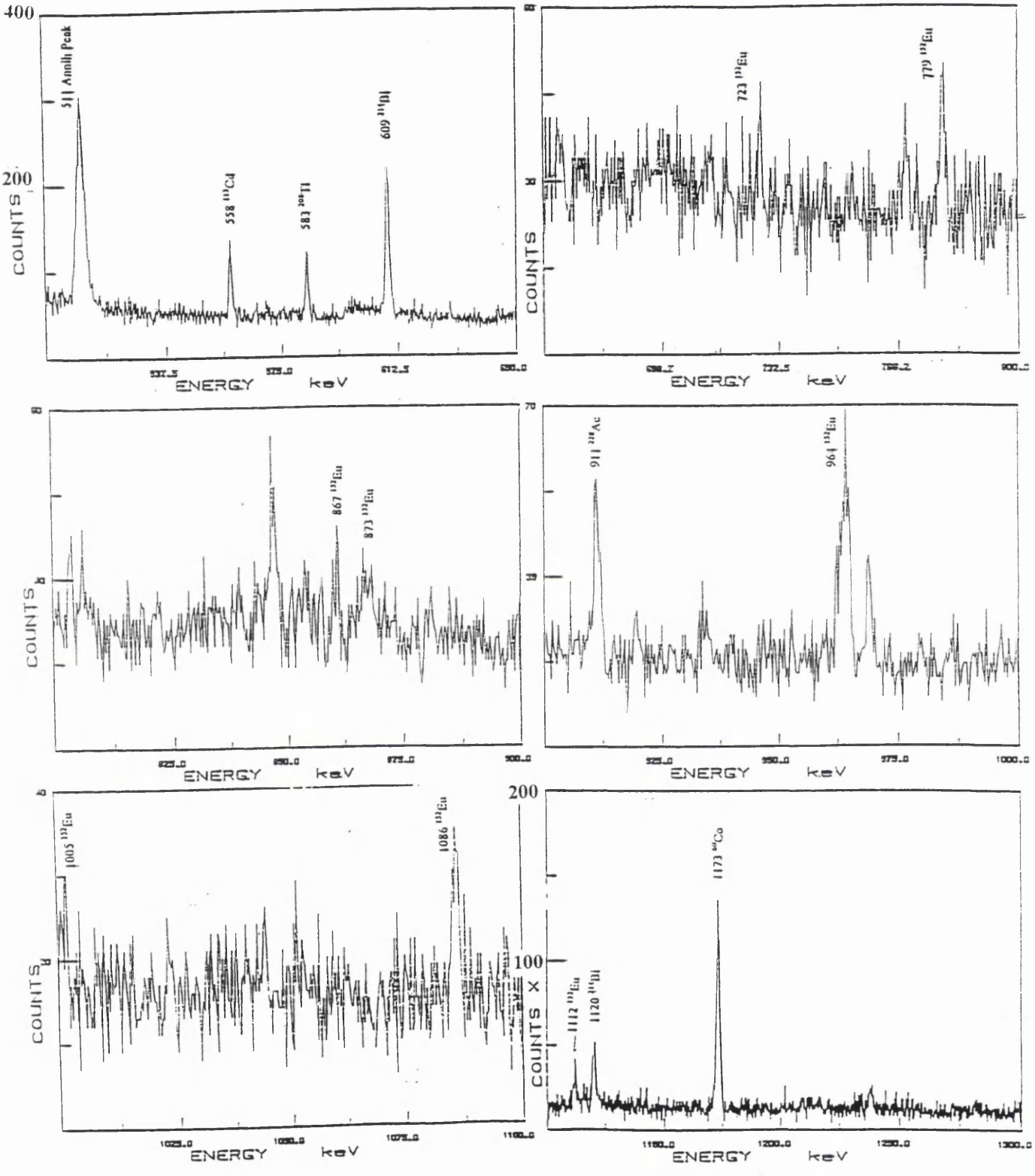
400
200
COUNTS
511 Annih Peak
558 ^{113}Cd
583 ^{208}Tl
609 ^{214}Bi
ENERGY keV
723 ^{152}Eu
779 ^{152}Eu
867 ^{152}Eu
873 ^{152}Eu
911 ^{228}Ac
964 ^{152}Eu
1005 ^{152}Eu
1086 ^{152}Eu
1112 ^{152}Eu
1120 ^{214}Bi
1173 ^{60}Co
COUNTS X
100

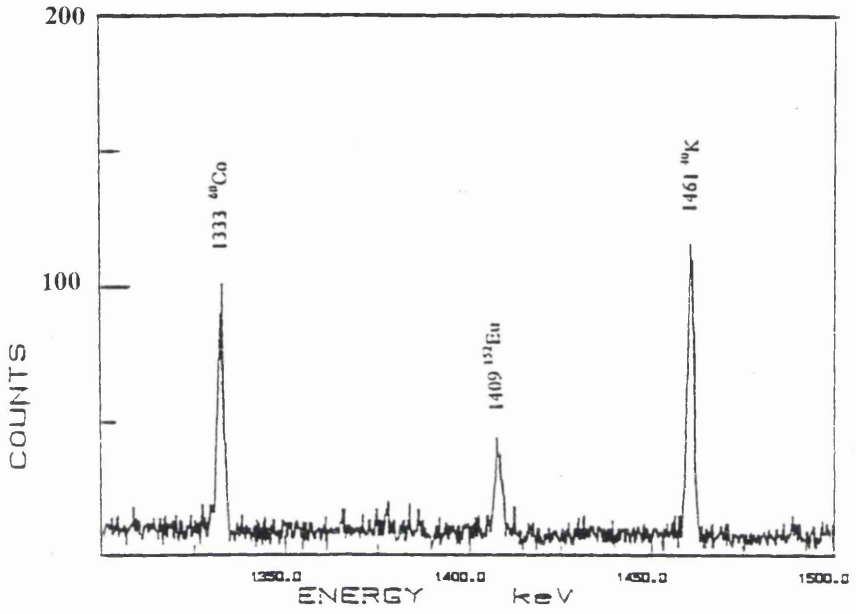
200
100
COUNTS
1333 60Co
1409 152Eu
1461 40K
1350.0
1400.0
1450.0
1500.0
ENERGY keV

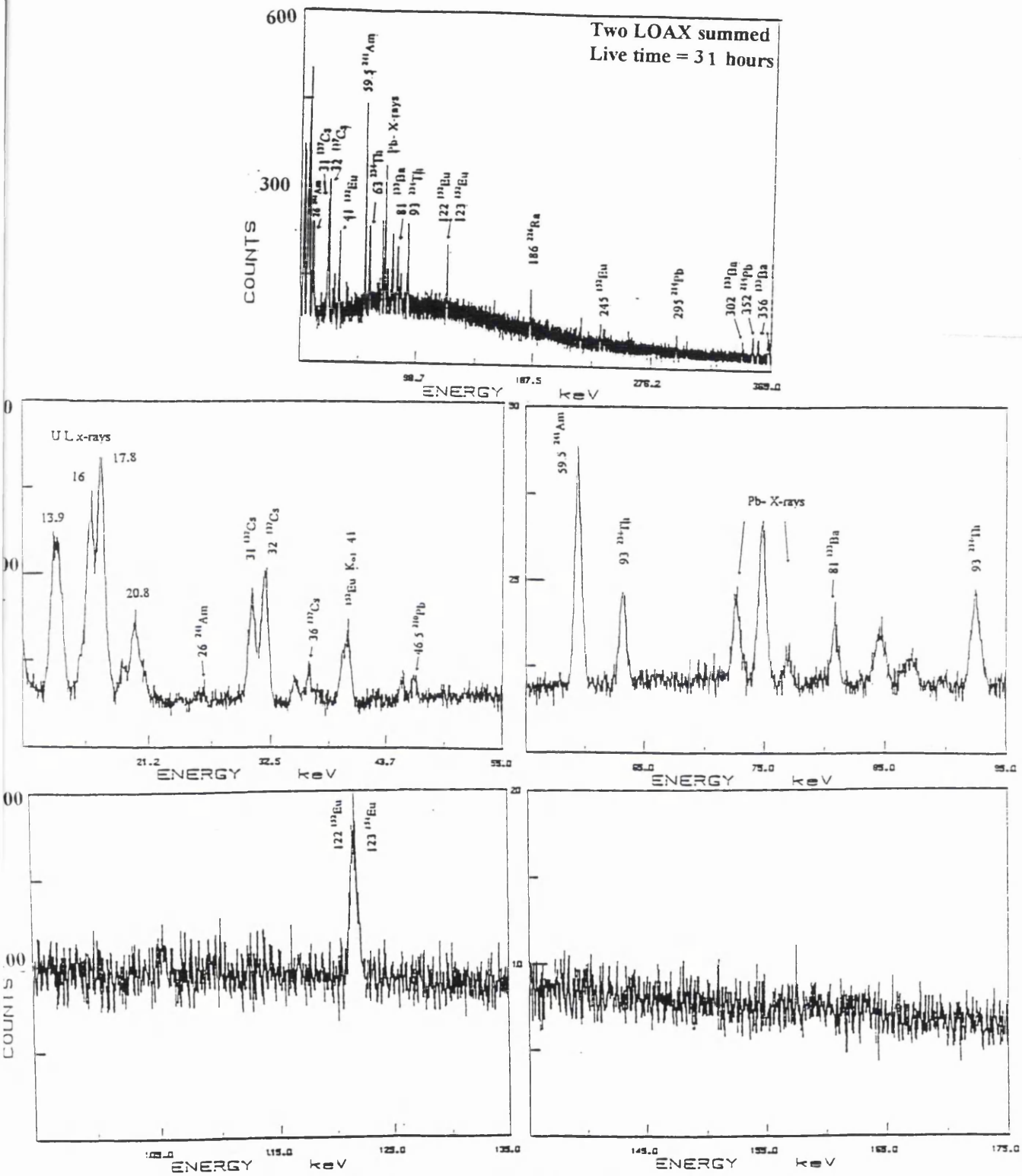

Figure A4 Long count of subject associated soil sample measured using the 2LOAX HPGe-detectors.